DEVELOPMENT OF BIOPOLYMERS BASED HYDROGELS FOR VARIOUS APPLICATIONS

A Thesis Submitted

in Partial Fulfillment of the Requirements for the

Degree of

DOCTOR OF PHILOSOPHY

By

INDU RANI

(2K19/PhD/AC/502)

Under the Supervision of

PROF. SUDHIR G.WARKAR

and

PROF. ANIL KUMAR

To the

Department of Applied Chemistry

DELHI TECHNOLOGICAL UNIVERSITY

(Formely Delhi College of Engineering)

Shahbad Daulatpur, Main Bawana Road, Delhi- 110042, India

December, 2024

Dedicated to my beloved family

ACKNOWLEDGEMENTS

"I am blessed with everything I need. I am working hard towards everything I want, and most of all, I appreciate and thank God for what I have."

Coming to the end of my Ph.D., I pour out my thoughts and hope that reflects the deep gratitude I hold for people who have made it possible for me to surmount this hurdle and achieve my dream. I am extremely fortunate to have **Prof. Sudhir G Warkar** as my mentor, an individual with years of experience and possibly the most encouraging person I have come across in my educational years. He is not only the person behind innumerable success stories of his doctoral students but also the one who established pioneering research ethics among young researchers. I am extremely grateful to **Prof. Anil Kumar** (Co-supervisor, and Head of Department of Applied Chemistry) for providing the necessary research facilities and an excellent working environment in the department. His work exhibits the ideal fusion of punctuality, enthusiasm, commitment, organization, and excellent administrative abilities. We are fortunate to have a visionary like him in our department. I would also like to thank Professor D. Kumar, Professor R. C. Sharma, Professor R. K. Gupta, Professor Ram Singh, Professor Roli Purwar, Dr. Richa Srivastava, Dr. Manish Jain, Dr. Raminder Kaur, and Dr. Poonam, faculty members, Department of Applied Chemistry, DTU for their time-to-time valuable support. No word and no language are ever adequate to express my heartfelt admiration for my respected **parents, Mrs. Sheela Devi (Mother), and Mr. Rishi Parkash (Father),** who have been pillars of inspiration for my academic expedition and I am thankful for their blessings and unconditional love, without which Iwould have failed to complete this work. I am grateful to **Mr. Gurmeet (Husband)** and my **parents-in-law** for their constant support and motivation to do well in my academic area.

I am grateful to all my labmates and my deepest thanks to **Dr. Himansh Goel** for his help and support whenever needed and for being such a good friend. I thank my daughter **Rudranshi** who allowed me to remain focused and finish my thesis without being distracted. I am grateful to **Prof. Prateek Sharma** (Vice Chancellor) and **Prof. Yogesh Singh** (former Vice Chancellor) of Delhi Technological University for giving me this opportunity to conduct my research work. I must also thank CIF-Delhi Technological University, USIC-University of Delhi, CIF-IIT Delhi, and SAIF-AIIMS Delhi for

providing various instrumentation facilities. I would like to thanks the Council of Scientific and Industrial Research (CSIR) for providing me the NET-JRF fellowship.

Thank you so much!!!!!

(Indu Rani)

DELHI TECHNOLOGICAL UNIVERSITY

(Formerly Delhi College of Engineering)

Shahbad Daulatpur, Main Bawana Road, Delhi-42

CANDIDATE'S DECLARATION

I **Indu Rani** hereby certify that the work which is being presented in the thesis entitled "**Development of Biopolymers Based Hydrogels for Various Applications"** in partial fulfillment of the requirements for the award of the Degree of Doctor of Philosophy, submitted in the Department of **Applied Chemistry**, Delhi Technological University is an authentic record of my own work carried out during the period from 10 January, 2020 to 2024 under the supervision of Prof. Sudhir G.Warkar and Prof. Anil Kumar. The matter presented in the thesis has not been submitted by me for the award of any other degree of this or any other Institute.

Candidate's Signature

This is to certify that the student has incorporated all the corrections suggested by the examiners in the thesis and the statement made by the candidate is correct to the best of our knowledge.

Signature of Supervisor (s) **Signature of External Examiner**

DELHI TECHNOLOGICAL UNIVERSITY

(Formerly Delhi College of Engineering)
Shahbad Daulatpur, Main Bawana Road, Delhi-42

CERTIFICATE BY THE SUPERVISOR(s)

Certified that **Indu Rani (**2K19/PHDAC/502) has carried out her research work presented in this thesis entitled **"Development of Biopolymers Based Hydrogels for Various Applications"** for the award of **Doctor of Philosophy**from Department of Applied Chemistry, Delhi Technological University, Delhi,under our supervision. The thesis embodies results of original work, and studiesare carried out by the student herself and the contents of the thesis do not formthe basis for the award of any other degree to the candidate or to anybody else from this or any other University/Institution.

Signature
Prof. Anil Kumar
(Co-Supervisor)
(Head of Department)
Department of Applied Chemistry

Signature
Prof.Sudhir G.Warkar
(Supervisor)
Department of Applied Chemistry

Date:

ABSTRACT

In this thesis, the research aims on the synthesis of tamarind kernel gum (TKG) and carboxymethyl tamarind kernel gum (CMTKG) based hydrogels and utilized different nanocomposite hydrogels for mainly drug delivery applications. Various inorganic fillers such as silver nanoparticles, zinc nanoparticles, and zeolites has been incorporated into hydrogels and used in different applications such as drug delivery and dye removal applications. This thesis has been summarized in 6 chapters.

Chapter 1 outlines different aspects regarding the properties, synthesis, and applications of hydrogels. This chapter gives insight about the hydrogels, their classification, and their methods of synthesis. The chapter also discusses the introduction of biopolymers, especially Tamarind Kernel Gum (TKG) and its derivative, Carboxymethyl Tamarind Kernel Gum (CMTKG), which can be used to synthesize hydrogels for different applications. The chapter also focuses on the applications of hydrogels, such as drug delivery systems, tissue engineering, wound healing, dye removal, agricultural, metal ion removal, biosensors, textile, and food industry.

In **Chapter 2,** a novel hydrogel network based on carboxymethyl tamarind kernel gum/poly (sodium acrylate) was synthesized by using polyethylene glycol diacrylate (PEGDA) as a cross-linker. Zinc Oxide nanoparticles (ZnO NPs) were prepared via hydrothermal synthetic method and developed ZnO NPs were embedded within CMTKG/poly(sodium acrylate (PSA) hydrogel for the controlled release studies of ciprofloxacin drug. Various techniques such as FTIR, XRD, FESEM, and TEM were used to characterize the synthesized ZnO NPs, pure hydrogel, and hydrogel nanocomposites. Various parameters such as drug loading, drug entrapment, gel content, and porosity were estimated for all the synthesized hydrogel nanocomposites. The swelling and rheological studies revealed that ZnO NPs embedded hydrogel composites exhibited increased swelling tendency and thermal stability.

The antibacterial action of CMTKG-based hydrogel nanocomposites was studied using *E. coli* (gram-negative) bacteria with the help of the disc diffusion method. The result showed that the incorporation of ZnO NPs enhanced the antimicrobial action of ciprofloxacin-loaded CMTKG-based hydrogels. The kinetic modelling of drug release

was done using Higuchi and Korsmeyer - Peppas model. The higher value of Regression coefficient (R^2) close to unity indicated that the mechanistic pathway of drug release from the hydrogels was more fitted in the Korsmeyer-Peppas model followed by Fickian diffusion.

Chapter 3, deals with the green synthesis of novel silver nanoparticles (Ag NPs) embedded TKG/PSA nanocomposite hydrogel without the use of any toxic materials. The developed hydrogels were characterized using XRD, FTIR, U V-visible, FE-SEM, and TEM techniques. Doxycycline was chosen as a model drug for release studies using TKG/PSA and Ag/TKG/PSA nanocomposite. The observation is that Ag/TKG/PSA hydrogel nanocomposite showed a pH-dependent swelling which is higher at pH 7.4 than at pH 1.2. Similarly, the cumulative drug release percentage using silver nanocomposite is higher at pH 7.4 than at pH 1.2. Also, the presence of Ag NPs decreased the swelling ratio of TKG/PSA hydrogel, which controls the Doxycycline drug's release rate. In addition, the Doxycycline release kinetics studies indicated that the drug release data was fitted in the Korsmeyer-Peppas model with a higher R^2 value. Thus, Ag/TKG/PSA nanocomposite showed satisfactory results for sustainable release of Doxycycline drug.

Chapter 4, describes the synthesis of hydrogel films comprising of CMTKG, polyvinyl alcohol (PVA), and guar gum (GG) using glutaraldehyde (GTA) as cross-linker. The synthesized hydrogel films were evaluated in terms of equilibrium swelling ratio, moisture content, thickness, wetting analysis, thermal analysis, and mechanical analysis. The tensile strength of the films lie in the range of 95.80 to 149.07 MPa while elongation at break value lies in the range of 1.51 to 5.20%. The synthesized hydrogel films were characterized by techniques such as FTIR, FE-SEM, TGA, and DTA.

The ciprofloxacin (CFX) drug was embedded in the best-swelled hydrogel film and in-vitro drug release behavior was studied at alkaline pH 7.4 phosphate buffer solution. It was found that the maximum drug release was to be 73 % after 24 hours at pH 7.4. Moreover, the release data was fitted in various kinetic models such as the First-order, Higuchi, and Korsmeyer-Peppas models. The best-fitted Korsmeyer-Peppas model suggested that the release of the drug follows Fickian diffusion and the value of diffusion exponent (n) was determined to be 0.38.

Chapter 5 deals with the synthesis of zeolite-loaded CMTKG based hydrogels as a potential adsorbent for the removal of crystal violet dye. Initially, the crosslinked hydrogel of CMTKG with sodium methacrylate (SMA) was prepared via a free radical mechanism using a methylene bisacrylamide (MBA) cross-linking agent and potassium persulfate (KPS) as initiator. In this way, various formulations of hydrogels were prepared by varying the content of zeolite. The swelling capacity of all the synthesized hydrogels was investigated and the composition of hydrogel which exhibited maximum swelling wasused for the characterization and dye removal experiment. Crystal violet (CV) was chosen as a model dye for the dye removal experiment. The structure of zeolite and zeolite-embedded hydrogel was elucidated by XRD, FTIR, and SEM-EDX analysis tools. The adsorption experiment was investigated by varying the CV concentration, hydrogel amount, temperature, dye solution pH, adsorption time, and ionic strength. The Langmuir and Freundlich isotherm models were used to fit the adsorption data and it was noticed that the data fitted well with the Langmuir model.

The hydrogel's maximum dye adsorption efficiency was found at 123.60 mg g^{-1}. The adsorption kinetic studies were followed by pseudo-first-order and intraparticle diffusion kinetic models. In addition, regeneration studies were performed for the best adsorbent hydrogel using ethanol solvent and the result concluded the desorption efficiency of hydrogel (82%) over four desorption cycles. Overall, the synthesized hydrogel material was used as an effective adsorbent for removing hazardous cationic dye from polluted water.

LIST OF PUBLICATIONS

From Thesis

- **Indu Rani,** S.G. Warkar and Anil Kumar, "Nano ZnO embedded Poly(ethylene glycol) diacrylate cross-linked carboxymethyl tamarind kernel gum and poly (sodium acrylate) composite hydrogels for oral delivery of ciprofloxacin and their antibacterial properties," ***Mater. TodayCommun.,*** vol. 35, no. June 2022, p. 105635, 2023, doi: 10.1016/j.mtcomm.2023.105635. **(I.F. = 3.8) (SCIE)**

- **Indu Rani**, S.G.Warkar and Anil Kumar, " Removal of cationic crystal dye using zeolite embedded carboxymethyl tamarind kernel gum (CMTKG)based hydrogel adsorbents," ***ChemistrySelect,*** vol. 8, no. 29, 2023, doi: 10.1002/ slct.202301434. **(I.F. = 2.3) (SCIE)**

- **Indu Rani,** S.G.Warkar and Anil Kumar, "A Silver nanoparticle embedded tamarind kernel gum/ poly (sodium acrylate) nanocomposite for sustainable release of doxycycline," ***ChemistrySelect,*** vol. 9, no. 14, p. 2024, 2024, doi: 10.1002/slct.202400168. **(I.F. = 2.3) (SCIE)**

- **Indu Rani,** S.G.Warkar and Anil Kumar, " Synthesis and characterization of novel carboxymethyl tamarind kernel gum- poly(vinyl alcohol)/ guar gum- based hydrogel film loaded with ciprofloxacin for biomedical applications," ***International Journal of Biological Macromolecules***, p.136766, 2024, doi: http://doi.org/10.1016/j.ijbiomac.2024.136766. **(I.F. =7.7) (SCIE)**

Other Publications

- **Indu Rani,** Ekta Yadav, Komal Pandey, Khusbhu, S.G.Warkar, Anil Kumar. Synthesis and application of zinc-loaded carboxymethyl tamarind kernel gum and xanthan gum-based superabsorbent hydrogels to investigatethe effect on sesame plant growth, ***Polym. Bull.,*** no. 0123456789, 2024, doi: 10.1007/s00289-024-05150-y. **(I.F. = 3.2) (SCIE)**

TABLE OF CONTENTS

LIST OF TABLES

LIST OF FIGURES

LIST OF ABBREVIATIONS

Ag	**:**	Silver
BET	**:**	Brunauer–Emmett–Teller
CFX	**:**	Ciprofloxacin
CMTKG	**:**	Carboxymethyl tamarind kernel gum
CV	**:**	Crystal violet
DL	**:**	Drug loading
DE	**:**	Drug entrapment
DOX	**:**	Doxycycline
E. Coli	**:**	Escherichia coli
ESR	**:**	Equilibrium swelling ratio
FTIR	**:**	Fourier transform infrared resonance
FWHM	:	Full width at half maximum
G'	**:**	Storage modulus
G''	:	Loss modulus
GG	**:**	Guar gum
GTA	:	Glutaraldehyde
MA	**:**	Methacrylic acid
MBA	**:**	Methylene bis acrylamide
NaOH	**:**	Sodium hydroxide
NP	**:**	Nanoparticles
KPS	**:**	Potassium persulfate
PBS	**:**	Phosphate buffer saline
PEGDA	**:**	Poly(ethylene glycol diacrylate)
PSMA	**:**	Poly (sodium methacrylate)
PZC	**:**	Point zero charge
Qe	**:**	Equilibrium adsorption
SPR	**:**	Surface plasma resonance
SAED	**:**	Selected area electron diffraction
TEM	**:**	Transmission electron microscope
TKG	**:**	Tamarind kernel gum

TGA	**:**	Thermogravimetric analysis
UTM	**:**	Universal testing machine
XRD	**:**	X-ray diffraction
ZnO	**:**	Zinc oxide
%	**:**	Percentage
cm	**:**	Centimeter
MW	**:**	Molecular weight
mL	**:**	milliliter
nm	**:**	nanometer
$\boldsymbol{\theta}$	:	Diffraction angle

CHAPTER 1

INTRODUCTION AND LITERATURE REVIEW

Graphical Abstract

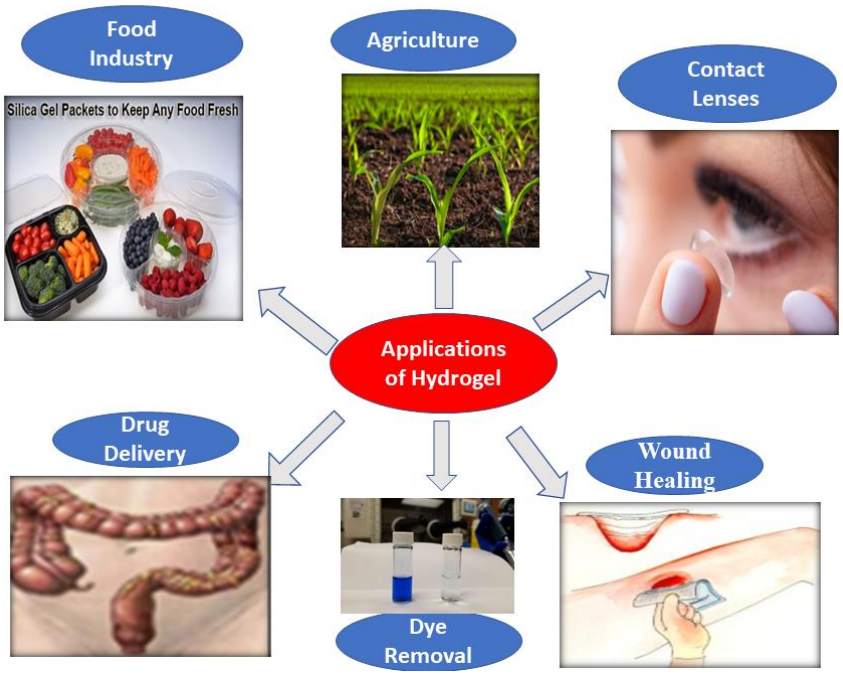

1.1. Introduction

Biopolymers are polymers composed of several monomers, or units, found within an organism. Since they are typically produced from plants and animals, they are readily renewable for numerous applications due to their biodegradable nature [1,2]. Biopolymers play a variety of roles in the body, including the synthesis of cell- based tissue, support for the integrity of connective tissue, including human cartilage, and the provision of molecules for the human endocrine system to use as signals [3]. Biopolymer materials that can be used for biomedical purposes such as drug delivery and tissue engineering can be made from polypeptides and polysaccharides. Biopolymers are used to synthesis hydrogels due to their specific properties such as they are cheap, biocompatible, biodegradable, hydrophilic, non-toxic, renewable, and highly abundant (Fig.1.1). Hydrogel is a three-dimensional network of hydrophilic

polymers that can swell and hold liquid when immersed in it. Because the polymer chains are cross-linked chemically or physically, they can preserve their structure [4,5]. It is interesting to understand how hydrogels can take and hold a lot of water or biological fluids inside their porous structures. They are made up of three- dimensional cross-linked polymeric networks. These hydrophilic materials have unique properties, including a high-water content, being soft, flexible, and biocompatible[6]. This makes them good choices for many uses in various applications, especially in the biomedical field [7,8]. Hydrogels can hold lot of water in it, anywhere from 10% to thousands of times its dry weight. Because hydrogels are made up of cross- linked networks, they can swell and hold water molecules without breaking. Their hydrophilic nature allows the uptake of water, nutrients, and other molecules through the gel matrix [9]. In the late 19^{th} century, scientists explored the cross-linked polymers which could uptake and hold water. In 1938, Wichterle and Lim made poly(2-hydroxyethyl methacrylate) (HEMA) hydrogels for use as contact lenses[10]. This was one of the first hydrogels ever made. This groundbreaking work paved the way for the development of modern hydrogels. Researchers at the U.S. Department of Agriculture made the first superabsorbent hydrogels in the 1960s. They were made from partly diluted poly (acrylic acid) and could soak up to 1000 times their weight in water[11]. Hydrogels can be used in many areas, such as cosmetic, food industry, metal ion and dye removal, agricultural field, and drug delivery applications. Hydrogels were synthesized through different ways such as radiation polymerization[12] and controlled radical polymerization [13], as well as the addition of functional groups and flexible qualities. In this research work, the main focuses were on the synthesis of composite hydrogels for the drug delivery and dye removal applications. The trapping of various fillers inside the hydrogel matrix, including clays, metallic nanoparticles, carbon-based materials, and organic fillers, results in the composite hydrogels, which exhibit improved mechanical, chemical, and thermal properties as well as adsorption capacity. Varied type of composite hydrogels can be used in the biological fields such as biosensors, tissue engineering, drug delivery systems, and wound treatments. They can release therapeutic agents slowly and safely, behave like the extracellular matrix to help tissues grow back [14], and keep the environment moist for wound healing [15]. This is because they are biocompatible and have properties that can be modified. In

pharmaceutical applications, hydrogels could be used for controlled drug delivery systems because they have properties like better bioavailability, and fewer side effects[16]. Hydrogels can also be used in the agricultural fields as seed coats, soil conditioners, and controlled-release systems for pesticides and fertilizers[12]. Water cleansing, wastewater cleaning, and cleanup of oil spills are environmental uses of hydrogels[17]. Hydrogels can be used as adsorbents to remove pollutants and other harmful substances from water sources because they can hold a lot of water and selectively adsorb certain substances like heavy metal ions, and dye molecules [18,19]. Due to their sensitive and selective qualities, hydrogels have also been looked at for use as biosensors [20], actuators [21], and separation membranes[22]. This work aims to provide a comprehensive and qualitative overview of the area, highlighting current advancements in hydrogel devices for different applications. Hydrogels are effective materials for drug absorption in aqueous media through physical or chemical interactions and the release of the drugs under physiological pH and temperature conditions. The rate of drug release from hydrogels depends on the pH, temperature, ionic strength, and pore size of hydrogels. There are some other factors which can influence the rate of drug release from hydrogels such as swelling, mesh size, pore diameter, and geometry of drug delivery devices. The drug can be released from hydrogel through a swelling-controlled, diffusion-controlled, or chemically-controlled mechanism. In the present research work, the aim was to synthesize hybrid hydrogels made by polymerizing synthetic monomers with biopolymers. There have been numerous natural biopolymer-based hydrogels used for the controlled release of drugs into the human body, including guar gum, chitosan, tamarind gum, sodium alginate, cellulose, Arabic gum, chitosan carboxymethyl guar gum, etc. However, the hydrogels based on Tamarind kernel gum (TKG) and its carboxymethyl derivative carboxymethyl tamarind kernel gum (CMTKG) are scarcely explored. TKG has been chemically modified to make CMTKG which is a hydrophilic, non-toxic, biodegradable, and biocompatible biopolymer. Because of this chemical alteration, the drug loading capacity, swelling capacity, biodegradability, and shelf-life of CMTKG were found higher than TKG [82]. The present research has mainly focused on TKG and CMTKG biopolymer-based hydrogels and their applications in different fields, specifically, in drug delivery and dye removal applications.

1.2. Types of Hydrogels

Hydrogels can be classified into different groups based on cross-linking, polymeric composition, sources, electrical charges, physical structure, and configuration.

1.2.1. Polymeric composition

Homopolymeric networks is formed from a single species of monomer which is the fundamental structural component of any polymer network. Depending on the type of monomer and polymerisation method, homopolymers have a cross-linked skeleton. However, copolymeric hydrogels are made up of two or more distinct monomer species bonded in a random, block, or alternating pattern throughout the polymer network's chain, each containing at least one hydrophilic component [5]. Multipolymer interpenetrating polymeric hydrogel (IPN) is composed of two cross-linked synthetic and natural polymer that are arranged in a network shape. To synthesize the semi-IPN hydrogels, two types of polymers in which one cross-linked and the other is non-cross-linked are used.

1.2.2. Based on configuration and electrical charges

Hydrogels can be classified into semi-crystalline, crystalline, and amorphous based on their configuration. However, based on electrical charges, hydrogels can be non-ionic (neutral), ionic (cationic or anionic), amphoteric, and zwitterionic [5].

1.2.3. Based on cross-linked networks

Hydrogels can be divided into physically or chemically cross-linked networks. Physically cross-linked hydrogels formed a polymeric network through the physical interactions like ionic interactions, hydrogen bonding, hydrophobic associations, and molecular entanglements, but not through covalent bonds as shown in Fig.1.2.[23]. These hydrogels are physically or chemically sensitive to specific environmental changes such as temperature, pressure, pH, electric field, magnetic field and ionic strength. The ionic interactions between the polymers for example, lead to the formation of alginate-based hydrogels by interacting with calcium ions and other divalent cations [24]. However, chitosan based physically cross-linked hydrogels were synthesized

through polymerization with tripolyphosphate anion [25]. Additionally, hydrogen bonding is a significant interaction that favors the formation of physically cross-linked hydrogels, especially based on proteins and polysaccharide polymers. For example, gelatin protein derived from collagen synthesizes thermo-reversible hydrogels by building triple-helical structures held together through hydrogen bonds [26]. The hydrophobic interactions between molecules are also involved in the formation of physically cross-linked hydrogels, especially thermosensitive hydrogels. After heating, these hydrogels change from sol to gel, and the hydrophobic parts of the polymer chains cross-linked to form a temporary network[27] .

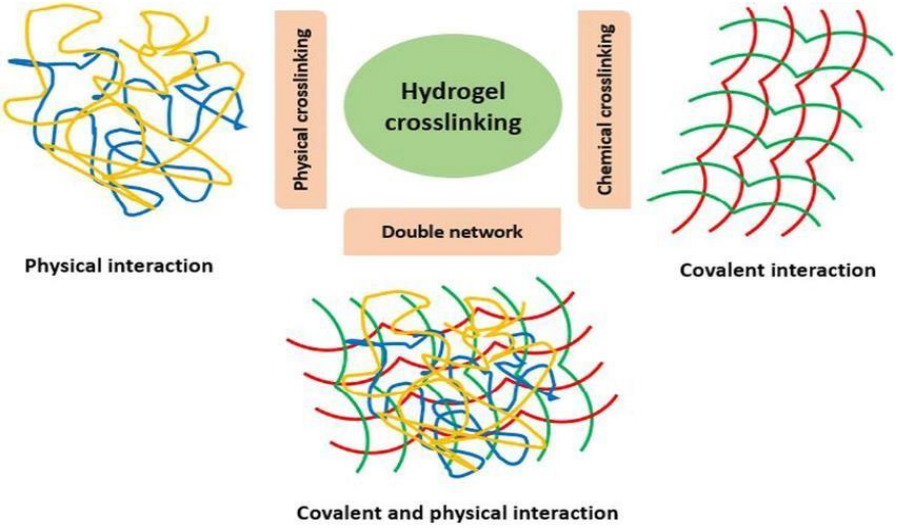

Fig.1.1: Structure of physically and chemically cross-linked hydrogel

Chemically crosslinked hydrogels formed the polymeric network through the covalent bonding as shown in **Fig.1.1.** Chemically cross-linked hydrogels are also called fixed or covalent hydrogels. There are different ways to cross-link polymers, such as through free radical polymerization, condensation reactions, grafting and enzymatic methods [28]. Chemically cross-linked hydrogels are more stable than physically cross-linked hydrogels. The most common way to synthesize chemically cross-linked hydrogels is a free radical chain polymerization [29]. In this method, vinyl monomers such as acrylic acid, acrylamide, or methacrylic acid formed free radicals using an initiator such as potassium persulphate and cross-linked using a cross-linking agent, for example, N, N'-methylene bisacrylamide (N,N'-MBA). However, in the condensation method, chemically cross-linked hydrogels are formed by the condensation reaction between the

functional groups of polymer moieties through the elimination of small molecules like water or alcohol. In the grafting method, hydrophilic polymer chains are covalently attached to a polymeric backbone. Chemically cross-linked hydrogels can also be synthesized through a covalent bond formation between vinyl monomers and polysaccharide backbones through radiation-induced copolymerization [30].

1.2.4. Based on sources

Polysaccharides such as alginate, chitosan, hyaluronic acid and proteins like collagen, gelatin, and silk fibroin are the building blocks of natural hydrogels[31]. Due to the biocompatible, biodegradable, and non-toxic properties of these hydrogels, they can be used in the biomedical applications especially for the tissue engineering and drug delivery applications. Natural hydrogels synthesized from Alginate biopolymer, obtained from brown seaweed, via formation of cross-linked through the interaction with divalent cations, such as calcium ions [32]. Additionally, various proteins like gelatin, collagen, and silk fibroin can also be used to synthesize natural hydrogels [33, 34]. Synthetic hydrogels can be made using synthetic polymers which have superior water-absorbing capacity, long life-span, and gel strength. However, compared to natural hydrogels, synthetic polymer-based hydrogels exhibit less biological and cytocompatibility activities. The different synthetic polymers such as polyacrylic acid, polyvinyl alcohol, polyethylene glycol, and their derivatives can be used to synthesize the synthetic hydrogels. In a study, poly(acrylic acid)-based synthetic hydrogel was prepared through a free radical polymerization and grafting methods [35]. Polyvinyl alcohol (PVA) is another synthetic polymer that is widely used to synthesize hydrogels, especially hydrogel films. In a study, PVA based hydrogels were formed by chemically cross-linking with glutaraldehyde or boric acid [36] and physically cross-linking with freeze-thaw cycles. Polyethylene glycol (PEG) is a example of synthetic polymer that is often used to make synthetic hydrogels due to its high biocompatibility and swelling capacity [37]. Moreover, both natural and synthetic polymers or monomers can be cross-linked to form hybrid hydrogels[38]. For example, natural polysaccharides like chitosan or alginate can be mixed with synthetic polymers like polyacrylic acid or polyethylene glycol to make hybrid hydrogels. Hybrid hydrogels showed higher swelling, thermal, mechanical, and rheological properties than their individual

units[39]. For example, collagen can be polymerized with polyacrylic acid and polyethylene glycol and the synthesized hybrid hydrogel showed better biocompatibility, thermal, and mechanical strength [40].

1.3. Methods of Preparation of Hydrogels

Hydrogels can be prepared using various techniques such as bulk, suspension and solution polymerization. However, different cross-linking strategy was adopted to synthesize physically and chemically cross-linked polymeric hydrogel.

1.3.1. Cross-linking strategy to synthesize physical hydrogels

1.3.1.1. Freeze thawing method

In this method, physically cross-linked hydrogels in microcrystal form were produced through the freeze and thaw cycle without using any cross-linking agent. Thus, physically cross-linked chains of hydrogels are linked through non-covalent interactions. For example, M. Gann et.al.[41], reported the synthesis of poly(vinyl alcohol) (PVA) and poly (acrylic acid) based physically cross-linked hydrogel using the freeze and thaw method. In another study, salecan and PVA based hybrid hydrogels were synthesized using freeze and thaw method [42].

1.3.1.2. Ionic interactions

Polyelectrolyte complex can be formed due to the significant interaction of the polymer chains having opposite charges. This method is often used with natural polymers such as chitin and alginate. Alginate is an anionic polysaccharide and forms physically cross-linked hydrogels by interacting with divalent cations like calcium ions ($Ca^{2+)}$ and barium ions (Ba^{2+})[32]. In the gelation process, sodium (Na^{+}) ions from the guluronic acid unit of alginate are exchanged with divalent cations[24]. However, chitosan is a cationic polysaccharide that can form polyelectrolyte complexes with polyanions such as tripolyphosphate (TPP) or citrate [25]. In this case, positively charged amino groups of chitosan attracted with the negatively charged ions of the polyanion, and formed a cross-linked hydrogel network[39].

1.3.1.3. Hydrogen bonding

A functional group with a high electron density combines with an electron-deficient hydrogen atom to form a hydrogen bond. The aqueous solution of polymers having carboxyl groups can be made into an H-bonded hydrogel by decreasing its pH. For example, through hydrogen bonding, a variety of novel pH-sensitive biodegradable hydrogels with self-healing properties were synthesized. These hydrogels are fabricated from modified hyaluronic acid (HA) and nucleobases such as cytosine and guanosine. A bridging unit between the nucleobase and HA is 1,6-hexamethylenediamine (HMDA) [26]. Moreover, a hydrogen bonded based poly(N-vinylpyrrolidone) and linear poly (acrylic acid) hydrogels were synthesized by lowering the pH of the reaction conditions [42]. Another example of hydrogen bonded cross-linked hydrogels is an agarose polysaccharide-based hydrogel [43].

1.3.1.4. Hydrophobic interactions

Physically cross-linked hydrogels can be formed due to the hydrophobic interactions of polymeric chains with each other. This process is often seen in thermosensitive hydrogels, in which the gelation occurs due to hydrophobic interactions. A thermosensitive polymer Poly (N-isopropylacrylamide) (PNIPAM) has a lower critical solution temperature (LCST) of about 32°C. Below the LCST, PNIPAM is hydrophilic, and can dissolve in water. However, when the temperature exceeds the LCST, the hydrophobic interactions between the isopropyl groups dominate [44], forming a physically cross-linked hydrogel. In another study, pluronic which is a tri-block copolymer, and composed with poly(ethylene oxide), and poly(propylene oxide) blocks was used to synthesize thermoreversible hydrogels [45]. In this case, the gelation process is caused by the hydrophobic poly(propylene oxide) blocks sticking together at high temperatures.

1.3.1.5. Stereo complex formation

The interactions between enantiomeric polymeric chains, or tiny molecules, with the same chemical composition but distinct stereochemistry are referred to as stereo-complexing. Stereo-complex grafting was used for cross-linking of natural polymers. For example, poly (lactic acid) (PLA) shows maximum ability to form stereo complexes [29]. However, the primary disadvantage of stereo-complexation is its limited range of possible polymer compositions. However, a small stoichiometry variation may decrease or eliminate the stereochemical interaction.

1.3.2. Cross-linking strategy to synthesize Chemical Hydrogels

1.3.2.1. Free radical mechanism

A common way to synthesize chemically cross-linked hydrogels is a free radical polymerization method. In this mechanism, vinyl monomers such as acrylic acid, acrylamide, and N,N-methacrylic acid are cross-linked with polymers using an activator and cross-linking agent. Mostly, ammonium persulfate (APS) or potassium persulfate (KPS) is used as an activator and methylene bisacrylamide (MBA) is used as a cross-linking agent [29]. The three steps are involved in the free radical chain polymerization process i.e. initiation, propagation, and termination. In the initiation step, the activator breaks down into free radicals and combines with the vinyl monomers to form a polymer chain. In the propagation step, these active polymer chains keep growing by interacting with more monomers and as the polymer chains grow, the cross-linking agent forms cross-linking network between them. In the last step of termination, the active polymer chains mix with other radical species and cease the polymerization process. Thus, chemically cross-linked hydrogels are synthesized by free radical chain polymerization. For example, pectin-g-poly(acrylic acid) and poly(vinylpyrrolidone) based hydrogel was synthesized using KPS initiator and MBA cross-linker [36].

1.3.2.2. Condensation

The process of condensation polymerization involves the loss of small molecules like water or alcohol, during the formation of the covalent linkage. Mostly, this method is used to synthesize hydrogels based on proteins and polysaccharides. The condensation

of -OH groups or -NH_2 with -COOH or derivatives can be used to produce polyesters and polyamides, respectively. The cross-linking of chitosan with glutaraldehyde is an example of condensation polymerization used to synthesize hydrogels [39]. Chitosan is a cationic polysaccharide that has primary amine groups and combines with glutaraldehyde's aldehyde groups to make Schiff bases and a cross-linked hydrogel network [46]. It is also possible to cross-link gelatin with genipin, which comes naturally from the seed of the *gardenia jasminoides plant* [47]. In this case, genipin forms a linkage with gelatin's main amine groups to form a covalent cross-link. Therefore, a chemically cross-linked hydrogel can be synthesized with significant thermal and mechanical properties.

1.3.2.3. Grafting

The polymerization of a monomer on the backbone of a polymer is known as grafting. In this process, either high energy radiation or chemical reagents, both activate the polymer chains. Thus, both the branching and subsequent cross-linking are caused by the expansion of functional monomers on activated macroradicals. The two types of grafting either chemical grafting or ray-induced grafting used for the synthesis of hydrogels. For example, Alginate and poly(N-isopropylacrylamide) (PNIPAAm) were used to synthesize semi-IPN hydrogels and comb-type grafts that are both pH- and temperature-sensitive. These comb-type graft hydrogels are grafted with PNIPAAm and consist of a network of cross-linked alginate. Their free and dynamic graft chains allowed them to respond quickly to changes in pH and temperature [30]. Ceric ion-initiated graft copolymerization is another way to grafting[48]. In this method, ceric ions (Ce^{4+}) are used to start the process of making free radicals on the backbone polymer. These radicals then start the graft copolymerization of vinyl monomers onto the backbone, and form a cross-linked hydrogel network.

1.3.2.4. Enzymatic method

Spray or injectable hydrogels was formed using enzymatic cross-linking under milder conditions and without the use of any toxic chemical substance which ensures the biocompatibility of hydrogels. In this method, both the enzyme and substrate get unionized and form a covalent bond within the cross-linking network of the hydrogel.

The advantages of this method are to control the cross-linking kinetics, high specificity of chemical reaction, and higher in-situ gelation rate of hydrogel formation. For example, Y. Lee et.al. [49], proposed that horseradish peroxide catalysed the cross-linking of gelatin hydrogels and used as a carrier of dermal fibroblasts. The synthesis of hyaluronic acid hydrogel catalysed by transglutaminase enzyme was reported by A. Ranga et.al. [50]. Moreover, tyrosinase enzyme catalysed the synthesis of gelatin and chitosan injectable hydrogel and utilized for tissue engineering applications [51]. Thus, the enzyme catalysed the synthesis of chemically cross-linked polymeric hydrogels.

1.4. Biopolymers Based Composite Hydrogels

1.4.1. Biopolymers

Biopolymers are formed from microorganisms, animals, and plants under natural conditions through a complex metabolic method. There are limited biopolymers that are generated inside the cytoplasm of the cell. For instance, starch, glycon, and poly(phosphate). However, biopolymers that are generated outside the cytoplasm of cells are chitosan, dextran, xanthan gum, alginate, and cellulose [52]. These are made from natural sources and useful in the synthesis of hydrogels for different applications. Polymers like proteins and polysaccharides have advantages like being non-toxic, biocompatible, biodegradable, and being able to be chemically modified [31]. Many types of polysaccharides such as chitosan, alginate, cellulose, and different gums such as guar gum, xanthan gum, acacia gum, and tamarind kernel gum are used to synthesize hydrogels which can be physically or chemically cross-linked [53]. In the past, researchers have also focused on the synthesis of hydrogels using proteins like collagen, gelatin, silk fibroin, and elastin [54]. The physiochemical properties of biopolymers can be modified by either grafting or cross-linking with other polymers and monomers. Biopolymers are hydrophilic, biodegradable, biocompatible, non-toxic, renewable raw materials, highly abundant, and have low processing cost. Thus, biopolymers-based hydrogels can be used in different applications such as drug delivery, tissue engineering, dye removal, agricultural, and metal ion removal applications [55].

1.4.2. Tamarind Kernel Gum (TKG)

TKG is a naturally occurring polysaccharide isolated from Tamarindus indica L. seeds and is found in the endosperm of tamarind seeds as a cell wall storage unit. It is made up of β-(1→4)-D-glucopyranose units, and on its side chains, there are single α-D-xylopyranose units connected by (1→6) links [56]. Organic solvents do not dissolve TKG. In warm water, TKG produces a highly viscous gel with good adhesive properties. TKG is stable at low pH, hydrophilic, and non-toxic. However, TKG suffers from drawbacks such as its drab color, low water solubility, unpleasant odor, and fast biodegradability due to which it is modified into its carboxyl derivative i.e. carboxymethyl tamarind kernel gum (CMTKG) form. TKG is a biocompatible, biodegradable, and cytocompatible biopolymer and these features are useful to synthesize hydrogels for biomedical applications [57]. This biopolymer can also be used to synthesize composite hydrogels which shows excellent potential for use in various fields such as dye removal, drug delivery, metal ion sensing, tissue engineering applications, and some other fields.

1.4.3. Carboxymethyl Tamarind Kernel Gum (CMTKG)

CMTKG is a carboxymethyl derivative of TKG and made by carboxymethylation of TKG (Fig.1.2)[60]. This chemical modification of TKG into CMTKG provides an anionic nature to CMTKG. This biopolymer has higher hydrophilicity, higher swelling ability, and larger self-life than TKG. However, the biodegradability of CMTKG is lower than TKG. Additionally, CMTKG contains higher in-situ gelation, broad pH tolerance, higher drug loading capacity, higher mucoadhesivity, higher stability and release kinetics compared to TKG [64,65]. To synthesize CMTKG, TKG is usually mixed with monochloroacetic acid in the presence of an alkaline catalyst like sodium hydroxide. However, the amount of carboxymethyl substitution can be varied by changing the reaction variables, like the temperature, reaction time and composition of reacting chemicals. Although, CMTKG showed lower biodegradability but thermal, mechanical, and antimicrobial properties of CMTKG was increased by loading of the metallic nanoparticles, inorganic clay particles, and zeolite particles. Fourier-transform infrared spectroscopy (FTIR), and Nuclear magnetic resonance (NMR) spectroscopy

are used to measure the degree of substitution (DS). The results of these studies showed the effect of molecular changes and the amount of carboxymethylation on the physicochemical properties of CMTKG [82].

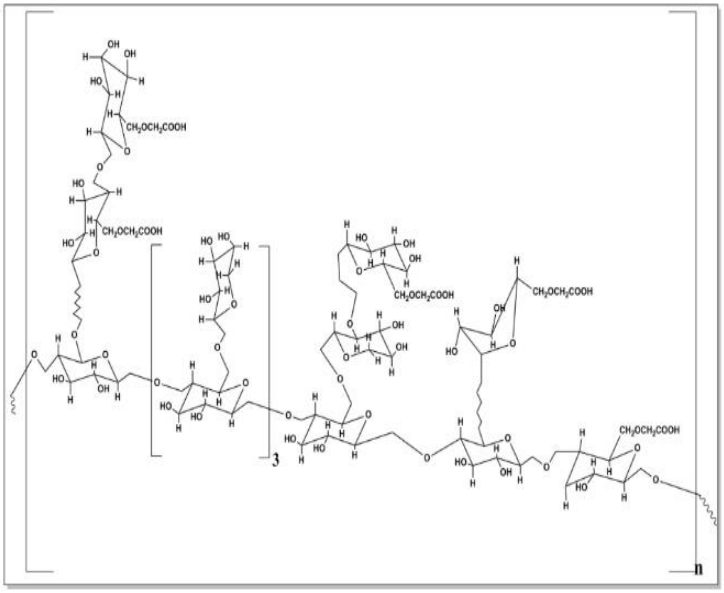

Fig.1.2: Structure of CMTKG

1.5. Various Applications of Composite Hydrogel

Hydrogels have enormous applications owing to unique properties like biocompatibility, biodegradability, hydrophilicity, swelling capacity, and porosity.

1.5.1. Drug delivery applications

Hydrogels have significant amount of porosity, which makes them efficient materials to absorb drugs in the aqueous mediums via physical or chemical interactions and subsequent release of the drug under physiological conditions. Several stimuli like pH, temperature, and ionic strength affect the drug release rate through the hydrogel. A high local concentration of the active pharmaceutical drugs can be maintained for an extended period through an appropriate release mechanism regulated by diffusion, swelling, and chemical reactions. Hydrogel therefore can be used for different biomedical applications. Various drug administration routes are oral, nasal, ocular, topical, parenteral, transdermal, and ocular drug delivery.

1.5.1.1. Oral drug delivery

A drug is mixed into hydrogels and administered locally to the oral cavity to treat conditions like stomatitis, fungal infections, periodontal disease, viral infections, and malignancies of the oral cavity. Hydrogels act as a carrier for drug delivery systems that are taken by mouth, such as gastro-retentive drug delivery systems and colon-targeted drug delivery systems [13]. Because hydrogels can grow and stick to the mucosa, they remain in the digestive system for longer, which enables the drugs to be absorbed and used more effectively. For example, a pH-sensitive hydrogel was synthesized based on poly(acrylic acid) and hydroxypropyl methylcellulose for the slow release of metronidazole drug in the stomach [83]. In another study, alginate-based hydrogels were synthesized for the colon targeted delivery of Diclofenac sodium drug [57]. The synthesis of guar gum-based hydrogel is also reported for the controlled delivery of intestine specific dexamethasone drug [58]. In a study, Moxifloxacin hydrochloride drug loaded TKG based hydrogel was synthesized through a physical gelation method and utilized for the antimicrobial oral delivery applications [59]. Additionally, biopolymers-based nanocomposite hydrogels have also been empolyed for the oral drug delivery. In a study, ZnO nanoparticles loaded carboxymethyl chitosan and sodium alginate nanocomposite hydrogel was used as a carrier for the oral delivery of Diclofenac sodium drug [60]. Another study reported the synthesis of Ag nanoparticles loaded dextran and polyacrylamide hydrogel for the controlled release of ornidazole drug[61]. The literature survey reveals that TKG and CMTKG based nanocomposite hydrogels have not yet been explored for the oral delivery of drugs to the best of my knowledge.

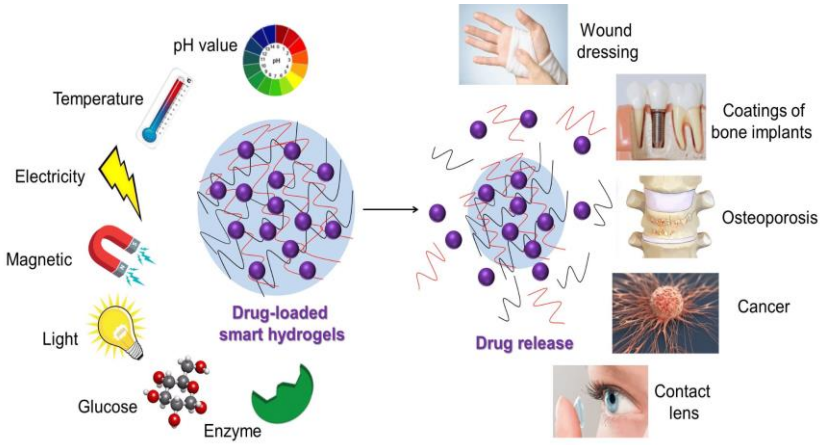

Fig. 1.3: Schematic representation of various drug delivery systems using hydrogels

1.5.1.2. Transdermal drug delivery

Hydrogels have unique properties like high water content, porosity, non-allergenicity, and elasticity which makes them useful for the transdermal drug delivery applications [103]. They are biocompatible and biodegradable, which enables them to be used for transdermal drug delivery applications. In a study, carboxymethyl guar gum and silica-based nanocomposite hydrogel loaded with diclofenac sodium was utilized for the controlled transdermal delivery [104]. In another study, gellan gum and ethylene glycol based hydrogel was synthesized and used for the transdermal delivery of Nebivolol drug and assessed through in-vivo studies[105]. Citric acid cross-linked CMTKG based hydrogel film was also used for transdermal drug delivery applications [72].

Table 1.1: Various biopolymers-based hydrogels used for drug delivery applications

Biopolymer	Co-polymer	Uses	References
Ghatti gum	Poly(acrylic acid-aniline)	For the delivery of amoxicillin trihydrate as colon specific drug.	[84]
Sterculia gum	Alginate and PVP	Delivery of Citicoline drug as brain specific drug carrier agent.	[85]
Tragacanth gum	Sodium alginate Chitosan	Prepared via ionotropic gelation method and used for Insulin delivery.	[86]
Almond gum	Poly(acrylamide)	For controlled delivery of antimicrobial drugs	[87]
Acacia gum	Carbopol Poly(vinyl imidazole)	For the release study of Lidocaine and gentamicin drugs for wound dressing applications.	[88]
Dammar gum	Acrylamide	Used as sustained release carrier of Atenolol drug.	[89]
Guar gum oleate	Poly(methacrylic acid)	Colon targeted delivery of Ibuprofen drug.	[90]
Karaya gum	Starch	Delivery of Paracetamol and Aspirin as oral delivery carrier.	[91]
Moringa gum	Sterculia gum and acrylamide	Release of Levofloxacin drug for wound dressing application.	[92]
Guar gum	Chitosan	Sustained release of Paracetamol drug.	[93]
Tragacanth gum	Poly(vinyl alcohol) and polyvinyl pyrrolidone	Used as wound dressing material via release of Lidocaine drug.	[94]
Xanthan gum	Chitosan	Used as carrier for release of Acyclovir antiviral drug.	[95]
Guar gum	Chitosan and PVP	Release study of Ciprofloxacin hydrochloride drug.	[96]

Biopolymer	Co-polymer	Uses	References
Xanthan gum	Starch	Release of Paracetamol and Aspirin as an oral delivery carrier.	[97]
Guar gum	Acrylamide and acrylamidoglycolic acid	Delivery of 5-Fluorouracil as anticancer drug.	[98]
Acacia gum	N-Vinylpyrrolidone	Used for Moxifloxacin drug release study.	[99]
Sesbania gum	Acrylamide	Sustained release study of 5-Flurouracil drug.	[100]
Carboxymethyl cellulose	Poly (dimethylaminoethyl methacrylate)	Having potential to release Bovine serum albumin protein.	[101]
Carboxymethyl guar gum	Gelatin	Used for Ciprofloxacin release study.	[102]

1.5.1.3. Ocular drug delivery

Hydrogels have less explored in ocular drug delivery applications. However, they are useful for the prolonged drug release and longer retention times of drug administration. Thus, they are used for delivering drugs to the eyes, mainly in contact lenses or ophthalmic inserts. Because they are clear, biocompatible, and can maintain the sustainable release of drugs, they are used for treating eyes conditions like glaucoma, dry eye syndrome, and eye diseases. Hydrogels may be administered more easily due to their stimuli-response ability [106] and combines with the ointments using eye drops to administer topical drugs effectively without the need for regular dosage schedules (as with eye drops). In a study, PVA- based hydrogel was synthesized and used for delivery of Timolol maleate, a drug used to treat glaucoma. This hydrogel showed a longer drug release and better absorption in the eye than regular eye drops [107]. In another study, gaur gum(GG) and xanthan gum (XG) biopolymers were mixed in a poloxamer 407 to develop in-situ gel formation for the delivery of Atropine sulfate drug [108].

1.5.1.4. Drug release through injection

Injectable hydrogels are widely used for biomedical applications because they can be used for minimally invasive drug delivery[16]. These hydrogels can be introduced as a liquid and then hardened, creating a depot for long-term drug release at the desired site. In addition to their distinct hydrophilicity and biocompatibility, hydrogels can also undergo phase transitions from sol (liquid) to gel (solid), forming solid like gel states

that can be used to administer and help encapsulate and release drugs, genes, DNA, proteins, and cells in a sustained and regulated manner. For example, a poly (lactide-co-glycoside) nanoparticles (NPs) loaded gellan gum-based nanocomposite hydrogel was synthesized for the release of Vancomycin drug for the treatment of osteomyelitis [63]. In another study, an injectable hydrogel device based on hydroxyapatite and gelatin was synthesized for delivery of the anti-cancer drug Paclitaxel over a long period [109]. Additionally, a mixture of guar adamantane and poly-β-cyclodextrin was lyophilized to make injectable hydrogel and deliver the bovine serum albumin drug for bone cell growth[110].

1.5.2 Tissue engineering

Hydrogels can act like extracellular matrix (ECM) and help for the growth and multiplication of cells. Therefore, they have become attractive templates for tissue engineering and regenerative medicine[111]. The biocompatibility, swelling ability, and porosity of hydrogels make them a good material for cells to stick together, grow, and change into different types of cells. Due to these properties, they are used for regenerating various tissues like skin, cartilage, and bone. They can provide the essential structural support for the tissue development. In one of the research, PVA-based hydrogels were fabricated for cell growth of bone cells[112]. In another study, chitosan, tamarind gum and nano-hydroxyapatite based nanocomposite hydrogel were fabricated for the bone tissue engineering field[113]. In another study, TKG, gelatin and CMTKG- based hydrogel films were synthesized using poly(ethylene glycol) as a plasticizer[114]. The hydrogel film showed good cell proliferation for human keratinocytes skin cells.

Table 1.2: TKG and CMTKG-based hydrogels used for biomedical applications

Biopolymers	**Monomers/ copolymers**	**Drug released**	**References**
CMTKG	Poly(vinylpyrrolidone)/ poly(acrylamide)	For the sustainable release of Diclofenac sodium drug	[66]
CMTKG	Poly(vinyl alcohol)	For Ciprofloxacin release studies and skin tissue engineering application	[67]
TKG	Poly(methacrylate) cyclodextrin	For the controlled release of Acyclovir drug	[68]
TKG	Chitosan/hydroxy apatite	For bone tissue engineering	[69]
TKG	Poly(methacrylic acid)	For faster release of Paracetamol in an alkaline medium	[70]
CMTKG/TKG	Gelatin	For skin tissue engineering applications	[71]
CMTKG	Citric acid	For controlled release of Moxifloxacin hydrochloride	[72]
CMTKG	Xanthan gum Poly (sodium acrylate)	For burst release of Metformin hydrochloride	[73]
CMTKG	Poly(acrylamide) Polyethylene glycol	For the controlled release of Etophylline drug	[74]
CMTKG	Poly (N-isopropyl acrylamide)	Used for lung cancer therapy	[75]
CMTKG	Poly(sodium acrylate) /poly(ethylene glycol) diacrylate	Used for release of antibiotic Ciprofloxacin drug	[76]
CMTKG/TKG	Gelatin	Used for sustainable release of Ciprofloxacin drug	[77]
CMTKG	Chitosan	For delivery of Aceclofenac drug	[78]
CMTKG	Alginate	For delivery of Acyclovir drug	[79]
TKG	Poly(sodium acrylate)	Used for release study of Doxycycline drug	[80]

1.5.3. Wound healing applications

Any damage or disturbance to live tissue, including skin, mucous membranes, or organs, is referred to as a wound. A wound may develop gradually over time because of underlying medical conditions such diabetes mellitus, venous/arterial insufficiency, or immunologic illness, or it may be the abrupt consequence of acute trauma (mechanical, thermal, or chemical). Among numerous factors, location of wound,

damage process, depth of injury, timing of onset (acute vs. chronic), and wound sterility can all significantly affect appearance of a wound. Hydrogels can keep an area wet, soak up fluids, and help tissue grow back for wound dressing and wound repair. They are biocompatible, flexible, and soak a lot of water, they are used to cover and protect wounds. Hydrogels are known for their high surface area-to-volume ratio, which enables maximum interaction and quick response with the surrounding tissue. They can also be mixed with different therapeutic agents to speed up the healing process. In a study, citric acid cross-linked CMTKG based hydrogel films were synthesized which was used for the wound healing applications[72]. However, nanocomposite hydrogels can also use for the treatment of chronic wounds. In a study, cerium oxide nanoparticles loaded PVA/Chitosan hydrogels were used as a wound dressing agent[115]. In another study, ZnO nanoparticles loaded gum acacia and sodium alginate nanocomposite hydrogels were used as a wound dressing for the fibroblast cells [116]. Thus, different biopolymers-based hydrogels were used for the wound healing applications.

1.5.4. Biosensors

Hydrogels have the ability to stick with proteins like enzymes, antibodies, or nucleic acids. Therefore, they are used to make biosensors and diagnostic tools [81]. Structurally stable hydrogels can offer enough permeability for the target analysis and a biocompatible microenvironment for enzymes to improve the sensitivity and stability of the sensors [129]. In a study, PVA and β-cyclodextrin polymers were used to make a skin patch sensor composed of electrospun hydrogel nanofibers [130]. The outcomes showed that the hydrogel patch sensor has enormous potential for use in clinical application and can assess the concentration of glucose in human serum. In another study, Gum tragacanth (GT) nanoparticles, acrylic acid, and fluorescein O, O′-diacrylate (FlA-DA) as cross- linker were used to make a superabsorbent biosensor hydrogel of extremely sensitive blood glucose. Moreover, the cross-linked network of hydrogels was used to immobilise CdTe quantum dots (QDs) and the glucose oxidise enzyme bioreceptor. Because of the synergistic interaction between QDs and FlA-DA, the produced hydrogel as a biosensor exhibited strong fluorescence. This biosensor successfully produced H_2O_2, a product that quenched the fluorescence light, by oxidising glucose under the guidance of an enzyme [131]. This showed that hydrogels

could be used to make diagnostic tools.

1.5.5. Agricultural

Hydrogels can be used to improve the soil quality, and to control the release of herbicides, micronutrients, and fertilizers for the crop production. Due to high water uptake capacity of hydrogels, they act as carrier for release of micronutrients into the soil [132]. Thus, various biopolymers-based hydrogel formulations were synthesized and utilized in the agricultural applications. Due to their high biocompatibility and biodegradability, they can be employed for growth of different plants through the release of micronutrient. In a study, sodium carboxymethyl cellulose and carrageenan-based hydrogel was developed for release of zinc micronutrient for the growth of wheatgrass plant [133]. In another study, water holding capacity (WHC) of soil was enhanced up to 66 % due to presence of pectin/guar gum/ polyacrylamide/ ZnO composite hydrogels that were cross-linked via gamma radiation[134]. Various inorganic fillers such as clay, nanoparticles, metals and zeolites can be embedded into hydrogels to improve their physiochemical properties. In a study, carboxymethyl cellulose- g- polyacrylamide/ zeolite-based hydrogel was synthesized for sustainable and slow release of zinc micronutrient[135]. In this hydrogel composite, zeolites act as inorganic fillers which would increase the surface area, porosity, and swelling capacity of hydrogels. Other than micronutrient, some metals such as Cu and Mn can also be released into soil using k-carrageenan based hydrogels and it was also found that these micronutrients were released slower in soil than in water[136].

1.5.6. Dye removal applications

Hydrogels can be used as an adsorbent for the removal of toxic dyes from textile and wastewater [137]. The porous sites and different functional groups present on hydrogels enable them to bind and remove the dye molecules effectively [138]. In a study, chitosan-based hydrogels have demonstrated excellent adsorption capacities for various anionic dyes owing to the protonated amino groups that can electrostatically attract the negatively charged dye molecules [139]. Chemical modifications such as cross-linking,

grafting, and composite formation with other polymers or nanomaterials have been employed to enhance the stability, reusability, and adsorption performance of chitosan hydrogels[140]. Alginate-based hydrogels have also been explored for dye removal, leveraging the carboxylate groups that can bind cationic dyes through ion exchange mechanisms[141]. Various derivatives of cellulose such as carboxymethyl cellulose, hydroxypropyl cellulose, and cellulose nanocrystals have been used to prepare hydrogel adsorbents with high surface area, porosity, and functionality [142]. Chemical modifications, such as grafting with acrylic monomers or incorporating metal oxides, have been employed to enhance the adsorption capacity and selectivity of cellulose hydrogels [143,150]. In a study, silver nanoparticles loaded pectin-based nanocomposite hydrogel were effectively used as adsorbent for removal of cationic crystal violet (CV) dye [154]. Moreover, in order to develop an effective adsorbent for the removal of Remazol Brilliant Blue R (RBBR) dye, zinc oxide nanoparticles were incorporated into the structure of a chitosan based composite hydrogel [155]. In a study, a composite hydrogel based on k-carrageenan, acrylamide, and methacrylic acid was synthesized for the removal of methylene blue dye and found that with the addition of 8 % of zeolite, a maximum swelling capacity of 3.481 % was achieved and a total of 99.9% dye removal was observed with 0.4 g L^{-1} hydrogel adsorbent[156]. However, zeolite loaded TKG and CMTKG hydrogel composite have not been explored for dye removal applications.

Table 1.3: Various application of TKG and CMTKG-based composite hydrogels

Polymer	Co-polymer	Applications	Reference
CMTKG	Poly(acrylamide)/silica	removal of methylene blue dye	[117]
CMTKG	Poly(acrylonitrile)	can be used as a diaper	[118]
CMTKG	Poly(methacrylate)	used in agricultural applications	[119]
TKG	Poly(methyl methacrylate)	removal of methylene blue and Congo red dyes	[120]
CMTKG	Zeolite/poly(methacrylate)	removal of cationic crystal violet dye	[121]
CMTKG	Poly(sodium acrylate)	used in zinc micronutrient release studies into soil	[122]
CMTKG	Carboxymethyl starch	used for printing of georgette fabric	[123]
CMTKG	Xanthan gum /methacrylate	used for release of zinc micronutrient for sesame plant	[124]

		growth	
TKG	_____	used to take Cu^{2+} from water bodies	[125]
CMTKG	Sodium Alginate	used as a thickener in cosmetics	[126]
CMTKG	Poly(acrylamide)	used as a flocculant	[127]
TKG	Poly(ethylene oxide-co-propylene oxide)	used as thickener in cosmetics	[128]

1.5.7. Heavy metal ion removal

In addition to organic pollutants, hydrogels are used for the removal of toxic heavy metal ions from aqueous solutions. The chelating ability of functional groups like amines, carboxylic acids, and alcohols present in polymetric networks of hydrogels allows them to bind metal ions strongly [129]. Various biopolymers such as alginate, chitosan, and cellulose are modified to prepare metal-adsorbing hydrogels for industrial wastewater treatment. In a research work, zeolite loaded sodium alginate and PVA - based composite hydrogel was synthesized and utilized as adsorbent for the removal of heavy metal ions[145]. Moreover, alginate-based hydrogels were also used for the removal of heavy metal ions, such as Cu(II), Pb(II), Cd(II), and Hg(II)[146]. In this study, the adsorption efficiency of hydrogels was increased by incorporating functional nanomaterials like graphene oxide, carbon nanotubes, and metal oxide nanoparticles into the alginate matrix[147]. In another study, chitosan-based hydrogels have also demonstrated excellent metal adsorption efficiency, attributed to the amino and hydroxyl groups that can form stable complexes with metal ions[148]. Additionally, chemical modifications such as cross-linking, grafting, and impregnation with metal oxides have been employed to improve the stability, selectivity, and reusability of these hydrogels for metal removal[149]. Also, cellulose-based hydrogels, particularly those derived from carboxymethyl cellulose and cellulose nanocrystals, have been explored for heavy metal adsorption. The abundant hydroxyl and carboxylate groups in these hydrogels can effectively bind metal ions through ion exchange and complexation mechanisms[150]. The use of composite hydrogels for heavy metal removal offers several advantages over conventional adsorbents like activated carbon, such as high adsorption capacity, selectivity, renewability, and the potential for stimuli-responsive behavior[151]. However, there are some challenges associated with use of hydrogels such as improved mechanical stability, regeneration efficiency, and cost-effectiveness for large-scale industrial

applications.

1.5.8. Food industry

Hydrogels were used for several applications in the food industry such as thickeners, stabilizers, and encapsulating agents[19]. Different biopolymers such as starch, pectin, carrageenan, and gelatin are commonly used as food additives to modify texture, consistency, and stability[130]. In a study, starch-based hydrogels were prepared through gelatinization and retrogradation processes and used as thickeners, stabilizers, and gelling agents in various food products, such as sauces, puddings, and baked goods[152]. Additionally, pectin can also form hydrogels in the presence of divalent cations like Ca^{2+} and is commonly used as a gelling agent, stabilizer, and texture modifier in jams, jellies, and fruit-based desserts[153]. Hydrogels have the efficiency to encapsulate bioactive compounds such as vitamins, antioxidants, and probiotics, protecting them during food processing and enabling their controlled release [157, 158]. In addition to their use as food additives and encapsulating agents, hydrogels have also found applications in edible coatings and active packaging materials. Hydrogels can also be incorporated into packaging materials to provide active functions such as oxygen scavenging, antimicrobial activity, and indicators for food quality and safety[159]. They provide several benefits, such as improving food texture, stability, and nutritional value. However, challenges such as ensuring food safety, regulatory compliance, and consumer acceptance must be addressed during the synthesis of hydrogels.

Table 1.4: Various applications of biopolymers-based composite hydrogel

Biopolymer	Other components	Application	References
Tragacanth gum	CdTe quantum dots Glucose oxidase	Analysis of blood sugar concentration	[160]
Karaya gum	SiC nanoparticles and poly(acrylic acid)	Used for removal of rhodamine B and malachite green dye	[161]
Tragacanth gum	Chitosan	Used for buccal application	[162]
Acacia gum	Polyaniline	Used for removal of methylene blue dye	[163]
Dialdehyde guar gum	Chitosan	Used as antibacterial pad for food packing applications	[164]

Biopolymer	Other components	Application	References
Xanthan gum	Cellulose fiber	Used as soil conditioner in forestry applications	[165]
Gum Ghatti	Acrylamide and methacrylic acid	For removal of crystal violet and methylene blue dyes	[166]
Katira gum	Poly (acrylamide-co-N-methyl acrylamide)	For the removal of textile dyes	[167]
Gum arabic	Poly(vinyl alcohol)	For removal of heavy metal ion for wastewater treatment	[168]
Carboxymethyl guar gum	Metabenziporphodimethene and polyacrylamide	For metal ion sensing applications	[169]
Gellan gum	Guar gum	Used for monitoring human motion and act as intelligent wearable device	[170]
Guar gum	Metaborate	Used for oily wastewater treatment	[171]
Arabic gum	Agar and acrylic acid	Used as soil conditioner in farming applications	[172]
Guar gum	Chitosan	Used for energy storage applications	[173]
Xanthan gum	Carboxymethyl cellulose	Used for agricultural applications	[174]
Guar gum	Acrylamide and borax	Used for removal of RB-19 dye	[175]
Acacia gum	Hydroxyapatite	Used for tissue engineering applications	[176]

1.6. Conclusions and future prospective

From the literature survey, it was concluded that there is a need to explore the development of novel hydrogels based on TKG and CMTKG biopolymers used for different applications. There is very limited composite hydrogels based on TKG and CMTKG biopolymers that were used for various applications, mainly for drug delivery and dye removal applications. Thus, TKG and CMTKG biopolymers have been used to synthesize nanocomposite hydrogels due to their specific properties such as high hydrophilicity, gel content, biocompatibility, biodegradability, high drug loading capacity, larger self-life, broad pH tolerance and high mucoadhesivity for the drug delivery applications. Due to these properties, TKG and CMTKG biopolymers-based hydrogels have the potential for several drug delivery methods, including oral, transdermal, ocular, subcutaneous and injectable routes. Moreover, TKG and CMTG

based hydrogel films need to be developed for wound dressing applications. It was also found that zeolite loaded TKG and CMTKG based composite hydrogel have not been reported. Zeolite has ion-exchange properties, therefore, zeolite loaded hydrogel can be used for dye removal and metal ion removal applications. Additionally, there is a need to explore the zeolites loaded hydrogels for different applications such as drug delivery, tissue engineering, agricultural field, dye removal, metal ion removal, textile, and food industry.

1.7. Research Gap

I. Very scarce literature is available on chemical cross linking of synthetic acrylic and methacrylic acid monomers with TKG and CMTKG based hydrogels for drug delivery applications.

II. TKG and CMTKG based nanocomposite hydrogels are very less explored for the drug delivery applications.

III. Zeolites have attracted significant research attention for controlled and targeted drug delivery purposes. However, zeolites have not been used with CMTKG based hydrogels till the date.

IV. There is a need to explore the role of zeolites in TKG and CMTKG based hydrogels for the different applications.

1.8. Research Objectives

I. To synthesize various TKG and CMTKG based composite hydrogels for the various applications.

II. To characterized the composite hydrogels using various techniques such as XRD, FTIR, SEM and TEM.

III. To perform the swelling studies of various synthesized hydrogels in the physiological pH solutions.

IV. To perform the drug loading and release experiments at physiological pH.

V. To study the drug release kinetic modelling using various mathematical models.

VI. To synthesize the zeolite embedded hydrogels and explored for the dye removal applications.

1.9. Overview of thesis

Chapter 1: The first chapter of the thesis provides information about the classifications, synthesis methods, and various applications of composite hydrogels. The primary focus of the literature survey is related to the various applications of TKG and CMTKG biopolymer-based hydrogels.

Chapter 2: focuses on the synthesis and characterization of ZnO NPs embedded CMTKG-based nanocomposite hydrogels for oral delivery of ciprofloxacin drug.

Chapter 3: The synthesis and characterization of Ag NPs embedded TKG-based hydrogels for sustainable doxycycline drug release studies has been discussed.

Chapter 4: This chapter deals with the synthesis and various parameters of CMTKG/PVA/GG hydrogel film for wound healing applications.

Chapter 5 discusses the synthesis of zeolite-embedded CMTKG-based hydrogels for crystal violet dye removal applications.

Chapter 6: This chapter deals with a discussion about the conclusion, social impact, and future prospects of the research that has been done.

References

[1] A. Mahmood, D. Patel, B. Hickson, J. Desrochers, and X. Hu, "Recent Progress in Biopolymer-Based Hydrogel Materials for Biomedical Applications," *Int. J. Mol. Sci.*, vol. 23, no. 3, 2022, doi: 10.3390/ijms23031415.

[2] C. R. Gough, K.Callaway, E.Spencer, K.Leisy, G. Jiang, S.Yang, and X.Hu, "Biopolymer-based filtration materials," *ACS Omega*, vol. 6, no. 18, pp. 11804–11812, 2021, doi: 10.1021/acsomega.1c00791.

[3] H. Tabani, M. Alexovič, J. Sabo, and M. Ramos Payán, "An overview on the recent applications of agarose as a green biopolymer in micro-extraction-based sample preparation techniques," *Talanta*, vol. 224, p. 121892, 2021, doi: 10.1016/j.talanta.2020.121892.

[4] C.M. Hassan, and N.A Peppas, "Structure and applications of poly (vinyl alcohol) hydrogels produced by conventional cross-linking or by freezing/thawing methods." Biopolymers, PVA Hydrogels, *Anionic Polymerization Nanocomposites,* 2000, 153-179.

[5] Z. Zhang, R. Zhang, L. Zou, L. Chen, Y. Ahmed, W. Al Bishri, K. Balamash, and D.J. McClements, "Encapsulation of curcumin in polysaccharide-based hydrogel beads: Impact of bead type on lipid digestion and curcumin bioaccessibility," Food *Hydrocolloids, 2016,* 58, 160-170.

[6] E. Caló, V.V. Khutoryanskiy, "Biomedical applications of hydrogels: A review of patents and commercial products," *European Polymer Journal,* 2015, 65, 252-267.

[7] T. R. Hoare, and D.S. Kohane, "Hydrogels in drug delivery: Progress and challenges," *Polymer,* 2008, 49(8), 1993-2007.

[8] J.P. Gong, Y. Katsuyama, T. Kurokawa, and Y. Osada, "Double-network hydrogels with extremely high mechanical strength," *Advanced Materials,* 2003, 15(14), 1155-1158.

[9] A.S. Hoffman, "Hydrogels for biomedical applications," Advanced *Drug Delivery Reviews,* 2012, 64, 18-23.

[10] M. K. Ashthiani, M. Zandi, P. Shokrollahi, M. Ehsani, H. Baharvand, "Surface

modification of poly (2-hydroxyethyl methacrylate) hydrogel for contact lens application," *Polym. Adv. T echnol.,* 1-7, doi: 10.1002/pat.4233.

[11] I. Meshram, V. Kanade, N. Nandanwar, and P. Ingle, "Super-Absorbent Polymer: A Review on the Characteristics and Application," *Int. J. Adv. Res. Chem. Sci.*, vol. 7, no. 5, pp. 8–21, doi: 10.20431/2349-0403.0705002.

[12] M.R. Guilherme, A.V. Reis, M. Takaki, A.F. Rubira, and E.C. Muniz, "Synthesis of a novel superabsorbent hydrogel by electron beam radiation based on PEG/chitosan/attapulgite compounds. Nuclear Instruments and Methods in Physics Research Section B: Beam Interactions with Materials and Atoms, 2005, 236(1-4), 391-395.

[13] C. Gao, G. Liu, P. Xue, M. Liu, and L. Chen, "Preparation and properties of a pH-sensitive semi-IPN hydrogel based on Konjac glucomannan and sodium alginate," *Carbohydrate Polymers,* 2009, 77(2), 292-298.

[14] K.Y. Lee, and D.J. Mooney, " Hydrogels for tissue engineering," *Chemical Reviews,* 2001, 101(7), 1869-1880.

[15] J.S. Boateng, K.H. Matthews, H.N. Stevens, and G.M. Eccleston, "Wound healing dressings and drug delivery systems: A review," Journal *of Pharmaceutical Sciences,* 2008 97(8), 2892-2923.

[16] S. Pacelli, F. Acosta, A.R. Chakravarti, S.G. Samanta, J. Whitlow, S. Modaresi, and A. Paul, "Nanomedicine for drug delivery and therapy," *Advanced Drug Delivery Reviews,* 2016, 130, 108-122.

[17] S. Kumaravel, and K. Thirumalai, "Hydrogels for environment management: Formation, characteristics, and applications. In S. Thirumalai & S. Muthuyah (Eds.)," *Advances in Polymer Materials and Technology*, 2016, 21-48.

[18] G. Crini, and P.M. Badot, "Application of chitosan, a natural amino polysaccharide, for dye removal from aqueous solutions by adsorption processes using batch studies: A review of recent literature," *Progress in Polymer Science,* 2008, 33(4), 399-447.

[19] D. Saha, and S. Bhattacharya, "Hydrocolloids as thickening and gelling agents

in food: A critical review," *Journal of Food Science and Technology,* 2010, 47(6), 587-597.

[20] R. Masteikova, Z. Chalupova, and Z. Sklutalka, "Stimuli-sensitive hydrogels in controlled and sustained drug delivery," *Medicina,* 2003, 39(2), 19-24.

[21] S. Dai, P. Ravi, and K.C. Tam, "pH-responsive polymers: Synthesis, properties and applications," *Soft Matter,*2008, 4(3), 435-449.

[22] Y.H. Kuan, R. Bhat, A. Patras, and A.A. Karim, "Radiation processing of food proteins: A review on the recent developments," *Trends in Food Science & Technology,* 2016, 27(2), 225-238.

[23] W.E. Hennink, and C.F. Van Nostrum, "Novel cross-linking methods to design hydrogels," *Advanced Drug Delivery Reviews,* 2002, 54(1), 13-36.

[24] A.D. Augst, J.H. Kong, and J.D. Mooney, "Alginate hydrogels as biomaterials." *Macromolecular Bioscience,* 2006, 6(8), 623-633.

[25] N. Bhattarai, J. Gunn, and M. Zhang, "Chitosan-based hydrogels for controlled, localized drug delivery," 2010, Advanced *Drug Delivery Reviews*, 62(1), 83-99.

[26] X. Ye, X. Li, Y. Shen, G. Chang, J. Yang, and Z. Gu, "Self-healing pH-sensitive cytosine- and guanosine-modified hyaluronic acid hydrogels via hydrogen bonding," *Polymer (Guildf).*, vol. 108, pp. 348–360, 2017, doi: 10.1016/j.polymer.2016.11.063.

[27] C. Chang, L. Zhang, J. Zhou, L. Zhang, and J.F. Kennedy, "Structure and properties of hydrogels prepared from cellulose in NaOH/urea aqueous solutions," *Carbohydrate Polymers,* 2010, 82(1), 122-127.

[28] M. F. Akhtar, M. Hanif, N.M. Ranjha, "A review of Methods of synthesis of hydrogels," *Saudi Pharmaceutical Journal,* 2016, 24, 554-559.

[29] H. Tsuji, "Poly(lactide) stereocomplexes: Formation, structure, properties, degradation, and applications," *Macromol. Biosci.*, vol. 5, no. 7, pp. 569–597, 2005, doi: 10.1002/mabi.200500062.

[30] H. K. Ju, S. Y. Kim, and Y. M. Lee, "pH/temperature-responsive behaviors of semi-IPN and comb-type graft hydrogels composed of alginate and poly(N-

isopropylacrylamide)," *Polymer (Guildf).*, vol. 42, no. 16, pp. 6851–6857, 2001, doi: 10.1016/S0032-3861(01)00143-4.

[31] A.S. Hoffman, "Hydrogels for biomedical applications, "*Advanced Drug Delivery Reviews,* 2002, 54(1), 3-12.

[32] K.Y. Lee, and D.J. Mooney, "Alginate: Properties and biomedical applications," Progress in Polymer Science, 2012, 37(1), 106-126.

[33] M. Bercea, and P. Navard, "Polysaccharides in phenolic foams–Cellulose, xylan and starch," *Journal of Applied Polymer Science,* 2000, 78(3), 624-642.

[34] S.O. Sarrigiannidis, J.M. Rey, O. Dobre, Gonzalez-García, M.J. Dalby, M. Salmeron-Sanchez, "A tough act to follow: collagen hydrogel modifications to improve mechanical and growth factor loading capabilities," *Material Today Bio.*, 2021,10, 100098.

[35] G. Sennakesavan, M. Mostakhdemin, L. K. Dkhar, A. Seyfoddin, and S. J. Fatihhi, "Acrylic acid/acrylamide based hydrogels and its properties - A review," *Polym. Degrad. Stab.*, vol. 180, p. 109308, 2020, doi: 10.1016/j.polymdegradstab.2020.109308.

[36] N. Ijaz *et al.*, "In vitro and toxicological assessment of dexamethasone sodium phosphate loaded pH sensitive Pectin-g-poly(AA)/PVP semi interpenetrating network," *Mater. Today Commun.*, vol. 25, no. June, p. 101325, 2020, doi: 10.1016/j.mtcomm.2020.101325.

[37] H.Y. Zhu, Y.Q. Fu, R. Jiang, J.Yao, L. Xiao, and G.M. Zeng, "Optimization of copper(II) adsorption onto novel magnetic calcium alginate/maghemite hydrogel beads using response surface methodology," *Industrial & Engineering Chemistry Research,* 2016, 53(10), 4059-4066.

[38] J. Shi, N.M. Alves, and J.F. Mano, "Drug release of pH/temperature-responsive calcium alginate/poly(N-isopropylacrylamide) semi-IPN beads," *Macromolecular Bioscience,* 2011, 6(5), 358-363.

[39] J. Berger, M. Reist, M.J. Mayer, O. Felt, A. N. Peppas, and R. Gurny, "Structure and interactions in covalently and ionically cross-linked chitosan hydrogels for

biomedical applications," *European Journal of Pharmaceutics and Biopharmaceutics,* 2004, 57(1), 19-34.

[40] J.L. Drury, D.J. Mooney, "Hydrogels for tissue engineering: Scaffold design variables and applications," *Biomaterials,* 2003, 24(24), 4337-4351.

[41] P.K. Dutta, J. Dutta, and V.S. Tripathi, "Chitin and chitosan: Chemistry, properties, and applications," *Journal of Scientific and Industrial Research,* 2009, 63(1), 20-31.

[42] M. J. Mc Gann, C. L. Higginbotham, L. M. Geever, and M. J. D. Nugent, "The synthesis of novel pH-sensitive poly(vinyl alcohol) composite hydrogels using a freeze/thaw process for biomedical applications," Int. J. Pharm., vol. 372, no. 1–2, pp. 154–161, 2009, doi: 10.1016/j.ijpharm.2009.01.008.

[43] X. Qi, X. Hu, W. Wei, H. Yu, J. Li, J. Zhang, W. Dong, "Investigation of Salecan/poly(vinyl alcohol) hydrogels prepared by freeze/thaw method," *carbohydrate* polymer, vol. 118, 2015, http://dx.doi.org/doi:10.1016/ j.carbpol.2014.11.021.

[44] M. J. Ansari , R. R. Rajendran, S. Mohanto, U. Agarwal , K. Panda. K. Dhotre, R. Manne, A. Deepak, A. Zafar, M. Yasir, and S. Pramanik, "Poly(N-isopropylacrylamide)-Based Hydrogels for Biomedical Applications: A Review of the State-of-the-Art," *Gels*, vol. 8, no. 7, 2022, doi: 10.3390/gels8070454.

[45] G. Bonacucina, M. Cespi, G. Mencarelli, G. Giorgioni, and G. F. Palmieri, "Thermosensitive self-assembling block copolymers as drug delivery systems," *Polymers (Basel).*, vol. 3, no. 2, pp. 779–811, 2011, doi: 10.3390/ polym3020779.

[46] F. Hong , P. Qiu , Y. Wang , P. Ren , J. Liu , J. Zhao , and D. Gou, "Chitosan-based hydrogels: From preparation to applications, a review," *Food Chem. X*, vol. 21, no. 8326, p. 101095, 2024, doi: 10.1016/j.fochx.2023.101095.

[47] A. Bigi, G. Cojazzi, S. Panzavolta, K. Rubini, and N. Roveri, "Mechanical and thermal properties of gelatin films at different degrees of glutaraldehyde cross-linking. Biomaterials," 2002, 22(8), 763-768.

[49] Y. Lee, J. W. Bae, J. W. Lee, W. Suh, and K. D. Park, "Enzyme-catalyzed in situ forming gelatin hydrogels as bioactive wound dressings: Effects of

fibroblast delivery on wound healing efficacy," *J. Mater. Chem. B*, vol. 2, no. 44, pp. 7712–7718, 2014, doi: 10.1039/c4tb01111b.

[50] A. Ranga, M. P. Lutolf, J. Hilborn, and D. A. Ossipov, "Hyaluronic Acid Hydrogels Formed in Situ by Transglutaminase-Catalyzed Reaction," *Biomacromolecules*, vol. 17, no. 5, pp. 1553–1560, 2016, doi: 10.1021/acs.biomac.5b01587.

[51] E. H. Kim, S. Lim, T. E. Kim, I. O. Jeon, and Y. S. Choi, "Preparation of in situ Injectable Chitosan/Gelatin Hydrogel Using an Acid-tolerant Tyrosinase," *Biotechnol. Bioprocess Eng.*, vol. 23, no. 5, pp. 500–506, 2018, doi: 10.1007/s12257-018-0315-4.

[52] R. Gheorghita, L. Anchidin-Norocel, R. Filip, M. Dimian, and M. Covasa, "Applications of biopolymers for drugs and probiotics delivery," *Polymers (Basel).*, vol. 13, no. 16, 2021, doi: 10.3390/polym13162729.

[53] T. G. Barclay, C. M. Day, N. Petrovsky, and S. Garg, "Review of polysaccharide particle-based functional drug delivery," *Carbohydr. Polym.*, vol. 221, pp. 94–112, 2019, doi: 10.1016/j.carbpol.2019.05.067.

[54] Y. Li, J. Rodrigues, and H. Tomás, "Injectable and biodegradable hydrogels: Gelation, biodegradation and biomedical applications," *Chemical Society Reviews,* 2012, 41(6), 2193-2221.

[55] S . Dhawan, A.K. Singla, and V.R. Sinha, "Evaluation of mucoadhesive properties of chitosan microspheres prepared by different methods," *AAPS PharmSciTech,* 2004 5(4), 67-76.

[56] V. Khanna, T.V. Ranganathan, C. Pande, D.N. Yadav, and P.A. Williams, "A new galactomannan from Tamarind kernel," Journal of Macromolecular Science, Part A: Pure and Applied Chemistry, 1996, 33(10), 1605-1615.

[57] P. Ilgin, H. Ozay, and O. Ozay, "Synthesis and characterization of pH responsive alginate based-hydrogels as oral drug delivery carrier," *J. Polym. Res.*, vol. 27, no. 9, 2020, doi: 10.1007/s10965-020-02231-0.

[58] S. Das and U. Subuddhi, "PH-Responsive guar gum hydrogels for controlled delivery of dexamethasone to the intestine," *Int. J. Biol. Macromol.*, vol. 79, pp.

856–863, 2015, doi: 10.1016/j.ijbiomac.2015.06.008.

[59] V. Sharma *et al.*, "Preparation and characterization of novel tamarind gum-based hydrogels for antimicrobial drug delivery applications," *Chem. Pap.*, vol. 72, no. 8, pp. 2101–2113, 2018, doi: 10.1007/s11696-018-0414-x.

[60] B. Niu *et al.*, "In vitro and in vivo release of diclofenac sodium-loaded sodium alginate/carboxymethyl chitosan-ZnO hydrogel beads," *Int. J. Biol. Macromol.*, vol. 141, pp. 1191–1198, 2019, doi: 10.1016/j.ijbiomac. 2019.09.059.

[61] K. Prusty and S. K. Swain, "Nano silver decorated polyacrylamide/dextran nanohydrogels hybrid composites for drug delivery applications," *Mater. Sci. Eng. C*, vol. 85, no. June 2017, pp. 130–141, 2018, doi: 10.1016/ j.msec.2017.11.028.

[62] G. Kaur, S. Jain, and A. K. Tiwary, "Chitosan-carboxymethyl tamarind kernel powder interpolymer complexation: Investigations for colon drug delivery," *Sci. Pharm.*, vol. 78, no. 1, pp. 57–78, 2010, doi: 10.3797/scipharm.0908-10.

[63] A. Giri, T. Ghosh, A. B. Panda, S. Pal, and A. Bandyopdhyay, "Tailoring carboxymethyl guargum hydrogel with nanosilica for sustained transdermal release of diclofenac sodium," *Carbohydr. Polym.*, vol. 87, no. 2, pp. 1532–1538, 2012, doi: 10.1016/j.carbpol.2011.09.050.

[64] S. Kumar, S.L. Harikumar, and T.K. Chaki, "Carboxymethyl tamarind gum-based nanocarriers for sustained delivery of doxorubicin," *Drug Development and Industrial Pharmacy*, 2013. 39(8), 1240-1249.

[65] S. Jain, N. Sharma, B. Singh, N. Bhandari, and A.C. Rana, "Carboxymethylated tamarind gum: A novel excipient for sustained release of hydrophobic drug," *International Journal of Biological Macromolecules*, 2012, 51(5), 841-847.

[66] P. Meena, P. Singh, S.G. Warkar, "Development and assessment of carboxymethyl tamarind kernel gum- based pH-responsive hydrogel for release of diclofenac sodium," *European Polymer Journal*, 2023, 197, 112340.

[67] I. Yadav,1, V.S. S. Rathnama, Y. Yogalakshmia, S. Chakraborty, I. Banerjee, A. Anis, K. Pal, "Synthesis and characterization of polyvinyl alcohol-carboxymethyl tamarind gum based composite films," *Carbohydrate Polymers*,

2017, 165, 159–168.

[68] K. Shafiq, A. Mahmood, M. M. S. Bekhit, R. M. Sarfraz, A. S. Algarni, E. I. Taha, A. A. Mansour, S. A. Zahrani, and Y. Benguerba, "Development and Optimization of Tamarind Gum-β-Cyclodextrin-g-Poly (Methacrylate) pH-Responsive Hydrogels for Sustained Delivery of Acyclovir," *Pharmaceuticals,* 2022, 15, 1527. https://doi.org/10.3390/ ph15121527.

[69] M. Shakir, I. Zia, A. Rehman, and R. Ullah, "Fabrication and characterization of nanoengineered biocompatible n-HA/Chitosan-Tamarind seed polysaccharide: Bio-inspired nanocomposites for bone tissue engineering," *Biological Macromolecules,* 2018, DOI: https://doi.org/10.1016/j.ijbiomac. 2018.01.035.

[70] A. Saha, K. Mukherjee, B. Ghosh, T. K. Giri, "Grafted tamarind kernel polysaccharide based Al^{3+} cross-linked hydrogel matrices for sustained release of drug in the gastrointestinal milieu," *Pharmaceutical Science Advances, 2024,* 100022.

[71] G. S. Shaw, D. Biswal, B. Anupriya, I. Banerjee, K. Pramanik, A. Anis & Kunal Pal, "Preparation, Characterization and Assessment of the Novel Gelatin-Tamarind Gum/ Carboxymethyl Tamarind Gum Based Phase-Separated Films for Skin Tissue Engineering Applications," *Polymer-Plastics Technology and Engineering,* DOI: 10.1080/03602559.2016.1185621.

[72] K. K. Mali, S. C. Dhawale, R. J. Dias, "Synthesis and characterization of hydrogel films of carboxymethyl tamarind gum using citric acid," *International Journal of Biological Macromolecules,* 2017, 105, 463–470.

[73] Tushar, Y. Saraswat, P. Meena, S.G. Warkar, "Synthesis and characterization of novel xanthan gum-based pH-sensitive hydrogel for metformin hydrochloride release," *Colloid Polym Sci* 301, 1147–1158 (2023). https://doi.org/10.1007/s00396-023-05135-9.

[74] Kajal, R. Kumar, P. Meena, S.G. Warkar, "Development and characterization of pH-responsive CMTKG/PAM/PEG hydrogel for oral administration of etophylline," *colloid and polymer science,* 2023, 301, 1313-1323.

[75] H. Bera Y.F. Abbasi , L. Lee Ping, D. Marbaniang , B. Mazumder, P. Kumar, P. Tambe, V. Gajbhiye, D. Cun, M. Yang, "Erlotinib-loaded carboxymethyl tamarind gum semi-interpenetrating nanocomposites," *Carbohydrate Polymers*, 2019.

[76] I. Rani, A. Kumar, S. G. Warkar, "Nano ZnO embedded poly (ethylene glycol) diacrylate cross-linked carboxymethyl tamarind kernel gum (CMTKG)/poly (sodium acrylate) composite hydrogels for oral delivery of ciprofloxacin drug and their antibacterial properties," *Materials Today Communications,* 2023, 35, 105635.

[77] G. S. Shaw, D. Biswal, B. Anupriya, I. Banerjee, K. Pramanik, A. Anis, and K. Pal (2016), "Preparation, Characterization and Assessment of the Novel Gelatin-Tamarind Gum/ Carboxymethyl Tamarind Gum Based Phase-Separated Films for Skin Tissue Engineering Applications," *Polymer-Plastics Technology and Engineering,* 2016, DOI: 10.1080/03602559.2016.1185621.

[78] K. K. Mali, S.C Dharwale, R. J Dias, V. D. Havaldar, P. R. Kavitake, "Interpenetrating networks of carboxymethyl tamarind gum and chitosan for sustained delivery of aceclofenac," *Marmara Pharmaceutical Journal,* 2017, 771-782, DOI: 10.12991/mpj.2017.20.

[79] S. Jana, R. Sharma, S. Maiti, K. K. Sen, "Interpenetrating hydrogels of O-carboxymethyl Tamarind gum and alginate for monitoring the delivery of acyclovir," *International Journal of Biological Macromolecules*, 2016, 92, 1034–1039.

[80] I. Rani, S. G. Warkar, and A. Kumar, "A Silver Nanoparticle-Embedded Tamarind Kernel Gum/Poly (Sodium Acrylate) Nanocomposite for Sustainable Release of Doxycycline," *ChemistrySelect*, vol. 9, no. 14, p. 2024, 2024, doi: 10.1002/slct.202400168.

[81] K. Mali, S. Dhawale, R. Dias, and V. Ghorpade, "Delivery of drugs using tamarind gum and modified tamarind gum: A review," *Bull. Fac. Pharmacy, Cairo Univ.*, vol. 57, no. 1, pp. 1–24, 2019, doi: 10.21608/bfpc.2019.47260.

[82] Khushbu and S. G. Warkar, "Carboxymethyl Tamarind Kernel Gum based Controlled Drug Delivery Excipients: A Review," *J. Eng. Res.*, vol. 10, pp. 27–40, 2022, doi: 10.36909/jer.ICAPIE.15061.

[83] G. Ponchel, F. Touchard, D. Wouessidjewe, D. Duchêne, and N. A. Peppas, "Bioadhesive analysis of controlled-release systems. III. Bioadhesive and release behavior of metronidazole-containing poly(acrylic acid)-hydroxypropyl methylcellulose systems," *Int. J. Pharm.*, vol. 38, no. 1–3, pp. 65–70, 1987, doi: 10.1016/0378-5173(87)90098-6.

[84] K. Sharma, V. Kumar, B. Chaudhary, B. S. Kaith, S. Kalia, and H. C. Swart, "Application of biodegradable superabsorbent hydrogel composite based on Gum ghatti-co-poly(acrylic acid-aniline) for controlled drug delivery," *Polym. Degrad. Stab.*, vol. 124, pp. 101–111, 2016, doi: 10.1016/j.polymdegradstab. 2015.12.021.

[85] B. Singh, A. Kumar, and Rohit, "Synthesis and characterization of alginate and sterculia gum based hydrogel for brain drug delivery applications," *Int. J. Biol. Macromol.*, vol. 148, pp. 248–257, 2020, doi: 10.1016/j.ijbiomac.2020.01.147.

[86] S. Cikrikci, B. Mert, and M. H. Oztop, "Development of pH Sensitive Alginate/Gum Tragacanth Based Hydrogels for Oral Insulin Delivery," *J. Agric. Food Chem.*, vol. 66, no. 44, pp. 11784–11796, 2018, doi: 10.1021/acs .jafc.8b02525.

[87] I. Syed Ahamed Hussain and V. Jaisankar, "An eco-friendly synthesis, characterization and antibacterial applications of novel almond gum – poly(acrylamide) based hydrogel silver nanocomposite," *Polym. Test.*, vol. 62, pp. 154–161, 2017, doi: 10.1016/j.polymertesting.2017.06.021.

[88] B. Singh and A. Dhiman, "Design of Acacia Gum-Carbopol-Cross-Linked-Polyvinylimidazole Hydrogel Wound Dressings for Antibiotic/Anesthetic Drug Delivery," *Ind. Eng. Chem. Res.*, vol. 55, no. 34, pp. 9176–9188, 2016, doi: 10.1021/acs.iecr.6b01963.

[89] P. Sharma, H. Mittal, R. Jindal, D. Jindal, and S. M. Alhassan, "Sustained delivery of atenolol drug using gum dammar crosslinked polyacrylamide and zirconium based biodegradable hydrogel composites," *Colloids Surfaces A Physicochem. Eng. Asp.*, vol. 562, pp. 136–145, 2019, doi: 10.1016/j.colsurfa. 2018.11.039.

[90] D. S. Seeli and M. Prabaharan, "Guar gum oleate-graft-poly (methacrylic acid) hydrogel as a colon-specific controlled drug delivery carrier," *Carbohydr. Polym.*, vol. 158, pp. 51–57, 2017.

[91] S. Sethi, B. S. Kaith, M. Kaur, N. Sharma, and S. Khullar, "Study of a cross-linked hydrogel of Karaya gum and Starch as a controlled drug delivery system," *J. Biomater. Sci. Polym. Ed.*, vol. 30, no. 18, pp. 1687–1708, 2019, doi: 10.1080/09205063.2019.1659710.

[92] B. Singh, V. Sharma, and R. and A. Kumar, "Designing moringa gum-sterculia gum-polyacrylamide hydrogel wound dressings for drug delivery applications," *Carbohydr. Polym. Technol. Appl.*, vol. 2, no. February, p. 100062, 2021, doi: 10.1016/j.carpta.2021.100062.

[93]A.J.Sami, M. Khalid, T. Jamil, S. Aftab, S.A.Mangat, A.R. Shakoori, S. Iqbal,"Formu lation of novel chitosan guargum based hydrogels for sustained drug release of paracetamol," *Int. J. Biol. Macromol.*, vol. 108, pp. 324–332, 2018, doi: 10.1016/j.ijbiomac.2017.12.008.

[94] B. Singh, L. Varshney, S. Francis, and Rajneesh, "Synthesis and characterization of tragacanth gum based hydrogels by radiation method for use in wound dressing application," *Radiat. Phys. Chem.*, vol. 135, no. January, pp. 94–105, 2017, doi: 10.1016/j.radphyschem.2017.01.044.

[95] N. S.Malik, M. Ahmad, M. U. Minhas, R. Tulain , K. Barkat , I. Khalid and Q. Khalid, "Chitosan/Xanthan Gum Based Hydrogels as Potential Carrier for an Antiviral Drug: Fabrication, Characterization, and Safety Evaluation," *Front. Chem.*, vol. 8, no. February, pp. 1–16, 2020, doi: 10.3389/fchem.2020.00050.

[96] Z. H. Ghauri , A. Islam, M. A. Qadir , N. Gull , B. Haider , R. U. Khan, and Tabinda Riaz, "Development and evaluation of pH - sensitive biodegradable ternary blended hydrogel films (chitosan / guar gum / PVP) for drug delivery application," *Sci. Rep.*, pp. 1–10, 2021, doi: 10.1038/s41598-021-00452-x.

[97] S. Sethi, Saruchi, B. S. Kaith, M. Kaur, N. Sharma, and V. Kumar, "Cross-linked xanthan gum–starch hydrogels as promising materials for controlled drug delivery," *Cellulose*, vol. 27, no. 8, pp. 4565–4589, 2020, doi: 10.1007/s10570-020-03082-0.

[98] G. Viswanatha Reddy, N. Sivagangi Reddy, K. Nagaraja, and K. S. V. K. Rao, "Synthesis of pH responsive hydrogel matrices from guar gum and poly(acrylamide-co-acrylamidoglycolicacid) for anti-cancer drug delivery," *J.*

Appl. Pharm. Sci., vol. 8, no. 8, pp. 084–091, 2018, doi: 10.7324/JAPS. 2018.8813.

[99] B. Singh, S. Sharma, and A. Dhiman, "Acacia gum polysaccharide based hydrogel wound dressings: Synthesis, characterization, drug delivery and biomedical properties," *Carbohydr. Polym.*, vol. 165, pp. 294–303, 2017, doi: 10.1016/j.carbpol.2017.02.039.

[100] P. Pal, J. P. Pandey, and G. Sen, "Sesbania gum based hydrogel as platform for sustained drug delivery: An 'in vitro' study of 5-Fu release," *Int. J. Biol. Macromol.*, vol. 113, pp. 1116–1124, 2018, doi: 10.1016/j.ijbiomac.2018.02.143.

[101] A. Salama, M. El-Sakhawy, and S. Kamel, "Carboxymethyl cellulose based hybrid material for sustained release of protein drugs," *Int. J. Biol. Macromol.*, vol. 93, pp. 1647–1652, 2016, doi: 10.1016/j.ijbiomac.2016.04.029.

[102] S.K. Ghosh, A. Das , A.Basu, A. Halder, S. Das, S.Basu, M. F.Abdullah, A. Mukherjee, and S. Kundu, "Semi-interpenetrating hydrogels from carboxymethyl guar gum and gelatin for ciprofloxacin sustained release," *Int. J. Biol. Macromol.*, vol. 120, pp. 1823–1833, 2018, doi: 10.1016/j.ijbiomac. 2018.09.212.

[103] P. Gupta, K. Vermani, and S. Garg, "Hydrogels: From controlled release to pH-responsive drug delivery," *Drug Discovery Today,* 2002, 7(10), 569-579.

[104] A. Giri, T. Ghosh, A. B. Panda, S. Pal, and A. Bandyopdhyay, "Tailoring carboxymethyl guargum hydrogel with nanosilica for sustained transdermal release of diclofenac sodium," *Carbohydr. Polym.*, vol. 87, no. 2, pp. 1532–1538, 2012, doi: 10.1016/j.carbpol.2011.09.050.

[105] A. B. Nair, J. Shah, B. M. Aljaeid, B. E. Al-Dhubiab, and S. Jacob, "Gellan gum-based hydrogel for the transdermal delivery of nebivolol: Optimization and evaluation," *Polymers (Basel).*, vol. 11, no. 10, pp. 1–17, 2019, doi: 10.3390/polym11101699.

[106] D. Gulsen, A. Chauhan, "Ophthalmic drug delivery through contact lenses," *Investigative Ophthalmology & Visual Science*, 2005, 46(7), 2342-2347.

[107] H. Gupta, S. Jain, R. Mathur, P. Mishra, A. K. Mishra, and S.P. Vyas, "Sustained ocular drug delivery from a temperature and pH triggered novel in situ gel

system," *Drug Delivery*, 2007, 14(8), 507-515.

[108] M. Bhowmik , P. Kumari, G. Sarkar, M.K.Bain,B. Bhowmick, M.M. Mollick , D. Mondal, D. Maity, D. Rana , D. Bhattacharjee ,and D. Chattopadhyay, "Effect of xanthan gum and guar gum on in situ gelling ophthalmic drug delivery system based on poloxamer-407," *Int. J. Biol. Macromol.*, vol. 62, pp. 117–123, 2013, doi: 10.1016/j.ijbiomac.2013.08.024.

[109] M. Y. Wu, I. F. Kao, C. Y. Fu, and S. K. Yen, "Effects of Adding Chitosan on Drug Entrapment Efficiency and Release Duration for Paclitaxel-Loaded Hydroxyapatite—Gelatin Composite Microspheres," *Pharmaceutics*, vol. 15, no. 8, 2023, doi: 10.3390/pharmaceutics15082025.

[110] H. Poudel, A. B. RanguMagar, P. Singh , A. Oluremi, N. Ali, F. Watanabe, J. B.Mpouma, J. W. Kim , and A. Ghosh, "Guar-Based Injectable Hydrogel for Drug Delivery and In Vitro Bone Cell Growth," *Bioengineering*, vol. 10, no. 9, 2023, doi: 0.3390/bioengineering10091088.

[111] N. Annabi, A. Tamayol, J.A. Utiuzian, M. Akbari, S.M. Borhan, J.E. Kocur, and A. Khademhosseini, "Rational design and applications of hydrogels in regenerative medicine, "*Advanced Materials*, 2014, 26(1), 85-124.

[112] A. P.Thankam, Q.A. Anbaky, Z.A.Karakooly, A.B.Rangumagar, B.P.Chhetri, N.Ali, and A.Ghosh, "Fabrication and characterization of hydroxypropyl guar-poly (vinyl alcohol)-nano hydroxyapatite composite hydrogels for bone tissue engineering," *J. Biomater. Sci. Polym. Ed.*, vol. 29, no. 17, pp. 2083–2105, 2018, doi: 10.1080/09205063.2018.1494437.

[113] M. Shakir, I. Zia, A. Rehman, and R. Ullah, "Fabrication and characterization of nanoengineered biocompatible n-HA/chitosan-tamarind seed polysaccharide: Bio-inspired nanocomposites for bone tissue engineering," *Int. J. Biol. Macromol.*, vol. 111, pp. 903–916, 2018, doi: 10.1016/ j.ijbiomac.2018.01.035.

[114] G. S. Shaw, D.Biswal, B.Anupriya, I.Banerjee, K.Pramanik, A.Anis, and K.Pal, "Preparation, Characterization and Assessment of the Novel Gelatin–tamarind Gum/Carboxymethyl Tamarind Gum-Based Phase-Separated Films for Skin Tissue Engineering Applications," *Polym. - Plast. Technol. Eng.*, vol. 56, no. 2, pp. 141–152, 2017, doi: 10.1080/03602559.2016.1185621.

[115] K. Kalantari, E. Mostafavi, B. Saleh, P. Soltantabar, and T. J. Webster, "Chitosan/PVA hydrogels incorporated with green synthesized cerium oxide

nanoparticles for wound healing applications," *Eur. Polym. J.*, vol. 134, no. June, p. 109853, 2020, doi: 10.1016/j.eurpolymj.2020.109853.

[116] R. Raguvaran, B.K. Manuja, M. Chopra, R. Thakur, T. Anand, A. Kalia, and A. Manuja, "Sodium alginate and gum acacia hydrogels of ZnO nanoparticles show wound healing effect on fibroblast cells," *Int. J. Biol. Macromol.*, vol. 96, pp. 185–191, 2017, doi: 10.1016/j.ijbiomac.2016.12.009.

[117] S. Pal, S. Ghorai, C. Das, S. Samrat, A. Ghosh, and A. B. Panda, "Carboxymethyl tamarind-g-poly(acrylamide)/silica: A high performance hybrid nanocomposite for adsorption of methylene blue dye," *Ind. Eng. Chem. Res.*, vol. 51, no. 48, pp. 15546–15556, 2012, doi: 10.1021/ie301134a.

[118] Meenkashi, M. Ahuja, and P. Verma, "MW-assisted synthesis of carboxymethyl tamarind kernel polysaccharide-g- polyacrylonitrile: Optimization and characterization," *Carbohydr. Polym.*, vol. 113, pp. 532–538, 2014, doi: 10.1016/j.carbpol.2014.07.041.

[119] R. Malik, S. G. Warkar, and R. Saxena, "Carboxy-methyl tamarind kernel gum based bio-hydrogel for sustainable agronomy," *Mater. Today Commun.*, vol. 35, no. January, p. 105473, 2023, doi: 10.1016/j.mtcomm.2023.105473.

[120] A. Pal and S. Pal, "Amphiphilic copolymer derived from tamarind gum and poly (methyl methacrylate) via ATRP towards selective removal of toxic dyes," *Carbohydr. Polym.*, vol. 160, pp. 1–8, 2017, doi: 10.1016/j.carbpol.2016.12.008.

[121] I. Rani, S. G. Warkar, and A. Kumar, "Removal of Cationic Crystal Violet dye using Zeolite- Embedded Carboxymethyl Tamarind Kernel Gum (CMTKG) based Hydrogel Adsorbents," *ChemistrySelect*, vol. 8, no. 29, 2023, doi: 10.1002/slct.202301434.

[122] Khushbu, S. G. Warkar, and N. Thombare, "Correction to: Zinc micronutrient-loaded carboxymethyl tamarind kernel gum-based superabsorbent hydrogels: controlled release and kinetics studies for agricultural applications (Colloid and Polymer Science, (2021), 299, 7, (1103-1111), 10.1007/s00396-021-," *Colloid Polym. Sci.*, vol. 299, no. 9, p. 1505, 2021, doi: 10.1007/s00396-021-04857-y.

[123] L. Wang, R. Li, C. Wang, J. Shao, M. Wu, and W. Wang, "Mixture from carboxymethyl tamarind gum and carboxymethyl starch on double-sided

printing of georgette fabric," *Cellulose*, vol. 24, no. 8, pp. 3545–3554, 2017, doi: 10.1007/s10570-017-1346-2.

[124] E. Yadav. K. Pandey and I. Rani, "tamarind kernel gum and xanthan gum - based superabsorbent hydrogels to investigate the effect on sesame plant growth," *Polym. Bull.*, no. 0123456789, 2024, doi: 10.1007/s00289-024-05150-y.

[125] C. M. Niu, S. Y. Li, and F. Lan, "Adsorption of Cu2+ from aqueous solution by crosslinked carboxymethyl tamarind," *Adv. Mater. Res.*, vol. 781–784, no. 3, pp. 2100–2105, 2013, doi: 10.4028/www.scientific.net/AMR.781-784.2100.

[126] L. Wang, R. Li, J. Shao, and Z. Wang, "Rheological behaviors of carboxymethyl tamarind gum as thickener on georgette printing with disperse dyes," *J. Appl. Polym. Sci.*, vol. 134, no. 26, pp. 1–7, 2017, doi: 10.1002/app.45000.

[127] G. Sen and S. Pat, "Polyacrylamide grafted carboxymethyl tamarind (CMT-g-PAM): Development and application of a novel polymeric flocculant," *Macromol. Symp.*, vol. 277, no. 1, pp. 100–111, 2009, doi: 10.1002/masy. 200950313.

[128] N.R. Gupta, A.Torrish,, P. Wadgaonkar, P.R. Rajamohanan, G. Ducouret, D. Hourdet, C. Creton , M. V. Badiger, "Synthesis and characterization of PEPO grafted carboxymethyl guar and carboxymethyl tamarind as new thermo-associating polymers," *Carbohydr. Polym.*, vol. 117, pp. 331–338, 2015, doi: 10.1016/j.carbpol.2014.09.073.

[129] S.H. Gehrke, L.H. Uhden, and J.F. McBride, "Enhanced loading and activity of metal ions on hydrogen polymers," U.S. Patent No. 5, 1993, 235,039.

[130] G. J. Kim and K. O. Kim, "Novel glucose-responsive of the transparent nanofiber hydrogel patches as a wearable biosensor via electrospinning," *Sci. Rep.*, vol. 10, no. 1, pp. 1–12, 2020, doi: 10.1038/s41598-020-75906-9.

[131] S. Qasemi and M. Ghaemy, "Highly sensitive and strongly fluorescent gum tragacanth based superabsorbent hydrogel as a new biosensor for glucose optical detection," *J. Mater. Chem. C*, vol. 8, no. 12, pp. 4148–4156, 2020, doi: 10.1039/c9tc07014a.

[132] W.A. Laftah, and Z. Hashisho, "Polymer hydrogels for enhanced soil remediation: A review," Soil and Sediment Contamination: An International

Journal, 2015, 24(2), 142-169.

[133] G. O. Akalin and M. Pulat, “Controlled release behavior of zinc-loaded carboxymethyl cellulose and carrageenan hydrogels and their effects on wheatgrass growth,” *J. Polym. Res.*, vol. 27, no. 1, 2020, doi: 10.1007/s10965-019-1950-y.

[134] A. Sayed, M. M. Mohamed, M. E. S. Abdel-raouf, and G. A. Mahmoud, “Radiation Synthesis of Green Nanoarchitectonics of Guar Gum-Pectin/Polyacrylamide/Zinc Oxide Superabsorbent Hydrogel for Sustainable Agriculture,” *J. Inorg. Organomet. Polym. Mater.*, vol. 32, no. 12, pp. 4589–4600, 2022, doi: 10.1007/s10904-022-02465-z.

[135] D. J. Sarkar, A. Singh, P. Mandal, A. Kumar, and B. S. Parmar, “Synthesis and Characterization of Poly (CMC-g-cl-PAam/Zeolite) Superabsorbent Composites for Controlled Delivery of Zinc Micronutrient: Swelling and Release Behavior,” *Polym. - Plast. Technol. Eng.*, vol. 54, no. 4, pp. 357–367, 2015, doi: 10.1080/03602559.2014.958773.

[136] G. O. Akalin and M. Pulat, “Preparation and characterization of κ-carrageenan hydrogel for controlled release of copper and manganese micronutrients,” *Polym. Bull.*, vol. 77, no. 3, pp. 1359–1375, 2020, doi: 10.1007/s00289-019-02800-4.

[137] W. Al-Getham, M. A. Qamar, M.Shariq, A. N. M. A. Alaghaz, A. Farhan, A. A. Areshi and M. Hisham Alnasir, “Emerging environmentally friendly bio-based nanocomposites for the efficient removal of dyes and micropollutants from wastewater by adsorption: a comprehensive review,” *RSC Adv.*, vol. 14, no. 4, pp. 2804–2834, 2024, doi: 10.1039/d3ra06501d.

[138] G. Crini, "Recent developments in polysaccharide-based materials used as adsorbents in wastewater treatment," *Progress in Polymer Science*, 2005, 30(1), 38-70.

[139] M. Vakili, M. Rafatullah, B. Salamatinia, A.Z. Abdullah, M.H. Ibrahim, K.B. Tan, Z. Gholami, and P. Amouzgar, "Application of chitosan and its derivatives as adsorbents for dye removal from water and wastewater: A review," *Carbohydrate Polymers*, 2014, 113, 115-130.

[140] J. Wang, and C. Chen, "Chitosan-based biosorbents: Modification and application for biosorption of heavy metals and radionuclides," *Bioresource*

Technology, 2014, 160, 129-141.

[141] S. Peretz, and O. Cinteza, "Removal of some nitrophenol contaminants using alginate gel beads," *Colloids and Surfaces A: Physicochemical and Engineering Aspects*, 2008, 319(1-3), 165-172.

[142] G.R. Mahdavinia, S. Mousanezhad, H. Hosseinzadeh, F. Darvishi, and M. Sabzi, "Magnetic hydrogel beads based on PVA/sodium alginate/laponite RD and studying their BSA adsorption," *Carbohydrate Polymers*, 2017, 147, 379-391.

[143] G. Zhou, C. Luo, Z. Zhou, R. Xing, Z. Ding, and Z. Bai, "Adsorption of anionic dyes on poly(vinylamine)-modified cellulose acetate viscose fiber," *Journal of Applied Polymer Science*, 2011, 120(3), 1717-1723.

[144] J.P. Gong, Y. Katsuyama, T. Kurokawa, and Y. Osada, "Double-network hydrogels with extremely high mechanical strength," *Advanced Materials*, 2003, 15(14), 1155-1158.

[145] H. Isawi, "Using Zeolite/Polyvinyl alcohol/sodium alginate nanocomposite beads for removal of some heavy metals from wastewater," *Arab. J. Chem.*, vol. 13, no. 6, pp. 5691–5716, 2020, doi: 10.1016/j.arabjc.2020.04.009.

[146] S.K.Papageorgiou, E.P. Kouvelos, E.P. Favvas, A.A. Sapalidis, G.E. Romanos, and F.K. Katsaros, "Metal–carboxylate interactions in metal–alginate complexes studied with FTIR spectroscopy, " *Carbohydrate Research*, 2010, 345(4), 469-473.

[147] J. Wang, J. Wei, J. Li, and H. Cao, "Preparation of a novel chitosan-based magnetic adsorbent modified with polyacrylic acid for the efficient removal of Cu(II) from aqueous solutions," *Colloids and Surfaces A: Physicochemical and Engineering Aspects*, 2016, 508, 327-336.

[148] W.S. Wan Ngah, L.C. Teong, and M.A.K.M. Hanafiah, "Adsorption of dyes and heavy metal ions by chitosan composites: A review," *Carbohydrate Polymers*, 2011, 83(4), 1446-1456.

[149] P. Miretzky, and A.F. Cirelli, " Hg(II) removal from water by chitosan and chitosan derivatives: A review. Journal of Hazardous Materials," 2009, 167(1-3), 10-23.

[150] X. Yu, S. Tong, M. Ge, L. Wu, J. Zuo, C. Cao, and W. Song, "Adsorption of heavy metal ions from aqueous solution by carboxylated cellulose nanocrystals.

Journal of Environmental Sciences," 2013, 25(5), 933-943.

[151] Y. Zhou, Y. Min, H. Qiao, Q. Huang, E. Wang, and T. Ma, "Improved removal of malachite green from aqueous solution using chemically modified cellulose by anhydride. International Journal of Biological Macromolecules, " 2016, 74, 271-277.

[152] N. Singh, J. Singh, L. Kaur, N.S. Sodhi, and B.S. Gill, "Morphological, thermal and rheological properties of starches from different botanical sources," *Food Chemistry,* 2007, 81(2), 219-231.

[153] J.B. Hirsch, and J.L. Kokini, "Understanding the mechanism of cross-linking agents (POCl3, STMP, and EPI) through swelling behavior and pasting properties of cross-linked waxy maize starches, "*Cereal Chemistry*, 2002, 79(1), 102-107.

[154] A. K. Kodoth and V. Badalamoole, "Silver nanoparticle-embedded pectin-based hydrogel for adsorptive removal of dyes and metal ions," *Polym. Bull.*, vol. 77, no. 2, pp. 541–564, 2020, doi: 10.1007/s00289-019-02757-4.

[155] A. Reghioua, D. Barkat, A. H. Jawad, A. S. Abdulhameed, S. Rangabhashiyam, M. R. Khan, and Z. A. Alothman, "Magnetic Chitosan-Glutaraldehyde/Zinc Oxide/Fe3O4 Nanocomposite: Optimization and Adsorptive Mechanism of Remazol Brilliant Blue R Dye Removal," *J. Polym. Environ.*, vol. 29, no. 12, pp. 3932–3947, 2021, doi: 10.1007/s10924-021-02160-z.

[156] H. Mittal, A. Al Alili, and S. M. Alhassan, "High efficiency removal of methylene blue dye using κ-carrageenan-poly(acrylamide-co-methacrylic acid)/AQSOA-Z05 zeolite hydrogel composites," *Cellulose*, vol. 27, no. 14, pp. 8269–8285, 2020, doi: 10.1007/s10570-020-03365-6.

[157] Z. Zhang, R. Zhang, L. Zou, L. Chen, Y. Ahmed, W. Al Bishri, K. Balamash, and D.J. McClements, "Encapsulation of curcumin in polysaccharide-based hydrogel beads: Impact of bead type on lipid digestion and curcumin bioaccessibility," *Food Hydrocolloids*, 2016, 58, 160-170.

[158] W.R. Gombotz, and S.F. Wee, "Protein release from alginate matrices," *Advanced Drug Delivery Reviews*, 2012, 64, 194-205.

[159] K.L. Yam, P.T. Takhistov, and J. Miltz, "Intelligent packaging: Concepts and

applications," *Journal of Food Science,* 2005, 70(1), R1-R10.

[160] S. Qasemi and M. Ghaemy, "Novel superabsorbent biosensor nanohydrogel based on gum tragacanth polysaccharide for optical detection of glucose," *Int. J. Biol. Macromol.*, vol. 151, pp. 901–908, 2020, doi: 10.1016/j.ijbiomac. 2020.02.231.

[161] H. Mittal, A. Maity, and S. S. Ray, "Gum karaya based hydrogel nanocomposites for the effective removal of cationic dyes from aqueous solutions," *Appl. Surf. Sci.*, vol. 364, no. 2016, pp. 917–930, 2016, doi: 10.1016/j.apsusc.2015.12.241.

[162] J. Potaś, E. Szymańska, A. Basa, A. Hafner, and K. Winnicka, "Tragacanth gum/chitosan polyelectrolyte complexes-based hydrogels enriched with xanthan gum as promising materials for buccal application," *Materials (Basel).*, vol. 14, no. 1, pp. 1–15, 2021, doi: 10.3390/ma14010086.

[163] T. Jayaramudu, R. D. Pyarasani, A. Akbari-Fakhrabadi, D. Abril-Milan, and J. Amalraj, "Synthesis of Gum Acacia Capped Polyaniline-Based Nanocomposite Hydrogel for the Removal of Methylene Blue Dye," *J. Polym. Environ.*, vol. 29, no. 8, pp. 2447–2462, 2021, doi: 10.1007/s10924-021-02066-w.

[164] L. Y. Maroufi, M. Tabibiazar, M. Ghorbani, and A. Jahanban-Esfahlan, "Fabrication and characterization of novel antibacterial chitosan/dialdehyde guar gum hydrogels containing pomegranate peel extract for active food packaging application," *Int. J. Biol. Macromol.*, vol. 187, no. July, pp. 179–188, 2021, doi: 10.1016/j.ijbiomac.2021.07.126.

[165] A. Sorze, F. Valentini, A. Dorigato, and A. Pegoretti, "Development of a Xanthan Gum Based Superabsorbent and Water Retaining Composites for Agricultural and Forestry Applications," *Molecules*, vol. 28, no. 4, 2023, doi: 10.3390/molecules28041952.

[166] H. Mittal, A. Maity, and S. S. Ray, "Effective removal of cationic dyes from aqueous solution using gum ghatti-based biodegradable hydrogel," *Int. J. Biol. Macromol.*, vol. 79, pp. 8–20, 2015, doi: 10.1016/j.ijbiomac.2015.04.045.

[167] S. Jana, J. Ray, S. K. Bhanja, and T. Tripathy, "Removal of textile dyes from

single and ternary solutions using poly(acrylamide-co-N-methylacrylamide) grafted katira gum hydrogel," *J. Appl. Polym. Sci.*, vol. 135, no. 10, pp. 1–20, 2018, doi: 10.1002/app.45958.

[168] S. Nasef, E. Elnesr, F. Hafez, N. Badawy, and S. Slim, "Gamma Irradiation Induced Preparation of Gum Arabic/ Poly (Vinyl Alcohol) Copolymer Hydrogels for Removal of Heavy Metal Ions from Wastewater," *Arab J. Nucl. Sci. Appl.*, vol. 0, no. 0, pp. 0–0, 2019, doi: 10.21608/ajnsa.2019.15587.1246.

[169] D. Chauhan, A. Kumar, and S. G. Warkar, "Synthesis, characterization and metal ions sensing applications of meta-benziporphodimethene-embedded polyacrylamide/carboxymethyl guargum polymeric hydrogels in water," *Environ. Technol. (United Kingdom)*, vol. 43, no. 7, pp. 991–1002, 2022, doi: 10.1080/09593330.2020.1812730.

[170] D. Cao, Y. Lv, Q. Zhou, Y. Chen, and X. Qian, "Guar gum/gellan gum interpenetrating-network self-healing hydrogels for human motion detection," *Eur. Polym. J.*, vol. 151, no. October 2020, p. 110371, 2021, doi: 10.1016/j.eurpolymj.2021.110371.

[171] L. Dai, B. Wang, X. An, L. Zhang, A. Khan, and Y. Ni, "Oil/water interfaces of guar gum-based biopolymer hydrogels and application to their separation," *Carbohydr. Polym.*, vol. 169, pp. 9–15, 2017, doi: 10.1016/j.carbpol.2017.03.096.

[172] V. Hasija, K. Sharma, V. Kumar, S. Sharma, and V. Sharma, "Green synthesis of agar/Gum Arabic based superabsorbent as an alternative for irrigation in agriculture," *Vacuum*, vol. 157, pp. 458–464, 2018, doi: 10.1016/j. vacuum.2018.09.012.

[173] L.Dai, Y.Wang, Z. Li, X. Wang, C. Duan [a], Wei Zhao, C. Xiong, S. Nie, Y. Xu, and Y. Ni, "A multifunctional self-crosslinked chitosan/cationic guar gum composite hydrogel and its versatile uses in phosphate-containing water treatment and energy storage," *Carbohydr. Polym.*, vol. 244, p. 116472, 2020, doi: 10.1016/j.carbpol.2020.116472.

[174] R. Yadav, Ayush, Manu, and A. Rani, "Synthesis and characterization of xanthan gum and carboxymethylcellulose sodium salt based ionic crosslinked hydrogels for agricultural application," *Bulg. Chem. Commun.* , vol. 55, pp. 131–137, 2023, doi: 10.34049/bcc.55.A.0021.

[175] A. Mahto and S. Mishra, "The removal of textile industrial Dye-RB-19 using

Guar gum-based adsorbent with thermodynamic and kinetic evaluation parameters," *Polym. Bull.*, vol. 79, no. 5, pp. 3353–3378, 2022, doi: 10.1007/s00289-021-03663-4.

[176] V. P. Padmanabhan, R. Kulandaivelu, and S. N. T. S. Nellaiappan, "New core-shell hydroxyapatite/um-Acacia nanocomposites for drug delivery and tissue engineering applications," *Mater. Sci. Eng. C*, vol. 92, no. June, pp. 685–693, 2018, doi: 10.1016/j.msec.2018.07.018.

CHAPTER 2

NANO ZNO EMBEDDED POLY (ETHYLENE GLYCOL) DIACRYLATE CROSS-LINKED CARBOXYMETHYL TAMARIND KERNEL GUM AND POLY (SODIUM ACRYLATE) NANOCOMPOSITE HYDROGELS FOR ORAL DELIVERY OF CIPROFLOXACIN DRUG AND THEIR ANTIBACTERIAL PROPERTIES

2.1. Introduction

Hydrogels are cross-linked polymeric systems made up of synthetic monomers and natural polymers such as polysaccharides, proteins and biopolymers. Hydrogels have a significant amount of porosity, making them efficient materials to absorb drugs in the aqueous mediums via physical or chemical interactions and subsequent release of the drug under physiological conditions[1]. Several stimuli like pH, temperature, and ionic strength affect the drug release rate through the hydrogel. The amount of drug release depends on the water uptake capacity of the hydrogels and the mechanism of diffusion of fluid into the matrix of hydrogel [2]. Other than the drug delivery applications, hydrogels can be used in other fields such as agriculture, metal ion sensing, heavy metal ion removal, toxic dyes removal, textile, and food industry [3]. Till now, a large number of natural biopolymer-based hydrogels such as carboxymethyl guar gum[4], chitosan[5], sodium alginate [6], carboxymethyl cellulose[7] were used for the controlled release of the drug into the human body. However, a biopolymer carboxymethyl tamarind kernel gum (CMTKG) based hydrogels have not been much explored for the drug delivery applications. CMTKG is a natural, non-toxic, biodegradable, and biocompatible biopolymer which is a chemically modified form of tamarind gum. It contains the polysaccharide units of D-Xylose, D-Glucose, and D-Galactose[8]. This chemical modification resulted in an enhanced life shell, swelling capacity, drug loading, and drug release capacity[9]. There are only a few numbers of CMTKG-based hydrogel reported for biomedical applications. For instance, K. Mali et.al., group have reported the formation of CMTKG-based hydrogel film cross-linked through citric acid [10]. In another research, alginate and CMTKG based hydrogels were synthesized for the delivery of acyclovir

drug[11]. Additionally, CMTKG-based nanoparticles were also synthesized for the ocular delivery of tropicamide [12]. Over the past few years, the incorporation of inorganic materials such as nanoparticles into the hydrogel matrix have gained a significant research attention. Nanocomposite hydrogels showed higher swelling, thermal and mechanical properties. Moreover, bio-composites can be formed by the combination of natural polymers with inorganic materials such as ZnO[13], Fe_2O_3[14], CuO[15], and Ag nanoparticles[16]. Among numerous nanoparticles, zinc oxide nanoparticles are non-toxic, antibacterial, and eco-friendly [17]. A study reported the synthesis of Poly acrylic acid/Polyethylene glycol/ZnO mucoadhesive nanocomposite hydrogels for the delivery of propranolol HCl[18]. The green synthesis of carboxymethyl cellulose/ZnO nanocomposite hydrogel was also reported [19]. In this study, the ciprofloxacin drug was used as a model drug for drug delivery application.

Ciprofloxacin is an antibiotic, broad-spectrum, synthetic, and chemotherapeutic agent belonging to fluoroquinolones[20]. Mainly, this drug was chosen because it is a superior antibiotic drug to others. However, the half-life of ciprofloxacin drug is 4 hours. It is a broad-spectrum antibiotic and used to treat the infections caused by gram-negative and gram-positive bacteria[21]. Mahdavinia reported the synthesis of chitosan and hydroxyapatite nanocomposite hydrogel cross-linked with k-carrageenan for the sustained release of ciprofloxacin drug [22]. It was found from literature that Poly (ethylene glycol diacrylate) (PEGDA) based hydrogels can be easily synthesized and have great biocompatibility. PEGDA can be used as a cross-linking agent in free radical polymerization methods using potassium persulfate as an initiator[23]. Only a few numbers of PEGDA cross-linked hydrogels have been reported till the date.

In the present study, hybrid hydrogels are fabricated from cross-linking of synthetic organic monomers (Acrylic acid) with biopolymers. Acrylic acid is a synthetic and anionic monomer soluble in water, containing a shorter lifetime, and ionizable acidic-COOH group sensitive to various stimuli such as temperature and pH[3]. In this study, CMTKG was cross-linked with poly (sodium acrylate) (PSA) using PEGDA cross-linker, resulting in CMTKG/PSA hydrogel formation. Zinc oxide nanoparticles (ZnO NPs) were synthesized through a hydrothermal synthetic method and loaded into CMTKG/PSA hydrogel to enhance the properties such as drug loading, drug entrapment,

biocompatibility, and controlled drug release. The synthesized ZnO NPs and CMTKG-based nanocomposite hydrogel were characterized using FTIR, XRD, FE-SEM, TEM, and UV-Visible techniques. Additionally, the impact of the presence of ZnO NPs on the parameters such as swelling capacity, porosity, gel content, rate of drug release, and mechanism of drug release were evaluated. The drug release kinetic modelling was done for the CMTKG/PSA hydrogel and ZnO NPs loaded CMTKG/ PSA nanocomposite hydrogel using the Higuchi model and Korsmeyer- Peppas model. Furthermore, antibacterial studies of CMTKG/PSA hydrogel, ZnO NPs and drug loaded CMTKG/PSA hydrogels were performed against the *E. coli* bacteria.

2.2. Experimental Sections

2.2.1. Materials

Carboxymethyl tamarind gum (CMTKG) having 0.20° substitution (courtesy Hindustan Gum Limited, Rewari), Acrylic acid (AA, CDH), Poly (ethylene glycol diacrylate) (PEGDA, Mn = 2000, Sigma Aldrich), Sodium hydroxide, Potassium persulfate (KPS, Fischer), Zinc acetate (Sigma Aldrich), were used as received. Ciprofloxacin drug was gifted by M/S Unicure India limited. Buffer solutions of pH 7.4 and pH 1.2 were prepared in the laboratory. Double distilled water was used to perform all the experiments.

2.2.2. Synthesis of CMTKG /Poly (sodium acrylate) hydrogel

A free radical polymerization method was employed to synthesize CMTKG- poly (sodium acrylate) hydrogel. Initially, 0.15 g of CMTKG was allowed to disperse in 10 mL of distilled water for one hour while stirring at 500 rpm. Potassium persulfate was added as a free radical initiator after complete dispersion of CMTKG and stirred for 10 minutes. After that 5 mL of acrylic acid with 5 mL (2N), sodium hydroxide was added, and stirring was continued for 20 minutes. Subsequently, PEGDA was added to the reaction mixture as a cross-linker and stirred for 30 minutes. Then, the reaction mixture was poured into test tubes and maintained at 60°C for 2 hours in a water bath. The resulting product was then put on petri plates and dried in an oven at 50 °C temperature. Thus, the achieved hydrogel is termed as CMTKG/PSA hydrogel.

2.2.3. Synthesis of ZnO nanoparticles

The hydrothermal synthetic method was used to prepare the ZnO NPs[24]. Initially, a solution of 0.05 M zinc acetate dihydrate (Zn. $(CH_3COO)_2.2H_2O$) and 0.1 M NaOH were prepared separately in the distilled water. To synthesize, ZnO NPs, the prepared zinc acetate solution was slowly added with a continuous stirring to NaOH solution which was placed in an oven at 100ºC for 2 hours. This solution reacted to give a white-colored zinc oxide precipitate which upon centrifugation at 2000 rpm for 20 minutes gave ZnO NPs. The particles were dried in the oven at 60 °C for further use.

2.2.4. Preparation of ZnO NPs loaded CMTKG/Poly (sodium acrylate) nanocomposite

A series of CMTKG/PSA nanocomposite hydrogel was prepared by varying the weight of ZnO NPs. A fixed amount of ZnO NPs such as 0.03g, 0.05g, and 0.1 g was mixed into the CMTKG and sodium acrylate reaction mixture before the addition of PEGDA as a cross-linker. The rest of the procedure is same as explained in section 2.2.2 to obtain nanocomposite hydrogel. The composition of a series of CMTKG/PSA/ZnO nanocomposite hydrogel is mentioned in the **Table 2.1**.

Table 2.1: Composition of series of CMTKG/ PSA nanocomposite hydrogel with varying amounts of ZnO

Sample Code	CMTKG (g)	AA (mL)	PEGDA (mL)	KPS (g)	ZnO NPs (g)
E1	0.15	5	2	0.025	0
E2	0.15	5	2	0.025	0.03
E3	0.15	5	2	0.025	0.05
E4	0.15	5	2	0.025	0.1

2.2.5. Swelling Studies

To determine the water absorption capacity of CMTKG/PSA hydrogels and ZnO NPs loaded hydrogels, the swelling studies were done gravimetrically in which a predetermined amount of xerogels were transferred into 100 mL of distilled water, pH 7.4 and pH 1.2 buffer solution. At different time intervals, the weight of the swollen hydrogel was recorded. The value of the swelling ratio (SR) was calculated using the given expression in Equation 2.1 [25].

$$SR\ (g/g) = \frac{W_s - W_0}{W_0} \quad (2.1)$$

where W_s represents the mass of hydrogel taken after t time and W_0 is the mass of the dry hydrogel sample. To estimate the equilibrium swelling ratio (ESR), W_s was substituted by W_e, i.e. weight of the maximum swelled hydrogel taken after 48 hours.

2.2.6. Modelling of swelling data

There are many mathematical models which were used to quantitatively study the dynamic swelling behavior of hydrogels. Here, the Power function model as a time-dependent model was used to study the fractional water uptake using the Equation 2.2[26].

$$F = \frac{M_t}{M_\infty} = k.t^n \quad (2.2)$$

Where M_t denotes the amount of water absorbed or swelling content of hydrogels at time t and M_∞ denotes the maximum water uptake or swelling content at equilibrium. The parameters such as n and k correspond to the water uptake index and the gel characteristic constant respectively. To further investigate the swelling behavior of hydrogels, the Schott model (second-order) was used. In this model, the water uptake rate constant (k_2) was evaluated using Equation 2.3[27].

$$\frac{t}{Mt} = \frac{1}{k_2 M^2{}_\infty} + \frac{t}{M_\infty} \quad (2.3)$$

Where M_t denotes the swelling (g/g) of the hydrogel at t time and M_∞ denotes the value of maximum swelling (g/g) of the hydrogel at equilibrium**.** Moreover, K_2 is the kinetic rate constant of water. However, the applicability of the given models can be known based on the higher value of the regression coefficient (R^2) close to unity.

2.2.7. Porosity and Gel content

The liquid displacement technique was used to determine the porosity of produced hydrogels [18]. A predetermined amount of hydrogel (W_d) was submerged in ethanol till saturation. The initial weight of hydrogel in ethanol was noted as (W_l). The hydrogel

sample was taken out after 24 hours from ethanol and weighed (W_w) after removing the surface liquid with the help of tissue paper. The porosity of the hydrogel was estimated by using Equation 2.4[28].

$$\text{Porosity (\%)} = \frac{W_w - W_d}{W_w - W_l} \times 100 \quad (2.4)$$

To calculate the gel content of the hydrogel, the freshly prepared xerogels with initial weight (W_0) were swollen in distilled water for 48 hours. They were dried at room temperature after being taken out from distilled water to reach the stage of complete deswelling. Then, the hydrogels were weighed (W_e) after drying in an oven at 40 ºC to remove moisture completely. The gel content (%) was calculated using the given Equation (2.5)[29].

$$\text{Gel content (\%)} = \frac{W_e}{W_o} \times 100 \quad (2.5)$$

2.2.8. Drug loading and entrapment efficiency

The drug loading efficiency of hydrogels is the ratio of the weight of the loaded drug to the weight of hydrogels while the drug entrapment efficiency is the ratio of the weight of the loaded drug to the weight of the unloaded drug. To evaluate the maximum loading of a drug into the hydrogel, a predetermined amount of xerogel (Wi) was added to 100 mL solution of pH 7.4 containing a specific amount (W_0) of ciprofloxacin drug. After 48 hours, the drug-loaded hydrogel was taken out from the buffer solution and dried at room temperature. Further, it was dried in an oven for 48 hours at 60 °C and weighed (W_d). Thus, the drug loading (DL%) and drug entrapment (DE%) efficiency of the hydrogels were calculated using Equation 2.6 and 2.7 respectively [30].

$$\text{DL} = \frac{W_d - W_i}{W_i} \times 100 \quad (2.6)$$

$$\text{DE} = \frac{W_d - W_i}{W_o} \times 100 \quad (2.7)$$

2.2.9. In vitro drug release study

The drug release studies of ciprofloxacin drug were carried out in physiological pH 7.4 at 37ºC. The specific weight of drug-loaded hydrogels was placed in 50 mL, pH 7.4 phosphate buffer solution in an orbital shaker incubator with constant shaking at 50 rpm. The absorbance of the drug released was measured using a UV-visible spectrophotometer at a wavelength of 278 nm after removing 2 ml of the supernatant liquid at regular intervals. The total volume of buffer solution was kept constant by adding 2 ml of fresh phosphate buffer solution every time. This absorbance corresponded to the concentration of the released drug as followed by the Beer-Lambert law. The amount of drug released was calculated using a standard calibration curve for the ciprofloxacin drug. Thus, drug release (%) was calculated using the given Equation 2.8[21].

$$\text{Drug Release } (\%) = \frac{A_t}{A_O} \times 100 \tag{2.8}$$

where A_t represents the amount of drug released at t time and A_0 represents the amount of drug loaded in the hydrogel.

2.2.10. Antibacterial Activity

The antibacterial effects of CMTKG/PSA, ZnO NPs loaded CMTKG/PSA, and CFX loaded ZnO/CMTKG/PSA nanocomposite hydrogel were investigated against *E. coli* NCIMB-1. The disc diffusion test (AATCC-30) was used in this study to determine their antibacterial activity [23]. Hydrogel samples (100 mg) were placed separately in the middle of the agar plates for the bacterial strain cultures under consideration. The samples were then incubated for 24 hours at 37 °C to evaluate the area of inhibition. In this study, CFX drug as a broad-spectrum antibiotic was utilized as a positive control.

2.2.11. Characterizations

ZnO nanoparticles, CMTKG/PSA hydrogel, and ZnO nanoparticles loaded CMTKG/PSA nanocomposite were characterized by FTIR, UV-visible, XRD, FE-SEM, and TEM techniques. The Fourier transform infrared resonance (FTIR) spectra were recorded using the Perkin Elmer Spectrum Model across the frequency range 400-

4000 cm^{-1}. Moreover, FE-SEM imaging of ZnO NPs and ZnO NPs loaded hydrogel was carried out using the ZEISS EVO model along with EDX analysis. Additionally, TEM imaging of ZnO NPs was carried out using TECNAI G 20 (200 KV). Zeta potential measurement of ZnO NPs colloidal solution in ethanol was done using a Zetasizer (Model ZSP, Malvern instrument, UK). The surface plasmon resonance (SPR) was recorded by dispersing ZnO NPs loaded hydrogel in ethanol and scanning under a UV-visible spectrophotometer. XRD spectra of ZnO NPs and CMTKG/PSA/ZnO hydrogel were recorded using powder X-ray diffraction with a high-resolution Bruker spectrophotometer over a range of angle 2θ = 0 to 80° with a scan rate of 1sec/step. Rheological measurements were performed using stress-controlled AR- 500 rheometers (TA Instrument, U.K) using a cone plate geometry (2°, 25 mm). The frequency sweep range from 0.1 to 100 rad/s was used to measure the mechanical spectra in terms of the storage modulus((G') and loss modulus (G'').

2.2.12 Statistical analysis

In this study, the numerical data was expressed as the mean ± SD. The data was statistically analyzed by using one-way ANOVA followed by Tukey's test with the level of significance set at $p < 0.05$.

2.3. Results and discussion

2.3.1. Mechanistic pathway of the reaction

CMTKG/PSA hydrogel was formed through a free radical chain polymerization mechanism. Here, potassium persulfate (free radical initiator) was decomposed and produced sulfate radicals at 60ºC [8]. These radicals formed a chain by the removal of the hydrogen atom of the -OH group present on the backbone of CMTKG. These reactive radicals reacted with the C=C double bond present at the terminal position of the PEGDA cross-linker and new radicals formed will react with the C=C bond of sodium acrylate to give a highly crosslinked network as shown in **Figure 2.1.** Nanocomposite hydrogels were formed by the incorporation of ZnO NPs. These particles showed electrostatic interactions with an oxygen atom and carboxyl groups present on the backbone of hydrogel. Additionally, there may be hydrogen bonding

interactions of ZnO nanoparticles with -OH group present on the surface of the CMTKG biopolymer.

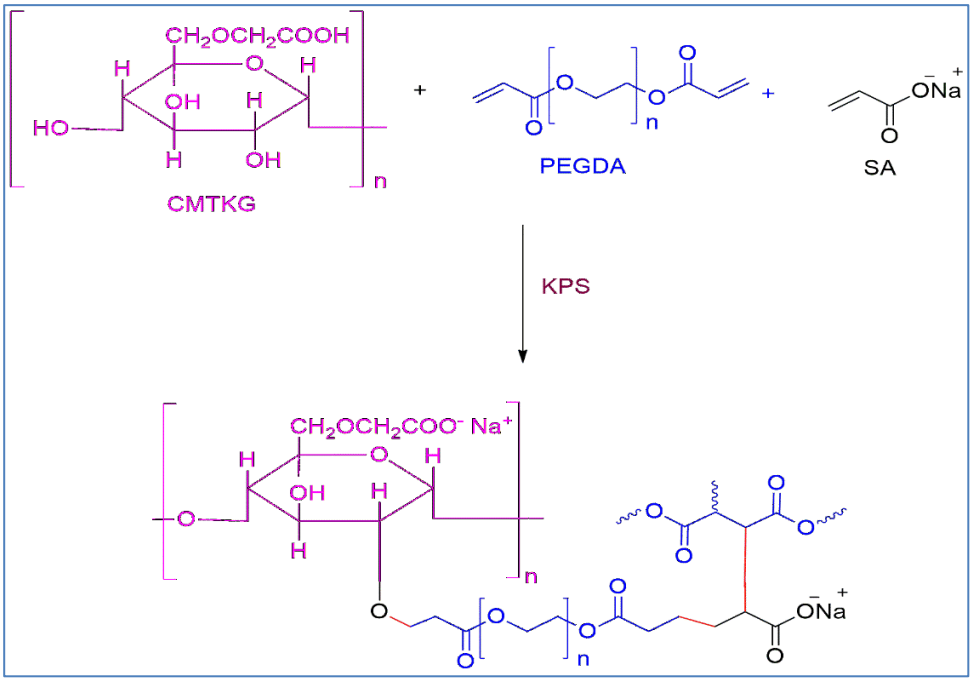

Figure 2.1: Proposed mechanism for CMTKG/PSA hydrogel

2.3.2. Swelling studies

Swelling studies of all the synthesized hydrogels were performed in double distilled water, pH 7.4 and pH 1.2 buffer solutions respectively. The maximum swelling capacity was noted for hydrogel containing 0.03 g ZnO NPs. The most probable cause of maximum swelling for 0.03 g ZnO NPs loaded hydrogel may be due to the maximum interaction of the oxygen atom of ZnO with the hydrogen atom of the water molecule. Also, ZnO is a polar amphoteric tetrahedrally coordinated structure of Zn^{+2} and O^{-2} ions[26]. It was also found that increasing the amount of ZnO up to 0.05 g and 0.1 g decreased the swelling capacity of the hydrogel. The increased concentration of ZnO NPs may lead to additional H-bonding interaction of negatively charged polar atom of oxygen with the hydroxyl group of CMTKG resulting in the decrease of swelling as shown in **Figure 2.2a.** [26].

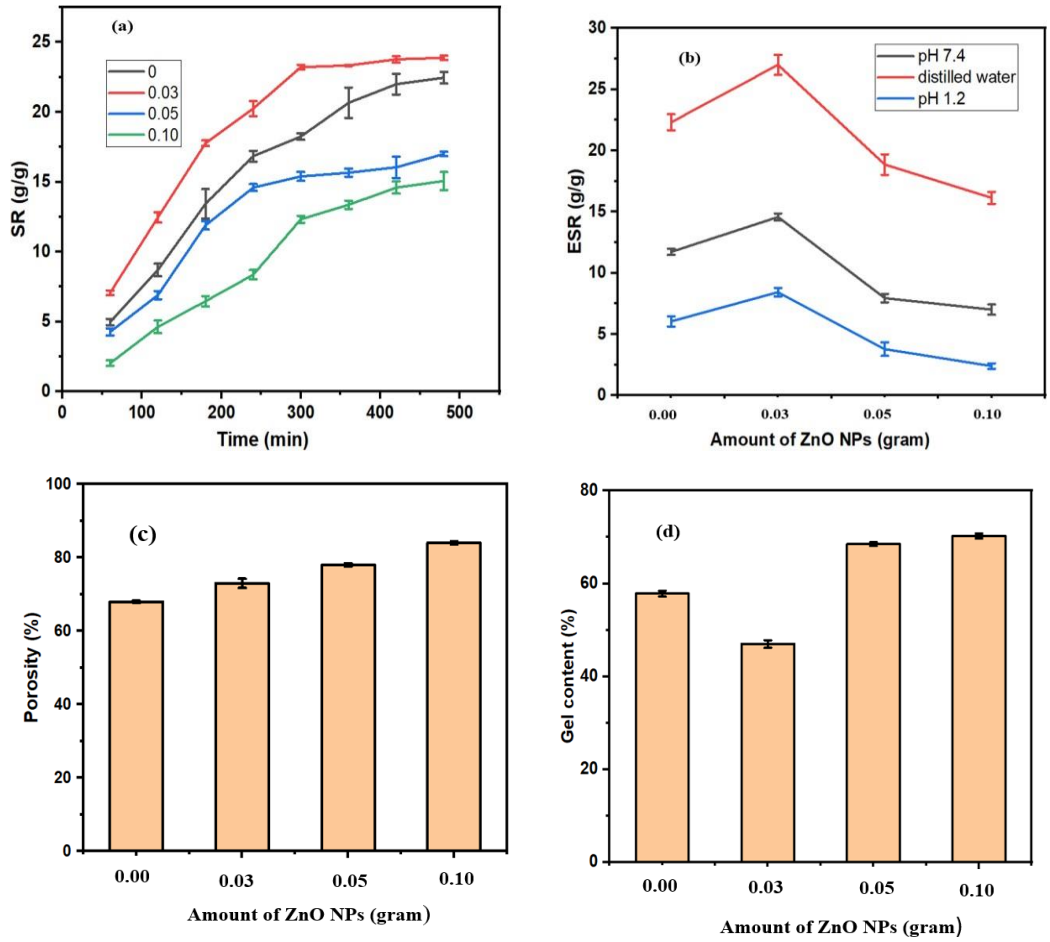

Figure 2.2: (a) SR (g/g) **(b)** ESR (g/g) **(c)** Porosity (%) **(d)** Gel Content (%) for E1 to E4 hydrogel

It was observed that nanocomposite hydrogel showed the highest ESR(g/g) value in distilled water. It may be due to the absence of interfering ions that can interact with the opposite charges present in the hydrogel matrix. At pH 7.4, nanocomposite hydrogel showed higher swelling than at pH 1.2 as shown in **Figure 2.2(b).** In the basic medium, there were many negatively charged carboxylate ions due to proper ionization of the -COOH group, the electrostatic repulsion between these groups allowed hydrogel to expand. In an acidic medium, the hydrogel showed the least swelling. It may be due to improper ionization and protonation of the -COOH group. Also, hydrogen bonding takes place that would decrease the electrostatic repulsions between negatively charged groups present in hydrogel[3]. Additionally, the dynamic water absorption data of hydrogel in distilled water was fitted in the power function model and Schott model as shown in **Figure 2.3**. In the case of the power function model, a linear plot of ln F vs

ln t was plotted **(Figure 2.3a).** The different parameters such as n, k, and R^2 were estimated and tabulated in **Table 2.2**. The value of n corresponded to the diffusion exponent, n=0.45 indicated a Fickian diffusion, the value of n between 0.45 and 0.89 for non-Fickian or anomalous diffusion, and n = 0.89 for case II diffusion mechanism. The calculated value of n for all nanocomposite hydrogels (E1 to E4) indicated a non-Fickian swelling behavior of hydrogel. In the case of the Schott model, a linear plot of t/M_t vs t was plotted as shown in **Figure 2.3b**. All parameters related to this model are given in **Table 2.2.** It was found that M_∞ (exp) values were nearly the same as M_∞(theor) values. Based on values of R^2, it was concluded that the dynamic swelling data was better fitted in the Schott model.

Table 2.2: Models used to evaluate the dynamic water absorption for various CMTKG/PSA hydrogels

Sample Code	Power function model	k	R^2	Schott kinetic model	M_∞(exp) (g/g)	$K_2 \times 10^{-4}$ (g/g min^{-1})	R^2
	n			M_∞(Theo) (g/g)			
E1	0.5197	0.0415	0.9981	8.35	8.50	17	0.9932
E2	0.5492	0.035	0.9875	10.78	8.89	7	0.9940
E3	0.5045	0.046	0.9749	8.26	6.54	10	0.9890
E4	0.4620	0.048	0.9430	7.83	5.40	4	0.9931

2.3.3. Porosity and Gel content

The gel fraction of a hydrogel is related to the cross-linking density which depends on the interaction between various components present in the hydrogel. The gel content of all the synthesized nanocomposite hydrogel (E1 to E4) was calculated by using **Equation. (2.5)** as shown in **Figure 2.2d**. It was noticed that with the addition of 0.03 g of ZnO NPs into the hydrogel, gel content was decreased. However, with the further addition of ZnO NPs, gel content was increased. It may be due to the significant interaction of a functional group of nanoparticles with a three-dimensional network of polymeric matrix[32]. In a study, Kalantari et.al., have reported that with an increase in the amount of CeO_2-NPs, gel content was decreased[28]. Hydrogels have porous structures which provide the space for the encapsulation of various drugs. It was observed that the porosity of the synthesized hydrogel was increased with an increasing

amount of ZnO NPs [29]. The observed range of porosity lied in range from 68 to 84% as shown in **Figure 2.2c.** The porosity of a hydrogel is responsible for its efficacy in absorbing a significant amount of exudate from a wound surface and allowing cells to proliferate. Thus, the synthesized nanocomposite hydrogel can also be employed for wound healing [19].

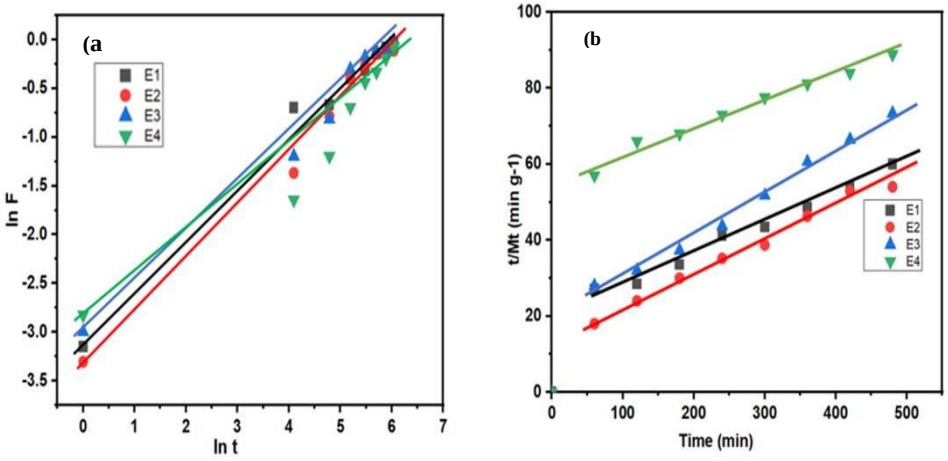

Figure 2.3: (a) Power function **(b)** Schott function model for the dynamic swelling data of all synthesized hydrogel (E1 to E4)

2.3.4. Drug loading and drug entrapment efficiency

The estimated value of DL (%) and DE (%) for all the nanocomposite hydrogel was shown in **Table 2.3.** The drug loading efficiency was calculated with respect to the mass of hydrogel while drug entrapment efficiency was calculated with respect to the mass of the drug in the hydrogel matrix. It was observed that the efficiency of loading and entrapment of the drug was enhanced with an increasing amount of zinc oxide nanoparticles. It may be due to their knotting behavior in which they can form the chelate ring with some -OH and -COO groups present in the polymeric matrix[13].

Secondly, the relative biocompatibility and the role of ZnO NPs as a nano-reservoir were responsible for the higher loading and entrapment efficiency of nanocomposite hydrogel.

Table 2.3: Drug loading (%DL) and drug entrapment (%DE) values for all the synthesized nanocomposite hydrogel (E1 to E4)

Sample Code	Amount of ZnO NPs	DL (%)	DE (%)
E1	0.00	10± 0.04	58.67±0.89
E2	0.03	21±0.57	65±0.81
E3	0.05	24±0.40	67.50±0.40
E4	1.00	28±0.12	70.65±0.23

2.3.5. Characterizations

2.3.5.1.XRD

At room temperature, XRD of ZnO NPs, CMTKG/PSA, and ZnO/CMTKG/PSA nanocomposite hydrogels were carried out, as shown in **Figure 2.4.** It was found that the XRD pattern of ZnO NPs revealed crystalline in nature. To estimate the average crystallite size of ZnO NPs, Debye-Scherrer **Equation (2.9)** was used [32].

$$D = \frac{0.89\,\lambda}{\beta\cos\theta} \tag{2.9}$$

Where λ represents the wavelength of X-ray (0.15418 nm), β is FWHM (Full Width at Half Maximum) in radian, θ indicates diffraction angle and D indicates crystal particle size (nm). X'Pert High Score Plus software was used to estimate d-spacing values. All the calculated parameters were tabulated in **Table 2.4.** Additionally, XRD plot of ZnO NPs was shown in **Figure 2.4a** indicated various diffraction bands at 2θ values of 31.92°, 34.52º, 36.36°, 47.68°, 56.76º, 62.96º, 68.08°, and 69.20° which assigned to (100), (002), (101), (102), (110), (103), (112), and (201) diffractions of zinc oxide nanoparticles[33]. Moreover, the XRD of CMTKG, CMTKG/PSA, and CMTKG/PSA/ZnO nanocomposite hydrogel is shown in **Figure 2.4b**. XRD pattern of CMTKG showed diffraction bands at 19.24º, 31.95º, 34.18º, and 45.16º which may be due to the semi-crystalline nature of CMTKG biopolymer. However, XRD of acrylic acid monomer showed a broad diffraction peak at 21.20º which was assigned to the amorphous nature of acrylic acid. In the case of XRD of CMTKG/PSA hydrogels, two broad diffraction peaks at 16.25º and 31.80º indicate the amorphous nature of hydrogel.

However, the intensity of peaks of CMTKG decreased after cross- linking with amorphous sodium acrylate monomer. Moreover, XRD pattern of CMTKG/PSA/ZnO nanocomposite hydrogel showed some sharp diffraction peaks at 25.72º and 38.10º. Moreover, the significant reduction in the diffraction pattern of ZnO NPs after loading into the CMTKG/PSA hydrogel suggested that the crystalline nature of ZnO NPs was converted in amorphous form.

Table 2.4: Detailed analysis of XRD and estimation of various parameters for ZnO NPs

Sample	d-spacing	FWHM	Crystallite size(nm)
ZnO NPs	2.4657	0.43	20

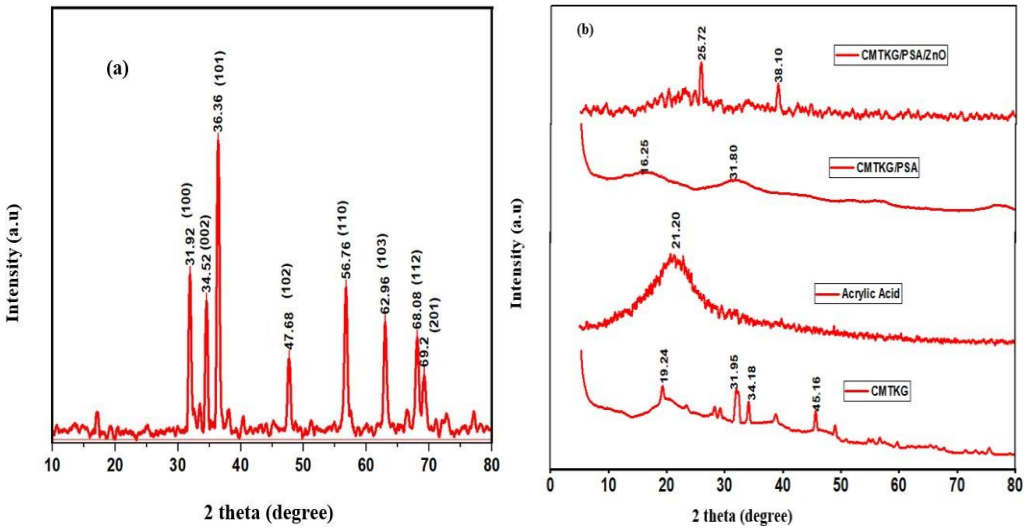

Figure 2.4: XRD plot of **(a)** ZnO NPs **(b)** CMTKG, acrylic acid, CMTKG/PSA and CMTKG/PSA/ZnO nanocomposite hydrogel

2.3.5.2. Surface plasmon resonance (SPR)

Surface plasmon resonance is a characteristic optical property of metal oxide nanoparticles. The optical properties of metallic nanoparticles are dependent on SPR. The plasmon term in SPR signifies the collective oscillation of free electrons within the inorganic nanoparticles and the width of the plasmon peak depends on the type, geometry, and size of the metal nanoparticles [34]. UV-visible absorbance spectra of the zinc oxide nanoparticles incorporated in hydrogel have been illustrated in **Figure 2.5.** which showed that these particles exhibited a strong, and sharp characteristic peak

at 364 nm. This has confirmed the successful synthesis of zinc oxide nanoparticles.

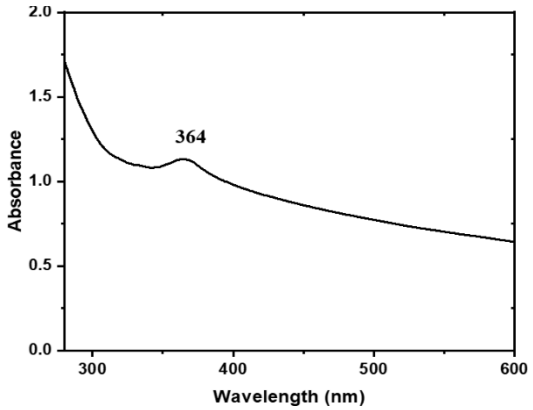

Figure 2.5: Surface plasma resonance (SPR) of ZnO NPs

2.3.5.3. FTIR Analysis

FTIR spectrum of CMTKG biopolymer as shown in **Figure 2.6a** indicated a broad peak at 3340 cm^{-1} for vibration of -OH group while the peaks at 1415 cm^{-1} and 1593 cm^{-1} were related to symmetric and asymmetric vibration of $-COO^-$ groups respectively. The peaks observed in the acrylic acid at 1633 cm^{-1} and 1718 cm^{-1} were related to C=C and C-O vibration respectively. The FTIR spectrum of PEGDA showed a band at 2676 cm^{-1} due to vibration of $-CH_2$ group, whereas the peaks at 1255 cm^{-1} and 864 cm^{-1} were attributed to the C-O stretching and C=C bending. In the FTIR spectrum of CMTKG/PSA hydrogels, there was an -OH stretching band at 3400 cm^{-1}, $-COO^-$ symmetric vibration band at 1415 cm^{-1}, and O-H bending vibration at 1400 cm^{-1}.

However, one common peak at 1415 cm^{-1} related to the vibration of $-COO^-$ groups was noticed in CMTKG, AA, PEGDA and CMTKG/PSA hydrogel. The FTIR spectrum (**Figure 2.6b)** for ZnO NPs showed a band at 644 cm^{-1} assigned to the stretching vibration of the Zn-O bond. However, due to the hygroscopic nature of ZnO NPs, a broad peak at 3302 cm^{-1} was observed which was assigned to the stretching of the hydroxyl group. The bands observed at 1514 and 1411 cm^{-1} in zinc oxide nanoparticles corresponded to the stretching vibration and asymmetric vibration of the -C=O group respectively [35]. FTIR spectra of ciprofloxacin drug as shown in **Figure 2b** showed the characteristic band at 1707 cm^{-1} corresponded to the C=O group, 3527 cm^{-1} due to vibration of O-H bond, 1448 cm^{-1} corresponded to C- N stretching vibration. However,

the presence of carboxylic acid was confirmed by the presence of the peak at 1271 cm^{-1} due to the bending vibration of the O-H group [36]. FTIR spectra of ZnO-loaded hydrogels showed a broad peak at 3400 cm^{-1} due to vibration of the -OH group. Other bands at 1392 cm^{-1} and 1566 cm^{-1} were assigned to the stretching of C-O and C=O stretching vibration of carboxylic acid. A peak at 644 cm^{-1} related to the vibration of ZnO bond was noticed in CMTKG/PSA/ZnO hydrogel indicating the loading of nanoparticles in the hydrogel matrix. Moreover, both peaks at 644 cm^{-1} and 1448 cm^{-1} related to characteristics of ZnO NPs and ciprofloxacin drug respectively were also present in CFX loaded CMTKG/PSA/ZnO nanocomposite hydrogel. However, some common peaks were noticed in the FTIR spectrum of ZnO, CFX drug, and drug-loaded CMTKG/PSA/ZnO nanocomposite. All the related peaks of ZnO nanoparticles were present in the ZnO-loaded hydrogels which confirmed the formation of nanocomposite hydrogel. In FTIR spectra of without drug and drug-loaded nanocomposite hydrogel, it was seen that all the related peaks of the drug were present in a drug-loaded hydrogel which signified the successful loading of the ciprofloxacin drug into the hydrogel matrix.

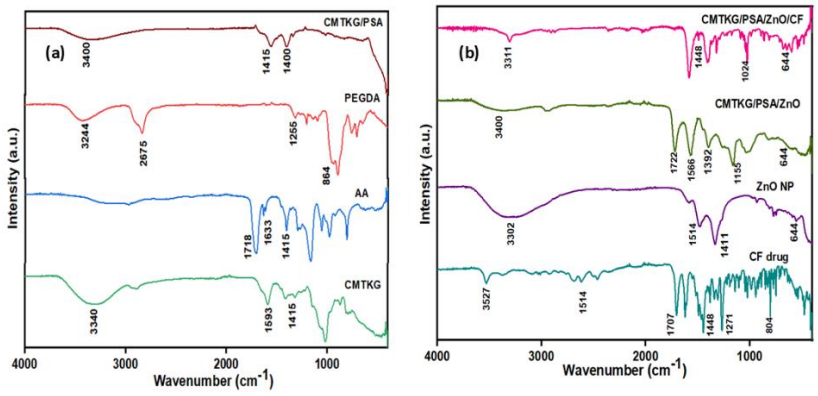

Figure 2.6: FTIR plots of **(a)** CMTKG, AA, PEGDA, and CMTKG/PSA hydrogel **(b)** CFX drug, ZnO NPs, CMTKG/PSA/ZnO, and CMTKG/PSA/ZnO/CFX hydrogel

2.3.5.4. FE-SEM analysis

The surface morphology of ZnO NPs, CMTKG/PSA, and CMTKG/PSA/ZnO nanocomposite hydrogels was studied by the FE-SEM analysis[38]. The surface morphology of ZnO NPs is shown in **Figure 2.7a** indicating that they have a flower-shaped morphology. However, the surface morphology of CMTKG/PSA hydrogel

showed a lot of interspatial voids and spongy surfaces as shown in **Figure 2.7b.** However, the surface morphology of CMTKG/PSA/ZnO nanocomposite showed that flower-shaped ZnO NPs were embedded in the polymeric hydrogel matrix. Moreover, the average size of ZnO nanoparticles was estimated using ImageJ software which was found as 118 nm. Moreover, EDX analysis was used to analyze the composition of various elements present in the synthesized hydrogel. It revealed the presence of Zn, Na, C, and O elements in the nanocomposite hydrogel as shown in **Figure 2.8.**

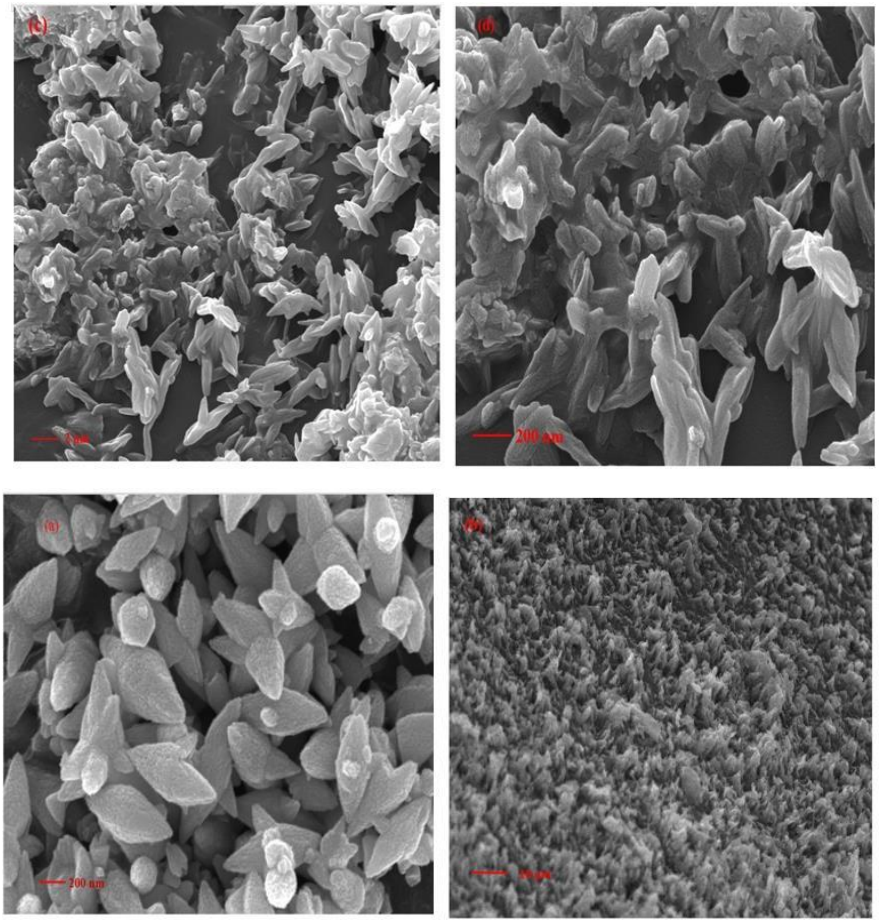

Figure 2.7: FE-SEM images of **(a)** ZnO NPs at 200 nm scale **(b)** CMTKG/PSA at 10µm scale **(c)** CMTKG/PSA/ZnO at 2 µm scale **(d)** CMTKG/PSA/ZnO at 200 nm scale

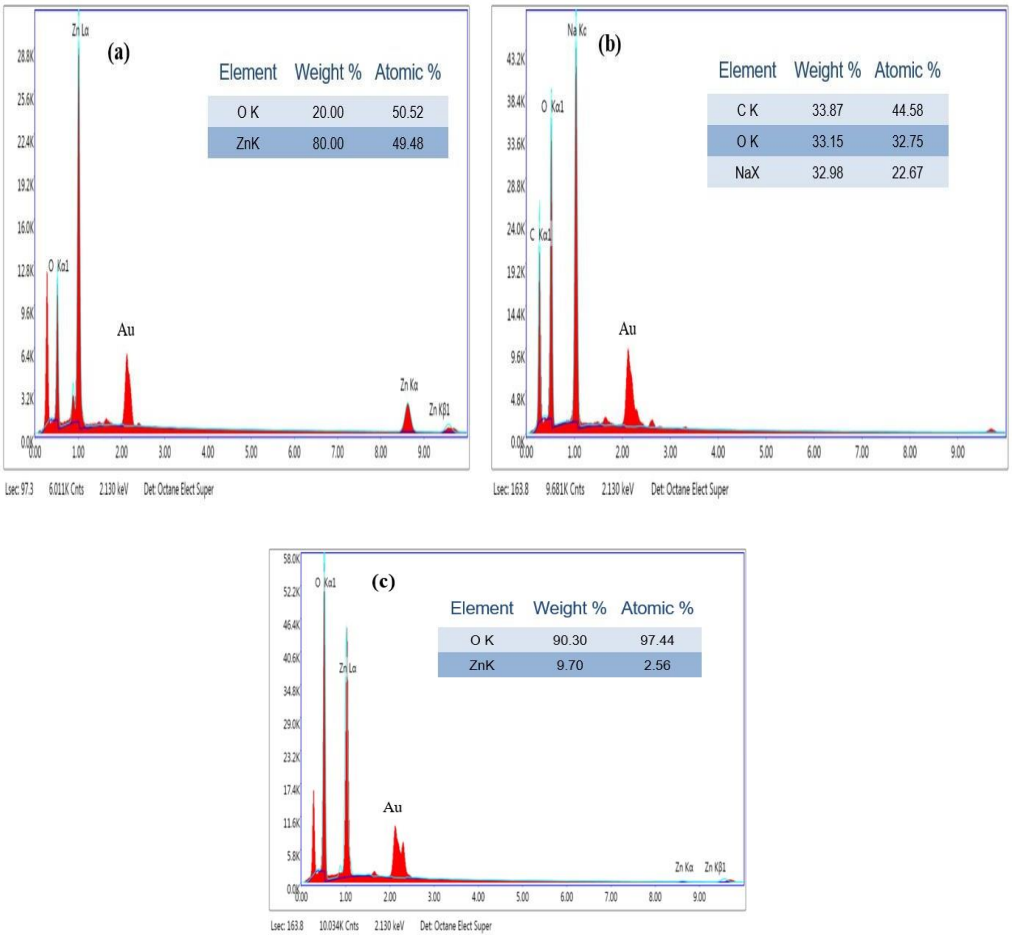

Figure 2.8: EDX analysis of (a) ZnO NPs (b) CMTKG/PSA hydrogel (c) CMTKG/PSA/ZnO nanocomposite hydrogel

2.3.5.5. TEM analysis

The TEM image of synthesized ZnO nanoparticles in **Figure 2.9a** showed that particles have aggregated spherical shapes. The average particle size of ZnO nanoparticles was estimated using ImageJ software to be 37 nm. However, the estimated particle size determined by XRD was equal to 20 nm which is in good agreement with the size determined by TEM analysis[39]. In the SAED pattern (**Figure 2.9b**), specific bright spots were observed which corresponded to the hexagonal wurtzite polycrystalline structure of ZnO NPs. The SAED pattern showed the diffraction peaks at (002), (310), (330), and (321) corresponded to ZnO nanoparticles. The interplanar spacing d (A°) was calculated for different regions of the SAED pattern using ImageJ software. The estimated value of d spacing (angstrom unit) is 3 Å, 2.38 Å, 1.95 Å and 1.46 Å for (310), (330), (321), and (002) planes respectively. However, a strong diffraction peak

at (002) plane in the XRD of ZnO NPs was consistent with their SAED pattern. Thus, both the characterizations confirmed the Wurtzite structure and synthesis of ZnO nanoparticles.

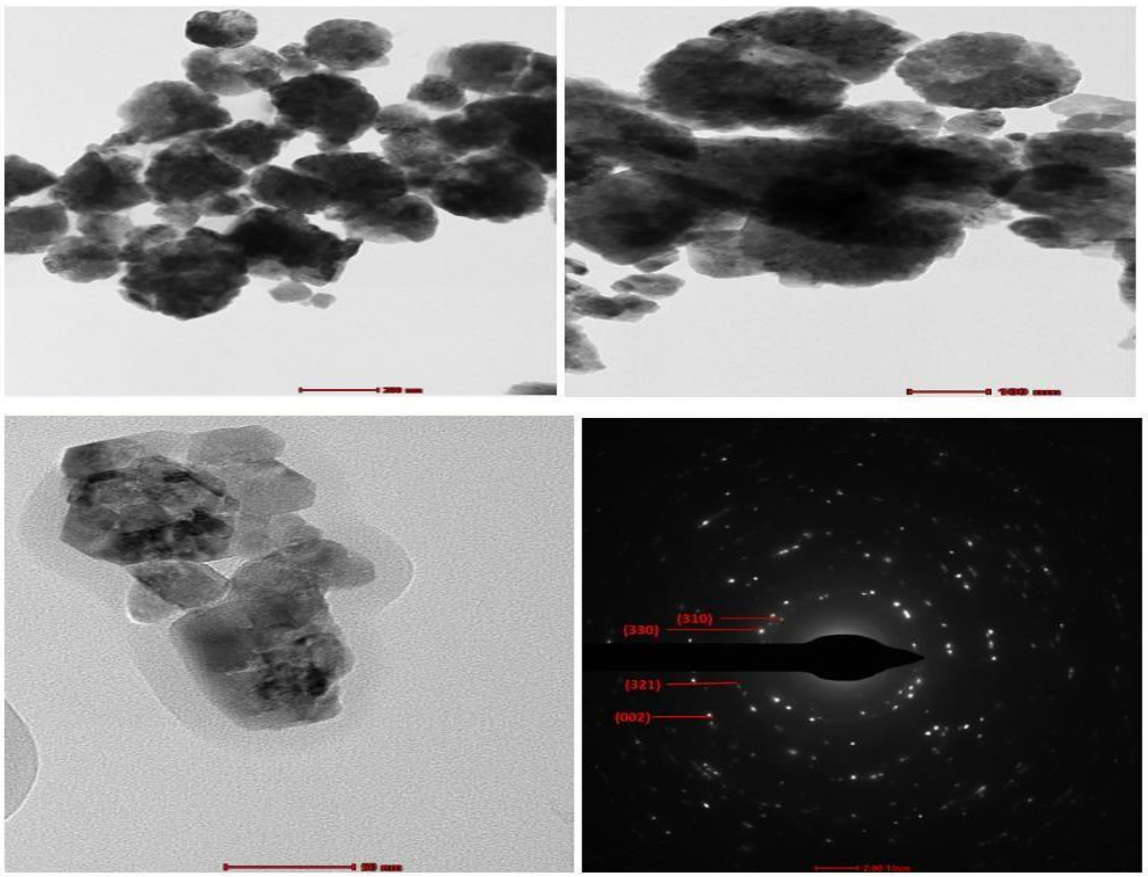

Figure 2.9: TEM micrograph of ZnO NPs at **(a)** 200 nm **(b)** 100 nm **(c)** 50 nm scales **(d)** SAED pattern

2.3.5.6. Zeta Potential measurement

The zeta potential was used to investigate the surface charges and stability of metallic nanoparticles. The zeta potential of produced zinc oxide nanoparticles was measured using ethanol as a dispersant as shown in **Figure 2.10**. In the present study, it was measured as 21.7mV which indicated the strong anionic behavior as well as the stability of the colloidal suspension of ZnO nanoparticles.

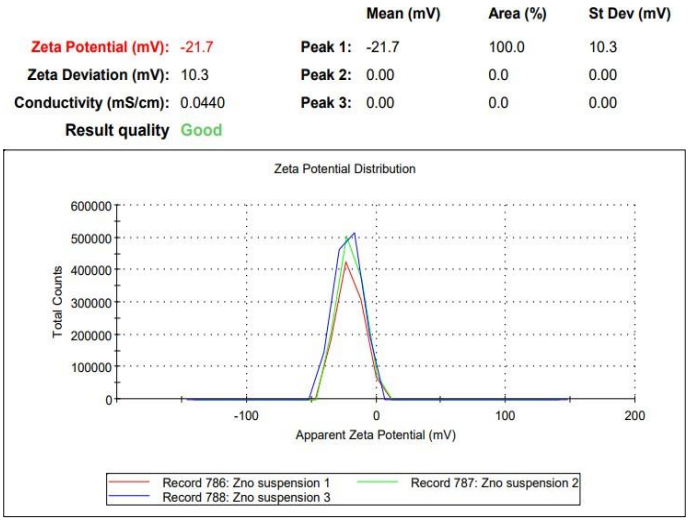

Figure 2.10: Zeta potential of synthesized ZnO nanoparticles

2.3.6. Rheological analysis

The rheological behavior of CMTKG/PSA hydrogel and CMTKG/PSA/ZnO nanocomposite hydrogel was studied based on change of storage modulus (G'), loss modulus (G''), and complex viscosity as a function of angular frequency. The storage modulus corresponded to the elastic component while the loss modulus corresponded to the viscous component. The storage modulus (G') of pure hydrogel and nanocomposite hydrogel is illustrated in **Figure 2.11(a).** It is observed that G' of nanocomposite hydrogel was higher than pure hydrogel. It indicated that the loading of ZnO NPs increased the cross-linking strength of hydrogel due to the physical interactions of these particles with the hydrogel polymeric network [40]. It was also observed that along with the storage modulus (G'), the loss modulus(G'') increased with an increase in the angular frequency from 1 Hz to 100 Hz as shown in **Figure 2.11(b).** At the lower frequency region, the value of loss modulus for pure hydrogel was higher than ZnO loaded hydrogels. The reason may be that there may be a possibility of the formation of a physical cross-links network in absence of zinc oxide nanoparticles at a lower frequency region[41]. However, the presence of zinc oxide nanoparticles provided more stability, rigidity, and thickness to the hydrogel matrix. It showed the pseudo-elastic behavior of nanocomposite hydrogel[42].

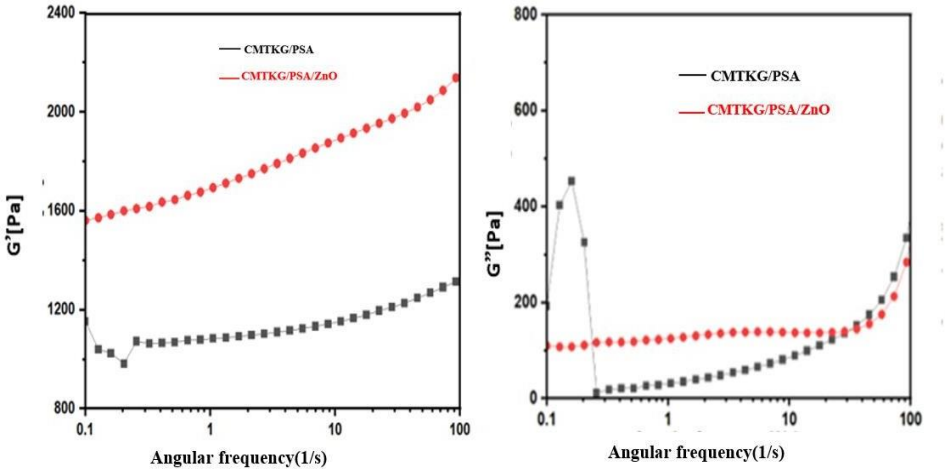

Figure 2.11: (a) Storage modulus (G') **(b)** Loss modulus (G'') of pure hydrogels and ZnO NPs embedded hydrogel nanocomposite

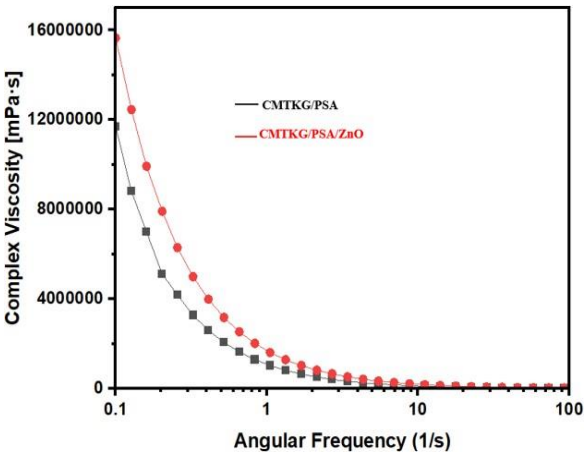

Figure 2.12: A plot of complex viscosity vs angular frequency

The decrease in value of complex viscosity with an increase in the angular frequency changes from 0.1 to 100 rad/s as shown in **Figure 2.12** indicated that hydrogels are pseudoplastic fluid and showed thixotropic behavior [43]. It was also found that the complex viscosity of ZnO NPs embedded hydrogel is higher than unloaded hydrogel because of the higher value of storage modulus (G') for nanocomposite hydrogel. Hence, ZnO loaded hydrogel act as better drug delivery carriers than pure hydrogel which was also confirmed by the values of DL (%) and DE (%) efficiency given in **Table 2.2**.

2.3.7. Antibacterial studies

Antibacterial performance of CMTKG/PSA, CMTKG/PSA-CFX, and CMTKG/ PSA/ ZnO-CFX were studied via a disc diffusion method against gram-negative *E. coli* (NCIMB-1) bacteria as shown in **Figure 2.13.** The zone of inhibition (mm) for hydrogel, drug-loaded hydrogel, and drug-loaded nanocomposite hydrogel was measured as shown in **Figure 2.14**. Ciprofloxacin was an antibiotic drug which would increase the bacteriostatic behavior of hydrogels. ZnO nanoparticles themselves exhibited antibacterial properties by interacting with the bacterial surface[44]. The loading of antibacterial ZnO NPs and ciprofloxacin drug increased the antibacterial action of hydrogels.

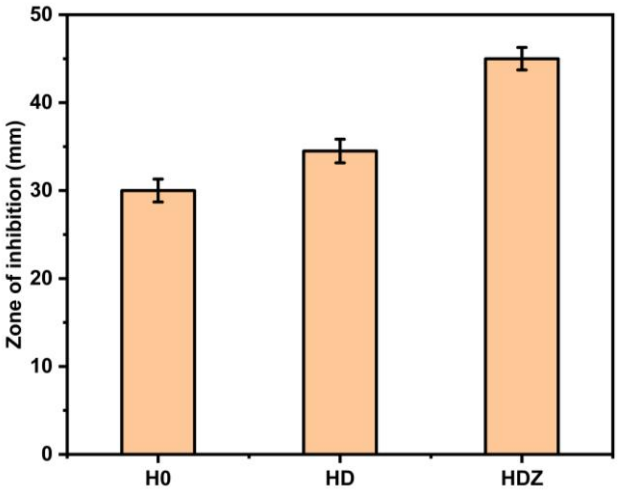

Figure 2.13: Size of the zone of inhibition (mm) exhibited by CMTKG/PSA hydrogel (H0), CMTKG/PSA-CFX (HD), and CMTKG/PSA/ZnO-CFX (HDZ) nanocomposite

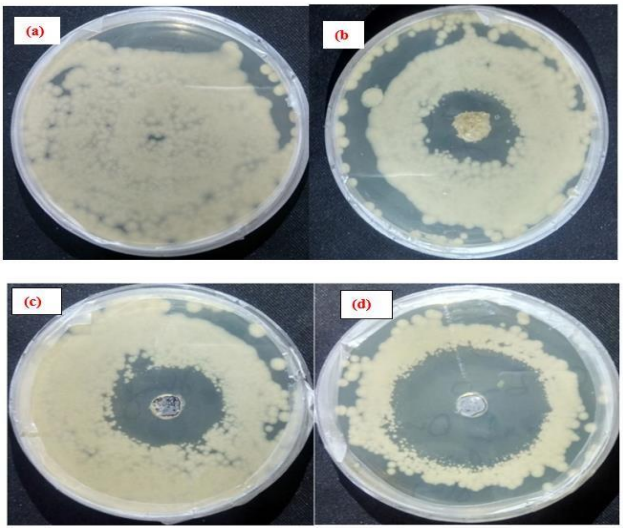

Figure 2.14: Antibacterial actions **(a)** blank sample **(b)** CMTKG/PSA **(c)** CMTKG/PSA- CFX **(d)** CMTKG/PSA/ZnO-CFX against *E. coli* bacteria.

2.3.8. Drug Release Studies

The release mode of ciprofloxacin drug from CMTKG/PSA hydrogels and ZnO-loaded nanocomposite hydrogel was illustrated in **Figure 2.15**. The drug release behavior of hydrogels was studied in physiological buffer solution of pH 7.4 at 37 ºC using a UV-Visible spectrophotometer. The drug release was performed for up to 9 hours and it was seen that after 6 hours, a plateau region of the drug release curve was observed. The release of ciprofloxacin drug was thus relying on the swelling of hydrogel[45]. The result concluded that ZnO loaded nanocomposite hydrogel showed more controlled release than pure hydrogel. This may be due to the knot-tying function of ZnO nanoparticles[31]. Thus, a chelated ring was formed via the interaction of zinc oxide nanoparticles with hydroxyl and carboxyl groups of CMTKG biopolymer[46]. As a result, it was difficult for the ciprofloxacin drug to release from such tightened network of nanocomposite hydrogel. Thus, ZnO loaded hydrogel showed a slow and controlled release of ciprofloxacin drug.

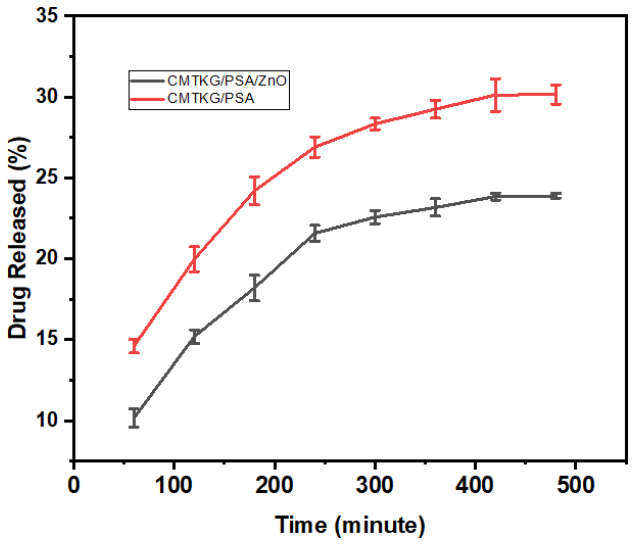

Figure 2.15: Drug release (%) with time of CMTKG/PSA and CMTKG/PSA/ZnO hydrogel nanocomposite

2.3.9. Drug Release Mechanism

The release of drug from the hydrogel matrix was studied with the help of Higuchi and Korsmeyer-Peppas models as shown in **Figure 2.16.** The Higuchi model is dependent on the Fickian diffusion process. It is useful to explain the release of hydrophilic and hydrophobic drugs from the polymeric system. The drug release mechanism in the case

of Korsmeyer- Peppas model is dependent on the diffusion exponent value [47].

The various parameters such as K, K_h, n, and R^2 were calculated using these models as shown in **Table 2.5.** Several physical and chemical phenomena affect the drug release kinetics such as swelling of hydrogel, mesh size, porosity, and chemical interaction of drug with polymers. The Higuchi model and Korsmeyer -Peppas models is expressed in given Equation (2.10) and Equation (2.11) respectively[48].

$$\frac{M_t}{M_\infty} = K_h . t^{0.5} \tag{2.10}$$

$$\frac{M_t}{M_\infty} = K_h . t^{n} \tag{2.11}$$

Where M_t represents the amount of drug released at t time and M_∞ represents the amount of drug released at equilibrium. K and K_h are rate constants for drug release corresponding to the Korsemeyer-Pepass and Higuchi models. The value of diffusion exponent n decided the mechanism of drug release. In this case, the value of n less or equal to 0.5 indicated Fickian, 1> n > 0.5 non-Fickian, and n =1 case II anomalous diffusion[18]. Since the calculated value of n for CMTKG/PSA hydrogel (E1) and ZnO-loaded hydrogel (E2) is less than 0.5, therefore drug release followed a Fickian law of diffusion. It clearly showed that drug release from hydrogel depends on purely diffusivity phenomena and for both samples, the solvent diffusion was higher than polymeric chain relaxation[49]. The value of R^2 was compared for CMTKG/PSA hydrogel and ZnO-loaded hydrogel. It was found that the drug release data was more fitted in the Korsmeyer-Peppas model.

Table 2.5: Model followed for drug release studies using ciprofloxacin loaded CMTKG/ PSA hydrogel (E1) and CMTKG/PSA/ZnO (E2) nanocomposite hydrogel

Sample	Different parameters associated with models for the drug release				
	Korsmeyer -Peppas Model			Higuchi Model	
	K	n	R^2	Kh	R^2
CMTKG/PSA	0.069	0.25	0.9951	0.060	0.9885
CMTKG/PSA/ZnO	0.042	0.32	0.9932	0.069	0.9921

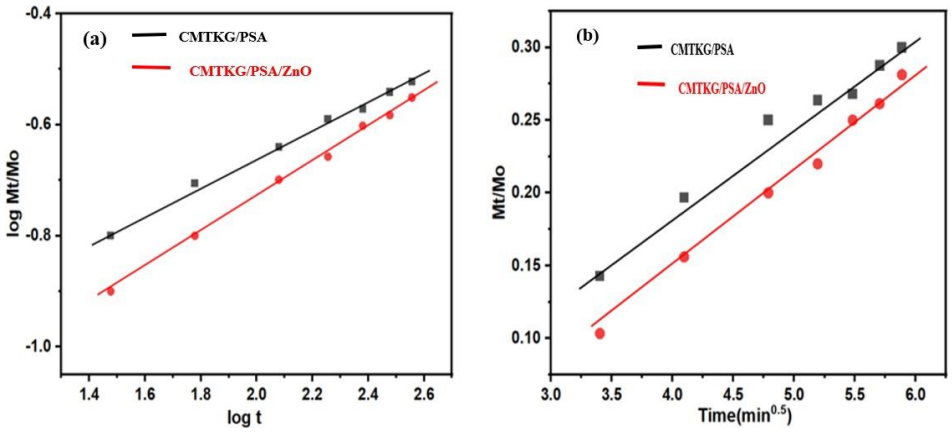

Figure 2.16: (a) Korsmeyer-Peppas model (b) Higuchi model for CMTKG/PSA and CMTKG/PSA/ZnO nanocomposite hydrogel

2.4. Conclusion

In this research work, ZnO NPs loaded CMTKG/PSA nanocomposite hydrogels were synthesized using a PEGDA cross-linker. ZnO NPs were formed via a hydrothermal method while the synthesis of CMTKG/PSA hydrogels was done through a free radical mechanism. The synthesized ZnO NPs and nanocomposite hydrogel were characterized using FTIR, XRD, FE-SEM, and TEM techniques. The swelling studies of hydrogels were performed at different pH solutions. The dynamic swelling data were fitted in the Power function model and Schott model. The result concluded that swelling data fitted more in the Schott model with R^2 value close to unity. The synthesized CMTKG/PSA hydrogel and ZnO-loaded nanocomposite hydrogel were used for *in-vitro* release studies of the ciprofloxacin drug. The various parameters such as porosity, drug loading, and entrapment efficiency of CMTKG/PSA hydrogel increased in the presence of ZnO NPs due to the knot typing function of ZnO NPs. Rheological studies for CMTKG/PSA hydrogel and ZnO-loaded hydrogels were performed. The results showed that the elasticity of CMTKG/PSA hydrogel was increased in the presence of ZnO NPs. The antibacterial studies against *E. coli* bacteria indicated that due to incorporation of antibacterial ZnO NPs, the antibacterial action of drug-loaded CMTKG/PSA hydrogels was increased. Additionally, the drug release results indicated that CMTKG/PSA/ZnO nanocomposite hydrogel showed a controlled and slow drug release than CMTKG/PSA hydrogel. The drug release kinetics concluded that the release of the drug from both CMTKG/PSA hydrogel and nanocomposite hydrogel was followed by Korsmeyer-Peppas model. In brief, the synthesized nanocomposite hydrogel could be a better candidate for the oral delivery of ciprofloxacin drug.

References

[1] G. R. Bardajee, F. Mizani, and S. S. Hosseini, "pH sensitive release of doxorubicin anticancer drug from gold nanocomposite hydrogel based on poly(acrylic acid) grafted onto salep biopolymer," *J. Polym. Res.*, vol. 24, no. 3, 2017, doi: 10.1007/s10965-017-1197-4.

[2] L. Ali, M. Ahmad, M. N. Aamir, M. U. Minhas, H. H. Shah, and M. A. Shah, "Cross- linked pH-sensitive pectin and acrylic acid-based hydrogels for controlled delivery of metformin," *Pak. J. Pharm. Sci.*, vol. 33, no. 4, pp. 1483–1491, 2020, doi: 10.36721/PJPS.2020.33.4.REG.1483-1491.1.

[3] N. Ajaz, I.U. Khan, I. Khalid, R.U. Khan, H.A. Khan, S. Asghar, S.H. Khalid, Y. Shahzad, A.M. Yousaf, T. Hussain and N. Sabir, 2020. "In vitro and toxicological assessment of dexamethasone sodium phosphate loaded pH sensitive Pectin-g-poly(AA)/PVP semi-interpenetrating network," *Mater. Today Commun.*, vol. 25, no. June, p. 101325, 2020, doi: 10.1016/ j.mtcomm.2020.101325.

[4] S. K. Ghosh, A. Das, A. Basu, A. Halder, S. Das, S. Basu, M. F. Abdullah, A. Mukherjee, and S. Kundu, "Semi-interpenetrating hydrogels from carboxymethyl guar gum and gelatin for ciprofloxacin sustained release," *Int. J. Biol. Macromol.*, vol. 120, pp. 1823–1833, 2018, doi: 10.1016/j.ijbiomac. 2018.09.212.

[5] V. F. Lotfy and A. H. Basta, "Optimizing the chitosan-cellulose based drug delivery system for controlling the ciprofloxacin release versus organic/inorganic crosslinker, characterization and kinetic study," *Int. J. Biol. Macromol.*, vol. 165, pp. 1496–1506, 2020, doi: 10.1016/j.ijbiomac. 2020.10.047.

[6] M. Rawooth, D. Qureshi, M. Hoque, M. G. Prasad, B. Mohanty, M. A. Alam, A. Anis,P. Sarkar, and K. Pal "Synthesis and characterization of novel tamarind gum and rice bran oil-based emulgels for the ocular delivery of antibiotics," *Int. J. Biol. Macromol.*, vol. 164, pp. 1608–1620, 2020, doi: 10.1016/j.ijbiomac.2020.07.231.

[7] Z. Naderi, J. Azizian, E. Moniri, and N. Farhadyar, "Synthesis and Characterization of Carboxymethyl Cellulose/β-Cyclodextrin/Chitosan Hydrogels and Investigating the Effect of Magnetic Nanoparticles (Fe3O4) on a Novel Carrier for a Controlled Release of Methotrexate as Drug Delivery," *J. Inorg. Organomet. Polym. Mater.*, vol. 30, no. 4, pp. 1339–1351, 2020, doi:

10.1007/s10904-019-01301-1.

[8] Khushbu, S. G. Warkar, and A. Kumar, "Synthesis and assessment of carboxymethyl tamarind kernel gum based novel superabsorbent hydrogels for agricultural applications," *Polymer (Guildf).*, vol. 182, no. July, p. 121823, 2019, doi: 10.1016/j.polymer.2019.121823.

[9] Khushbu and S. G. Warkar, "Potential applications and various aspects of polyfunctional macromolecule- carboxymethyl tamarind kernel gum," *Eur. Polym. J.*, vol. 140, no. September, p. 110042, 2020, doi: 10.1016/j.eurpolymj.2020.110042.

[10] K. K. Mali, S. C. Dhawale, and R. J. Dias, "Synthesis and characterization of hydrogel films of carboxymethyl tamarind gum using citric acid," *Int. J. Biol. Macromol.*, vol. 105, pp. 463–470, 2017, doi: 10.1016/j.ijbiomac.2017.07.058.

[11] S. Jana, R. Sharma, S. Maiti, and K. K. Sen, "Interpenetrating hydrogels of O-carboxymethyl Tamarind gum and alginate for monitoring delivery of acyclovir," *Int. J. Biol. Macromol.*, vol. 92, pp. 1034–1039, 2016, doi: 10.1016/j.ijbiomac.2016.08.017.

[12] H. Kaur, M. Ahuja, S. Kumar, and N. Dilbaghi, "Carboxymethyl tamarind kernel polysaccharide nanoparticles for ophthalmic drug delivery," *Int. J. Biol. Macromol.*, vol. 50, no. 3, pp. 833–839, 2012, doi: 10.1016/j.ijbiomac. 2011.11.017.

[13] X. Sun, C. Liu, A. M. Omer, W. Lu, S. Zhang, X. Jiang, H. Wu, D. Yu and X. K. Ouyang, "pH-sensitive ZnO/carboxymethyl cellulose/chitosan bio-nanocomposite beads for colon-specific release of 5-fluorouracil," *Int. J. Biol. Macromol.*, vol. 128, pp. 468–479, 2019, doi: 10.1016/j.ijbiomac.2019.01.140.

[14] R. Patwa, O. Zandraa, Z. Capáková, N. Saha, and P. Sáha, "Effect of iron-oxide nanoparticles impregnated bacterial cellulose on overall properties of alginate/casein hydrogels: Potential injectable biomaterial for wound healing applications," *Polymers (Basel).*, vol. 12, no. 11, pp. 1–21, 2020, doi: 10.3390/polym12112690.

[15] Y. Ahmadian, A. Bakravi, H. Hashemi, and H. Namazi, "Synthesis of polyvinyl alcohol/CuO nanocomposite hydrogel and its application as drug delivery agent," *Polym. Bull.*, vol. 76, no. 4, pp. 1967–1983, 2019, doi:10.1007/s00289-018-2477.

[16] K. Virk, K. Sharma, S. Kapil, V. Kumar, V. Sharma, S. Pandey and V. Kumar, "Synthesis of gum acacia-silver nanoparticles-based hydrogel composites and their comparative anti-bacterial activity," *J. Polym. Res.*, vol. 29, no. 4, pp. 1–15, 2022, doi: 10.1007/s10965-022-02978-8.

[17] M. T. Khorasani, A. Joorabloo, A. Moghaddam, H. Shamsi, and Z. Mansoorimoghadam, "International Journal of Biological Macromolecules Incorporation of ZnO nanoparticles into heparinized polyvinyl alcohol / chitosan hydrogels for wound dressing application," *Int. J. Biol. Macromol.*, vol. 114, pp. 1203– 1215, 2018, doi: 10.1016/j.ijbiomac.2018.04.010.

[18] G. A. Mahmoud, A. E. H. Ali, A. I. Raafat, N. A. Badawy, and M. F. Elshahawy, "Development of (acrylic acid/ polyethylene glycol)-zinc oxide mucoadhesive nanocomposites for buccal administration of propranolol HCl," *Radiat. Phys. Chem.*, vol. 147, no. July 2017, pp. 18–26, 2018, doi: 10.1016/j. radphyschem.2018.01.020.

[19] R. Priyadarshi, B. Kumar, and J. W. Rhim, "Green and facile synthesis of carboxymethylcellulose/ZnO nanocomposite hydrogels crosslinked with Zn2+ ions," *Int. J. Biol. Macromol.*, vol. 162, pp. 229–235, 2020, doi: 10.1016/j.ijbiomac.2020.06.155.

[20] D. H. Hanna and G. R. Saad, "Bioorganic Chemistry Encapsulation of ciprofloxacin within modified xanthan gum- chitosan based hydrogel for drug delivery," *Bioorg. Chem.*, vol. 84, no. October 2018, pp. 115–124, 2019, doi: 10.1016/j.bioorg.2018.11.036.

[21] K. Prusty, A. Biswal, S. B. Biswal, and S. K. Swain, "Synthesis of soy protein/polyacrylamide nanocomposite hydrogels for delivery of ciprofloxacin drug," *Mater. Chem. Phys.*, vol. 234, no. May, pp. 378–389, 2019, doi: 10.1016/j.matchemphys.2019.05.038.

[22] G. R. Mahdavinia, M. H. Karimi, M. Soltaniniya, and B. Massoumi, "In vitro evaluation of sustained ciprofloxacin release from κ-carrageenan-crosslinked chitosan/hydroxyapatite hydrogel nanocomposites," *Int. J. Biol. Macromol.*, vol. 126, pp. 443–453, 2019, doi: 10.1016/j.ijbiomac.2018.12.240.

[23] K. McAvoy, D. Jones, and R. R. S. Thakur, "Synthesis and Characterizations of

Photo crosslinked poly(ethylene glycol) diacrylate Implants for Sustained Ocular Drug Delivery," *Pharm. Res.*, vol. 35, no. 2, 2018, doi: 10.1007/s11095-017-2298-9.

[24] D. A. M. O. Osman and M. A. Mustafa, "Synthesis and Characterization of Zinc Oxide Nanoparticles using Zinc Acetate Dihydrate and Sodium Hydroxide," *J. Nanosci. Nanoeng.*, vol. 1, no. 4, pp. 248–251, 2015, [Online]. Available: http://www.aiscience.org/journal/jnnhttp://creativecommons.org/licenses/by-nc/4.0/.

[25] S. Jana, A. Banerjee, K. K. Sen, and S. Maiti, "Gelatin-carboxymethyl tamarind gum bio composites: In vitro characterization & anti-inflammatory pharmacodynamics," *Mater. Sci. Eng. C*, vol. 69, pp. 478–485, 2016, doi: 10.1016/j.msec.2016.07.008.

[26] S. K. Bajpai, M. Jadaun, and S. Tiwari, "Synthesis, characterization and antimicrobial applications of zinc oxide nanoparticles loaded gum acacia/poly(SA) hydrogels," *Carbohydr. Polym.*, vol. 153, pp. 60–65, 2016, doi: 10.1016/j.carbpol.2016.07.019.

[27] M. V. Nagarpita, P. Roy, S. B. Shruthi, and R. R. N. Sailaja, "Synthesis and swelling characteristics of chitosan and CMC grafted sodium acrylate-co-acrylamide using modified nanoclay and examining its efficacy for removal of dyes," *Int. J. Biol. Macromol.*, vol. 102, pp. 1226–1240, 2017, doi: 10.1016/j.ijbiomac.2017.04.099.

[28] K. Kalantari, E. Mostafavi, B. Saleh, P. Soltantabar, and T. J. Webster, "Chitosan/PVA hydrogels incorporated with green synthesized cerium oxide nanoparticles for wound healing applications," *Eur. Polym. J.*, vol. 134, no. June, p. 109853, 2020, doi: 10.1016/j.eurpolymj.2020.109853.

[29] S. Batool, Z. Hussain, M. B. K. Niazi, U. Liaqat, and M. Afzal, "Biogenic synthesis of silver nanoparticles and evaluation of physical and antimicrobial properties of Ag/PVA/starch nanocomposites hydrogel membranes for wound dressing application," *J. Drug Deliv. Sci. Technol.*, vol. 52, no. April, pp. 403–414, 2019, doi: 10.1016/j.jddst.2019.05.016.

[30] S. Ganguly and N. C. Das, "Synthesis of a novel pH responsive phyllosilicate loaded polymeric hydrogel based on poly (acrylic acid-co-N-vinylpyrrolidone) and

polyethylene glycol for drug delivery: modelling and kinetics study for the sustained release of an antibiotic drug." *RSC Advances*, 2015, *5*(24), pp.18312-18327.

[31] A. Tanwar, P. Date, and D. Ottoor, "ZnO NPs incorporated gelatin grafted polyacrylamide hydrogel nanocomposite for controlled release of ciprofloxacin," *Colloid Interface Sci. Commun.*, vol. 42, no. December 2020, p. 100413, 2021, doi: 10.1016/j.colcom.2021.100413.

[32] I. Gholamali and M. Yadollahi, "Doxorubicin-loaded carboxymethyl cellulose/Starch/ZnO nanocomposite hydrogel beads as an anticancer drug carrier agent," *Int. J. Biol. Macromol.*, vol. 160, pp. 724–735, 2020, doi: 10.1016/j.ijbiomac.2020.05.232.

[33] S. R. Brintha and M. Ajitha, "Synthesis and characterization of ZnO nanoparticles via aqueous solution, sol-gel and hydrothermal methods," *IOSR J. Appl. Chem.*, vol. 8, no. 11, pp. 66–72, 2015, doi: 10.9790/5736-081116672.

[34] M. A. Islam and I. Khan, "ZnO/Ag Composite Nanoparticles for Surface Plasmon Resonance Based Sensor Application in UV-Vis Region," *Int. J. Adv. Res. Technol.*, vol. 1, no. 5, 2012.

[35] S. Nilavazhagan, D. Anbuselvan, A. Santhanam, and N. Chidhambaram, "Effect of an alkali hydroxide concentration on the structural, optical, and surface morphological properties of ZnO nanoparticles," *Appl. Phys. A Mater. Sci. Process.*, vol. 126, no. 4, pp. 1–8, 2020, doi: 10.1007/s00339-020-3462-3.

[36] R. Nithya and N. Meenakshi Sundaram, "Biodegradation and cytotoxicity of ciprofloxacin-loaded hydroxyapatite-polycaprolactone nanocomposite film for sustainable bone implants," *Int. J. Nanomedicine*, vol. 10, no. October 2015, pp. 119– 127, 2015, doi: 10.2147/IJN.S79995.

[37] S. A. Sadeek, W. H. El-Shwiniy, W. A. Zordok, and A. M. El-Didamony, "Spectroscopic, structure and antimicrobial activity of new Y(III) and Zr(IV) ciprofloxacin," *Spectrochim. Acta - Part A Mol. Biomol. Spectrosc.*, vol. 78, no. 2, pp. 854–867, 2011, doi: 10.1016/j.saa.2010.12.048.

[38] A. C. Mohan and B. Renjanadevi, "Preparation of Zinc Oxide Nanoparticles and

its Characterization Using Scanning Electron Microscopy (SEM) and X-Ray Diffraction(XRD)," *Procedia Technol.*, vol. 24, pp. 761–766, 2016, doi: 10.1016/j.protcy.2016.05.078.

[39] V. Srivastava, D. Gusain, and Y. C. Sharma, "Synthesis, characterization and application of zinc oxide nanoparticles (n-ZnO)," *Ceram. Int.*, vol. 39, no. 8, pp. 9803– 9808, 2013, doi: 10.1016/j.ceramint.2013.04.110.

[40] S. Murali, S. Kumar, J. Koh, S. Seena, P. Singh, A. Ramalho and A. J. Sobral "Bio- based chitosan/gelatin/Ag@ZnO bio nanocomposites: synthesis and mechanical and antibacterial properties," *Cellulose*, vol. 26, no. 9, pp. 5347–5361, 2019, doi: 10.1007/s10570-019-02457-2.

[41] M. Arab, M. Jallab, M. Ghaffari, E. Moghbelli, and M. R. Saeb, "Synthesis, rheological characterization, and antibacterial activity of polyvinyl alcohol (PVA)/ zinc oxide nanoparticles wound dressing, achieved under electron beam irradiation, *"Iran. Polym. J. (English Ed.*, vol. 30, no. 10, pp. 1019–1028, 2021, doi: 10.1007/s13726-021-00952-7.

[42] K. Prusty, S. Patra, and S. K. Swain, "Nano ZnO imprinted dextran hybrid poly (N- isopropylacrylamide)/poly ethylene glycol composite hydrogels for in vitro release of ciprofloxacin," *Mater. Today Commun.*, vol. 26, no. December 2019, 2021, doi: 10.1016/j.mtcomm.2020.101869.

[43] A. Nanodispersion, F. Cuomo, M. Cofelice, and F. Lopez, "Rheological Characterization of Hydrogels from," 2019, doi: 10.3390/polym11020259.

[44] A. Sirelkhatim, S. Mahmud, A. Seeni, N.H.M. Kaus, L.C. Ann, S.K.M. Bakhori, H. Hasan and D. Mohamad "Review on zinc oxide nanoparticles: Antibacterial activity and toxicity mechanism," *Nano-Micro Lett.*, vol. 7, no. 3, pp. 219–242, 2015, doi: 10.1007/s40820-015-0040-x.

[45] M. K. Younis, A. Z. Tareq, and I. M. Kamal, "Optimization of Swelling, Drug Loading and Release from Natural Polymer Hydrogels," *IOP Conf. Ser. Mater. Sci. Eng.*, vol. 454, no. 1, 2018, doi: 10.1088/1757-899X/454/1/012017.

[46] Z. Zare-Akbari, H. Farhadnejad, B. Furughi-Nia, S. Abedin, M. Yadollahi, and

M. Khorsand-Ghayeni, "PH-sensitive bio nanocomposite hydrogel beads based on caborboxymethyl cellulose/ZnO nanoparticle as drug carrier," *Int. J. Biol. Macromol.*, vol. 93, pp. 1317–1327, 2016, doi: 10.1016/j.ijbiomac.2016.09.110.

[47] M. A. Lungan, M. Popa, S. Racovita, G. Hitruc, F. Doroftei, J. Desbrieres and S. Vasiliu, "Surface characterization and drug release from porous microparticles based on methacrylic monomers and xanthan," *Carbohydr. Polym.*, vol. 125, pp. 323–333,2015, doi: 10.1016/j.carbpol.2015.02.058.

[48] J. David and B. Mahanty, "Optimized ciprofloxacin release from citric acid crosslinked starch - PVA hydrogel film : modelling with mixture design," *J. Polym. Res.*, pp. 1– 11, 2021, doi: 10.1007/s10965-020-02397-7.

[49] I. Permanadewi, A. C. Kumoro, D. H. Wardhani, and N. Aryanti, "Modelling of controlled drug release in gastrointestinal tract simulation," *J. Phys. Conf. Ser.*, vol. 1295, no. 1, 2019, doi: 10.1088/1742-6596/1295/1/012063.

CHAPTER 3

A SILVER NANOPARTICLE EMBEDDED TAMARIND KERNEL GUM AND POLY(SODIUM ACRYLATE) NANOCOMPOSITE HYDROGELS FOR CONTROLLED RELEASE OF DOXYCYCLINE DRUG

3.1. Introduction

Hydrogels can uptake large quantities of water due to the presence of various hydrophilic functional groups. The composite hydrogel can be synthesized by loading various inorganic materials such as zeolite [1], silica[2], metal nanoparticles[3], etc. Nanocomposite hydrogels can be used for different applications in the drug delivery fields. It was found that various noble metals such as silver [4], gold [5], and platinum[6]-based nanoparticles can be used in the biomedical field. However, the researchers have focused on the synthesis of biocompatible nanoparticles. Out of many nanoparticles, silver nanoparticles (Ag NPs) based nanocomposite hydrogels have gained significant research attention from the last few decades [7]. Because of their cytotoxic effects on living systems, silver nanoparticles cannot be employed directly for biomedical applications. Consequently, to prevent NPs from penetrating into living systems, they should be integrated into a polymer matrix prior to use in any biomedical application. Therefore, Ag NPs were incorporated into the hydrogel to increase properties such as electrical conductivity, optical properties, mechanical toughness, high deformability, and transparency [8]. However, the uniform dispersion of Ag NPs without any formation of aggregation can be achieved by embedding Ag^{+} ions into a hydrogel matrix and reduction using reducing agent like sodium borohydride. These reagents are highly toxic and they can reduce the efficiency of Ag-loaded hydrogels. Therefore, the green synthesis is more preferred to synthesize Ag NPs using biocompatible biopolymers[9]. There are many reported methods to synthesize Ag NPs. However, for the in-situ synthesis of Ag NPs, hydrogels can be used as porous templates with controlled size and appropriate stability[10]. Biopolymers based hydrogel acts as a reducing and stabilizing agent for the silver ions. Therefore, biopolymer-based nanocomposites hydrogel is widely used in the biomedical applications due to their biocompatible and biodegradable properties. Various biopolymer such as sodium

alginate, pectin, chitosan, and guar gum [11] have been used for the development of nanocomposite hydrogels. Till the date, tamarind kernel gum (TKG) has not been explored for the various applications. In a study, tamarind gum-co-poly(acrylamidoglycolic acid) and their silver nanocomposite hydrogel were used for release study of doxorubicin drug[11]. In another research, the co-precipitation method was used to fabricate the nano-hydroxyapatite/chitosan-tamarind seed nanocomposite for bone tissue engineering[12].

In the present study, TKG and poly (sodium acrylate) (PSA) hydrogel was synthesized through a free radical chain polymerization mechanism. Additionally, Ag NP-loaded TKG/PSA nanocomposite hydrogel was used in biomedical applications. TKG is a non-toxic, biodegradable, and biocompatible polymer used in medical applications due to its viscosity-modulating properties[13]. TKG contains β-(1,4)-D-glucan with chains of α- (1,4)-D-xylopyranose and glucose residue linked with β-D-glucopyranosyl-(1,2)-α-D-xylopyranose[14]. TKG can increase the mucoadhesive properties of hydrogels. Recently, researches have been devoted to synthesize the metal nano-particle containing nanocomposite hydrogel. In a study, M. Sabzi et.al., have synthesized PVA/Citric acid/ Ag nanocomposite hydrogel for the release study of ciprofloxacin drug[15]. The Ag-based nanocomposite hydrogels have been used for increasing the antimicrobial properties of hydrogels due to their large surface area, non-toxic behavior, and high fraction of surface atoms [16]. The Ag-based nanocomposite hydrogel exhibited excellent antibiotic properties[17]. In the present study, the doxycycline drug was used as a model drug. Doxycycline as a member of the semi- synthetic tetracycline group is a broad-spectrum drug (**Figure 3.1**). Doxycycline is a water soluble, non-toxic, and inexpensive drug. It has a half-life of 18 to 22 hours. It is administered to treat acute A. phagocytophilum, malaria prophylaxis, and falciparum malaria[18]. It can rapidly diffuse into many body parts but its high concentration can be excreted in unchanged medicine form from the urine. It is used to treat many bacterial infections by affecting gram-positive bacteria, gram-negative bacteria, and other parasites[19]. Doxycycline can be embedded into nanocomposite hydrogels which increases the antibacterial capacity of nanocomposite hydrogels. Due to this property, these nanocomposite hydrogels have a potential application in wound dressing applications[20]. In this

research work, Ag NPs loaded TKG/PSA nanocomposite hydrogel was synthesized through a free-radical mechanism. The synthesized nanocomposite hydrogel was characterized using UV-visible, XRD, FTIR, FE-SEM, and TEM techniques. The dynamic swelling data of TKG/PSA hydrogel and Ag/TKG/PSA nanocomposite hydrogel was fitted in the Power function model and Schott model. The effect of silver nanoparticles on the gel fraction of TKG/PSA was also evaluated.

Doxycycline drug was used as a model drug for release using Ag/TKG/PSA nanocomposite hydrogel at physiological pH 7.4 and pH 1.2 buffer solution. The drug release kinetics were performed using the Korsmeyer-Peppas and Higuchi model. Moreover, the cytotoxicity analysis of Ag/TKG/PSA hydrogel was carried out using an MTT assay against CCD 841 CoN cell lines.

3.2. Experimental

3.2.1. Materials

Silver nitrate ($AgNO_3$) was used as a precursor for the synthesis of Ag NPs. Tamarind Kernel gum (TKG, Courtesy Hindustan Gum Limited, Rewari), Acrylic acid (AA, CDH), Sodium hydroxide (NaOH Fischer Scientific, Mumbai), Potassium persulfate (KPS, Fischer scientific), *N*, *N*'- Methylenebisacrylamide (MBA, Merck Germany), Doxycycline (Merck India) were used. Double Distilled water was used to perform the experiments.

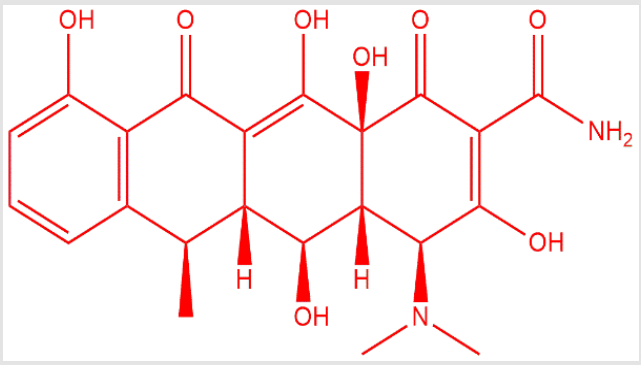

Figure 3.1: Structure of Doxycycline drug

3.2.2. Synthesis of Ag/TKG/PSA nanocomposite hydrogel

TKG/PSA hydrogel was synthesized through a free radical chain polymerization mechanism. Initially, 0.25 g of tamarind kernel gum (TKG) was added to 15 mL of double distilled water in a beaker and continuously stirred for 20 minutes. After the complete uniform dispersion of TKG, 5 mL of acrylic acid along with sodium hydroxide (2.5 g) solution was added to the reaction mixture and stirred for 25 minutes. Then, 0.15 g of KPS initiator, and 0.25 g of *N, N'*- MBA were added to the above solution with a constant stirring for 20 minutes till a viscous and homogenous fluid system was achieved. After that, the content of the beaker was poured into test tubes and placed in a water bath at 60 °C for 3 hours. A similar procedure was adopted to synthesize the Ag/TKG/PSA nanocomposite hydrogel. In this case, after complete dispersion of TKG and acrylic acid, 25 mM $AgNO_3$ solution was added into the continuously stirred beaker and stirred until a yellowish-brown color was obtained. Thus, the Ag NPs embedded hydrogel was obtained by breaking the test tubes and named Ag/TKG/PSA nanocomposite hydrogel as shown in **Figure 3.2.**

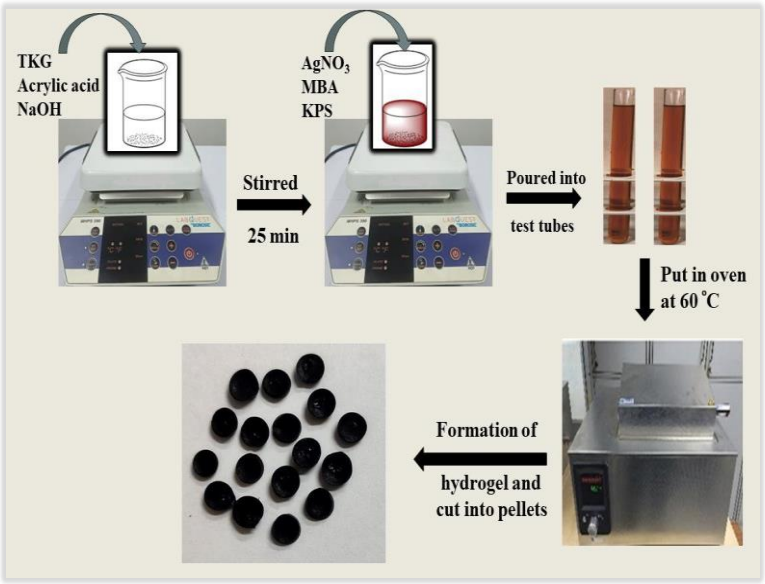

Figure 3.2: Layout of synthesis of Ag/TKG/PSA nanocomposite hydrogel

3.2.3. Swelling Analysis

To determine the water uptake capacity of TKG/PSA hydrogel and Ag/TKG/PSA nanocomposite hydrogel, swelling studies were performed gravimetrically. Initially, a

fixed amount of hydrogel was transferred in 50 mL buffer solutions of pH 7.4 and pH 1.2. The weight of the swollen hydrogel was measured at different time intervals until the constant weight of the hydrogel was achieved. Thus, the swelling ratio (g/g) was determined using the given Equation (3.1)[7].

$$SR\ (g/g) = \frac{W_s - W_0}{W_0} \tag{3.1}$$

Where W_s indicates the mass of hydrogel taken after t time and W_0 indicates the mass of the dried hydrogel. Moreover, various models such as the Power function model (first-order) and the Schott model (second-order)[21] were used to study the kinetics of dynamic swelling of TKG/PSA hydrogel and Ag/TKG/PSA nanocomposite hydrogel using the given **Equation (3.2)** and **(3.3)** respectively. In the power function model, M_∞ is the highest swelling ratio and M_t is the swelling ratio with respect to time t. The value of k signifies the gel characteristics of the hydrogel matrix. However, in the Schott model, M_∞ indicates the theoretical value of the highest swelling ratio.

$$\frac{M_t}{M_\infty} = k.t^n \tag{3.2}$$

$$\frac{t}{Mt} = \frac{1}{k_2 M^2{}_\infty} + \frac{t}{M_\infty} \tag{3.3}$$

3.2.4. Gel content

The gel content of TKG/PSA hydrogel and Ag/TKG/PSA nanocomposite hydrogel was determined to evaluate the cross-linked content present in the polymeric network. To determine the gel content, a dried hydrogel sample (W_1) was allowed to swell in distilled water up to the equilibrium swelling at room temperature. Afterward, the swollen sample was withdrawn from distilled water, dried in the oven and reweighed (W_2) till constant weight. The gel content (%) was computed using the given Equation (3.4)[22].

$$\text{Gel Content (\%)} = \frac{W_2}{W_1} \times 100 \tag{3.4}$$

3.2.5. Doxycycline loading and entrapment efficiency

To determine the maximum loading of doxycycline drug into the nanocomposite hydrogel, a fixed amount of Ag/TKG/PSA nanocomposite hydrogel (Wi) was placed in a 100 mL phosphate buffer saline solution (pH 7.4) containing a specific amount (W_0) of doxycycline drug. After 48 hours, nanocomposite hydrogel was taken out from the buffer solution, initially dried at room temperature, and then dried in an oven for 48 hours at 60 °C and weighed (W_d) till constant weight. Thus, percent drug loading (DL%) and percent drug entrapment efficiency (DE%) were determined using Equation (3.5) and (3.6) respectively[23].

$$\% \text{ DL (mg/g)} = \frac{W_d - W_i}{W_i} \times 100 \tag{3.5}$$

$$\% \text{ DE (mg/g)} = \frac{W_d - W_i}{W_o} \times 100 \tag{3.6}$$

3.2.6. Characterizations

X-ray diffraction (XRD) analysis of TKG/PSA and Ag/TKG/PSA nanocomposite was carried over a range of angles from 0-80^O with a scan rate of 1 sec/step using a Bruker instrument. The Zeta potential of TKG/PSA hydrogel and Ag/TKG/PSA nanocomposite hydrogel was studied using a Zetasizer (Model ZSP, Malvern instrument, UK). Surface plasma resonance (SPR) of Ag NPs was studied using a UV-visible spectrophotometer. Fourier Transform infrared resonance (FTIR) spectra were recorded for TKG/PSA and Ag/TKG/PSA nanocomposite hydrogel over a frequency range from 400 cm^{-1} to 4000 cm^{-1} using a Perkin-Elmer spectrum model. Moreover, the field emission scanning electron microscope (FE-SEM) along with EDX were studied to compare the surface morphology of TKG/PSA and Ag/TKG/PSA nanocomposite using the ZEISS EVO model. Also, TEM imaging of silver nanocomposite hydrogel was captured with a TECNAI G 20 (200 kv) instrument to determine the shape and the average particle size of silver nanoparticles.

3.2.7. In vitro drug Release

The drug release study of the doxycycline drug was executed in buffer solutions of pH 7.4 and pH 1.2 at 37 ºC in the incubator. For this purpose, a fixed amount of drug-loaded Ag/TKG/PSA nanocomposite hydrogel in powdered form was placed in 50 mL of phosphate buffer solution (PBS) of pH 7.4 and subjected to constant shaking at 100 rpm. Then, the absorbance of the drug-released supernatant solution (2 mL) was measured using a UV-visible spectrophotometer at a maximum wavelength of 274 nm after a regular interval of time. Thus, the amount of drug release was determined using the given **Equation (3.7)[**15].

$$\text{Doxycycline release (\%)} = \frac{A_t}{A_0} \times 100 \tag{3.7}$$

Where A_t is the amount of drug released at any time and A_0 is the amount of drug loaded in the nanocomposite hydrogel.

3.2.8. Release kinetic analysis

Various models such as the Korsmeyer-Peppas model, First-order, and Higuchi model [16] have been reported for the determination of the release kinetic studies of drugs from nanocomposite hydrogel as a function of time. The doxycycline release data at both pH 7.4 and pH 1.2 were fitted in these models to understand the release mechanism. The best-fit model was selected based on the highest value of the coefficient of determination (R^2). The first-order model represented by **Equation (3.8)** depends only on the amount of drug as a reactant. Here, $\frac{M_t}{M_\infty}$ signifies the fraction of drug released with respect to time. However, K_1 indicates the First-order rate constant. In case of Higuchi model expressed in Eq.(3.9) signifies the diffusion of the drug from the insoluble polymeric matrix. In this model, K_H indicates the Higuchi release rate constant. However, in Korsmeyer-Peppas model given by Eq.(3.10), the value of diffusion exponent (n) signifies the type of drug release mechanism. In the case when $n < 0.45$, indicate Fickian diffusion, if $0.45 \leq n \leq 0.89$, indicate non-Fickian diffusion, and if $n > 0.89$, indicate super case II[24].

$$\log\left(1 - \frac{M_t}{M_\infty}\right) = K_1 . \frac{t}{2.303} \tag{3.8}$$

$$\frac{M_t}{M_\infty} = K_H . t^{0.5} \tag{3.9}$$

$$\frac{M_t}{M_\infty} = K.t^n \qquad (3.10)$$

3.2.9. MTT assay

The cytotoxicity analysis of Ag/TKG/PSA nanocomposite hydrogel against CCD 841 CoN cell lines (procured from the National Centre for Cell Science, Pune) was determined by MTT assay [43]. The cells (10000 cells/well) were cultured in 96 well plates for 24 h in DMEM medium (Dulbecco's Modified Eagle Medium-AT149-1L) supplemented with 10% FBS (Fetal Bovine Serum - HIMEDIA-RM 10432) and 1% antibiotic solution at 37°C with 5% CO_2. The next day, cells were treated with different concentrations (0, 1, 10, 50, 100, 250, 500, 1000 µg/ml). Cells without treatment were considered as Control and cells without MTT were considered as Blank. After incubation for 24 hours, MTT solution was added to cell culture and further incubated for 2 h. At the end of the experiment, the culture supernatant was removed, and the cell layer matrix was dissolved in 100 µl Dimethyl Sulfoxide and read in an Elisa plate reader (iMark, Biorad, USA) at 540 nm and 660 nm wavelength.

3.3. Results and discussion

3.3.1. Mechanism of TKG/PSA hydrogel synthesis

TKG/PSA hydrogels were formed by a free radical chain polymerization mechanism[25]. Here, potassium persulfate (free radical initiator) was decomposed and produced sulfate radicals at 60 ºC. These radicals initiated the polymerization of sodium acrylate by breaking the vinyl bond of sodium acrylate and produces the radicals of sodium acrylate and the chain propagation step continued which led the formation of poly (sodium acrylate). These radicals of sodium acrylate abstracted hydrogen atoms of the -OH group present on the backbone of TKG and linked with the vinyl bond present at the terminal position of the *N, N'*- MBA cross-linker. The other end of *N, N'*-MBA has cross-linked with the PSA as shown in Figure 3.3.

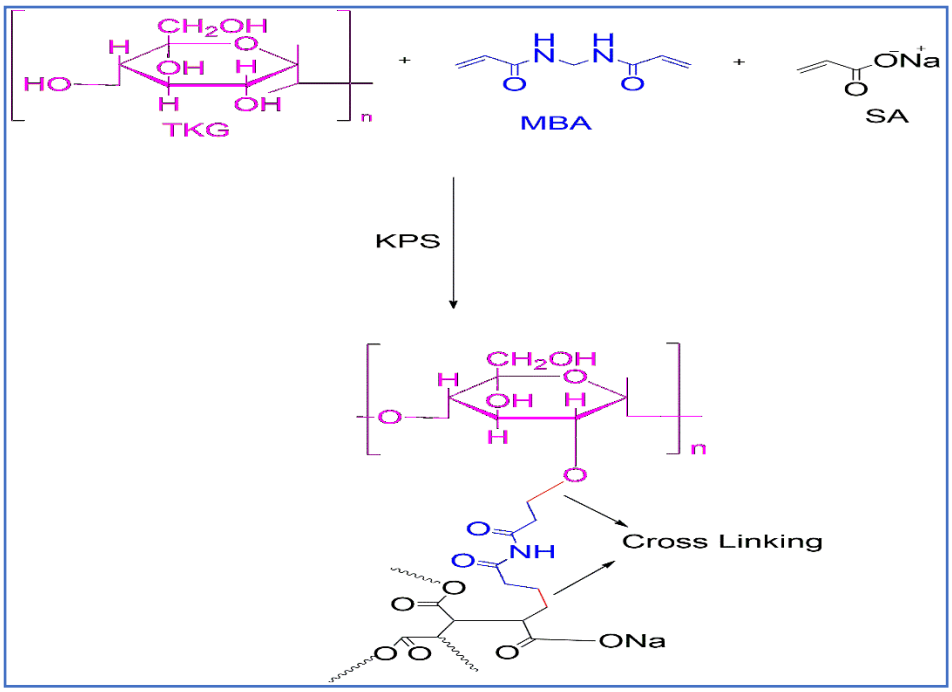

Figure 3.3: Mechanism of synthesis of TKG/PSA hydrogel

3.3.2. XRD analysis

This technique was used to evaluate the structural properties of synthesized TKG/PSA hydrogel and Ag/TKG/PSA nanocomposite hydrogel (**Figure 3.4.).** XRD of TKG/PSA hydrogel showed a broad peak at 2θ value of 22.84° due to the amorphous nature of hydrogel[26]. However, XRD of Ag/TKG/PSA nanocomposite hydrogel showed peaks at 32.2°, 38.12°, and 46.20° related to (110), (200), and (220) crystalline planes of silver nanoparticles [27].

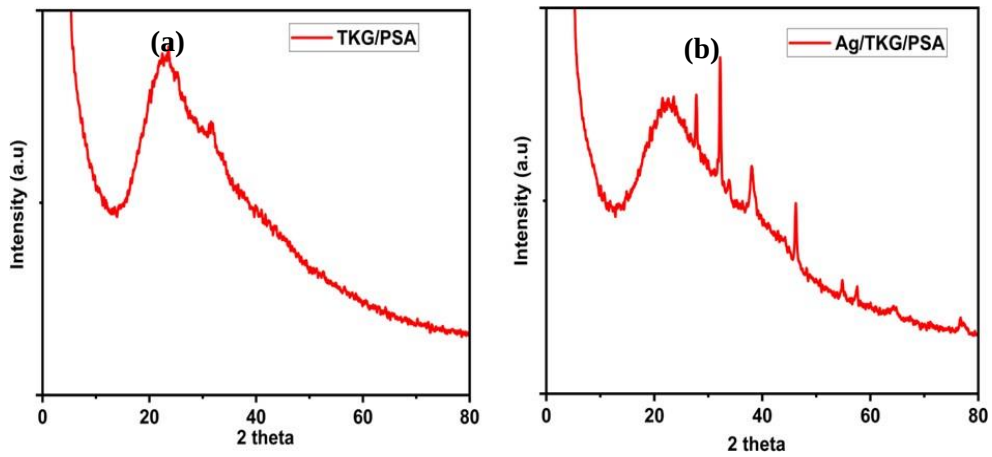

Figure 3.4: XRD of **(a)** TKG/PSA hydrogel **(b)** Ag/TKG/PSA nanocomposite hydrogel

3.3.3. Effect of Ag NPs on swelling capacity and gel content

The swelling studies of TKG/PSA hydrogel and Ag/TKG/PSA nanocomposite hydrogel were studied at physiological pH 7.4 and pH 1.2 as shown in **Figure 3.5.** It was observed that the presence of Ag NPs decreased the swelling capacity of Ag/TKG/PSA nanocomposite hydrogel. It may be due to the knot typing function of Ag NPs which was an important factor to understand the lesser swelling of silver nanocomposite hydrogels[28]. Ag NPs would restrict the expansion of the polymeric chain due to the chelation of some hydroxyl groups present on the surface of hydrogels. Additionally, the presence of Ag NPs would reduce the vacant space. As a result, silver nanocomposite's water uptake capacity was lower than TKG/PSA hydrogel. Also, it was detected that the swelling capacity of hydrogels at pH 7.4 was higher than at pH 1.2. When pH was higher than the pKa of hydrogel, there were many negatively charged CH_2O^- and O^- ions that repelled each other. As a result, the creation of rapid relaxation in the polymeric chain led to higher swelling of the hydrogel at pH 7.4.

However, in an acidic medium, where pH was less than pKa of hydrogels, -OH functional groups present in hydrogel remained in non-ionized states and thus less electrostatic repulsion occurred, responsible for less swelling of the hydrogel at pH 1.2.[29]. Moreover, gel content (%) was calculated for TKG/PSA hydrogel and Ag/TKG/PSA nanocomposite hydrogel as presented in **Table 3.1.** It was observed that the presence of Ag NPs increased the gel content of the TKG/PSA hydrogel which may be due to the coordinated interactions of Ag NPs with the functional groups such as OH^- and $-COO^-$ present in the hydrogel.

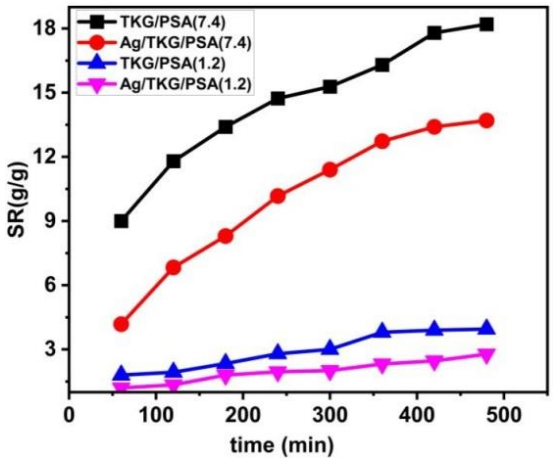

Figure 3.5: Swelling ratio (SR) of TKG/PSA hydrogel and Ag/TKG/PSA nanocomposite hydrogel at pH 7.4 and 1.2.

Table 3.1: Estimation of gel content (%), DL (%) and DE (%) for TKG/PSA hydrogel and Ag/TKG/PSA nanocomposite hydrogel

Hydrogel	Gel Content (%)	DL (%)	DE (%)
TKG/PSA	68.32	11± 0.42	58.32±0.81
Ag/TKG/PSA	72.34	23±0.53	67.53±0.40

3.3.4. Modelling of dynamic swelling data

The dynamic swelling data was fitted in mathematical models such as the Power function model (first-order) and Schott model(second-order) as shown in **Figure 3.6.** All the related parameters were tabulated in **Table 3.2**. However, the highest value of the coefficient of determination (R^2) close to unity showed that the Power function model is the better-fitted model over the Schott model. In the case of the Power function model, for TKG/PSA hydrogel, the diffusion constant value (n) was 0.338 which indicated a Fickian diffusion while for Ag/TKG/PSA nanocomposite, the value of n was 0.580 which indicated a non-Fickian diffusion [30].

Table 3.2: Modelling of dynamic swelling data using Power function and Schott kinetic models

Hydrogel	Power function model			Schott kinetic model			
	n	k	R^2	M_∞(Theo) (g/g)	M_∞(exp) (g/g)	$K_2 \times 10^{-4}$ (g/g min^{-1})	R^2
TKG/PSA	0.338	0.1178	0.9924	21.50	21	98	0.9901
Ag/TKG/PSA	0.580	0.02548	0.9938	21.03	18	38	0.9921

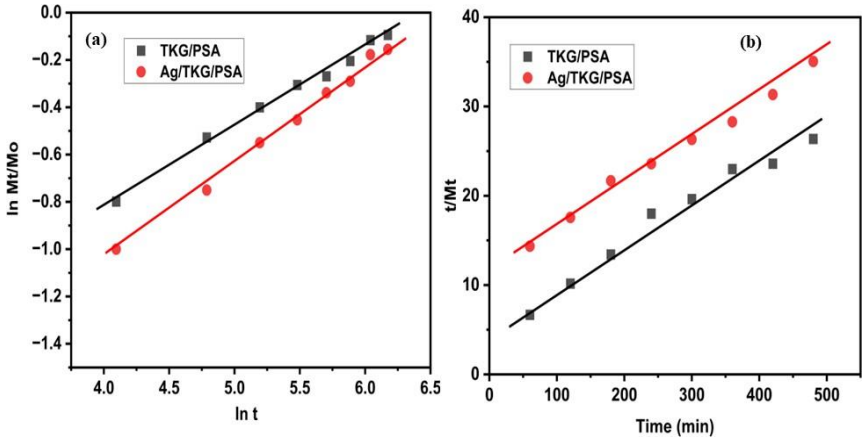

Figure 3.6: (a) Power function n model (b) Schott model for TKG/PSA hydrogel and Ag/TKG/PSA nanocomposite hydrogel

3.3.5. UV-Visible Spectra

The synthesis of Ag NPs was confirmed by UV-Visible spectra. A broad band at 420 nm as shown in **Figure 3.7** indicated the characteristic surface plasmon resonance (SPR) peak of AG NPs[31]. SPR gives characteristic optical spectra of the metal oxide nanoparticles and the width of the plasmon peak depends on various factors such as oxidation state, geometry, and size of the metal [32]. However, no peaks other than 420 nm is present which confirmed the non-aggregation of Ag NPs.

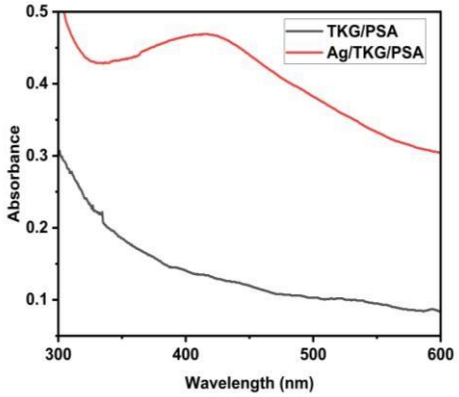

Figure 3.7: UV-visible spectra of TKG/PSA and Ag/TKG/PSA hydrogel

3.3.6. Zeta potential

Zeta potential of TKG/PSA hydrogel **(Figure 3.8)** was observed at -12.6mV which may be due to presence of -COO^- functional group present in the hydrogel. Moreover, the zeta potential of Ag/TKG/PSA nanocomposite hydrogel was observed at -16.3 mV **(Figure 3.9).** Although, there was not any significant difference between the two zeta potentials but higher negative value signified higher colloidal stability and anionic nature[33].

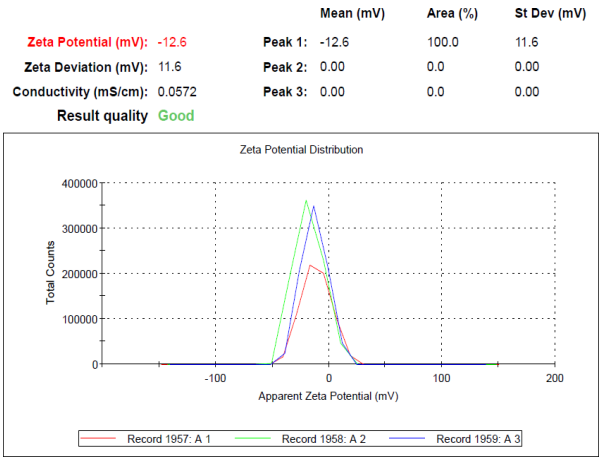

Figure 3.8: Zeta potential of TKG/PSA hydrogel

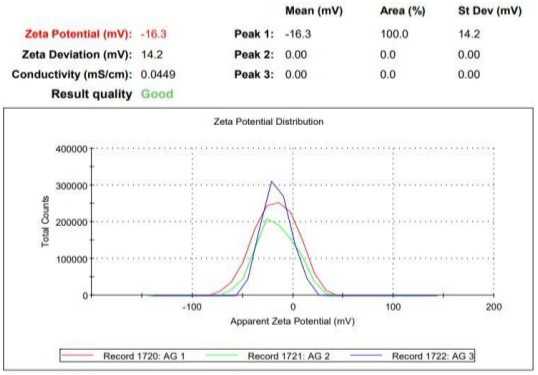

Figure 3.9: Zeta potential of Ag/TKG/PSA nanocomposite hydrogel

3.3.7. Fourier Transform Infrared Spectra

FTIR spectra of TKG/PSA hydrogel and Ag/TKG/PSA nanocomposite was shown in **Figure 3.10.** FTIR spectra of TKG/PSA hydrogel showed a broad peak at 3406 cm^{-1} indicating the presence of an aliphatic -O-H group, while a band appearing at 2975 cm^{-1} was due to -C-H group. The two bands appearing at 1407 cm^{-1} and 1563 cm^{-1} indicated the presence of $-COO^-$ symmetric and asymmetric vibration while peaks at 866 cm^{-1} and 1261cm^{-1} indicated the presence of O=C-N and C-N groups of cross- linker MBA[29]. All these peaks are present in the FTIR of silver nanocomposite hydrogel but shifted to lower wavenumber due to coordinated interactions of Ag NPs with functional groups of hydrogels [34]. The functional groups such as -OH and $-COO^-$ present in hydrogels can form coordination bonds with Ag NPs as reported in the literature[17].

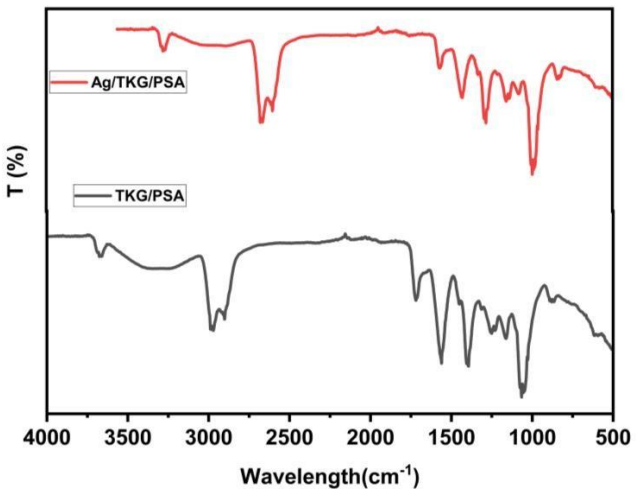

Figure 3.10: FTIR of TKG/PSA and Ag/TKG/PSA nanocomposite

3.3.8. FE-SEM Analysis

The surface morphology of TKG/PSA and Ag/TKG/PSA nanocomposite hydrogel was provided by the FE-SEM micrographs. It has been observed that TKG/PSA hydrogel showed a distinct, rough, and spongy surface having the presence of interstitial voids as shown in **Figure 3.11a**. However, the surface morphology of Ag NPs embedded hydrogel showed that Ag NPs are spherical [35]. This was also confirmed that Ag NPs were successfully embedded in the hydrogel matrix without any aggregation as shown in **Figure 3.11 (b, c)**. The chemical composition of Ag NPs embedded hydrogel was also confirmed by EDX analysis as shown in **Figure 3.11d.**

3.3.9. Transmission Electron Microscope [TEM]

The transmission electron microscope (TEM) image of the TKG/PSA hydrogel (**Figure 3.12a**) containing Ag NPs revealed that the nanoparticles were spherical and distributed within the hydrogel matrix. [36]. The average particle size of the Ag NPS falls within the range of 10 to 25 nm. [37]. The SAED pattern (**Figure 3.12b**) of Ag NPs indicated a polycrystalline and FCC-type structure of synthesized Ag NPs[38].

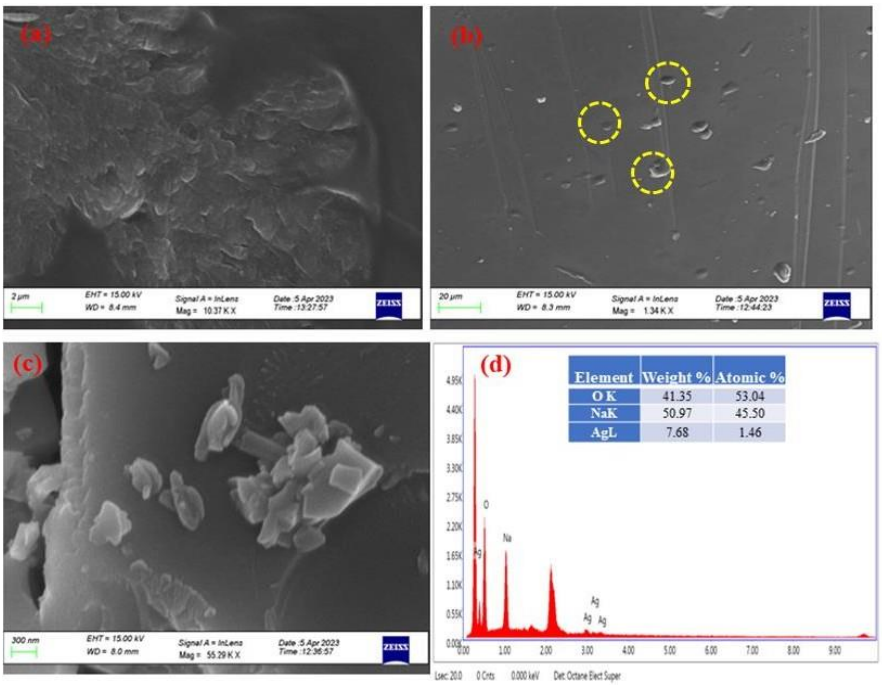

Figure 3.11: Surface morphology of **(a)** TKG/PSA at 2 µm scale **(b, c)** Ag/TKG/PSA at 20 µm and 300 nm scale **(d)** EDX spectra of Ag/TKG/PSA nanocomposite

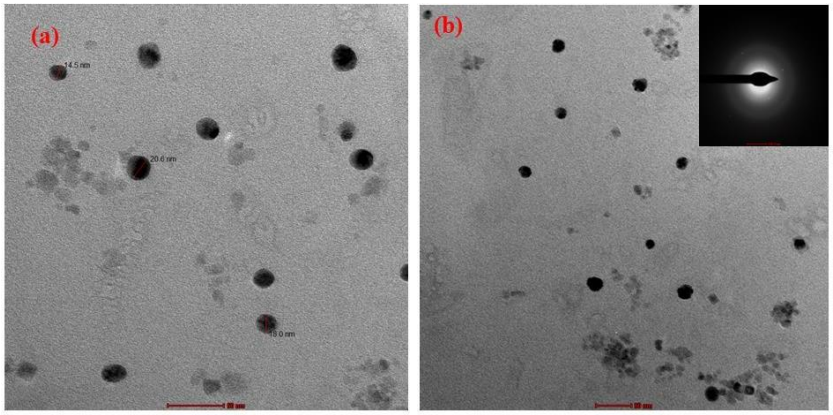

Figure 3.12: (a) TEM image of Ag NPs **(b)** SAED pattern of Ag NPs

3.3.10. In-vitro release of doxycycline drug

The drug release analysis from silver nanocomposite hydrogel was performed in a simulated intestinal fluid solution of pH 7.4 and simulated stomach gastric fluid of pH 1.2 solutions at 37ºC placed in an incubator using a UV-visible spectrophotometer.

The Ag/TKG/PSA hydrogel nanocomposite was selected for the drug release study because the drug's ability to spread through the hydrogel was influenced by how much the hydrogel swelled. [39]. This study was performed for 8 hours as shown in **Figure 3.13.** It was observed that the doxycycline release (%) was much higher at pH 7.4 than at pH 1.2. Again, it may be due to the diffusion of drug from a more swelled polymeric matrix[40]. Thus, silver nanocomposite shows a controlled and slow release of doxycycline drug.

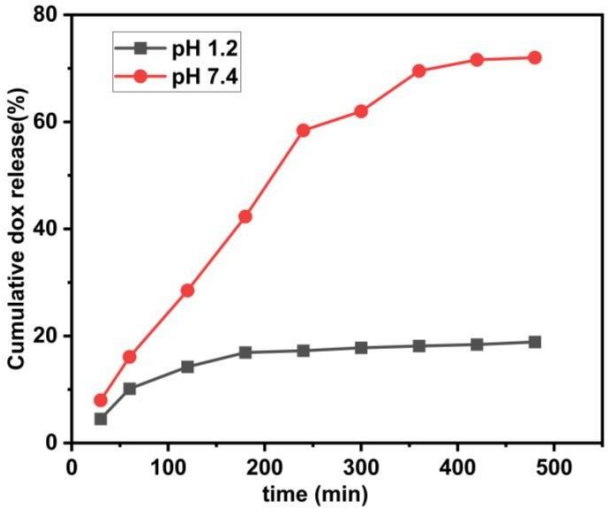

Figure3.13: Doxycycline release (%) from Ag/TKG/PSA nanocomposite hydrogel at pH 1.2 and pH 7.4

3.3.11. Kinetic modelling of released doxycycline

The doxycycline release data at both pH 7.4 and pH 1.2 were fitted in the various mathematical kinetic models such as First-order, Higuchi, and Korsmeyer-Peppas models[41] to understand the drug release mechanism. All the estimated parameters along with the coefficient of determination (R^2) were tabulated in **Table 3.3.** It was observed that the drug release data was best fitted in the Korsmeyer-Peppas model as the value of R^2 was close to unity. Thus, the drug release from silver nanocomposite hydrogel followed the Korsmeyer-Peppas model. In this model, a plot was made between log (M_t/M_o) vs log t as shown in **Figure 3.14**. The diffusion exponent value (n) for drug release at pH 7.4 and pH 1.2 buffer solutions have values of 0.82 and 0.46 respectively, which strongly suggested a non-Fickian diffusion. A non-Fickian diffusion signified a significant interaction between the hydrogel and drug, due to which both erosion and diffusion factors were responsible for the drug release behavior[42].

Table 3.3: Kinetic modelling of doxycycline release using Ag/TKG/PSA nanocomposite hydrogel

pH	Higuchi model		Korsmeyer-Peppas model			First-Order	
	KH	R^2	K	n	R^2	K1	R^2
7.4	0.058	0.9731	0.007	0.819	0.9801	0.0084	0.9732
1.2	0.036	0.9693	0.060	0.461	0.9923	0.0039	0.9694

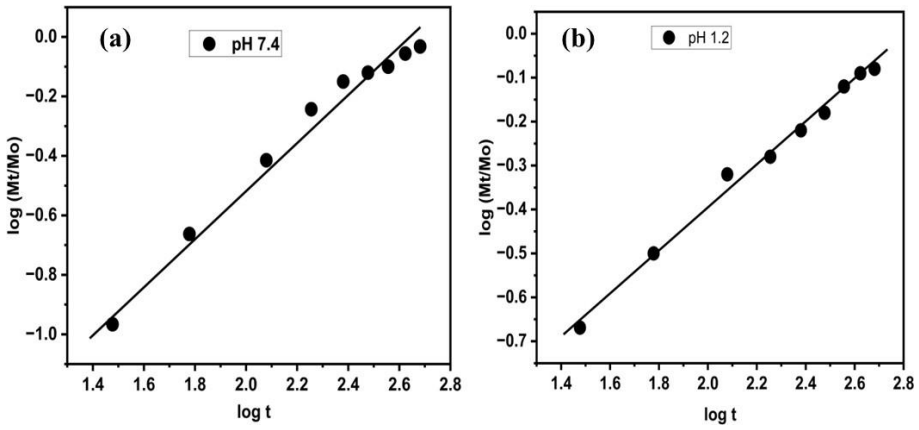

Figure 3.14: Korsmeyer-Peppas model for Ag/TKG/PSA in (a) pH 7.4 (b) pH 1.2 buffer solutions

3.3.12. MTT assay

MTT assay was carried out for the different concentrations (0, 1, 10, 100, 250, 500, 1000 μg/ml) of synthesized nanocomposite hydrogel against CCD 841 CoN cell lines as shown in **Figure 3.15.** It was observed that Ag/TKG/PSA nanocomposite hydrogel shows 44.77 % cell viability at a maximum concentration of 1000 μg/ml. However, 87.97 % of cell viability was observed at 1 μg/ml concentration. This indicated the cytocompatibility of the synthesized nanocomposite hydrogel. This behavior is expected due to the presence of biologically active sites in TKG biopolymer which contribute to the cytocompatibility of the hydrogel.

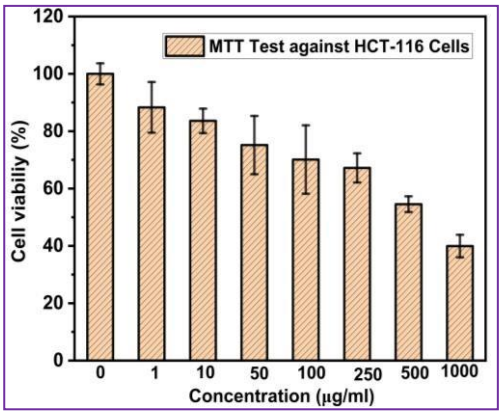

Figure 3.15: MTT assay of TKG/PSA with different concentrations against CCD 841 CoN cell lines

3.4. Conclusion

These results demonstrated the in-situ generation of Ag NPs in hydrogel termed as Ag/TKG/PSA nanocomposite hydrogel. The interesting aspect of this study was to control the swelling and drug release behavior of TKG/PSA hydrogel in the presence of Ag NPs. The dynamic swelling data of TKG/PSA and Ag/TKG/PSA in pH 1.2 and pH 7.4 was fitted in the Power function model and Schott model and the results showed the swelling data was more fitted in the Power function model in which the diffusion coefficient value for TKG/PSA and Ag/TKG/PSA was determined to be 0.338 and 0.580 indicating Fickian and non-Fickian diffusion respectively. The structural properties of Ag/TKG/PSA nanocomposite hydrogel were evaluated using XRD, FTIR, UV-visible, FE-SEM, and TEM techniques. Moreover, the average particle size of Ag NPs was estimated using the TEM technique in the range of 10 to 25 nm. Also, the UV-

visible SPR peak at 420 nm indicated the successful synthesis of Ag NPs in TKG/PSA hydrogel. The doxycycline release study using Ag/TKG/PSA nanocomposite hydrogel was performed at pH 1.2 and pH 7.4 at a physiological temperature of 37 °C. However, drug release (%) was higher at pH 7.4 than at pH 1.2 due to higher swelling of nanocomposite at pH 7.4. It was also found that doxycycline release data at both pH followed the Korsmeyer-Peppas model and showed non-Fickian diffusion. The MTT analysis of Ag/TKG/PSA nanocomposite hydrogel against CCD 841 CoN cell lines showed the cytocompatibility of the nanocomposite hydrogel. Thus, the developed Ag/TKG/PSA nanocomposite hydrogels act as a good carrier for the sustainable and controlled release of doxycycline drug.

References

[1] P. Abasian, M. Radmansouri, M. Habibi, M.Vaez, "Incorporation of magnetic NaX zeolite/DOX into the PLA/chitosan nanofibers for sustained release of doxorubicin against carcinoma cells death in vitro," *Int. J. Biol. Macromol.*, vol. 121, pp. 398–406, 2019, doi: 10.1016/j.ijbiomac.2018.09.215.

[2] P. Zhao, H.Liu, H.Deng, L.Xiao, "A study of chitosan hydrogel with embedded mesoporous silica nanoparticles loaded by ibuprofen as a dual stimuli-responsive drug release system for surface coating of titanium implants," *Colloids Surfaces B Biointerfaces*, vol. 123, pp. 657–663, 2014, doi: 10.1016/j.colsurfb.2014.10.013.

[3] K. Roshanbinfar, M.K.Gray, M. Angeloni, S.Schruefer, M.Fiedler, D.W.Schubert, F. Ferrazzi, V.Krstic, F.B. Engel, "Collagen Hydrogel Containing Polyethylenimine-Gold Nanoparticles for Drug Release and Enhanced Beating Properties of Engineered Cardiac Tissues," *Adv. Healthc. Mater.*, vol. 2202408, pp. 1–20, 2023, doi: 10.1002/adhm.202202408.

[4] S. H. Hussein-Al-Ali, S. M. Abudoleh, Q. I. A. Abualassal, Z. Abudayeh, Y. Aldalahmah, and M. Z. Hussein, "Preparation and characterization of ciprofloxacin-loaded silver nanoparticles for drug delivery," *IET Nanobiotechnology*, vol. 16, no. 3, pp. 92–101, 2022, doi: 10.1049/nbt2.12081.

[5] S. Siddique and J. C. L. Chow, "Gold nanoparticles for drug delivery and cancer therapy," *Appl. Sci.*, vol. 10, no. 11, 2020, doi: 10.3390/app10113824.

[6] A. Abed *et al.*, "Platinum Nanoparticles in Biomedicine: Preparation, Anti-Cancer Activity, and Drug Delivery Vehicles," *Front. Pharmacol.*, vol. 13, no. February, pp. 1–23, 2022, doi: 10.3389/fphar.2022.797804.

[7] A. K. Kodoth, V. M. Ghate, S. A. Lewis, B. Prakash, and V. Badalamoole, "Pectin-based silver nanocomposite film for transdermal delivery of Donepezil," *Int. J. Biol. Macromol.*, vol. 134, pp. 269–279, 2019, doi: 10.1016/j.ijbiomac.2019.04.191.

[8] L. A. Austin, M. A. MacKey, E. C. Dreaden, and M. A. El-Sayed, "The optical, photothermal, and facile surface chemical properties of gold and silver nanoparticles in bio diagnostics, therapy, and drug delivery," *Arch. Toxicol.*, vol. 88, no. 7, pp. 1391–1417, 2014, doi: 10.1007/s00204-014-1245-3.

[9] J. H. Lee, D. Jeong, and P. Kanmani, "Study on physical and mechanical properties of the biopolymer/silver based active nanocomposite films with antimicrobial activity," *Carbohydr. Polym.*, vol. 224, p. 115159, 2019, doi: 10.1016/j.carbpol.2019.115159.

[10] K. Alaqad and T. A. Saleh, "Gold and Silver Nanoparticles: Synthesis Methods, Characterization Routes and Applications towards Drugs," *J. Environ. Anal. Toxicol.*, vol. 6, no. 4, 2016, doi: 10.4172/2161-0525.1000384.

[11] K. M. Rao, "acid) -Based pH Responsive Semi-IPN Hydrogels and Their Ag and Inactivation of Multi-Drug-Resistant Bacteria," 2021.

[12] M. Shakir, I. Zia, A. Rehman, and R. Ullah, "Fabrication and characterization of nanoengineered biocompatible n-HA/chitosan-tamarind seed polysaccharide: Bio-inspired nanocomposites for bone tissue engineering," *Int. J. Biol. Macromol.*, vol. 111, pp. 903–916, 2018, doi: 10.1016/j.ijbiomac. 2018.01.035.

[13] Khushbu and S. G. Warkar, "Potential applications and various aspects of polyfunctional macromolecule- carboxymethyl tamarind kernel gum," *Eur. Polym. J.*, vol. 140, no. September, p. 110042, 2020, doi:10.1016/j.eurpolymj. 2020.110042.

[14] D. Qureshi, K.P.Behera, D.Mohanty, S.K.Mahapatra, "Synthesis of novel poly (vinyl alcohol)/tamarind gum/bentonite-based composite films for drug delivery applications," *Colloids Surfaces A Physicochem. Eng. Asp.*, vol. 613, no. December 2020, p. 126043, 2021, doi: 10.1016/j.colsurfa.2020.126043.

[15] M. Sabzi, M. J. Afshari, M. Babaahmadi, and N. Shafagh, "pH-dependent swelling and antibiotic release from citric acid crosslinked poly(vinyl alcohol) (PVA)/nano silver hydrogels," *Colloids Surfaces B Biointerfaces*, vol. 188, no. December 2019, p. 110757, 2020, doi: 10.1016/j.colsurfb.2019.110757.

[16] A. Shah, M. A. Yameen, N. Fatima, and G. Murtaza, "Chemical synthesis of chitosan/silver nanocomposites films loaded with moxifloxacin: Their characterization and potential antibacterial activity," *Int. J. Pharm.*, vol. 561, no. November 2018, pp. 19–34, 2019, doi: 10.1016/j.ijpharm.2019.02.029.

[17] J. Chalitangkoon, M. Wongkittisin, and P. Monvisade, "Silver loaded hydroxyethylacryl chitosan/sodium alginate hydrogel films for controlled drug release wound dressings," *Int. J. Biol. Macromol.*, vol. 159, pp. 194–203, 2020, doi: 10.1016/j.ijbiomac.2020.05.061.

[18] S. K. Bajpai, M. Jadaun, M. Bajpai, P. Jyotishi, F. F. Shah, and S. Tiwari, "Controlled release of Doxycycline from gum acacia/poly(sodium acrylate) microparticles for oral drug delivery," *Int. J. Biol. Macromol.*, vol. 104, pp. 1064–1071, 2017, doi: 10.1016/j.ijbiomac.2017.06.108.

[19] Z. Yang, H. Peng, W. Wang, and T. Liu, "Crystallization behavior of poly(ε-caprolactone)/layered double hydroxide nanocomposites," *J. Appl. Polym. Sci.*, vol. 116, no. 5, pp. 2658–2667, 2010, doi: 10.1002/app.

[20] X. Yi, J. He, X. Wei, H. Li, X. Liu, and F. Cheng, "A mussel-inspired multifunctional hydrogel reinforced by bacterial cellulose for wound healing: sustained drug release, enhanced adhesion and self-healing property," *Cellulose*, vol. 30, no. 10, pp. 6523–6538, 2023, doi: 10.1007/s10570-023- 05297-3.

[21] S. K. Bajpai, M. Jadaun, and S. Tiwari, "Synthesis, characterization and antimicrobial applications of zinc oxide nanoparticles loaded gum acacia/poly(SA) hydrogels," *Carbohydr. Polym.*, vol. 153, pp. 60–65, 2016, doi: 10.1016/j.carbpol.2016.07.019.

[22] S. M. Nasef, E. E. Khozemy, E. A. Kamoun, and H. El-Gendi, "Gamma radiation-induced crosslinked composite membranes based on polyvinyl alcohol/chitosan/AgNO3/vitamin E for biomedical applications," *Int. J. Biol. Macromol.*, vol. 137, pp. 878–885, 2019, doi: 10.1016/j.ijbiomac.2019.07.033.

[23] I. Rani, S. G. Warkar, and A. Kumar, "Nano ZnO embedded poly (ethylene glycol) diacrylate cross-linked carboxymethyl tamarind kernel gum (CMTKG)/poly (sodium acrylate) composite hydrogels for oral delivery of ciprofloxacin drug and their antibacterial properties," *Mater. Today Commun.*, vol. 35, no. June 2022, p. 105635, 2023, doi: 10.1016/j.mtcomm.2023.105635.

[24] K. Virk, K.Sharma, S.Kapil, V.Kumar, V.Sharma, S.Pandey, "Synthesis of gum acacia-silver nanoparticles based hydrogel composites and their comparative anti-bacterial activity," *J. Polym. Res.*, vol. 29, no. 4, pp. 1–15, 2022, doi: 10.1007/s10965-022-02978-8.

[25] R. Malik, S. G. Warkar, and R. Saxena, "Carboxy-methyl tamarind kernel gum based bio-hydrogel for sustainable agronomy," *Mater. Today Commun.*, vol. 35, no. January, p. 105473, 2023, doi: 10.1016/j.mtcomm.2023.105473.

[26] Z. Zare-Akbari, H. Farhadnejad, B. Furughi-Nia, S. Abedin, M. Yadollahi, and M. Khorsand-Ghayeni, "PH-sensitive bionanocomposite hydrogel beads based on caborboxymethyl cellulose/ZnO nanoparticle as drug carrier," *Int. J. Biol. Macromol.*, vol. 93, pp. 1317–1327, 2016, doi: 10.1016/j.ijbiomac.2016.09.110.

[27] S. Mohamadi Zahedi and Y. Mansourpanah, "Construction of chitosan-carboxymethyl β-cyclodextrin silver nanocomposite hydrogel to improve antibacterial activity," *Plast. Rubber Compos.*, vol. 47, no. 6, pp. 273–281, 2018, doi: 10.1080/14658011.2018.1475166.

[28] M. Yadollahi, S. Farhoudian, and H. Namazi, "One-pot synthesis of antibacterial chitosan/silver bio-nanocomposite hydrogel beads as drug delivery systems," *Int. J. Biol. Macromol.*, vol. 79, pp. 37–43, 2015, doi: 10.1016/j.ijbiomac.2015.04.032.

[29] Khushbu, S. G. Warkar, and A. Kumar, "Synthesis and assessment of carboxymethyl tamarind kernel gum based novel superabsorbent hydrogels for agricultural applications," *Polymer (Guildf).*, vol. 182, no. July, p. 121823, 2019, doi: 10.1016/j.polymer.2019.121823.

[30] Khushbu, S. G. Warkar, and N. Thombare, "Correction to: Zinc micronutrient-loaded carboxymethyl tamarind kernel gum-based superabsorbent hydrogels: controlled release and kinetics studies for agricultural applications (Colloid and Polymer Science, (2021), 299, 7, (1103-1111), 10.1007/s00396-021-," *Colloid Polym. Sci.*, vol. 299, no. 9, p. 1505, 2021, doi: 10.1007/s00396-021-04857-y.

[31] R. Anith Jose, D. Devina Merin, T. S. Arulananth, and N. Shaik, "Characterization Analysis of Silver Nanoparticles Synthesized from Chaetoceros calcitrans," *J. Nanomater.*, vol. 2022, 2022, doi: 10.1155/2022/4056551.

[32] S. Batool, Z. Hussain, M. B. K. Niazi, U. Liaqat, and M. Afzal, "Biogenic synthesis of silver nanoparticles and evaluation of physical and antimicrobial properties of Ag/PVA/starch nanocomposites hydrogel membranes for wound dressing application," *J. Drug Deliv. Sci. Technol.*, vol. 52, no. April, pp. 403–414, 2019, doi: 10.1016/j.jddst.2019.05.016.

[33] R. M. Elamawi, R. E. Al-Harbi, and A. A. Hendi, "Biosynthesis and characterization of silver nanoparticles using Trichoderma longibrachiatum and their effect on phytopathogenic fungi," *Egypt. J. Biol. Pest Control*, vol. 28, no. 1, pp. 1–11, 2018, doi: 10.1186/s41938-018-0028-1.

[34] G. Karthiga Devi, P. Senthil Kumar, and K. Sathish Kumar, "Green synthesis of novel silver nanocomposite hydrogel based on sodium alginate as an efficient biosorbent for the dye wastewater treatment: prediction of isotherm and kinetic parameters," *Desalin. Water Treat.*, vol. 57, no. 57, pp. 27686–27699, 2016, doi: 10.1080/19443994.2016.1178178.

[35] M. Goudarzi, N. Mir, M. Mousavi-Kamazani, S. Bagheri, and M. Salavati-Niasari, "Biosynthesis and characterization of silver nanoparticles prepared from two novel natural precursors by facile thermal decomposition methods," *Sci. Rep.*, vol. 6, no. August, pp. 1–13, 2016, doi: 10.1038/srep32539.

[36] C. Talodthaisong, W. Boonta, S. Thammawithan, R. Patramanon, N. Kamonsutthipaijit, J.A. Hutchison, S. Kulchat, "Composite guar gum-silver nanoparticle hydrogels as self-healing, injectable, and antibacterial biomaterials," *Mater. Today Commun.*, vol. 24, no. February, p. 100992, 2020, doi: 10.1016/j.mtcomm.2020.100992.

[37] N. Pande, D. K. Jaspal, J. Ambekar, and J. V. P, "Ecofriendly synthesis and applications of silver nanoparticles," *J. Chem. Pharm. Res.*, vol. 6, no. 9, pp. 403–410, 2014.

[38] M. Lopez-Carrizales *et al.*, "Characterization, antibiofilm and biocompatibility properties of chitosan hydrogels loaded with silver nanoparticles and ampicillin: an alternative protection to central venous catheters," *Colloids Surfaces B Biointerfaces*, vol. 196, no. April, p. 111292, 2020, doi: 10.1016/j.colsurfb.2020.111292.

[39] N. Zeng, L. He, L. Jiang, S. Shan, and H. Su, "Synthesis of magnetic/pH dual responsive dextran hydrogels as stimuli-sensitive drug carriers," *Carbohydr. Res.*, vol. 520, no. April, p. 108632, 2022, doi: 10.1016/j.carres.2022.108632.

[40] A. Tanwar, P. Date, and D. Ottoor, "ZnO NPs incorporated gelatin grafted polyacrylamide hydrogel nanocomposite for controlled release of ciprofloxacin," *Colloid Interface Sci. Commun.*, vol. 42, no. December 2020, p. 100413, 2021, doi: 10.1016/j.colcom.2021.100413.

[41] Tushar, Y. Saraswat, P. Meena, and S. G. Warkar, "Synthesis and characterization of novel xanthan gum-based pH-sensitive hydrogel for metformin hydrochloride release," *Colloid Polym. Sci.*, no. 0123456789, 2023, doi: 10.1007/s00396-023-05135-9.

[42] Y. Huang, H. Yu, and C. Xiao, "pH-sensitive cationic guar gum/poly (acrylic acid) polyelectrolyte hydrogels: Swelling and in vitro drug release," *Carbohydr. Polym.*, vol. 69, no. 4, pp. 774–783, 2007, doi: 10.1016 /j.carbpol.2007.02.016.

[43] D. H. Hanna, R. Osailan, and H. A. Ahmed, "Stevia rebaudiana Methanolic Leaf Extract in Egypt: Phytochemical Analysis, Antioxidant, Antilipid Peroxidation, Antihemolytic, Antimetastatic, and Anticancer Properties," *J. Food Biochem.*, vol. 2023, 2023, doi: 10.1155/2023/7161091.

CHAPTER 4

SYNTHESIS AND CHARACTERIZATION OF CARBOXYMETHYL TAMARIND KERNEL GUM POLY(VINYL ALCOHOL) AND GUAR GUM BASED HYDROGEL FILM FOR CIPROFLOXACIN RELEASE STUDIES

4.1. Introduction

Skin plays a crucial role in protecting the human body against various types of bacterial and viral infections. Skin helps to control fluid maintenance, temperature regulation, and sensing mechanisms of the body[1]. In the medical field, skin injuries are the most common problem and to resolve this, there is a high demand for the development of wound dressing materials in the medical field[2]. One of the most promising dressing materials is the hydrogel. Hydrogels are pH-sensitive, hydrophilic, and physically or chemically cross-linked networks. The hydrophilic functional groups present in the hydrogels are responsible for the interaction of hydrogel with various biological tissues. The external environmental conditions such as pH, temperature, and ionic strength can break the physically cross-linked networks of hydrogels. Therefore, chemically cross-linked hydrogels are required to be developed using the cross-linker agents. These are attractive materials in wound healing applications due to their specific properties such as high swelling capacity, moisture uptake, and bioactivity[3] which makes them efficient dressing materials [4]. They can absorb the wound exudates, have good flexibility, prevent bacterial growth, keep the moist restorative surroundings, and inhibit anaerobic bacteria proliferation [5]. The flexibility of the 3-D network of hydrogel allows the entrapment and transportation of antibacterial drugs [6]. The diffusion of drugs from hydrogel depends on various factors such as pH, temperature, pressure, and swelling solvent [7]. The antibacterial properties of hydrogel can be enhanced by incorporating antibiotic drugs in the hydrogel matrix [8]. In this study, the ciprofloxacin (CFX) drug was selected as a model drug. CFX is a synthetic, broad-spectrum, and chemotherapeutic agent belonging to the fluoroquinolone family. It is one of the most important biocompatible and antimicrobial drugs used for wound healing applications [9]. The half-life of the CFX drug is 4 hours and it can inhibit DNA replication by preventing the production of folate [10]. Moreover, CFX can enhance the effectiveness of hydrogel film in wound healing. Biopolymer-based hydrogels have garnered considerable attention in recent years owing to their adaptable characteristics,

rendering them suitable for pharmaceutical applications. [11]. These materials exhibit exceptional water absorption capacity, viscosity enhancement properties, and possess unique biological attributes such as antifungal, antibacterial, and wound-healing capabilities. [12].

Among the variety of available biopolymers, carboxymethyl tamarind kernel gum (CMTKG) is not much explored for wound healing applications. In the present study, the CMTKG was chosen as a biopolymer due to its higher resistance to microbial degradation and its ability to promote cell proliferation [13]. CMTKG can decrease the extracellular matrix and is suitable for skin tissue applications [14]. A study developed CMTKG / Gelatin–Tamarind kernel gum films for wound healing applications [15]. Additionally, nanofibers made of CMTKG and graphene oxide were synthesized for neuronal cell proliferation [16]. Besides CMTKG, Guar gum (GG) is another natural polymer was used that consists of a linear cross-linked form of D-mannose and D-galactose[17]. It has high solubility in water and can be cross-linked with synthetic monomers using cross-linking agents such as glutaraldehyde, citric acid, sodium borate, N,N'-Methylenebisacrylamide. Thus, the thermal and mechanical properties of the GG biopolymer were enhanced, making it more suitable for biomedical applications. [18]. Additionally, poly (vinyl alcohol) (PVA) was chosen as a water-soluble and synthetic polymer that is widely used to synthesize hydrogel films for wound dressing applications due to its excellent thermal, and mechanical properties[19]. However, the physiochemical properties of PVA-based hydrogel films can further be increased by cross-linking of PVA with biopolymers. The hydrogel films of PVA with biopolymers such as chitosan[20], gum acacia[21], cellulose[22], alginate[23], and dextran[24] are reported in the literature. It is pertinent to mention that very scarce literature is available on the formulation of CMTKG-based hydrogel film.

In this study, we have synthesized several compositions of CMTKG/PVA/GG hydrogel film (S1 to S9) by changing the quantity of GG, PVA, and CMTKG biopolymers. Hydrogel films were characterized using FE-SEM, FTIR, Thermal, and Mechanical analysis. The various parameters such as thickness, moisture content, equilibrium swelling ratio (ESR), and wetting analysis were evaluated for all the compositions of hydrogel films. An antibiotic drug, CFX was loaded into the best-swelled hydrogel film (S2). The in-vitro release studies of the CFX drug were performed in a phosphate saline solution (pH 7.4) and release data was fitted in various mathematical models such as

the First-order, Higuchi, and Korsmeyer-Peppas models to determine the mechanism of drug release. In this study, the prepared hydrogel film is found superior to the reported earlier CMTKG/PVA film [25]. The hydrogel films demonstrated improved properties, such as swelling capacity, drug loading efficiency, and mechanical stability, compared to PVA-based hydrogel films. The presence of hydrophilic biopolymers, such as GG and CMTKG, enhanced the hydrophilicity, gel fraction, and cross-linking density of PVA-based hydrogel films. Moreover, the cytocompatibility of PVA-based hydrogel films can also be increased in the presence of CMTKG and GG biopolymers due to their biocompatibility and biodegradability. The antibacterial activity of film showed higher antibacterial activity against *S. aureus* than *E.coli.* Additionally, the MTT assay indicated the cytocompatibility of film against HaCaT human keratinocyte cell lines. The prepared hydrogel film also showed good cytocompatibility and antibacterial properties.

4.2. Experimental

4.2.1. Materials

Carboxymethyl tamarind kernel gum (CMTKG) (0.2° substitution, Mol. wt.= 9.14×10^5 g/mol, Hindustan Gum Ltd., Rewari), Poly (vinyl alcohol) (PVA, Mol. wt.= 1,25,000 g/mol, Moly Chem Pvt. Ltd., India), Glutaraldehyde (GTA, Mol. Wt.=100 g/mol, Thomas Baker, India), and Guar gum (GG, Dabur Ltd., India) was used as received. Ciprofloxacin (CFX) drug was provided by M/S Unicure Pvt. Ltd., India. Distilled water was used to perform all the experimental sections.

4.2.2. Synthesis of CMTKG/PVA/GG hydrogel film

The solvent casting method was used to synthesize hydrogel film. In brief, 0.15 g (0.75% w/v) of CMTKG was dissolved in 20 mL of distilled water using a magnetic stirrer (700 rpm) at room temperature. After the complete homogenization, 0.05 g (0.5 % w/v) of GG solution was added to the CMTKG solution. Further, 20 % w/v of PVA solution was prepared and added to continuous stirring CMTKG-GG suspension and homogenized for 15 minutes. To this mixture, 2 mL of glutaraldehyde (composition: 10 ml GTA + 0.1 ml HCl + 10 ml ethanol) cross-linking agent was added and again homogenized for 15 min. After that, 15 mL of the suspended reaction mixture was poured onto Petri dishes and kept in a hot air oven for pre-drying at 60 °C for 24 h.

Further, hydrogel film was cured at 120 °C for 15 min to enhance the crosslinking between polymeric chains. The schematic representation for the synthesis of CMTKG/PVA/GG hydrogel film is shown in **Figure 4.1.** The various formulations of hydrogel films were also prepared by varying the amount of CMTKG, PVA, GG, and glutaraldehyde as shown in Table **4.1.**

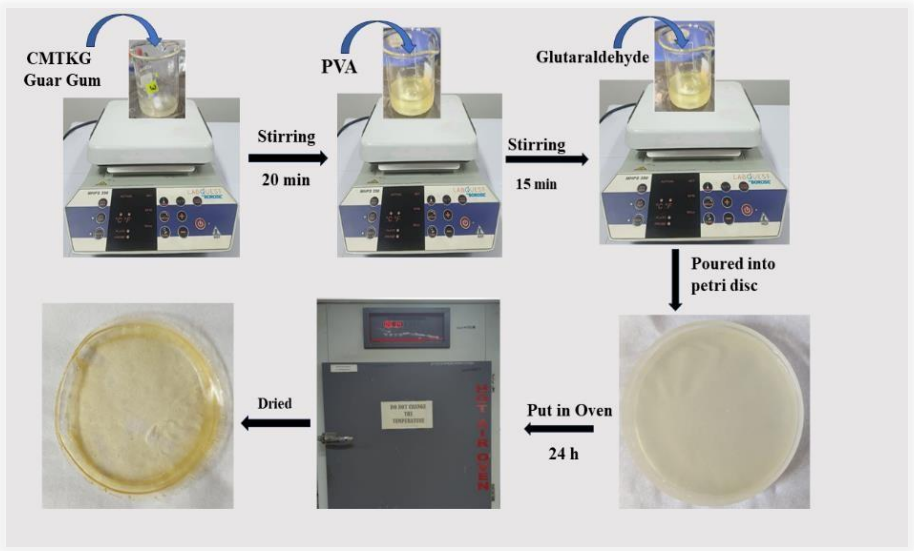

Figure 4.1: Layout of synthesis of CMTKG/PVA/GG hydrogel film

Table 4.1: Composition of various reactants involved in CMTKG/GG/PVA film synthesis

Sample Code	CMTKG (g); %(w/v)	GG (g); %(w/v)	PVA (g); %(w/v)	GTA (mL)
S1	0.15; 0.75	0.05; 0.5	2.24; 20	2
S2	**0.10; 0.50**	0.05; 0.5	2.24; 20	2
S3	**0.05; 0.25**	0.05; 0.5	2.24; 20	2
S4	0.15; 0.75	**0.03; 0.3**	2.24; 20	2
S5	0.15 ; 0.75	**0.07; 0.7**	2.24; 20	2
S6	0.15; 0.75	0.05; 0.5	2.24; 20	**4**
S7	0.15 ; 0.75	0.05;0.5	2.24; 20	**6**
S8	0.15; 0.75	0.05; 0.5	**1.24; 11**	2
S9	0.15 ; 0.75	0.05; 0.5	**3.20; 29**	2

4.2.3. Swelling study

To investigate the swelling capacity of the hydrogel films, a phosphate buffer solution with a pH of 7.4 was employed. The pre-weighed (0.15 g) rectangular-shaped hydrogel

films were immersed in 20 mL of the buffer solution at 37°C for 24 hours. After this period, the swollen films were carefully removed and blotted with tissue paper to remove excess buffer solution before being weighed again. This weight change was then used to calculate the equilibrium swelling ratio (ESR) using **Equation (4.1)** [26].

$$\mathrm{ESR}\left({}^{\mathrm{g}}/_{\mathrm{g}}\right) = \frac{W_T - W_0}{W_T} \tag{4.1}$$

Where W_T is the weight of swollen hydrogel film and W_0 is the dry weight of hydrogel film. Thus, ESR (g/g) was calculated for each synthesized hydrogel film.

4.2.4. Synthesis of CFX-loaded CMTKG/PVA/GG hydrogel film

After the evaluation of the swelling ratio of synthesized hydrogel films, the best-swelled hydrogel film (S2) was chosen for the loading of the CFX drug. Then, 0.1 g of CFX drug was dissolved in 5 mL of ethanol, added to the beaker containing the CMTKG/PVA/GG reaction mixture and continuously stirred for 20 min. Afterward, a glutaraldehyde cross-linker was added to the beaker, and the same procedure was followed as given in **section 4.2.2.** In this way, CFX-loaded hydrogel film was synthesized.

4.2.5. Drug loading efficiency (%)

Drug loading and encapsulation efficiency for CFX-loaded hydrogel film was evaluated by placing 0.2 g of CFX-loaded hydrogel film in 50 mL of phosphate saline buffer (pH 7.4) for 48 h. After that, 2 mL buffer solution was withdrawn, and absorbance was measured using a UV-visible spectrophotometer at 276 nm wavelength. Thus, the CFX loading and encapsulation efficiency was calculated using the given **Equation (4.2) and (4.3),** respectively [27,30].

$$\text{CFX loading } (\%) = \frac{\text{amount of CFX in hydrogel film}}{\text{amount of hydrogel film}} \times 100 \tag{4.2}$$

$$\text{CFX encapsulation } (\%) = \frac{\text{amount of CFX in hydrogel film}}{\text{theotical amount of CFX in hydrogel fim}} \times 100 \tag{4.3}$$

4.2.6. Thickness and moisture content (%)

Thickness of hydrogel films were measured using a Vernier caliper instrument. Moreover, to evaluate the moisture content (%), a pre-weighed hydrogel film (W_i) was put in a desiccator containing silica gel. After 48 hours, the weight of the film was recorded and repeated the steps until constant weight (W_d) was achieved. Thus, Moisture content (%) was calculated using the given **Equation (4.4)** [28]:

$$\text{Moisture content (\%)} = \frac{W_i - W_d}{W_d} \times 100 \quad (4.4)$$

4.2.7. In vitro drug release study

The drug release study of the CFX drug was performed in phosphate buffer (pH 7.4) at 37 °C in the incubator. Initially, 0.1 g of CFX-loaded hydrogel film was placed in a beaker containing 100 mL of phosphate buffer solution. After a regular interval of

time, 2 mL of the sample was withdrawn and its absorbance was measured using a UV-visible spectrophotometer at 276 nm[29]. At the same time, 2 mL of phosphate buffer solution was added to the beaker to keep the total volume constant. Thus, the drug release behaviors of optimized hydrogel film were performed in triplicate.

4.2.8. Kinetics of Drug Release Study

To understand the kinetics and mechanism of CFX drug release behavior in phosphate buffer solution pH 7.4, various mathematical models were used. The drug release study of CFX drug was studied with time using the First-order, Higuchi model, and Korsmeyer-Peppas model [30] as expressed in **Equations (4.5), (4.6), and (4.7)** respectively.

$$\log\left(1 - \frac{M_t}{M_\infty}\right) = K_1 . \frac{t}{2.303} \quad (4.5)$$

$$\frac{M_t}{M_\infty} = K_H . t^{0.5} \quad (4.6)$$

$$\frac{M_t}{M_\infty} = K . t^n \quad (4.7)$$

It was observed that the First-order model depends only on the concentration of the drug as a reactant. Here, $\frac{Mt}{M\infty}$ indicates the fraction of drug released in t time and K_1 is the First-order rate constant. Moreover, the Higuchi model signifies diffusion of the drug from an insoluble polymeric matrix and K_H indicates the Higuchi release rate constant. However, the value of diffusion exponent (n) signifies the type of drug release mechanism in the Korsmeyer-Peppas model. In the case when $n < 0.45$, indicates Fickian diffusion, if $0.45 \leq n \leq 0.89$ indicate non-Fickian diffusion, and if $n > 0.89$, indicates super case II as reported in literature[36].

4.2.9. Characterization

4.2.9.1.FTIR

The FTIR spectra of the CFX drug, CMTKG/PVA/GG film, and CFX-embedded CMTKG/PVA/GG film were analyzed to identify the functional groups present in each sample. The KBr pellet method was used to prepare the samples for FTIR analysis, and the spectra were recorded in the wavelength range of 4000 cm^{-1} to 400 cm^{-1}.

4.2.9.2. FE-SEM

The FE-SEM imaging of synthesized CMTKG/PVA/GG film was carried out using the ZEISS EVO model. The EDX analysis was also done at a voltage of 20 kV to investigate the composition of various elements present in the hydrogel film.

4.2.9.3. TGA-DTA

TGA-DTA analysis of CFX drug, CMTKG/PVA/GG film, and CFX embedded CMTKG/PVA/GG film was performed from 30 to 800 °C with 10 °C/min heating rate under an N_2 atmosphere using Perkin Elmer TGA 4000 instruments.

4.2.9.4. Wetting analysis

The water contact angle instrument was utilized to determine the hydrophobicity and hydrophilicity ratio of hydrogel film[30]. The static contact angles of the prepared hydrogel film were investigated using a contact angle analyzer (Phoenix 300).

4.2.9.5. Mechanical analysis

The mechanical properties such as tensile strength (MPa) and elongation at break (%) of hydrogel films of size 1 cm^2 were analyzed by static UTM (Zwick Roell, Germany static UTM Z010) instrument.

4.2.9.6. Antibacterial assay

The Antibacterial activity was evaluated using the zone inhibition method (Kirby-Bauer method) [45]. The MHA plates were inoculated with 100 microliters of bacterial cultures, *Staphylococcus aureus* and *Escherichia coli*. The inoculum was prepared by adjusting the cell density to 0.5 McFarland units (approximately 1.5 x 10^8 CFU/mL) in Mueller-Hinton broth. The discs containing 10 microliters of various concentrations were then placed onto the inoculated plates. One disc in each plate was loaded with the solvent alone, which served as a control for the vehicle, and a ciprofloxacin disc (10 µg) was used as a positive control. The plates containing *Staphylococcus aureus* and *Escherichia coli* were incubated at 37 °C for 24 hours (Basil Scientific Corp., India). The clear zones surrounding each disc were measured and recorded.

4.2.9.7. MTT assay

The cytotoxicity of the synthesized hydrogel film to HaCaT cells, a human keratinocyte cell line (RRID:CVCL_0038, obtained from NCCS Pune), was evaluated using the MTT assay [46]. The cells (10000 cells/well) were cultured in 96 well plate for 24 h in DMEM medium (Dulbecco's Modified Eagle Medium-AT149-1L) supplemented with 10% FBS (Fetal Bovine Serum - HIMEDIA-RM 10432) and 1% antibiotic solution at 37°C with 5% CO_2. The following day, cells were treated with different concentrations of the hydrogel film, ranging from 0 to 2.0 µg/ml (i.e 0, 0.5, 1.0, 1.5, 2.0). The Cells that were not treated were considered as the control group, and cells without MTT were considered as the blank.

After incubating the cells for 24 hours, MTT solution was added to the cell culture and incubated for an additional 2 hours. At the end of the experiment, the culture supernant was removed, and the cell layer matrix was dissolved in 100 µL of dimethyl sulfoxide. The solution was then analyzed using an ELISA plate reader (iMark, Bio-Rad, USA) at wavelengths of 540 nm and 660 nm. The optical microscopic images were captured under an inverted microscope (Olympus ek2) using a Camera (Am Scope digital camera 10 MP Aptima CMOS).

4.2.9.8. Statistical analysis

In this study, the results of the experiments which were studied in triplicates have been expressed as mean ±SD. The results were analyzed using Microsoft Excel software (t-test) with the level of significance at $p < 0.05$.

4.3. Results and discussion

4.3.1. Swelling analysis

The effect of the amount of CMTKG, GG, PVA, and GTA cross-linker on the swelling capacity of hydrogel film was studied as shown in **Figure 4.2.** The equilibrium swelling ratio (ESR (g/g)) was calculated by swelling studies in physiological pH 7.4 buffer solution. It was noticed that with an increase in the amount of CMTKG biopolymer, the swelling capacity of hydrogel film was increased as shown in **Figure 4.2(a)**. This could be due to the increased number of COO- groups, which might lead to greater electrostatic repulsion. Furthermore, increasing the concentration of counter ions, especially sodium ions, might improve osmotic swelling pressure and chain relaxation within the hydrogel gel network [32,33]. The effect of varying amounts of guar gum (GG) on the ESR of the hydrogel film was also studied as shown in **Figure 4.2(b).** It was observed that with an increased content of GG biopolymer from 0.03 to 0.05 g, the ESR of hydrogel film was increased while a further increase in its amount up to 0.07 g led to a decrease in the ESR of hydrogel film. The initial increase in ESR was attributed to the expansion of the hydrophilic 3-D network of the hydrogel matrix while, a decrease in ESR may be due to the higher viscosity of hydrogel film which does not allow the expansion of the gel phase in water[34]. As depicted in **Figure 4.2(c)**, the influence of PVA was also examined. It was observed that increasing the PVA content

from 1.24 to 2.24 grams resulted in a higher ESR due to the presence of more hydrophilic groups in PVA, a hydrophilic polymer [35]. However, with further increase in amount of PVA up to 3.20 g, the ESR of the film was reduced. During the synthesis of the S9 sample, which contained 3.20 grams of PVA, the reaction mixture became viscous. This viscosity might have contributed to the lower swelling of the S9 sample. The influence of the cross-linker (GTA) was also studied, as depicted in **Figure 4.2(d)**. The results indicated that increasing the volume of the GTA cross-linker led to a decrease in the swelling capacity of the hydrogel film. This could be attributed to the decreased pore spaces between the polymeric chains caused by the increased cross-linking density of the polymeric network. As a result, the reduced accessible volume for water absorption led to a lower ESR value for the hydrogel films.

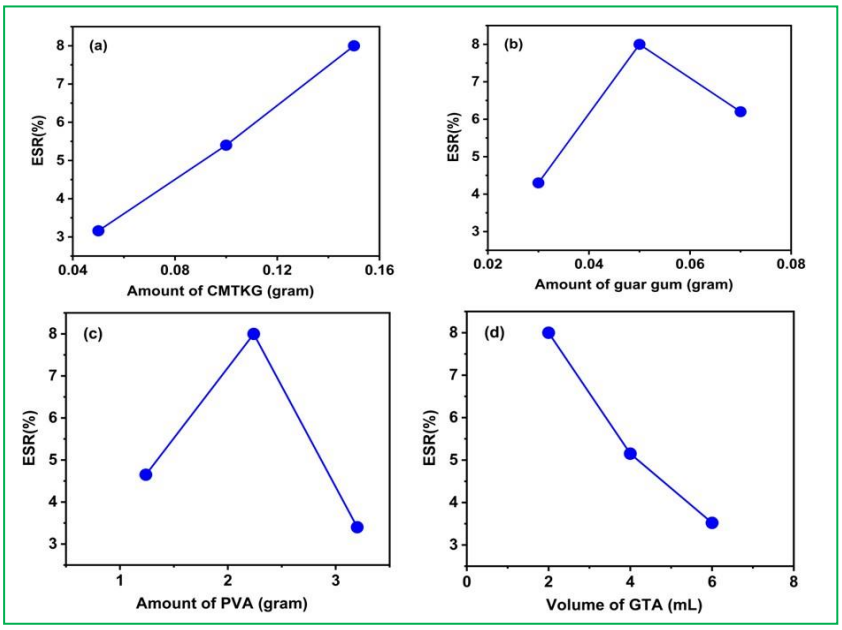

Figure 4.2: Effect of amount of (a) CMTKG (b) GG (c) PVA (d) GTA on ESR of hydrogel film at pH 7.4 buffer solution

4.3.2. FE-SEM

FE-SEM micrograph of CMTKG/PVA/GG hydrogel film at 2 μm and 3 μm scales at different magnifications are shown in **Figure 4.3(a-c)**. The surface morphology of the film manifests an irregular arrangement of compact and globular structures. Also, the rough surface of the hydrogel film showed the presence of both micro and macro pores in the hydrogel matrix [35]. Additionally, EDX analysis of the hydrogel film, as shown in **Figure 4.3d**, revealed the presence of oxygen and sodium elements within the film.

The weight percentage of oxygen was determined to be 73.79%, while that of sodium was found to be 26.21%.

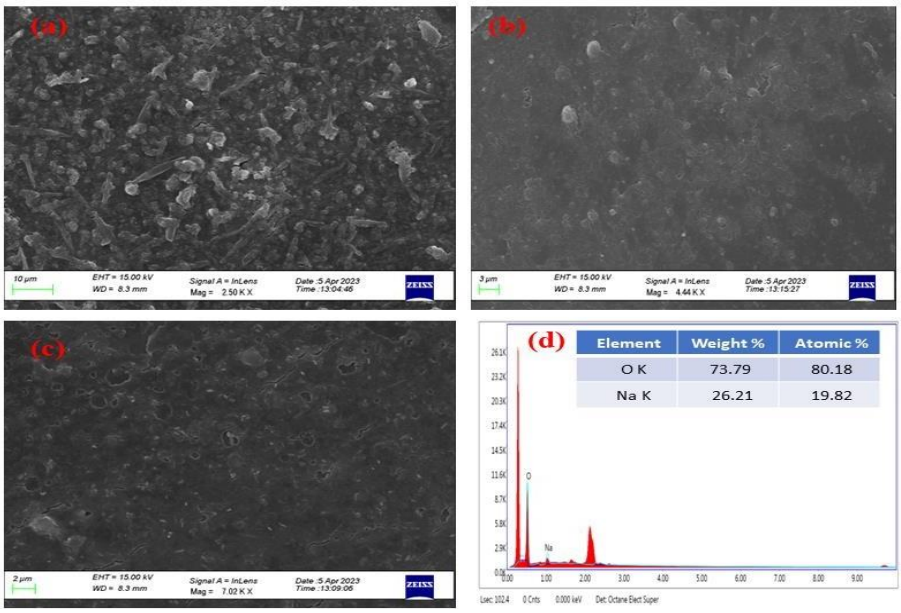

Figure 4.3: FE-SEM micrograph of CMTKG/PVA/GG film at (a) 10 µm 3 µm (c) 2 µm scales (d) EDX analysis

4.3.3. FTIR analysis

FTIR spectra of hydrogel film, CFX drug, and CFX-loaded hydrogel film are shown in **Figure 4.4.** In the case of FTIR spectra of CMTKG/PVA/GG hydrogel film, a characteristic peak at 3327 cm^{-1} was observed due to intermolecular H-bonding between various components of films. The other observable peaks at 2933 cm^{-1} were correlated to the -CH_2 group, 1732 cm^{-1} correlated to -C=O vibration, 1015 cm^{-1} correlated with -C-O stretching, and 823 cm^{-1} correlated to the C-C vibration of the alkane group[24]. In the case of FTIR of the CFX drug, peaks at 3528 cm^{-1} (O-H vibration), 1446 cm^{-1} (C-N stretching vibration), and 1706 cm^{-1}(C=O vibration) were observed. A peak at 1272 cm^{-1} corresponded to the bending stretching of the O-H functional group present in carboxylic acid[36]. In the case of CFX-loaded hydrogel film, few common peaks of CFX drug were observed which indicated successful loading of CFX into hydrogel film. This is also evidence that there is only physical interaction of the drug with a polymeric matrix of hydrogel film as there is no observable shifting of FTIR peaks of hydrogel film after loading the drug.

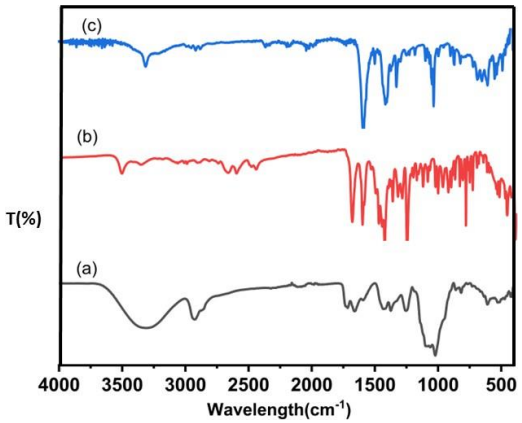

Figure 4.4: FTIR spectra of **(a)** CMTKG/PVA/GG hydrogel film **(b)** CFX CFX- loaded CMTKG/PVA/GG hydrogel film

4.3.4. TGA analysis

The thermal behavior of the CFX drug, CMTKG/PVA/GG hydrogel film, and CFX-loaded hydrogel film was analyzed using TGA and DTA curves **(Figure 4.5)**. According to the TGA analysis in Figure 4.5a, the CFX drug experienced an initial mass loss of 9.35% between 30 and 220 °C. This loss is attributed to the removal of the acetylene (C_2H_2) group.

The second and third stages of weight loss occur between 220 and 417 °C and 417- 500 °C, respectively, with mass losses of 46.54% and 66.03%. These losses may be attributed to the elimination of hydrogen, hydrogen fluoride, nitrogen oxide (NO), and ethylene [37]. In contrast, the first stage of weight loss for the CMTKG/PVA/GG film begins between 30 and 248 °C, with a loss of 26.87%, as illustrated in Figure 4.5b. [37]. In contrast, the next weight loss stage for the CMTKG/PVA/GG film occurred between 248 and 382 °C, with a loss of 57.53%. The final weight loss stage occurred between 382 and 486 °C, with a loss of 66.58%. However, in the case of the CFX-loaded hydrogel film, as shown in **Figure 4.5c**, the initial weight loss started at 30 °C and ended at 284 °C, with a weight loss of only 12.94%. This indicates that the thermal stability of the hydrogel film was improved after incorporating the CFX drug. The residual weight after decomposition at 506 °C was 33.21% for the drug-loaded film and 23.47% for the film without the drug.

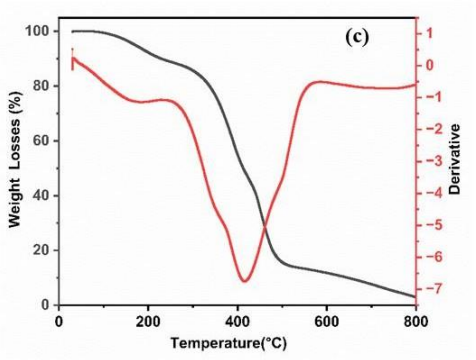

Figure 4.5: TGA-DTA analysis of **(a)** CFX drug **(b)** CMTKG/PVA/GG hydrogel film **(c)** CFX loaded hydrogel film

4.3.5. Mechanical Properties

The two parameters, tensile strength (MPa) and elongation at break (%) were chosen for the measurement of the tensile behavior of developed hydrogel films (S1 to S9) as shown in **Table 4.2.** It was observed from **Figure 4.6a** that the tensile strength value lies in the range of 95.80 to 149.07 MPa while elongation at break value lies in the range of 1.51 to 5.20 % as presented in **Figure 4.6b**. The good mechanical properties of films were observed because of strong cross-linked network due to physical interactions between PVA, CMTKG, and guar gum[14]. Therefore, hydrogel films with desirable mechanical properties can be applied in end-use applications. Literature reports reveal that tamarind gum and PVA-based composite films exhibit superior mechanical properties, making them ideal for controlled ciprofloxacin release [25, 38].

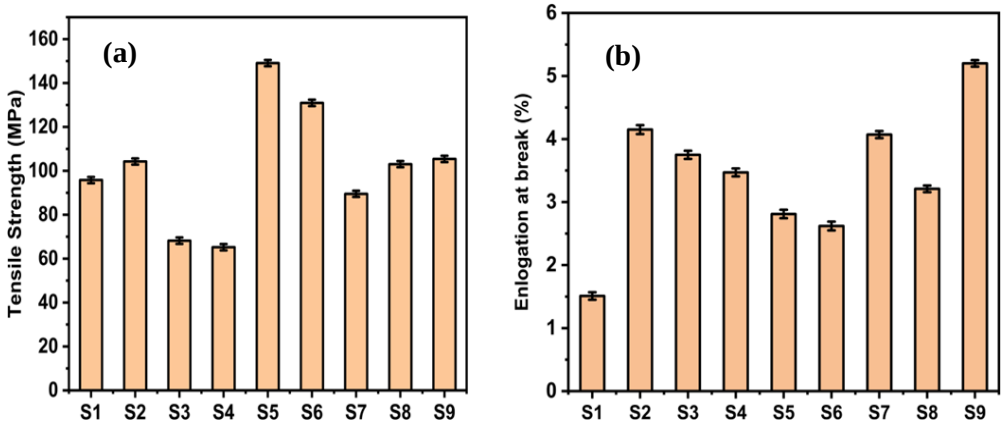

Figure 4.6: (a) Tensile strength (MPa) **(b)** Elongation at break (%)for S1 to S9 samples

Table 4.2: Results of physiochemical evaluation of hydrogel film

Sample Code	Thickness (mm)	Contact angle (degree)	Moisture content (%)	Tensile strength (MPa)	Elongation at break (%)
S1	0.06	39.58	4.51	95.8	1.51
S2	0.05	35.25	3.90	104.26	4.15
S3	0.09	69.85	3.29	68.18	3.75
S4	0.03	53.29	5.80	65.23	3.47
S5	0.05	43.58	6.65	149.07	2.81
S6	0.04	40.45	3.70	130.98	2.62
S7	0.03	64.28	4.69	89.53	4.07
S8	0.07	59.87	3.53	103.05	3.21
S9	0.08	75.70	3.12	105.43	5.20

4.3.6. Wetting analysis

The wetting analysis for all the synthesized hydrogel films (S1 to S9) was performed and estimated the water contact angle as given in **Table 4.2.** This analysis helps to determine the hydrophobicity and hydrophilicity of hydrogel films[39]. It was observed when the amount of CMTKG increased from 0.05 g to 0.1 g , contact angle was decreased for S2 film but with further increase in amount (0.15 g) of CMTKG, contact angle was increased for S1 film. Thus, the hydrophilicity nature of S2 film is higher than S1 and S3 films. However, with increasing the amount of guar gum biopolymer from 0.03 g to 0.05 g (from S4 to S1), contact angle was lowered for S1 film than S4 film. It may be due to higher cross-linking density of polymeric film which may cause unavailability of functional group for hydrogen bonding and led to higher hydrophobicity for S4 film[40]. However, further increase in amount up to 0.07 g of guar gum led to decrease in the contact angle for the S5 film. When the volume of GTA cross-linker was increased (from S1 to S7), the contact angle increased. This increase in contact angle is likely due to the denser cross-linking network of the hydrogel film, which made it more hydrophobic with a higher amount of cross-linker. Additionally, the contact angle increased when the amount of PVA was increased. This could be due to the higher of the reaction mixture, which might have interfered with the gel formation of the hydrogel film. Therefore, it can be concluded that the S2 film exhibited the highest hydrophilic nature.

4.3.7. CFX release study

The best-swelled hydrogel film (S2) was further used for drug-loading purpose. As mentioned earlier, the drug loading and encapsulation efficiency were evaluated using **Equations (4.2) and Eq.(4.3)**. The CFX loading and encapsulation efficiency was found to be 21.35 % and 70.63 %, respectively. Thus, S2 hydrogel film was used for the in-vitro drug release studies in PBS buffer solution (pH 7.4) because it exhibited the highest swelling in alkaline pH 7.4 solution[42]. The in-vitro CFX release studies from the CMTKG/PVA/GG hydrogel film were performed in PBS buffer solution at 37 °C in an incubator at 120 rpm as shown in **Figure 4.7.** The experiment was conducted over a period of 24 hours. The results showed that 48.34% of the drug was released in the initial hour. After eight hours, 69% of the drug release was observed, possibly due to the dynamic swelling of the hydrogel film. However, the highest drug release after 24 h was found to be 73 %.

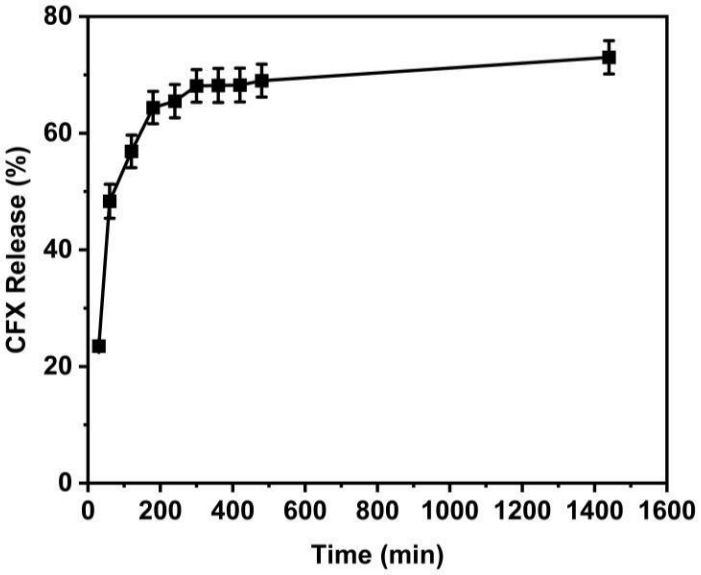

Figure 4.7: In-vitro release of CFX drug from S2 hydrogel film

Table 4.3: CFX releases data fitted in various mathematical models

Sample	Higuchi model		Korsmeyer-Peppas model			First order	
	KH	R^2	K	n	R^2	K1	R^2
S2	0.042	0.8207	0.1136	0.38	**0.9826**	0.0135	0.9718

4.3.8. Release Kinetic Study of CFX drug

The in-vitro CFX drug release data from S2 hydrogel film was fitted to different models such as the First-order, Higuchi, and Korsmeyer-Peppas models[43]. All the parameters related to these models are shown in **Table 4.3**. The regression coefficient (R^2) value, approaching unity, strongly suggested that the Korsmeyer-Peppas model was the best fit for the CFX release data. The calculated value of R^2 from this model was 0.9826. The calculated value of diffusion exponent (n) from the Korsmeyer-Peppas model was 0.388 which showed that drug release from the hydrogel film followed a Fickian diffusion mechanism[44]. **Figure 4.8** illustrates the release kinetics of the CFX drug from the hydrogel film, as modeled by the first-order, Higuchi, and Korsmeyer-Peppas models in a phosphate saline buffer solution with a pH of 7.4.

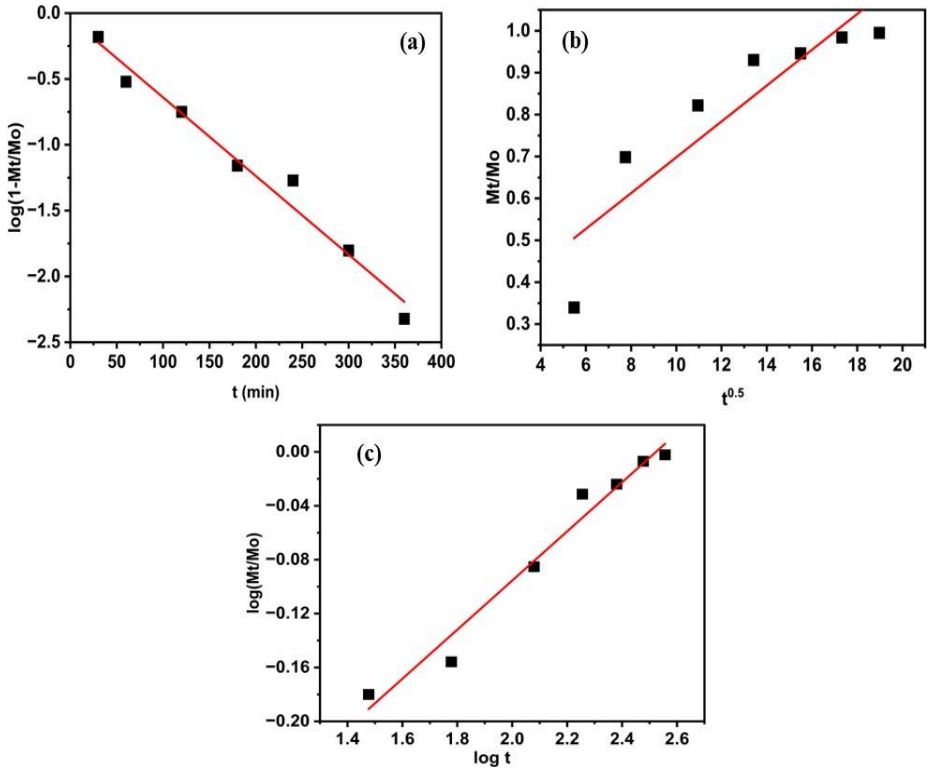

Figure 4.8: Release kinetics of CFX drug by (a) First-order model (b) Higuchi model (c) Korsmeyer-Peppas model

4.3.9. Antibacterial assay

Antibacterial properties of hydrogel film were evaluated against *S. aureus* and *E.coli* bacteria as shown in **Figure 4.9(a,b).** The Antibacterial activity was performed by using the zone inhibition method (Kirby-Bauer method). The zone of inhibition for hydrogel

film was measured as 15.66±1.15 mm and 17.66±0.57 mm for *E.coli* and *S. aureus*, respectively **(Figure 4.9(c)).** It was found that the hydrogel film showed stronger antibacterial properties against *S. aureus* than *E.coli.* Thus, the developed hydrogel film showed good antibacterial properties, which can be used in different biomedical applications.

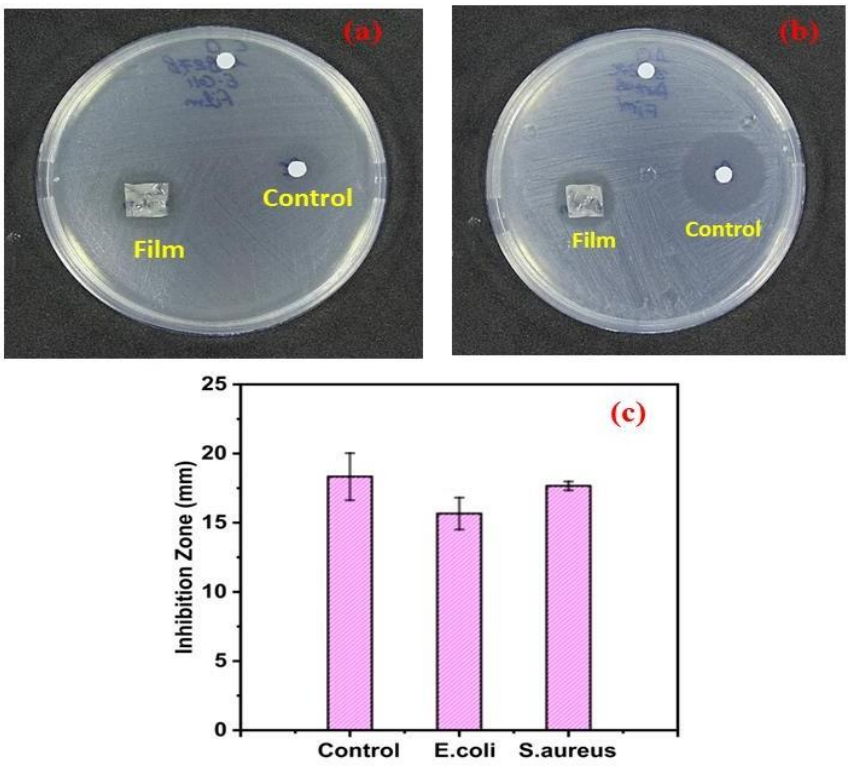

Figure 4.9: Antibacterial activity of hydrogel film against (a) E.coli (b) S. aureus (c) inhibition zone (mm) of hydrogel film against E. coli and S. aureus

4.3.10. Cytocompatibility analysis

The MTT assay was performed on HaCaT human keratinocyte cell lines using various concentrations (0, 0.5, 1.0, 1.5, and 2.0 µg/mL) of the synthesized hydrogel film for the S2 sample, as illustrated in **Figure 4.10.** The S2 film demonstrated 64% cell viability at the highest concentration of 2 µg/mL. However, at a concentration of 0.5 µg/mL, cell viability was observed to be 82%. This behavior is likely attributed to the presence of biologically active sites within the CMTKG and GG biopolymers.

The CMTKG and GG are biocompatible polymers that contribute to the cytocompatibility of hydrogel film. The inherent biocompatibility of PVA, a synthetic

polymer, contributes to the increased cytocompatibility of the hydrogel film[25]. □ Furthermore, microscopic examination of HaCaT cells revealed that both the hydrogel film-treated and control cell lines maintained a polygonal shape and similar cell density. This indicates that the hydrogel film had no significant effect on the morphology or viability of the cells.

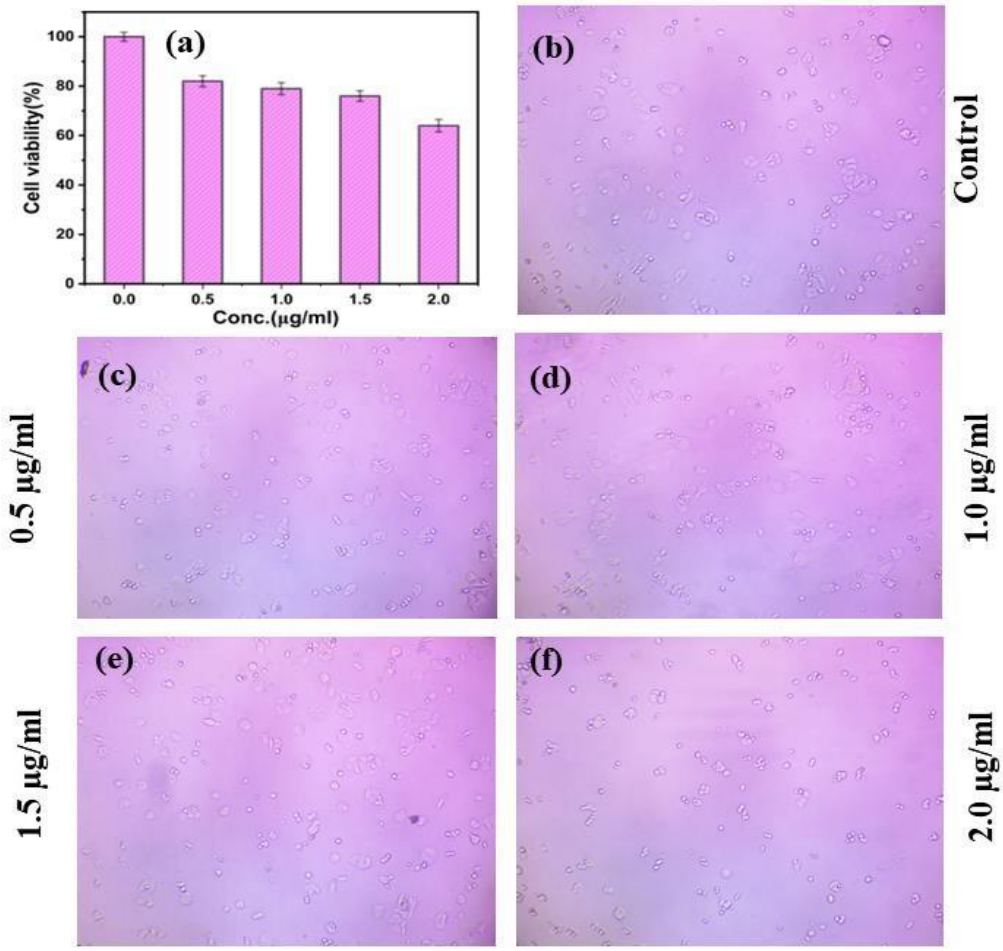

Figure 4.10: (a) MTT assay of hydrogel film with different concentrations on HaCaT cell lines, optical microscopic pictures of HaCaT cells treated with **(b)** control **(c)** 0.5 µg/ml **(d)** 1.0 µg/ml **(e)** 1.5 µg/ml **(f)** 2.0 µg/ml concentration of hydrogel film

4.4. Conclusion

The present study describes the synthesis of a novel CMTKG/PVA/GG hydrogel film cross-linked with glutaraldehyde. The impact of altering the quantities of different components, such as CMTKG, PVA, GG biopolymers, and GTA cross-linker, on the equilibrium swelling ratio of the hydrogel film was evaluated. The study evaluated various parameters of the hydrogel film, including thickness, moisture content, and

contact angle. The tensile strength of hydrogel films (S1 to S9) lies in the range of 95.80 to 149.07 MPa, and elongation at break (%) lies in the range of 1.51 to 5.20 %. Moreover, the wetting analysis indicated that the S2 hydrogel film showed maximum hydrophilicity while the S9 hydrogel film showed minimum hydrophilicity. Thus, the S2 hydrogel film was chosen for the loading of the CFX drug due to its highest hydrophilicity and swelling capacity. Moreover, the successful loading of the CFX drug was confirmed by FTIR spectroscopy. The surface morphology of hydrogel film showed the presence of rough surface and globular structures. The thermal analysis showed that the loading of the CFX drug increased the thermal stability of the hydrogel film. Moreover, the CFX release studies from S2 hydrogel film in PBS solution (pH 7.4) showed that 48.34 % of the drug was released in the initial first hour. After 24 hours, the highest drug release was found to be 73%. This release data was fitted in the First-order, Higuchi and Korsmeyer-Peppas models to understand its release mechanism. The best-fitted model was selected based on the highest value of regression coefficient (R^2) close to unity. Therefore, the observation was that the Korsmeyer-Peppas model was the best-fitted model, and the estimated value of diffusion exponent (n) was found to be 0.38. This value shows that drug release from the hydrogel film followed Fickian diffusion. The hydrogel film was analyzed for its antibacterial activity against *E. coli* and *S. aureus* bacteria. The results demonstrated that the CFX-loaded film exhibited antimicrobial properties, with a significant zone of inhibition. The cytocompatibility analysis with MTT assay indicated that the synthesized film showed good cell viability and biocompatibility against HaCaT cell lines. Thus, the overall results suggested that CMTKG/PVA/GG hydrogel film has significant potential for the delivery of ciprofloxacin drug in biomedical applications.

References

[1] H. Mahmood, I.U. Khan, M. Asif, R.U. Khan, S. Asghar, I. Khalid, S.H. Khalid, M. Irfan, F.Rehman, Y.Shahzad, A. M. Yousaf, A.Younus, Z. R. Niazi, M. Asim, In vitro and in vivo evaluation of gellan gum hydrogel films: Assessing the co impact of therapeutic oils and ofloxacin on wound healing, *Int. J. Biol. Macromol.*, vol. 166, pp. 483–495, 2021, doi: 10.1016/j.ijbiomac.2020.10.206.

[2] P. Picone, M. A. Sabatino, A. Ajovalasit, D. Giacomazza, C. Dispenza, and M. Di Carlo, Biocompatibility, hemocompatibility and antimicrobial properties of xyloglucan-based hydrogel film for wound healing application, *Int. J. Biol. Macromol.*, vol. 121, pp. 784–795, 2019, doi: 10.1016/j.ijbiomac.2018.10.078.

[3] B. Evranos, D. Aycan, and N. Alemdar, Production of ciprofloxacin loaded chitosan/gelatin/bone ash wound dressing with improved mechanical properties, *Carbohydr. Polym.*, vol. 222, no. June, p. 115007, 2019, doi: 10.1016/j.carbpol.2019.115007.

[4] O. Zandraa, F.A.Ngwabebhoh, R.Patwa, H.T.Nguyen, M.Motiei, N.Saha, T.Saha, P.Saha, Development of dual crosslinked mumio-based hydrogel dressing for wound healing application: Physico-chemistry and antimicrobial activity, *Int. J. Pharm.*, vol. 607, no. April, p. 120952, 2021, doi: 10.1016/ j.ijpharm.2021.120952.

[5] Y. Huan, Q. Kong, Q.Tang, Y. Wang, H. Mou, R. Ying, C. Li, Antimicrobial peptides/ciprofloxacin-loaded O-carboxymethyl chitosan/self-assembling peptides hydrogel dressing with sustained-release effect for enhanced anti-bacterial infection and wound healing, *Carbohydr. Polym.*, vol. 280, no. October 2021, p. 119033, 2022, doi: 10.1016/j.carbpol.2021.119033.

[6] E. A. Kamoun, E. R. S. Kenawy, and X. Chen, A review on polymeric hydrogel membranes for wound dressing applications: PVA-based hydrogel dressings, *J. Adv. Res.*, vol. 8, no. 3, pp. 217–233, 2017, doi: 10.1016/j.jare. 2017.01.005.

[7] R. Deka, P. Boruah, A.A. Ali, R. Dutta, P. Gogoi, J. K. Sarmah, Smart hydrogel with rapid self-healing and controlled release attributes for biomedical applications, *Smart mater. struct.* 31 095039, DOI: 10.1088/1361-665X/ac845d.

[8] L. Cao, G. Shao, F. Ren, M.Yang, Y. Nie, Q. Peng, P. Zhang, Cerium oxide nanoparticle-loaded polyvinyl alcohol nanogels delivery for wound healing care systems on surgery, *Drug Deliv.*, vol. 28, no. 1, pp. 390–399, 2021, doi: 10.1080/10717544.2020.1858998.

[9] M. Massaro, A. B. Sanchez, R. S. Espejo, C.V. Iborra, G. Cavallaro, F. G. Villen, S. Guernelli, G. Lazzara, D. Miele, C. Diaz, G. Sandri, S. Riela, Ciprofloxacin carrier systems based on hectorite/halloysite hybrid hydrogels for potential wound healing applications, *Appl. Clay Sci.*, vol. 215, no. September, 2021, doi: 10.1016/j.clay.2021.106310.

[10] I. Rani, S. G. Warkar, and A. Kumar, Nano ZnO embedded poly (ethylene glycol) diacrylate cross-linked carboxymethyl tamarind kernel gum (CMTKG)/poly (sodium acrylate) composite hydrogels for oral delivery of ciprofloxacin drug and their antibacterial properties, *Mater. Today Commun.*, vol. 35, no. June 2022, p. 105635, 2023, doi: 10.1016/j.mtcomm.2023.105635.

[11] K. Dharmalingam and R. Anandalakshmi, Functionalization of cellulose-based nanocomposite hydrogel films with zinc oxide complex and grapefruit seed extract for potential applications in treating chronic wounds, *Polymer (Guildf).*, vol. 202, p. 122620, 2020, doi: 10.1016/j.polymer.2020.122620.

[12] R. Patwa, O. Zandraa, Z. Capáková, N. Saha, and P. Sáha, Effect of iron-oxide nanoparticles impregnated bacterial cellulose on overall properties of alginate/casein hydrogels: Potential injectable biomaterial for wound healing applications, *Polymers (Basel).*, vol. 12, no. 11, pp. 1–21, 2020, doi: 10.3390/polym12112690.

[13] A. P. Pandit, K. R. Koyate, A. S. Kedar, and V. M. Mute, Spongy wound dressing of pectin/carboxymethyl tamarind seed polysaccharide loaded with moxifloxacin beads for effective wound heal, *Int. J. Biol. Macromol.*, vol. 140, pp. 1106–1115, 2019, doi: 10.1016/j.ijbiomac.2019.08.202.

[14] Khushbu and S. G. Warkar, Potential applications and various aspects of polyfunctional macromolecule- carboxymethyl tamarind kernel gum, *Eur. Polym. J.*, vol. 140, no. September, p. 110042, 2020, doi: 10.1016/j.eurpolymj. 2020.110042.

[15] G. S. Shaw, D. Biswal, B. Anupriya, I. Banerjee, K. Pramanik, A. Anis, K. Pal, Preparation, Characterization and Assessment of the Novel Gelatin–tamarind Gum/Carboxymethyl Tamarind Gum-Based Phase-Separated Films for Skin Tissue Engineering Applications, *Polym. - Plast. Technol. Eng.*, vol. 56, no. 2, pp. 141–152, 2017, doi: 10.1080/03602559.2016.1185621.

[16] P. Orsu, A. Koyyada, K. Lakshun Naidu, and S. Yadav, Nanofibers of carboxymethyl tamarind gum/reduced graphene oxide composite for neuronal cell proliferation, *J. Drug Deliv. Sci. Technol.*, vol. 66, no. September, p. 102870, 2021, doi: 10.1016/j.jddst.2021.102870.

[17] Z. H. Ghauri, A. Islam, M. A. Qadir, N. Gull, B. Haider, R. U. Khan, T.Riaz, Development and evaluation of pH - sensitive biodegradable ternary blended hydrogel films (chitosan / guar gum / PVP) for drug delivery application, *Sci. Rep.*, pp. 1–10, 2021, doi: 10.1038/s41598-021-00452-x.

[18] M. U. A. Khan, M.A. Raza, S. I. A. Razak, M. R. A. Kadir, A. Haider, S. A. Shah, A. H. M. Yusof, S. Haider, I. Shakir, S. Aftab, *Novel functional antimicrobial and biocompatible arabinoxylan/guar gum hydrogel for skin wound dressing applications*, vol. 14, no. 10. 2020.

[19] J. David and B. Mahanty, Optimized ciprofloxacin release from citric acid crosslinked starch - PVA hydrogel film : modelling with mixture design, *J. Polym. Res.*, pp. 1–11, 2021, doi: 10.1007/s10965-020-02397-7.

[20] J. H. Sung, M.R.Hwang, J.O. Kim, J. H. Lee, Y.I. Kim, J.H. Kim, S.W.Chang, S.G. Jin, J.A. Kim, W.S.Lyoo, S.S. Han, S.K.Ku, C.S.Yong, H.G.Choi, Gel characterization and in vivo evaluation of minocycline-loaded wound dressing with enhanced wound healing using polyvinyl alcohol and chitosan, *Int. J. Pharm.*, vol. 392, no. 1–2, pp. 232–240, 2010, doi: 10.1016/j.ijpharm.2010.03.024.

[21] L. Parwani, M. Bhatnagar, A. Bhatnagar, V. Sharma, and V. Sharma, "Gum acacia-PVA hydrogel blends for wound healing," *Vegetos*, vol. 32, no. 1, pp. 78–91, 2019, doi: 10.1007/s42535-019-00009-4.

[22] S. Song, Z. Liu, M.A. Abubaker, L.Ding, J. Zhang, S.Yang, Z.Fan, Antibacterial polyvinyl alcohol/bacterial cellulose/nano-silver hydrogels that effectively promote wound healing, *Mater. Sci. Eng. C*, vol. 126, no. February, p. 112171, 2021, doi: 10.1016/j.msec.2021.112171.

[23] J. O. Kim, J.K.Park, J.H.Kim, S.G.Jin, C.S.Yong, D.X.Li, J.Y.Choi,J.S.Woo, B.K.Yoo, W.S.Lyoo, J.A.Kim, H.G.Choi, Development of polyvinyl alcohol-sodium alginate gel-matrix-based wound dressing system containing nitrofurazone, *Int. J. Pharm.*, vol. 359, no. 1–2, pp. 79–86, 2008, doi: 10.1016/j.ijpharm.2008.03.021.

[24] M. R. Hwang, J.O. Kim, J.H.Lee, Y.I.Kim, J.H. Kim, S.W.Chang, S.G.Jin, J.A. Kim, W.S. Lyoo, S. S. Han, S. K. Ku, C.S.Yong, H.G.Choi, Gentamicin-loaded wound dressing with polyvinyl alcohol/dextran hydrogel: Gel characterization and in vivo healing evaluation, *AAPS PharmSciTech*, vol. 11, no. 3, pp. 1092–1103, 2010, doi: 10.1208/s12249-010-9474-0.

[25] I. Yadav, V. Rathnam, Y.Yogalakshmi, S.Chakraborty, I.Banerjee, A.Anis, K.Pal, Synthesis and characterization of polyvinyl alcohol- carboxymethyl tamarind gum based composite films," *Carbohydr. Polym.*, vol. 165, pp. 159– 168, 2017, doi: 10.1016/j.carbpol.2017.02.026.

[26] P. Orsu and S. Matta, Fabrication and characterization of carboxymethyl guar gum nanocomposite for application of wound healing, *Int. J. Biol. Macromol.*, vol. 164, pp. 2267–2276, 2020, doi: 10.1016/j.ijbiomac.2020.07.322.

[27] Tushar, Y. Saraswat, P. Meena, and S. G. Warkar, Synthesis and characterization of novel xanthan gum-based pH-sensitive hydrogel for metformin hydrochloride release, *Colloid Polym. Sci.*, no. 0123456789, 2023, doi: 10.1007/s00396-023-05135-9.

[28] H. Chopra, S. Bibi, S. Kumar, M. S. Khan, P. Kumar, and I. Singh, Preparation and Evaluation of Chitosan/PVA Based Hydrogel Films Loaded with Honey for Wound Healing Application, *Gels*, vol. 8, no. 2, 2022, doi: 10.3390/gels8020111.

[29] S. K. Ghosh, A.Das, A.Basu, A.Halder, S.Das, S.Basu, M.F.Abdullah, A.Mukherjee, S.Kundu, Semi-interpenetrating hydrogels from carboxymethyl guar gum and gelatin for ciprofloxacin sustained release, *Int. J. Biol. Macromol.*, vol. 120, pp. 1823–1833, 2018, doi: 10.1016/j.ijbiomac.2018. 09.212.

[30] D. H. Hanna and G. R. Saad, Encapsulation of ciprofloxacin within modified xanthan gum- chitosan based hydrogel for drug delivery, *Bioorg. Chem.*, vol. 84, no. November 2018, pp. 115–124, 2019, doi: 10.1016/j.bioorg.2018. 11.036.

[31] K. Kalantari, E. Mostafavi, B. Saleh, P. Soltantabar, and T. J. Webster, Chitosan/PVA hydrogels incorporated with green synthesized cerium oxide nanoparticles for wound healing applications, *Eur. Polym. J.*, vol. 134, p. 109853, 2020, doi: 10.1016/j.eurpolymj.2020.109853.

[32] Khushbu, S. G. Warkar, and N. Thombare, Controlled release and release kinetics studies of boron through the functional formulation of carboxymethyl tamarind kernel gum-based superabsorbent hydrogel, *Polym. Bull.*, vol. 79, no. 4, pp. 2287–2303, 2022, doi: 10.1007/s00289-021-03634-9.

[33] R. Malik, S. G. Warkar, and R. Saxena, Carboxy-methyl tamarind kernel gum based bio-hydrogel for sustainable agronomy, *Mater. Today Commun.*, vol. 35, no. January, p. 105473, 2023, doi: 10.1016/j.mtcomm.2023.105473.

[34] L. Ali, M. Ahmad, M. N. Aamir, M. U. Minhas, H. H. Shah, and M. A. Shah, Cross-linked pH-sensitive pectin and acrylic acid based hydrogels for controlled delivery of metformin, *Pak. J. Pharm. Sci.*, vol. 33, no. 4, pp. 1483–1491, 2020, doi: 10.36721/PJPS.2020.33.4.REG.1483-1491.1.

[35] S. Batool, Z. Hussain, M. B. K. Niazi, U. Liaqat, and M. Afzal, Biogenic synthesis of silver nanoparticles and evaluation of physical and antimicrobial properties of Ag/PVA/starch nanocomposites hydrogel membranes for wound dressing application, *J. Drug Deliv. Sci. Technol.*, vol. 52, no. April, pp. 403–414, 2019, doi: 10.1016/j.jddst.2019.05.016.

[36] R. Samanta, S. Nayak, B. Das, A. K. Nayak, chitosan -carboxymethyl tamarind gum in situ polyelectrolyte complex- based floating capsule of ofloxacin: In vitro -in vivo studies, *Int. J. Biol. Macromol.*, vol. 253 pp. 127507, 2023, doi: 10.1016/j.ijbiomac.2023.127507.

[37] D. Kowalczuk, A. Gładysz, M. Pitucha, D. M. Kamiński, A. Barańska, and B. Drop, Spectroscopic study of the molecular structure of the new hybrid with a potential two-way antibacterial effect, *Molecules*, vol. 26, no. 5, 2021, doi: 10.3390/molecules26051442.

[38] S. H. Hussein-Al-Ali, S. M. Abudoleh, Q. I. A. Abualassal, Z. Abudayeh, Y. Aldalahmah, and M. Z. Hussein, Preparation and characterisation of ciprofloxacin-loaded silver nanoparticles for drug delivery, *IET Nanobiotechnology*, vol. 16, no. 3, pp. 92–101, 2022, doi: 10.1049/nbt 2.1208 1.

[39] D. Qureshi, K.P.Behera, D.Mohanty, S.K.Mahapatra, S.Verma, P.Sukyai, I.Banerjee, S.K.Pal, B.Mohanty, D.Kim, K.Pal, Synthesis of novel poly (vinyl alcohol)/tamarind gum/bentonite-based composite films for drug delivery applications, *Colloids Surfaces A Physicochem. Eng. Asp.*, vol. 613, no. December 2020, p. 126043, 2021, doi: 10.1016/j.colsurfa.2020.126043.

[40] W. S. Al-Arjan, M. U. A. Khan, H. H. Almutairi, S. M. Alharbi, and S. I. A. Razak, pH-Responsive PVA/BC-f-GO Dressing Materials for Burn and Chronic Wound Healing with Curcumin Release Kinetics, *Polymers (Basel).*, vol. 14, no. 10, 2022, doi: 10.3390/polym14101949.

[41] B. D. Kevadiya, S. Rajkumar, H.C.Bajaj, S.S.Chettiar, K.Gosai, H.Brahmbhatt, A.S.Bhatt, Y.K.Barvaliya, G.S.Dave, R.K.Kothari, Biodegradable gelatin-ciprofloxacin-montmorillonite composite hydrogels for controlled drug release and wound dressing application, *Colloids Surfaces B Biointerfaces*, vol. 122, pp. 175–183, 2014, doi: 10.1016/j.colsurfb.2014. 06.051.

[42] A. Tanwar, P. Date, and D. Ottoor, ZnO NPs incorporated gelatin grafted polyacrylamide hydrogel nanocomposite for controlled release of ciprofloxacin, *Colloid Interface Sci. Commun.*, vol. 42, no. December 2020, p. 100413, 2021, doi: 10.1016/j.colcom.2021.100413.

[43] Khushbu, S. G. Warkar, and N. Thombare, "Correction to: Zinc micronutrient-loaded carboxymethyl tamarind kernel gum-based superabsorbent hydrogels: controlled release and kinetics studies for agricultural applications, *Colloid Polym. Sci.*, vol. 299, no. 9, p. 1505, 2021, doi: 10.1007/s00396-021-04857-y.

[44] J. Chalitangkoon, M. Wongkittisin, and P. Monvisade, Silver loaded hydroxyethylacryl chitosan/sodium alginate hydrogel films for controlled drug release wound dressings, *Int. J. Biol. Macromol.*, vol. 159, pp. 194–203, 2020, doi: 10.1016/j.ijbiomac.2020.05.061.

[45] M. H. Abu Elella, M. W. Sabaa, D. H. Hanna, M. M. Abdel-Aziz, and R. R. Mohamed, "Antimicrobial pH-sensitive protein carrier based on modified xanthan gum," *J. Drug Deliv. Sci. Technol.*, vol. 57, p. 101673, 2020, doi: 10.1016/j.jddst.2020.101673.

[46] D. H. Hanna, R. Osailan, and H. A. Ahmed, "Stevia rebaudiana Methanolic Leaf Extract in Egypt: Phytochemical Analysis, Antioxidant, Antilipid Peroxidation, Antihemolytic, Antimetastatic, and Anticancer Properties," *J. Food Biochem.*, vol. 2023, 2023, doi: 10.1155/2023/7161091.

CHAPTER 5

REMOVAL OF CATIONIC CRYSTAL VIOLET DYE USING ZEOLITE EMBEDDED CARBOXYMETHYL TAMARIND KERNEL GUM AND POLY(SODIUM METHACRYLATE) BASED HYDROGEL ADSORBENTS

5.1. Introduction

Polluted water due to synthetic toxic dyes has become a serious challenge to environmental scientists. In a few years, drinking water quality will greatly be diminished by the direct and indirect discharge of industrial toxic effluents[1]. Even a small trace of toxic dye can harm the aquatic life of flora and fauna by disturbing the photosynthesis process[2]. Therefore, these toxic dyes must be removed from aqueous solutions. Various technologies were used for this purpose including biological degradation, chemical oxidation, photocatalytic degradation, and adsorption [3]. However, the removal of dyes using hydrogel as adsorbent is one of the most effective approaches owing to its low operating cost [4]. In this study, Crystal violet (CV) was chosen for the dye removal experiment. CV, also known as methyl violet 10B, is a toxic dye with mutagenic and carcinogenic properties.[4]. It is used in the textile, wood, and paper industry [5]. Therefore, it is crucial to develop efficient methods for removing CV dye from wastewater. In the past few years, hydrogels based on natural biopolymers have been used as an adsorbent in the dye removal applications [6].

Hydrogels are three-dimensional hydrophilic networks synthesized from synthetic and natural biopolymers. They have high water absorption efficiency due to the presence of hydrophilic groups like hydroxy(-OH) and carboxylate($-COO^-$) [7]. Furthermore, hydrogels synthesized from biopolymers are known for their non-toxicity, biocompatibility, and biodegradability. Additionally, the limited use of polysaccharide-based hydrogels as adsorbents can be attributed to their poor surface area, limited ability to form hydrogen bonds, and low hydrodynamic volume. [8]. However, the surface properties of hydrogels can be modified by incorporating inorganic substances like zeolites, clays, and nanoparticles [9]. Zeolites are crystalline materials with a tetrahedral structure, composed of aluminosilicates. The large surface area and porosity

of zeolite are responsible for their water purification property. Few zeolite-based composite hydrogels have been documented for removing toxic dyes and heavy metal ions. [10]. Due to their negatively charged lattice and ion-exchange capacity, zeolite-loaded hydrogels have been employed as adsorbents in various studies. [11]. Composite hydrogel based on gum karaya with acrylic acid and N- isopropyl acrylamide loaded with zeolite – Y particles and used for the dye adsorption of brilliant green dye (BG) [12]. Another study synthesized a composite hydrogel based on poly(methacrylic acid) and zeolite for the adsorption of basic yellow 28 dye from an aqueous solution. [13]. ZSM-5 was loaded into PVA/CMC/SA membrane and utilized for the dye adsorption of malachite green dye [14].

The biopolymers such as guar gum, carboxymethyl guar gum, alginate, chitosan, chitin, xanthan gum, carboxymethyl cellulose, chitin, gelatin-based hydrogels were used as adsorbents for the adsorption of toxic dye from the polluted water [15]. Carboxymethyl tamarind gum (CMTKG)-based hydrogels have been less explored as adsorbents for dye removal compared to other materials. A study synthesized a hydrogel by grafting tamarind gum with poly(methyl methacrylate) using CuBr as a catalyst. This hydrogel was then used for the removal of toxic dyes [16]. Moreover, nanocomposite hydrogel based on CMTKG-g-PAM/SiO_2 was synthesized for the dye adsorption of methylene blue[17]. Furthermore, CMTKG-based hydrogels have potential applications in agriculture [18], biomedical fields [19], cosmetics [20], and tissue engineering. [21,22]. In this work, zeolite-loaded CMTKG-based hydrogels were synthesized, and utilized as an adsorbent for the CV dye adsorption. The CMTKG-based hydrogel was fabricated using sodium methacrylate (SMA) monomer, and N,N methylene bisacrylamide (MBA) as a cross-linker through a free radical polymerization method. Moreover, the various combinations of composite hydrogels were synthesized with varying amounts of zeolite. Among the different hydrogel combinations, the best adsorbent was chosen based on its water absorption capacity. The effect of zeolite on the dye removal efficiency of hydrogel was analyzed. Zeolite and zeolite-loaded hydrogel were characterized using XRD, SEM, and FTIR techniques. The adsorption isotherm was studied using Langmuir and Freundlich isotherm models. The adsorption kinetics was also evaluated using various models such as Pseudo first-order, First-order, Pseudo second-order, and intraparticle diffusion models.

5.2. Experimental

5.2.1. Materials

Carboxymethyl tamarind kernel gum (CMTKG) having 0.20° of substitution, Methacrylic acid (MA, CDH), N, N-Methylene bisacrylamide (MBA, Merck, Germany), Potassium persulfate (KPS, Fischer scientific), Crystal violet (CV, CDH), and Sodium hydroxide (Fischer scientific, Mumbai), were used as received. Zeolite was obtained in powder form with an average particle size (2-4 µm) from Sigma Aldrich.

5.2.2. Preparation of CMTKG/Poly(sodium methacrylate) (PSMA) hydrogels

To synthesize CMTKG/PSMA hydrogel, a fixed amount of CMTKG was dissolved in 10 mL distilled water and stirred continuously at 600 rpm until complete solubilization. Then, a fixed volume of methacrylic acid was added to 5mL of sodium hydroxide, and the resulting solution was mixed with the reaction mixture containing CMTKG. Then, initiator KPS and cross-linker MBA were added to the reaction mixture and stirred well. The resulting hydrogel was named CMTKG/PSMA hydrogel. A similar procedure was followed to synthesize zeolite-loaded hydrogel. For this, zeolite solution was prepared separately in distilled water and added to the reaction mixture before the addition of KPS initiator and MBA cross-linker. Thus, zeolite-loaded CMTKG/PSMA hydrogel was obtained as shown in **Figure 5.1.** In this way, various combinations of zeolite-loaded hydrogels were synthesized by varying the amount of zeolite as summarized in **Table 5.1.**

Figure 5.1: Synthesis of CMTKG/PSMA hydrogel

Table 5.1: Synthesis of CMTKG/PSMA hydrogels with varying amounts of zeolite with their equilibrium swelling ratio (ESR) in distilled water

Formulation	CMTKG (g)	MA (mL)	Zeolite (g)	KPS (g)	MBA (g)	ESR (g/g)
ZH-1	0.1/20	5	0	0.045	0.065	47.00
ZH-2	0.1/20	5	0.02	0.045	0.065	45.27
ZH-3	0.1/20	5	0.05	0.045	0.065	44.83
ZH-4	**0.1/20**	**5**	**0.08**	**0.045**	**0.065**	**54.25**
ZH-5	0.1/20	5	1.0	0.045	0.065	51.05

5.2.3. Swelling Studies

Hydrogels have efficiency to absorb water. To evaluate the swelling capacity of hydrogels, a fixed weight of hydrogel (W_0) was added to the distilled water. After 24 hours, the swollen hydrogel was taken from the water and weighed by removing surface water by tissue paper. The equilibrium swelling ratio (ESR) was calculated according to the **Equation (5.1)[**22].

$$\mathrm{ESR(g/g)} = \frac{W_s - W_0}{W_0} \tag{5.1}$$

where W_s and W_0 represented the weights of the swollen hydrogel at equilibrium and dry hydrogel sample respectively. Among the synthesized hydrogel composites, zeolite-loaded CMTKG/PSMA hydrogel (ZH-4) was selected for the characterization and dye adsorption studies that showed the highest swelling capacity.

5.2.4. Point Zero Charge analysis (PZC)

To study the surface charges, present on hydrogel, PZC analysis was performed using a pH meter. Initially, different pH solutions between 3 to 12 were prepared by adding hydrochloric acid and sodium hydroxide. Then, 0.1 g of hydrogel was immersed in different pH solutions. After 24 hours, the pH of the supernatant liquid was noted using a pH meter and a graph was plotted between the difference in the initial and final pH (Δ pH) vs initial pH [24]. When Δ pH = 0, it indicates that there has been no change in

the pH of the solution, suggesting that the surface charge of the material has reached a neutral state, which is the PZC.

5.2.5. Porosity Measurement

The liquid displacement method [25] was used to determine the porosity of various composite hydrogels. Briefly, a pre-determined amount of hydrogel sample (W_d) was placed in a beaker containing ethanol for 24 hours till saturation. The weight of hydrogel in ethanol was recorded as W_l. The hydrogel was taken out from the ethanol after 24 hours and weighed (W_w) by removing the liquid present on the surface of the hydrogel. The porosity of the hydrogel was calculated by using **Equation (5.2)**. [26].

$$\text{Porosity } (\%) = \frac{W_w - W_d}{W_w - W_l} \times 100 \tag{5.2}$$

5.2.6. Characterization

5.2.6.1. Rheological analysis

Stress-controlled AR- 500 rheometers (TA Instrument, U.K.) with a cone plate shape of 25 mm diameter were used for the rheological studies of CMTKG/PSMA hydrogel and Zeolite loaded hydrogel. Rheological properties were measured in terms of the storage modulus (G') and loss modulus (G'') between 0.1 to 100 rad/s.

5.2.6.2. FTIR analysis

The FTIR spectra of zeolite and zeolite-loaded CMTKG/PSMA hydrogel were analyzed to identify the functional groups present in each sample. The KBr pellet method was used to prepare the samples for FTIR analysis, and the spectra were recorded in the wavelength range of 600-4000 cm^{-1}. (Model: Perkin Elmer spectrum version 10.5.3).

5.2.6.3. FE-SEM

The FE-SEM imaging of zeolite and zeolite-loaded hydrogel was carried out using the ZEISS EVO model. EDX analysis was also done at a voltage of 20 kV to investigate the presence of various elements present in the zeolite-loaded CMTKG/PSMA hydrogel.

5.2.6.4. X-ray diffraction (XRD)

XRD spectra of zeolite and zeolite-loaded hydrogel were carried out using powder X-ray diffraction with a high-resolution Bruker diffractometer equipped with a point detector (scintillation counter), over a range of angle 2θ from 0-80° with a scan rate of 1sec/step.

5.2.6.5. Brunauer- Emmett-Teller (BET)

BET was recorded to determine the surface area of the zeolite-loaded hydrogel at 77 K using a Quanta chrome Nova-1000 instrument by N_2 adsorption-desorption isotherm.

5.2.7. Dye adsorption Study

The removal of CV dye using ZH-4 hydrogel composite from an aqueous solution was studied at 35ºC for 5 hours. The effects of contact time, initial CV dye concentration, adsorbent dosage, pH, temperature, ionic strength, and nature of dye (cationic or anionic) on the dye adsorption efficiency were investigated. Different stock solutions of CV dye were prepared in the range of 20 mgL^{-1} to 100 mgL^{-1} concentration. To study the effect of pH on dye removal efficiency, different pH solutions from 3 to 12 were used. All studies were done by immersing hydrogel powder in 20 mL of CV dye solution for 5 hours. Then, the absorbance of the dye supernatant liquid was monitored at 578 nm using a UV-visible spectrophotometer. Thus, the adsorption efficiency (%) and equilibrium adsorption (Q_e) for the ZH-4 hydrogel were calculated according to the given **Equation (5.3)** and **(5.4)** respectively [13].

$$Q_e = \frac{(C_0 - C_e) \times V}{m} \tag{5.3}$$

$$\%\ \text{Removal of CV dye} = \frac{(C_0 - C_e)}{C_O} \times 100 \tag{5.4}$$

where C_o is the initial concentration and C_e is the equilibrium dye concentration (mgL^{-1}). However, Q_e is equilibrium dye adsorption (mg g^{-1}), V is the volume of the dye solution (L), and m is the adsorbent weight (g). The adsorption capacity (Q_t, mg/g) of ZH-4 hydrogel at a specific time t was studied using **Equation (5.5)**.

$$Q_t = \frac{(C_t - C_e) \times V}{m} \tag{5.5}$$

where C_t represents the concentration of left CV dye in the solution at time t.

5.2.8. Regeneration studies

To perform the adsorption-desorption experiment, ethanol was selected as a desorption medium based on its polarity and functionalities. An amount of saturated dye adsorbed xerogels powder was added into 50 mL ethanol solution and agitated for 1 hour. After that, the hydrogel particles were filtered, rinsed with distilled water, dried, and reused for the next adsorption-desorption cycle. The desorption efficiency (%) was calculated according to **Equation (5.6)**[27].

$$\text{Desorption efficiency (\%)} = \frac{\text{Amount of CV dye desorbed}}{\text{Amount of CV dye adsorbed}} \times 100 \qquad (5.6)$$

5.3. Results and discussion

5.3.1. Mechanism of formation of hydrogel adsorbent

CMTKG/PSMA composite hydrogel was synthesized through a free radical chain mechanism using potassium persulfate as an initiator [23]. Initially, the initiator decomposed to generate sulfate radicals at 60 ^{O}C. These radicals subsequently formed a chain by abstracting hydrogen atoms from the hydroxyl groups present on the backbone of CMTKG. The reactive radicals reacted with the C=C double bond of SMA, creating covalent bonds and initiating polymer growth of SMA. The newly formed radicals from the growing PSMA chain then reacted with the functional groups of the MBA cross-linker, forming a cross-linked network with CMTKG **(Figure 5.2).** The synthesized hydrogels were used as an adsorbent for the cationic crystal violet dye that was adsorbed on the surface of the hydrogel via diffusion mechanism. The interactions involved in the adsorption process may be dipole-dipole interaction, hydrogen bonding, and electrostatic interactions [27]. In the case where the pH is greater than the point of zero charge (PZC), the negatively charged carboxylate groups on the surface of the hydrogels attracted the positively charged CV dye particles through electrostatic attraction. However, when the pH is less than the PZC, the -COO- group of CMTKG

interacted with the nitrogen (N) atom of the dye through hydrogen bonding, as illustrated in **Figure 5.3**. Additionally, the -OH group present on the surface of the hydrogel could form hydrogen bonds with the -N atom of the dye, while the carboxylate ion could interact with the =N+ group of the dye through electrostatic attraction [12].

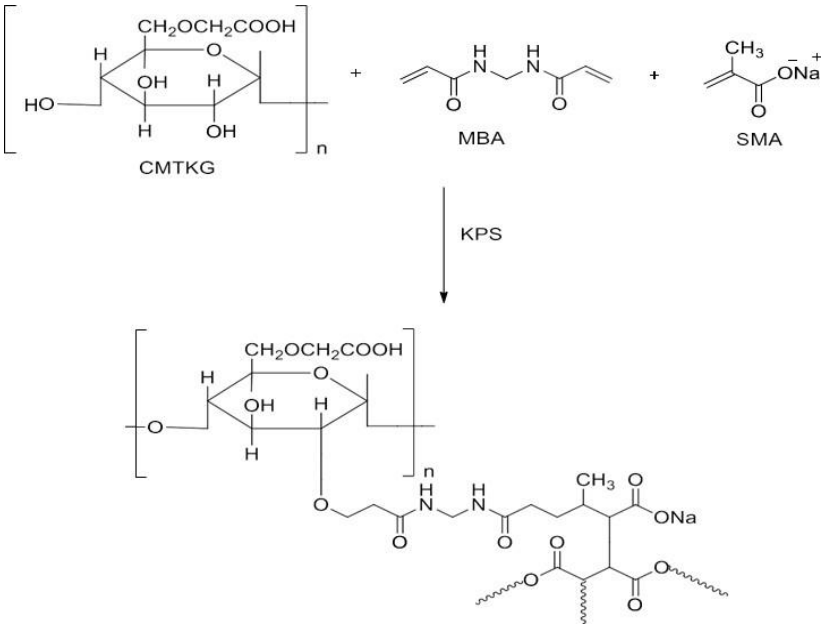

Figure 5.2: Mechanism of formation of CMTKG/PSMA hydrogel

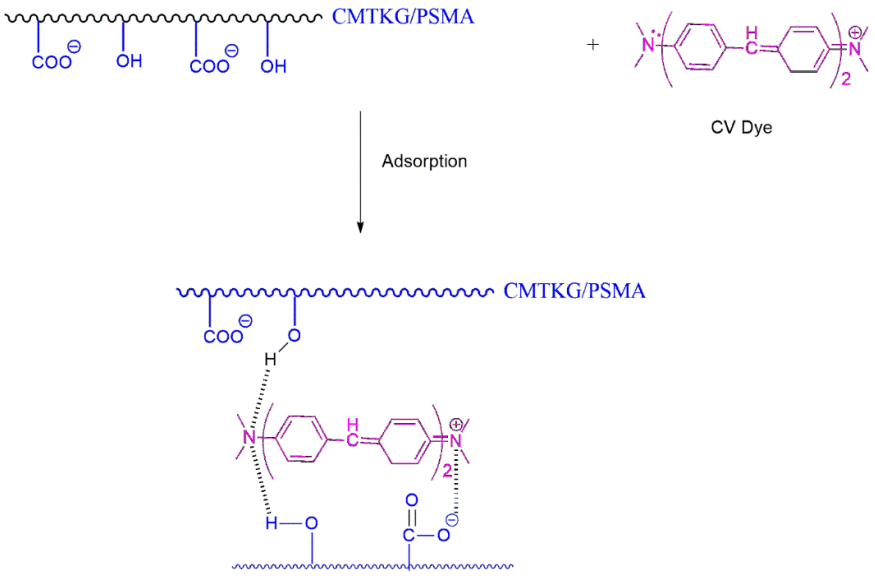

Figure 5.3: Possible mechanism of interaction of the dye with hydrogel network

5.3.2. Swelling studies

The swelling behavior for all the synthesized composite hydrogels was studied in the distilled water. The equilibrium swelling ratio (ESR(g/g)) was calculated and is presented in Figure 5.4. It was observed that as the amount of zeolite was increased from ZH-1 to ZH-3 hydrogel, the equilibrium swelling ratio decreased. However, further adding zeolite (0.08 g) to the ZH-4 hydrogel resulted in an increase in the ESR value. Conversely, when 0.1 g of zeolite was loaded in the ZH-5 hydrogels, the ESR value decreased again. The initial decrease in swelling for ZH-1 to ZH-3 hydrogels was observed due to the presence of a higher number of zeolite particles which significantly reduced the synergetic interactions between the zeolite and polymers present in the hydrogel matrix [30]. Moreover, the rigidity of hydrogels was also increased with an increase in the number of zeolite particles. However, ZH-4 hydrogel exhibited the highest swelling owing to the maximum synergetic interactions between zeolite and polymers present in the hydrogel matrix [12]. Overall, it was concluded that ZH-4 hydrogel exhibited the highest swelling in the distilled water. Therefore, ZH-4 hydrogel was used for all the characterization and dye removal experiments.

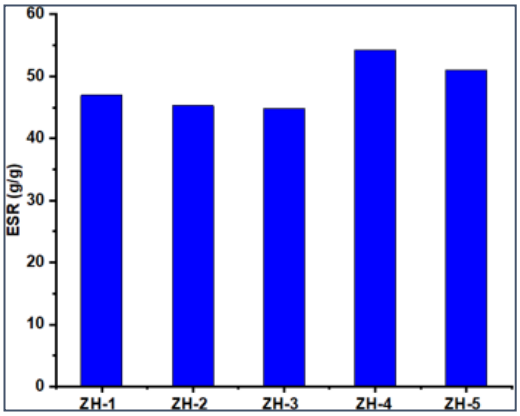

Figure 5.4: ESR (g/g) values for the synthesized hydrogels (ZH- 1 to ZH-5)

5.3.3. Porosity Measurement

The porosity of synthesized composite hydrogels was estimated by the liquid displacement method **(Figure 5.5).** It was observed that the porosity of hydrogels was increased by the loading of zeolite. The presence of zeolite also increased the hydrophilicity of hydrogels. The porosity of the hydrogels was observed to increase

from 63% to 80% as the zeolite content was raised. This enhancement is likely due to the larger surface area and negatively charged lattice sites of the zeolite. [31].

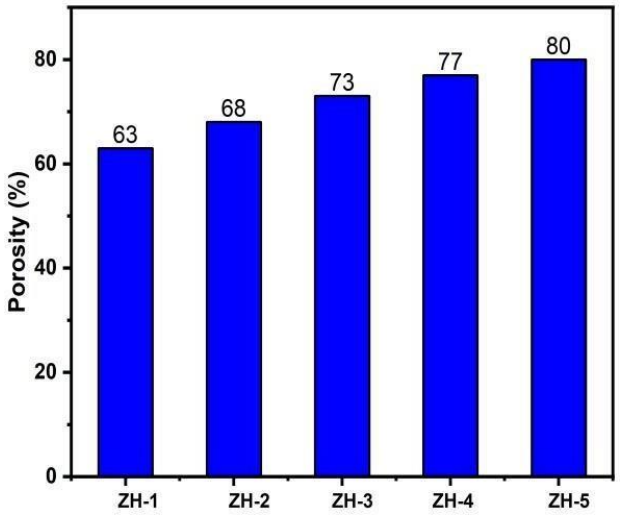

Figure 5.5: Porosity (%) measurement of zeolite-loaded hydrogels

5.3.4. Impact of the weight of adsorbent

The dye removal efficiency of ZH-4 hydrogel was calculated by varying the mass of the hydrogel adsorbent as shown in **Figure 5.6**. The dye removal efficacy was calculated with 5, 10, 20, and 40 mg hydrogel powder. The results showed that the dye removal efficiency of the hydrogels improved as the amount of hydrogel was increased from 5 to 20 mg. However, at a dosage of 40 mg, the dye removal efficiency decreased. This could be attributed to the increased active sites and surface area of the hydrogels at higher dosages, which may enhance the interaction between the dyes and hydrogel molecules. The maximum CV dye removal was achieved at an adsorbent quantity of 20 mg, reaching 93%. Beyond this point, agglomeration of adsorption sites occurred, leading to an increased diffusion path length. [12]. As a result, the dye removal efficiency of hydrogels above 20 mg amount was decreased. Similar results were reported for the removal of crystal violet dye using carboxymethylcellulose microbeads functionalized with p-benzoquinone and activated with iminodiacetic acid.[31].

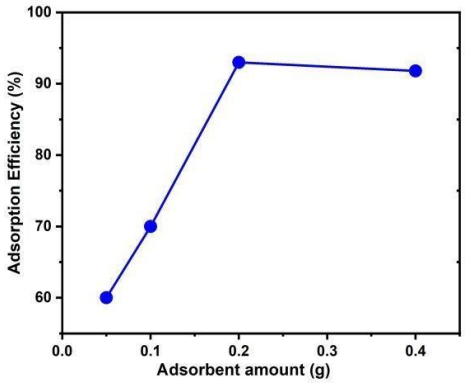

Figure 5.6: Effect of adsorbent amount on adsorption efficiency (%) of ZH-4 hydrogel

5.3.5. Impact of concentration of dye

The concentration of CV dye solution varied from 20 to 100 mgL^{-1} and their effect on the % adsorption of dye using ZH-4 hydrogel adsorbent was studied as shown in **Figure 5.7.** The observation revealed that the efficiency of hydrogels to adsorb the dye was decreased from 91 to 42 % by increasing the concentration of CV dye. At a lower concentration, a significant number of CV dye particles may adsorb on the surface of hydrogel, but at higher concentrations, active sites would become saturated. Consequently, the adsorption efficiency of hydrogels reduced as CV dye concentration increased. This observation is similar to the adsorption of CV dye using Arabic gum -cl- poly(acrylamide) nano hydrogel [32].

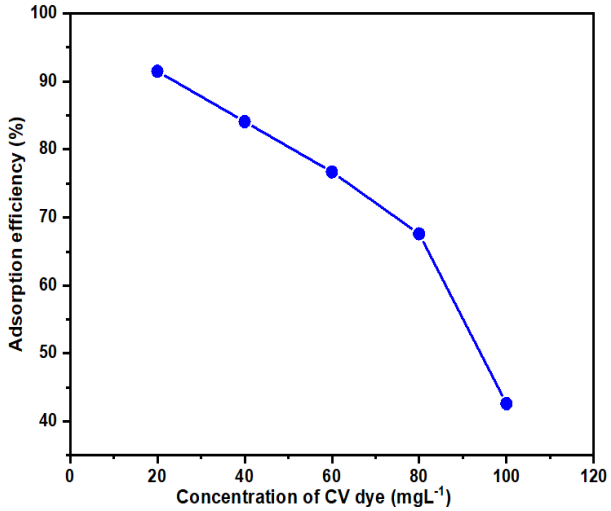

Figure 5.7: Effect of concentration of CV dye on adsorption efficiency (%) of ZH-4 hydrogel

5.3.6. Impact of temperature

The adsorption efficiency of the hydrogels can be altered by changing the temperature of the system. The temperature of the adsorption process varied from 7 to 45°C. The influence of temperature on ZH-4 hydrogel's adsorption efficiency was studied as shown in **Figure 5.8.** It was seen that as the temperature was increased from 7 to 35 ° C the adsorption efficiency of the hydrogel was also increased from 57.50 to 94 %. This incline may be associated with increasing diffusion and dispersion of dye as well as an increasing attractive forces between CV dye and hydrogel molecules, owing to enhancing the CV molecule's adsorption on ZH-4 hydrogel. However, at a higher temperature than 35ºC, a decline in adsorption of CV was observed due to an enhanced thermal effect which weakens the electrostatic attractive forces between the active sites on hydrogel and the CV molecules. Thus, ZH-4 hydrogel showed the highest adsorption efficiency at 35 °C.

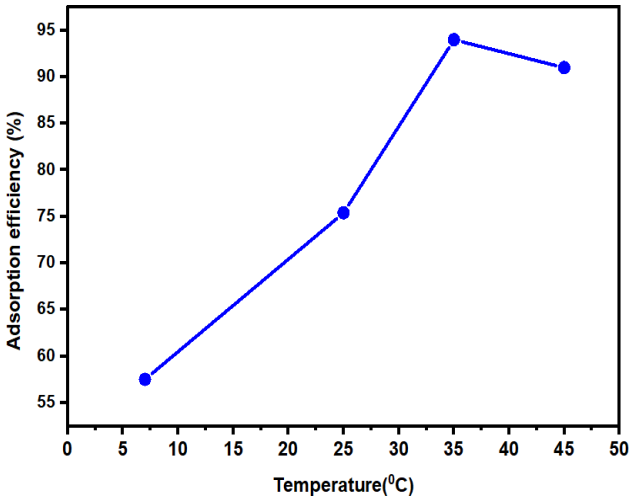

Figure 5.8: Effect of temperature on the adsorption efficiency of hydrogel

5.3.7. Impact of pH

To study the effect of pH, different CV dye solutions were prepared having pH 3 to 12. It was observed that increasing pH of the dye solution, the adsorption efficiency of ZH-4 hydrogel was increased **(Figure 5.9b).** In the hydrogel matrix, CMTKG and PSMA are anionic polymers that contain carboxylate anionic active sites for the adsorption of cationic CV dye. However, there was a large number of competing H^+ ions present in an acidic medium which would bind with the anionic groups present in the ZH-4

hydrogel leading to less dye removal efficiency of the hydrogel at a lower pH. Moreover, H+ ions, being smaller than CV, can more easily attach to the anionic carboxylate active sites. [33]. Also, with the increasing pH of the CV dye solution, a higher number of negatively charged OH^- ions and $-COO^-$ groups act as binding sites for the cationic CV dye present in the hydrogel which led to enhanced dye adsorption [17]. Hence, the maximum adsorption efficiency (%) of ZH-4 hydrogel was observed at pH 12. These results were correlated with PZC analysis of ZH-4 hydrogel as shown in **Figure 5.9a.** It was seen that at pH < PZC, lower adsorption of cationic CV dye took place due to the availability of protonated groups inside the hydrogel, while at pH > PZC, higher adsorption of CV dye was observed due to the availability of negatively charged binding sites present in the hydrogel [34].

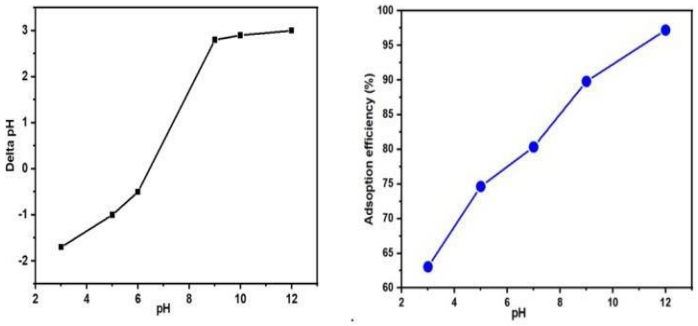

Figure 5.9: (a) PZC analysis **(b)** adsorption efficiency (%) variation with pH

5.3.8. Impact of Ionic strength

The impact of ionic strength on the dye removal efficiency of ZH-4 hydrogel was studied by using 0.1 N salt solution of NaCl, $CaCl_2$, and $AlCl_3$ as shown in **Figure 5.10.** For maximal dye adsorption, the optimum conditions were chosen, such as 20 mg of adsorbent in 20 mL of dye solution (100 mgL^{-1}), pH 12, 35°C, and 4 hours of equilibrium adsorption time. The results showed that by increasing the ionic strength of the dye solution, the hydrogel's adsorption efficacy was decreased. It was due to the competitive effect between the cationic CV dye particles and a cationic group of salt solutions which would bind with the anionic active sites on ZH-4 hydrogel. Furthermore, the result of ionic strength confirmed that there are electrostatic attractive forces that were responsible for the adsorption of CV dye onto anionic ZH-4 polymeric hydrogel [33]. These results are similar to the removal of crystal violet with Xanthan gum /Poly(vinyl alcohol) hydrogel [27].

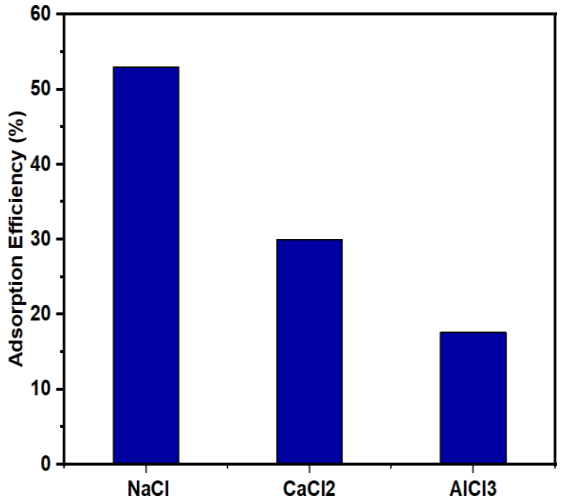

Figure 5.10: Effect of ionic strength on dye removal efficiency of ZH-4 hydrogel

5.3.9. Impact of contact time

A comparative dye removal study was performed for CMTKG/PSMA (ZH-1) and zeolite-loaded CMTKG/PSMA hydrogel (ZH-4) to evaluate the effect of zeolite particles on the dye adsorption efficiency of the hydrogel **(Figure 5.11).** The adsorption time was varied from 1 to 5 hours by keeping the other parameters fixed such as the mass of adsorbent used (20 mg), the concentration of dye solution (20 mgL^{-1}), pH (12), and 35° temperature. It was found that ZH-1 showed the maximum dye adsorption of up to 81 % while ZH-4 showed the maximum dye adsorption of up to 93 % in 4 hours and the removal of CV dye remains constant after 4 hours due to the saturation of the adsorption active sites present in the hydrogel [35]. Thus, the addition of zeolite particles increased the dye adsorption efficiency of hydrogel due to an increase in the swelling and porosity of hydrogel. The surface area of ZH-4 hydrogel was also increased in the presence of zeolite particles which would increase the number of adsorption sites for the dye removal [12]. As a result, higher adsorption efficiency of ZH-4 hydrogel was achieved in the presence of zeolite particles.

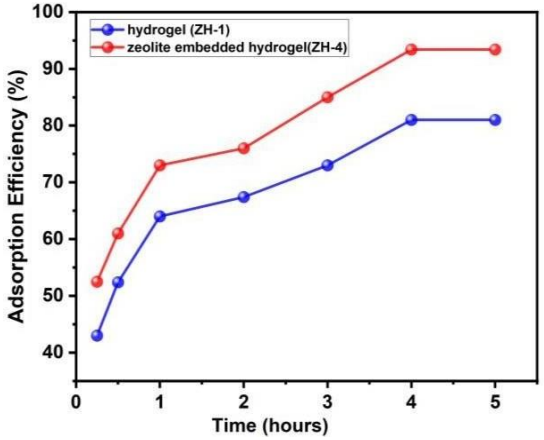

Figure 5.11: Influence of contact time on dye removal efficiency of hydrogel (ZH-1) and zeolite loaded hydrogel (ZH-4)

5.3.10. Comparison between various dyes

The hydrogel's efficiency in removing CV dye is significantly influenced by the charges present on the surface of CV dye. ZH-4 hydrogel was used as an adsorbent for the removal of cationic dyes such as methylene blue (MB), and crystal violet (CV), as well as for anionic dyes such as Congo red (CR) and methyl orange (MO) as shown in **Figure 5.12.** It was observed that ZH-4 hydrogel showed excellent adsorption efficiency for cationic dyes like MB, and CV while for anionic dyes like MO and CR, the adsorption efficiency of ZH-4 was comparatively very low. The difference in the adsorption efficiency was due to the electrostatic attractive forces and hydrogen bonding which would support the linkage of cationic dyes with the negatively charged linkage sites present on the surface of ZH-4 hydrogel.

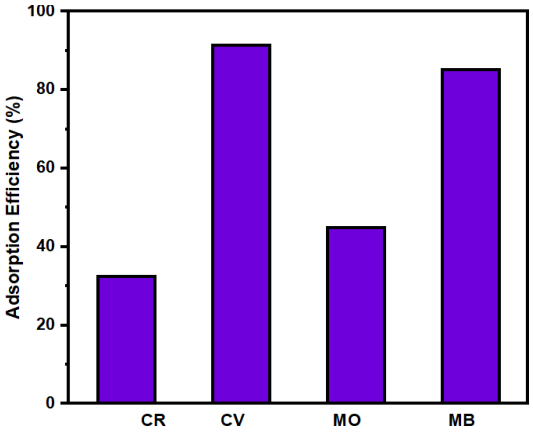

Figure 5.12: Comparison of various dyes for adsorption efficiency (%) of ZH-4 hydrogels

5.3.11. Rheological analysis

The rheological behavior of CMTKG/PSMA hydrogels (ZH-1) and zeolite-loaded hydrogels (ZH-4) was investigated by the variation of storage modulus (G') and loss modulus (G'') as a function of angular frequency as shown in **Figure 5.13**. The viscoelastic behavior of both the hydrogels was explained in terms of storage modulus (elastic nature) and loss modulus (viscous nature). It was observed that the value of storage modulus (G') increased with an increase in the angular frequency from 0.1 to 100 rad/s which indicated the increased elasticity of hydrogel. The addition of zeolite increased the degree and perfection of a cross-linking network of ZH-4 hydrogel [36]. As a result, the value of storage modulus (G') for zeolite-loaded hydrogel (ZH-4) was higher than for zeolite-unloaded hydrogel (ZH-1). The observation showed that the addition of zeolite to the hydrogel increased the elastic behavior and mechanical strength of the hydrogel [37]. The value of G' was higher than the G'' for both the ZH- 1 and ZH-4 hydrogels which indicated the dominant elastic behavior than the viscous behavior of hydrogels [38].

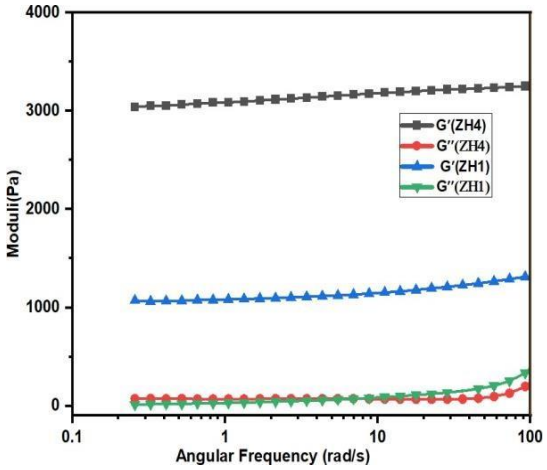

Figure 5.13: Storage (G') and loss modulus (G'') variation with angular frequency

5.4. Characterizations

5.4.1. XRD

XRD spectra of zeolite and zeolite-loaded ZH-4 hydrogel were recorded as shown in **Figure 5.14.** In the XRD of ZH-4 hydrogel **(Figure 5.14b)**, a broad diffraction peak at 20° at 2θ scale was observed which indicated the amorphous nature of ZH-4 hydrogel. In the XRD pattern of zeolite shown in **Figure 5.14a**, major peaks were observed at 8°,

23°, 25°, 29°and 33° at the2θ scale which indicated the crystalline nature of zeolite particles. However, these peaks were also found in the XRD of ZH-4 hydrogel and the intensity of these peaks was decreased in ZH-4 hydrogel due to loading zeolite particles into the polymeric matrix [12].

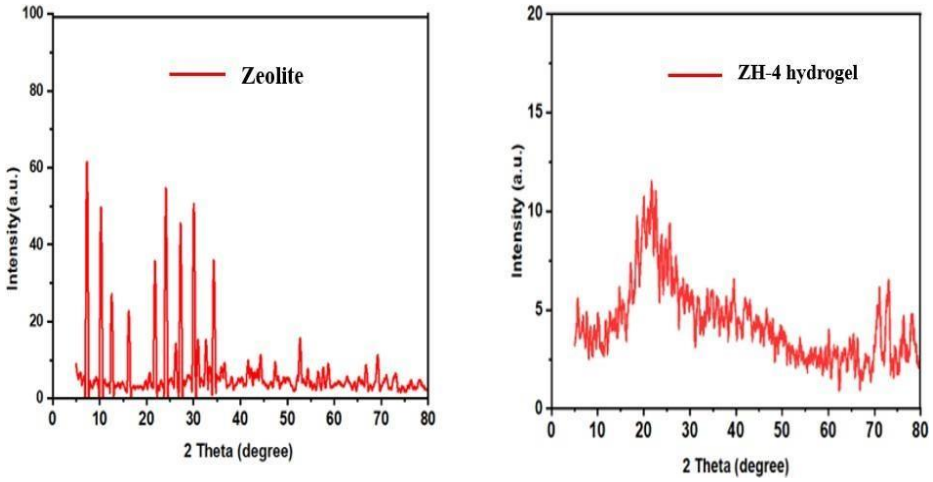

Figure 5.14: XRD plots of **(a)** Zeolite **(b)** ZH-4 hydrogel sample

5.4.2. FTIR

FTIR of zeolite as shown in **Figure 5.15a.** showed the characteristic adsorption peaks at 947 cm^{-1}, 671 cm^{-1}, and 459 cm^{-1} related to the symmetric vibration of Si-O-Si and Al- O-Si groups. A peak at 547 cm^{-1} corresponded to the vibration of tetrahedral units of Si or Al while another peak at 1654 cm^{-1} and 3375 cm^{-1} indicated the adsorbed water molecule by the zeolite material[39]. FTIR of the zeolite-loaded hydrogel as shown in **Figure 5.15b** indicated the stretching vibration of the -OH group of CMTKG at 3394 cm^{-1}. The stretching vibration of the $-COO^-$ groups present in the hydrogel was observed at 1720 cm^{-1}. However, the - O=C-N group present in MBA exhibited a vibrational frequency at 773 cm^{-1}, while the stretching vibration of the -CN group present in MBA was seen at a frequency of 1404 cm^{-1}[18]. It was observed that the characteristic band of zeolite at 550 cm^{-1} was also found in the FTIR spectra of ZH-4 hydrogel **(Figure 5.15b)** which indicated the successful trapping of zeolite particles into the ZH-4 hydrogel.

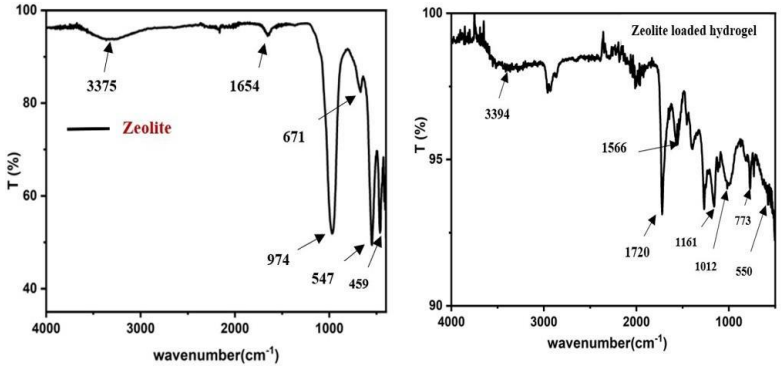

Figure 5.15: FTIR spectrum of **(a)** Zeolite **(b)** ZH-4 hydrogel

5.4.3. FE-SEM

The surface morphology of zeolite and zeolite-loaded ZH-4 hydrogel were analyzed using FE-SEM techniques. The micrograph in **Figure 5.16(a,b)** revealed the cubic morphology of zeolite particles. The average particle size of zeolite particles was estimated using ImageJ software to be 4.35 µm. Also, the surface morphology of ZH-4 hydrogel indicated the homogenous and uniform dispersion of zeolite particles into ZH-4 hydrogel matrix. It was observed that the shape of zeolite particles in the ZH-4 hydrogel remains the same as shown in **Figure 5.16(c,d).** In addition, the presence of various elements O, Na, Al, and Si in both zeolite and ZH-4 hydrogel was confirmed by EDX analysis as shown in **Figure 5.17 (a,b)**. The elemental mapping as shown in **Figure 5.17(c,d)** demonstrated the dispersion of O, Na, Al, and Si in the polymeric matrix.

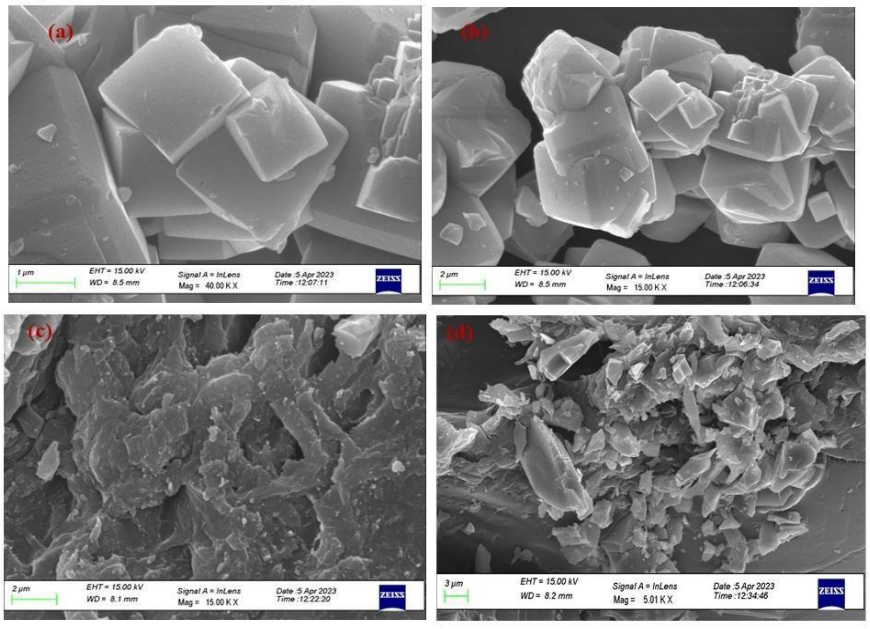

Figure 5.16: FE-SEM images of (a,b) zeolite particles and (c,d) Zeolite - loaded hydrogel

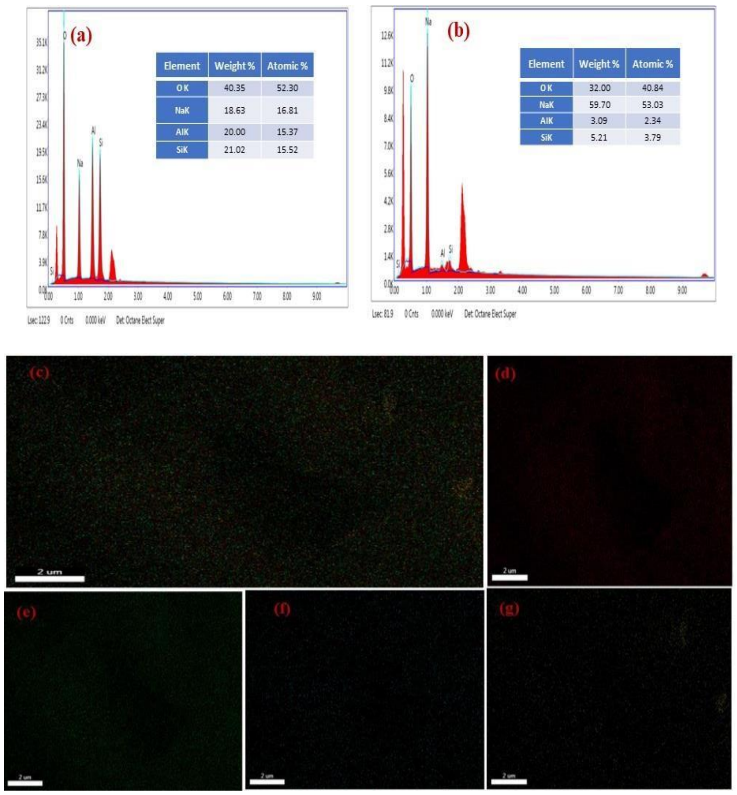

Figure 5.17: EDX spectrum of **(a)** zeolite **(b)** zeolite loaded hydrogel **(c)** elemental overlay and element maps ((d) O (e) Na (f) Al (g) Si

5.4.4. BET analysis

This analysis was carried out to determine the porosity and surface area of ZH-4 hydrogel. The N_2 adsorption/desorption isotherm was studied at 77 K as shown in **Figure 5.18a**, which showed the mesoporous nature of hydrogel particles used as an adsorbent. The specific surface area was estimated as 20.176 $m^2 g^{-1}$. Moreover, the pore size distribution plot shown in **Figure 5.18b** indicated that the estimated pore diameter and pore volume was to be 23.907 nm and 0.138 $cm^3 g^{-1}$, respectively.

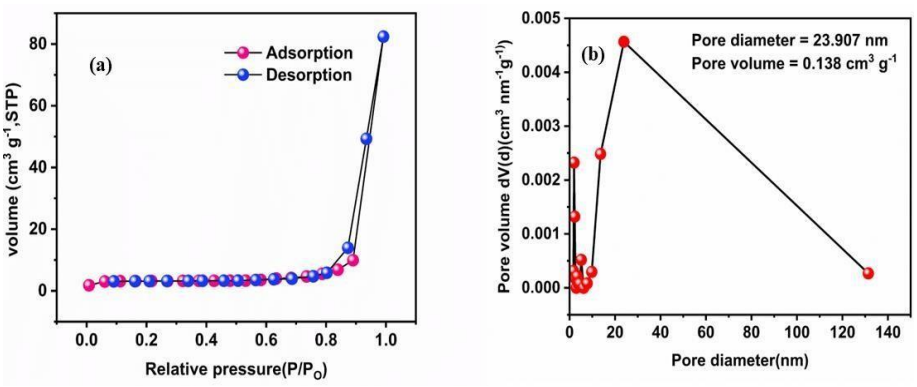

Figure 5.18: (a) adsorption-desorption isotherm **(b)** pore size distribution

5.4.5. Adsorption isotherm

The adsorption isotherm of CV dye on the surface of ZH-4 hydrogels was studied using Langmuir and Freundlich model. However, the Langmuir model expressed monolayer adsorption onto the homogeneous surface while the Freundlich model expressed multilayer adsorption with a condensation process onto the heterogeneous surface. The optimum conditions, such as 20 mg of hydrogel adsorbent in 20 mL of CV dye solution (20 ppm) at pH 12 and 35 $^{\circ}$C were used to study the adsorption isotherm on the hydrogel surface. A linear form as given in **Equation (5.7) and (5.8)** were used to analyze the adsorption data using the Langmuir and Freundlich isotherm models, respectively [32].

$$\frac{1}{Q_e} = \frac{1}{Q_{max}} + \frac{1}{bC_eQ_{max}} \tag{5.7}$$

$$\ln Q_e = \ln K_F + \frac{1}{n}\ln C_e \tag{5.8}$$

where Q_e is the maximum amount of adsorbed CV dye on ZH-4 hydrogel (mg g^{-1}). Q_{max} represents the hydrogel's greatest adsorption ability in terms of monolayer coverage (mg g^{-1}). C_e is the equilibrium concentration of CV dye (mg L^{-1}) and b is the Langmuir constant (L mg^{-1}) which can be affected by the affinity of the active sites and the adsorption's free energy. Also, the parameter K_F (Lg^{-1}) indicated the adsorption capacity while the parameter n indicated the adsorption intensity. Thus, adsorption isotherm was fitted in the Langmuir and Freundlich model as illustrated in **Figure 5.19**. All the related parameters of these models were tabulated in **Table 5.2**. The calculated maximum adsorption capacity (Q_{max}) from the Langmuir model was equal to 123.6 mg g^{-1} which led to a monolayer formation during the adsorption process of CV dye. Also, the value of the 1/n parameter related to the Freundlich model was found as 0.82, supporting favorable adsorption [37]. It was also observed that the Langmuir isotherm model having a higher R^2 value had been better correlated than the Freundlich model. Moreover, the separation factor (R_L) was used to calculate the affinity of CV dye onto ZH- 4 hydrogel using **Equation** (5.9) [40].

$$R_L = \frac{1}{1+b\,C_0} \tag{5.9}$$

where b is known as the Langmuir constant and C_0 is the initial concentration of CV dye (mgL^{-1}). The adsorption process is linear if R_L equals 1, irreversible if R_L equals 0, and favorable if $0 < R_L 1$. Since the calculated value of R_L is less than 1, it can be concluded that using ZH-4 hydrogel as an adsorbent to remove CV dye is an effective approach.

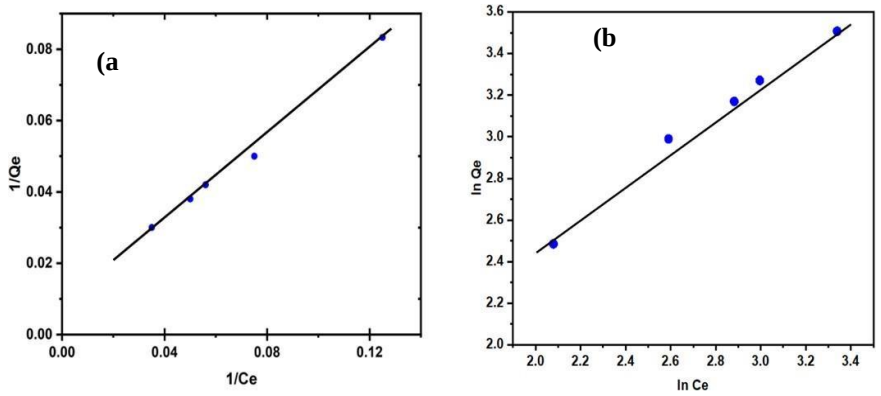

Figure 5.19: Graphs correspond to (a) Langmuir model and (b) Freundlich model for adsorption of CV dye on ZH-4 hydrogels

Table 5.2: Langmuir and Freundlich isotherm plot for removal of CV dye using hydrogel

Langmuir isotherm model		**Freundlich Isotherm model**			
Qmax (mg g^{-1})	B (Lmg^{-1})	R^2	KF (Lg^{-1})	1/n	R^2
123.60	0.0136	0.9942	2.3450	0.82	0.9743

5.4.6. Adsorption Kinetic

The multi-step process of the dye adsorption involves the migration of CV dye on the boundary layer along with the diffusion of dye onto the hydrogel's surface. The adsorption processes of CV dye on ZH-4 hydrogel were examined in the pseudo-first-order, second-order, and pseudo-second-order as given by following **Equation** (5.10), (5.11), and (5.12) respectively.

$$\ln(Q_e - Q_t) = \ln Q_e - K_1 t \qquad (5.10)$$

$$\frac{1}{Q_e - Q_t} = \frac{1}{Q_e} + K_2 t \qquad (5.11)$$

$$\frac{t}{Q_t} = \frac{1}{K_3 Q^2{}_e} + \frac{t}{Q_e} \qquad (5.12)$$

—

where Q_e and Q_t indicated the adsorption capacity of ZH-4 hydrogel to adsorb CV dye at equilibrium and time t, respectively. K_1 refers to the pseudo-first-order kinetic rate constant (min^{-1}), K_2 for the second order, and K_3 for the pseudo-second-order adsorption rate constant (g mg^{-1} min^{-1}). The plots of ln (Q_e -Q_t), 1/ (Q_e -Q_t), t/Q_t vs t, and Q_t vs $t^{-0.5}$ were shown in **Figure 5.20(a-c).** The results indicated that the experimental data was more correlated with the pseudo-first-order model (R^2 = 0.9843) while the pseudo-second-order and second-order models did not fit well in the experimental data. Pseudo-first-order parameters K_1 and Q_e were examined to be 0.0049 min^{-1} and 29.37 mg g^{-1}, respectively. However, for the second-order kinetics, the estimated values of K_2 and Q_e was to be 4.07×10^{-4} g mg^{-1} and 215.88 mg g^{-1}, respectively. To evaluate the diffusion of CV dye molecules onto the hydrogel's surface, the intraparticle diffusion kinetic model was studied. The linear equation for the model is represented by the following **Equation (5.13)[**12].

$$Q_t = K_4 t^{0.5} + C \qquad (5.13)$$

where K_4 is the intraparticle diffusion rate constant and C is the boundary layer thickness (mg $g^{-1}min^{-0.5}$). The boundary layer's thickness is determined by the non-zero intercept value. **Figure 5.20d** showed two linear sections in which the first section represented the quick adsorption of CV dye on the surface of ZH-4 hydrogel through the electrostatic attractive forces while the second one represented the diffusion of dye within the porous site of ZH-4 hydrogel through intraparticle diffusion. Thus, this was also confirmed that this intraparticle diffusion model participated along with the pseudo-first-order model in the CV dye adsorption mechanism.

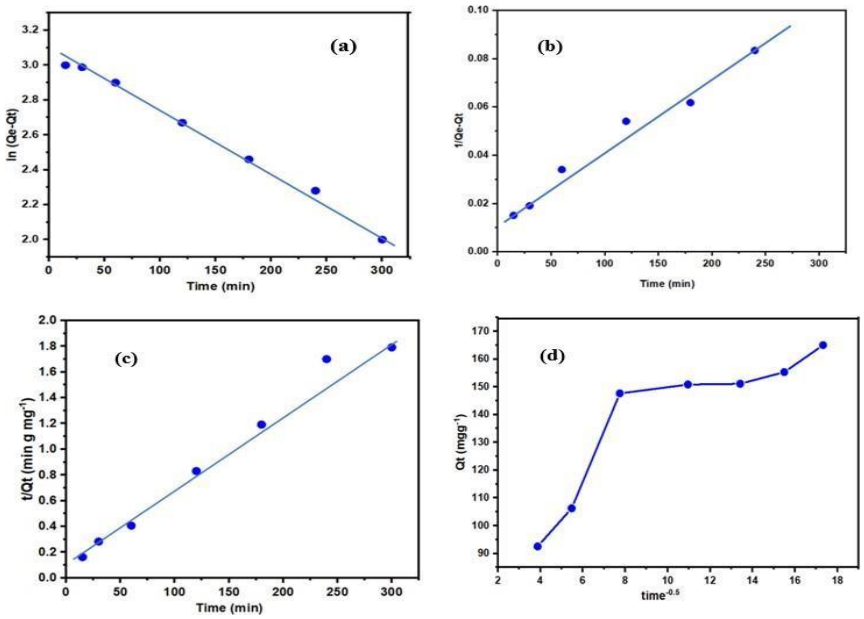

Figure 5.20: Kinetic Studies of dye adsorption on ZH-4 hydrogels using **(a)** Pseudo- first order **(b)**second order **(c)** pseudo-second-order **(d)** intraparticle diffusion model

5.4.7. Dye desorption studies

The best adsorbent material must have the maximum adsorption and desorption capacity. A hydrogel with the maximum desorption capacity can be reused leading to an economically viable process [17]. The dye adsorbed ZH-4 hydrogel powder was used for the regeneration experiment in the ethanol and four desorption cycles were performed to determine the reusability as shown in **Figure 5.21**. It was noticed that the maximum desorption efficiency of ZH-4 hydrogel was 82% and there was a small difference over the four cycles. Thus, zeolite-loaded hydrogel exhibited an excellent recycling performance.

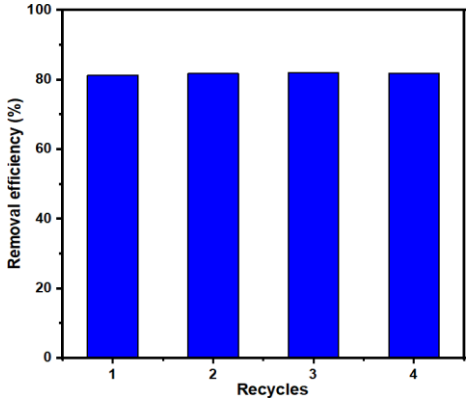

Figure 5.21: Dyes desorption cycles using ZH-4 hydrogels

5.5. Conclusion

The present work focused on the development of CMTKG/PSMA hydrogel and zeolite-loaded CMTKG/PSMA hydrogel for the potential application of cationic CV dye removal. The influence of zeolite on various factors such as maximum swelling capacity, porosity, morphology, and viscoelastic properties of CMTKG/PSMA hydrogel were investigated. The successful loading of zeolite particles into hydrogel matrix was confirmed by XRD, FTIR and FE-SEM characterization. Moreover, the BET analysis measured the estimated specific surface area of ZH-4 hydrogel as 20.176 m^2g^{-1} while the estimated pore diameter and pore volume were 23.907nm and 0.138 $cm^3\ g^{-\ 1}$, respectively. It was also found that CMTKG/PSMA hydrogel showed 81 % maximum CV dye removal while the presence of zeolite in ZH-4 hydrogel increased this value up to 93 %. The maximum adsorption capacity (Q_{max}) of ZH-4 hydrogel was found as 123.60 mg g^{-1}. The adsorption data was fitted more in the Langmuir model with $R^2 = 0.9942$. In addition, both pseudo-first-order and intraparticle diffusion kinetic models were used to follow the kinetic rate of the CV adsorption. Furthermore, the regeneration studies of CV dye were performed for ZH-4 hydrogels which showed 82% dye desorption efficiency. Thus, the prepared CMTKG/PSMA hydrogels can be used as a promising adsorbent for the removal of cationic dyes.

References

[1] B. K. Preetha and B. Vishalakshi, "Karaya gum-graft-poly (N, N'-dimethyl acrylamide) gel: A pH-responsive potential adsorbent for sequestration of cationic dyes," *J. Environ.Chem. Eng.*, vol. 8, no. 2, p. 103608, 2020, DOI: 10.1016/j.jece.2019.103608.

[2] Y. M. Slokar and A. Majcen Le Marechal, "Methods of decoloration of textile wastewaters," *Dye. Pigment.*, vol. 37, no. 4, pp. 335–356, 1998, doi: 10.1016/S0143- 7208(97)00075-2.

[3] S. Asadi, S. Eris, and S. Azizian, "Alginate-Based Hydrogel Beads as a Biocompatible and Efficient Adsorbent for Dye Removal from Aqueous Solutions," *ACS Omega*, vol.3, no. 11, pp. 15140–15148, 2018, DOI: 10.1021/acsomega.8b02498.

[4] M. R. Kulkarni, T. Revanth, A. Acharya, and P. Bhat, "Removal of Crystal Violet dye from aqueous solution using water hyacinth: Equilibrium, kinetics and thermodynamics study," *Resour. Technol.*, vol. 3, no. 1, pp. 71–77, 2017, doi: 10.1016/j.reffit.2017.01.009.

[5] M. Sarabadan, H. Bashiri, and S. M. Mousavi, "Removal of crystal violet dye by an efficient and low-cost adsorbent: Modeling, kinetic, equilibrium and thermodynamic studies," *Korean J. Chem. Eng.*, vol. 36, no. 10, pp. 1575–1586, 2019, doi: 10.1007/s11814-019-0356-1.

[6] K. K. Mali, S. C. Dhawale, R. J. Dias, V. D. Havaldar, and P. R. Kavitake, "Interpenetrating networks of carboxymethyl tamarind gum and chitosan for sustained delivery of aceclofenac," *Marmara Pharm. J.*, vol. 21, no. 4, pp. 771–782, 2017, doi: 10.12991/mpj.2017.20.

[7] N. Ajaz, I. Ullah, I. Khalid, R. Ullah, and H. Ahmad, "In vitro and toxicological assessment of dexamethasone sodium phosphate loaded pH sensitive Pectin- g-poly (AA)/ PVP semi-interpenetrating network," *Mater. Today Commun.*, vol. 25, no. May, p.101325, 2020, doi: 10.1016/ j.mtcomm.2020.101325.

[8] S. Ghorai, A. Sarkar, M. Raoufi, A. B. Panda, H. Schönherr, and S. Pal, "Enhanced removal of methylene blue and methyl violet dyes from aqueous solution using a nanocomposite of hydrolyzed polyacrylamide grafted xanthan gum and incorporated nanosilica," *ACS Appl. Mater. Interfaces*, vol. 6, no. 7, pp. 4766–4777, 2014, doi: 10.1021/am4055657.

[9] N. E. H. Fardjaoui, F. Z. El Berrichi, and F. Ayari, "Kaolin-issued zeolite A as

efficient adsorbent for Bezanyl Yellow and Nylomine Green anionic dyes," *Microporous Mesoporous Mater.*, vol. 243, pp. 91–101, 2017, doi: 10.1016/j.micromeso.2017.01.008.

[10] D. G. Trikkaliotis, N.M. Ainali, A.K. Tolkou, A.C. Mitropouos, D.A. Lambropoulou, D.N. Bikiaris, and G.Z. Kyzas, "Removal of Heavy Metal Ions from Wastewaters by Using Chitosan / Poly (Vinyl Alcohol) Adsorbents: A Review," pp. 403–425, 2022.

[11] M. Servatan, P. Zarrintaj, G. Mahamodi, S.J. Kim, M.R. Ganjali, M.R. Saeb. And M. Mozafari, "Zeolites in drug delivery: Progress, challenges and opportunities," *Drug Discov. Today*, vol. 25, no. 4, pp. 642–656, 2020, doi: 10.1016/j.drudis.2020.02.005.

[12] H. Mittal, R. Babu, A. A. Dabbawala, S. Stephen, and S. M. Alhassan, "Zeolite-Y incorporated karaya gum hydrogel composites for highly effective removal of cationic dyes," *Colloids Surfaces Physicochem. Eng. Asp.*, vol. 586, no. October 2019, p. 124161,2020, doi: 10.1016/j.colsurfa.2019.124161.

[13] V. V Panic and S. J. Vulakovich, "Removal of model cationic dye by adsorption onto poly (methacrylic acid)/ zeolite hydrogel composites: Kinetics, equilibrium study and image analysis," *Sep. Purif. Technol.*, vol. 122, pp. 384–394, 2014, doi: 10.1016/j.seppur.2013.11.025.

[14] S. Radoor, J. Karayil, A. Jayakumar, J. Parameswaranpillai, and S. Siengchin, "An efficient removal of malachite green dye from aqueous environment using ZSM-5 zeolite/polyvinyl alcohol/carboxymethyl cellulose/sodium alginate bio composite," *J. Polym. Environ.*, vol. 29, no. 7, pp. 2126–2139, 2021, doi: 10.1007/s10924-020- 02024-y.

[15] S. Pashaei-Fakhri, S. J. Peighambardoust, R. Foroutan, N. Arsalani, and B. Ramavandi, "Crystal violet dye sorption over acrylamide/graphene oxide bonded sodium alginate nanocomposite hydrogel," *Chemosphere*, vol. 270, p. 129419, 2021, doi: 10.1016/j.chemosphere.2020.129419.

[16] A. Pal and S. Pal, "Amphiphilic copolymer derived from tamarind gum and poly (methyl methacrylate) via ATRP towards selective removal of toxic dyes," *Carbohydr. Polym.*, vol. 160, pp. 1–8, 2017, doi: 10.1016/j.carbpol. 2016.12.008.

[17] S. Pal, S. Ghorai, C. Das, S. Samrat, A. Ghosh, and A. B. Panda,

"Carboxymethyl tamarind-g-poly(acrylamide)/silica: A high-performance hybrid nanocomposite for adsorption of methylene blue dye," *Ind. Eng. Chem. Res.*, vol. 51, no. 48, pp. 15546– 15556, 2012, doi: 10.1021/ie301134a.

[18] Khushbu, S. G. Warkar, and A. Kumar, "Synthesis and assessment of carboxymethyl tamarind kernel gum based novel superabsorbent hydrogels for agricultural applications," *Polymer (Guildf).*, vol. 182, no. July, p. 121823, 2019, doi: 10.1016/j.polymer.2019.121823.

[19] I. Yadav, S. Rathnam, Y. Yogalakshmi, S. Chakraborty, I. Banerjee, A. Anis, and K. Pal, "Synthesis and characterization of polyvinyl alcohol- carboxymethyl tamarind gum based composite films," *Carbohydr. Polym.*, vol. 165, pp. 159– 168, 2017, doi: 10.1016/j.carbpol.2017.02.026.

[20] N. R. Gupta, A. Torris, P. Wadgaonkar, R. Rajamohnan, G. Ducouret, D. Hourdet, C. Creton, and M.V. Badiger, "Synthesis and characterization of PEPO grafted carboxymethyl guar and carboxymethyl tamarind as new thermo-associating polymers," *Carbohydr. Polym.*, vol. 117, pp. 331–338, 2015, doi: 10.1016/j.carbpol. 2014.09.073.

[21] G. S. Shaw, K. Uvanesh, N. Gautham, V. Singh, K. Pramanik, I. Banerjee, N. Kumar, and K. Pal, "Preparation, Characterization and Assessment of the Novel Gelatin– tamarind Gum/Carboxymethyl Tamarind Gum-Based Phase- Separated Films for Skin Tissue Engineering Applications," *Polym. - Plast. Technol. Eng.*, vol. 56, no. 2, pp. 141– 152, 2017, doi: 10.1080/03602559. 2016.1185621.

[22] K. K. Mali, S. C. Dhawale, and R. J. Dias, "Synthesis and characterization of hydrogel films of carboxymethyl tamarind gum using citric acid," *Int. J. Biol. Macromol.*, vol. 105, pp. 463–470, 2017, doi: 10.1016/j.ijbiomac.2017.07.058.

[23] R Malik, S.G. Warkar, and R Saxena, "Carboxy-methyl tamarind kernel gum-based bio-hydrogel for sustainable agronomy, *Mater. Today Commun.*, vol. 35, no. Jan, p. 105473,2023, doi: 10.1016/j.mtcomm.2022.105473.

[24] S. Ganguly, and N.C. Das, "Synthesis of a novel pH responsive phyllosilicate loaded polymeric hydrogel based on poly (acrylic acid-co-N- vinylpyrrolidone) and polyethylene glycol for drug delivery: Modelling and kinetics study for sustained release of antibiotic drug" RSC Advances, 2015, 5(24), p.p.18312-18327.

[25] B. Singh, A. Kumar, and Rohit, "Synthesis and characterization of alginate and

sterculia gum-based hydrogel for brain drug delivery applications," *Int. J. Biol. Macromol.*, vol. 148, pp. 248–257, 2020, doi: 10.1016/j.ijbiomac.2020.01.147.

[26] K. Kalantari, E. Mostafavi, B. Saleh, P. Soltantabar, and T. J. Webster, "Chitosan/PVA hydrogels incorporated with green synthesized cerium oxide nanoparticles for wound healing applications," *Eur. Polym. J.*, vol. 134, no. June, p. 109853, 2020, doi: 10.1016/j.eurpolymj.2020.109853.

[27] M. H. Abu Elella, M. W. Sabaa, E. A. ElHafeez, and R. R. Mohamed, "Crystal violet dye removal using crosslinked grafted xanthan gum," *Int. J. Biol. Macromol.*, vol. 137, pp. 1086–1101, 2019, doi: 10.1016/j.ijbiomac.2019. 06.243.

[28] V. Malik, L. Saya, D. Gautam, S. Sachdeva, N. Dheer, D.K. Arya, G. Gambhir, and S.Hooda, " Review on adsorptive removal of metal ions and dyes from wastewater using tamarind-based bio-composites, no. 0123456789. Springer Berlin Heidelberg,2022.

[29] R. Karkhani and V. Javanbakht, "A polyurethane foam membrane filled with double cross-linked chitosan/carboxymethyl cellulose gel and decorated with ZSM-5 nano zeolite: Simultaneous dye removal," *Int. J. Biol. Macromol.*, vol. 213, no. May, pp. 699–717, 2022, doi: 10.1016/j.ijbiomac.2022.05.120.

[30] R. Sabarish and G. Unnikrishnan, "PVA/PDADMAC/ZSM-5 zeolite hybrid matrix membranes for dye adsorption: Fabrication, characterization, adsorption, kinetics and antimicrobial properties," *J. Environ. Chem. Eng.*, vol. 6, no. 4, pp. 3860–3873, 2018, doi: 10.1016/j.jece.2018.05.026.

[31] A. M. Omer, G. S. Elgarhy, G. M. El-Subruiti, R. E. Khalifa, and A. S. Eltaweil, "Fabrication of novel iminodiacetic acid-functionalized carboxymethyl cellulose microbeads for efficient removal of cationic crystal violet dye from aqueous solutions," *Int. J. Biol. Macromol.*, vol. 148, pp. 1072–1083, 2020, doi: 10.1016/j.ijbiomac.2020.01.182.

[32] G. Sharma A. Kumar, M. Naushad, A.G. Penas, Al. Muhtaseb, A. Ghfar, V. Sharma, T. Ahamad, and F.J. Stadler, "Fabrication and characterization of Gum arabic-cl- poly(acrylamide) nano hydrogel for effective adsorption of crystal violet dye," *Carbohydr. Polym.*, vol. 202, no. May, pp. 444–453, 2018, DOI: 10.1016/j.carbpol.2018.09.004.

[33] M. M. ALSamman and J. Sánchez, "Chitosan- and Alginate-Based Hydrogels

for the Adsorption of Anionic and Cationic Dyes from Water," *Polymers (Basel).*, vol. 14, no. 8, 2022, DOI: 10.3390/polym14081498.

[34] A. Salama, "Preparation of CMC-g-P(SPMA) super adsorbent hydrogels: Exploring their capacity for MB removal from wastewater," *Int. J. Biol. Macromol.*, vol. 106, pp. 940–946, 2018, doi: 10.1016/j.ijbiomac.2017.08.097.

[35] R. R. Mohamed, M. H. Abu, E. Magdy, and G. R. Saad, "Synthesis of an efficient adsorbent hydrogel based on biodegradable polymers for removing crystal violet dye from aqueous solution," *Cellulose*, vol. 25, no. 11, pp. 6513–6529, 2018, doi: 10.1007/s10570-018-2014

[36] B. Cursaru, A.L. Radu, F.X. Perrin, A. Sarbu, M. Teodorescu, A.M. Gavrila, C.M. Damian, T. Sandu, T.V. Lordache, and A. Zaharia, "Poly (ethylene glycol) Composite Hydrogels with Natural Zeolite as Filler for Controlled Delivery Applications," *Macromol. Res.*, vol. 28, no. 3,pp. 211–220, 2020, doi: 10.1007/s13233-020-8029-9.

[37] M. Shaban, M. R. Abukhadra, M. G. Shahien, and S. S. Ibrahim, "Novel bentonite/zeolite-NaP composite efficiently removes methylene blue and Congo red dyes," *Environ. Chem. Lett.*, vol. 16, no.1, pp. 275–280, 2018, doi: 10.1007/s10311-017-0658-7.

[38] A. Olad, H. Gharekhani, A. Mirmohseni, and A. Bybordi, "Study on the synergistic effect of clinoptilolite on the swelling kinetic and slow-release behavior of maize bran-based superabsorbent nanocomposite," *J. Polym. Res.*, vol. 23, no. 12, pp. 1–14, 2016, doi:10.1007/s10965-016-1140-0.

[39] R. A. Naikoo, S.U. Bhat, M.A. Mir, R. Tomar, W.A. Khanday, P. Dipak, and D.C. Tiwari, "Polypyrrole and its composites with various cation," *RSC Adv.*, vol. 6, no. November 2017, pp. 99202–99210, 2016, doi: 10.1039/C6RA19708F.

[40] G. R. Mahdavinia, H. Aghaie, H. Sheykhloie, M. T. Vardini, and H. Etemadi, "Synthesis of CarAlg/MMt nanocomposite hydrogels and adsorption of cationic crystal violet," *Carbohydr. Polym.*, vol. 98, no. 1, pp. 358–365, 2013, doi: 10.1016/j.carbpol.2013.05.096.

CHAPTER 6

CONCLUSION, FUTURE PROSPECTS AND SOCIAL IMPACT

6.1. Conclusion

The main focus of the research work was on the synthesis of biopolymers-based hydrogels to be utilized for different applications, especially drug delivery and dye removal applications. Among various biopolymers, tamarind kernel gum (TKG) and its derivative, carboxymethyl tamarind kernel gum (CMTKG), have been relatively underutilized in the development of composite hydrogels, particularly for drug delivery and water enrichment applications. A review of the literature suggests that zeolite and nanoparticle-loaded TKG and CMTKG-based hydrogels have limited exploration in various applications. Therefore, novel composite hydrogel systems incorporating TKG and CMTKG biopolymers need to be developed. In this study, a series of CMTKG-based hydrogels were synthesized and explored their applications as drug delivery vehicles and as an adsorbent for the removal of toxic dyes. To begin with, CMTKG/PSMA hydrogel and ZnO NPs-loaded CMTKG/PSA nanocomposite hydrogel were synthesized using PEGDA as a cross-linker. ZnO NPs were prepared using a hydrothermal method, while CMTKG/PSA hydrogels were synthesized through a free radical mechanism. The synthesis of CMTKG/PSMA and Zn NPs-loaded CMTKG/PSMA hydrogel composites was confirmed through various characterization techniques such as FTIR, XRD, FE-SEM, and TEM. The dynamic swelling data were fitted in the Korsmeyer-Peppas model and Schott model. The results indicated that the Schott model provided the best fit for the data, with a higher R^2 value closer to unity. The synthesized hydrogel and ZnO-loaded hydrogel nanocomposites were used in *in-vitro* release studies of the ciprofloxacin drug. The investigation of various parameters concluded that the porosity, drug loading, and drug entrapment efficiency of hydrogel were increased in the presence of ZnO NPs. The rheological studies of hydrogels and ZnO-loaded hydrogels were performed which inferred that the elasticity of hydrogels was increased in the presence of ZnO NPs. The antibacterial activity analysis showed that the presence of antibacterial ZnO NPs and Ciprofloxacin drug increased the zone of inhibition (mm) of ZnO NPs loaded CMTKG/PSA hydrogel. The in-vitro drug release results revealed that CMTKG/PSA/ZnO nanocomposite hydrogel showed a controlled

and slow drug release. The drug release kinetics analysis indicated that the release of the drug from both CMTKG/PSA hydrogel and ZnO-loaded hydrogel followed the Korsmeyer-Peppas model. Thus, CMTKG/PSA/ZnO nanocomposite hydrogel could be a promising candidate for the controlled oral delivery of ciprofloxacin. In brief, CMTKG/PSA/ZnO nanocomposite hydrogel could be a better candidate for the controlled oral delivery of ciprofloxacin drug.

Next, the synthesis of TKG/PSA hydrogel and Ag/TKG/PSA nanocomposite hydrogel was attempted. The interesting aspect of this study is to control the swelling and drug release behavior of TKG/PSA hydrogel in the presence of Ag NPs. The dynamic swelling data of TKG/PSA and Ag/TKG/PSA hydrogels in pH 1.2 and pH 7.4 buffer solutions were analyzed using the Power function model and the Schott model. The results indicated that the swelling data was best fitted in the Power function model. The diffusion coefficients for TKG/PSA and Ag/TKG/PSA were calculated to be 0.338 and 0.580, respectively, suggesting Fickian diffusion for TKG/PSA and non-Fickian diffusion for Ag/TKG/PSA.

The structural properties of Ag/TKG/PSA nanocomposite hydrogel were evaluated using XRD, FTIR, UV-visible, FE-SEM, and TEM techniques. Moreover, the average particle size of Ag NPs was in the range of 10 to 25 nm. The estimated zeta potential of Ag/TKG/PSA was determined as -16.3 mV which indicated the stability of Ag NPs. The successful synthesis of the Ag/TKG/PSA nanocomposite hydrogel was confirmed by a UV-visible peak at 420 nm, which is characteristic of surface plasmon resonance of Ag NPs. Since the nanocomposite hydrogel showed less swelling than hydrogel and the diffusion of the drug depends on the swelling of hydrogel. Therefore, Ag/TKG/PSA nanocomposite hydrogel was used for the controlled release of doxycycline drug at physiological pH 1.2 and pH 7.4 buffer solution at 37 °C. Moreover, the drug release (%) was higher at pH 7.4 than at pH 1.2. It was also observed that doxycycline release data at both pH followed the Korsmeyer-Peppas model and showed a non-Fickian diffusion. Thus, the developed Ag/TKG/PSA acts as a good carrier for the controlled release of doxycycline drug in the biomedical field.

Further, CMTKG/PVA/GG hydrogel film cross-linked with glutaraldehyde was

synthesized using the solvent casting method. The various parameters of hydrogel film such as thickness, moisture content, swelling capacity, tensile strength, elongation at break, thermal and wetting analysis were evaluated. The tensile strength for hydrogel films (S1 to S9) lies in the range of 95.80 to 149.07 MPa and elongation at break (%) lies in the range of 1.51 to 5.20 %. Moreover, the wetting analysis indicated that the S2 hydrogel film showed maximum hydrophilicity while the S9 hydrogel film showed minimum hydrophilicity. Thus, the S2 hydrogel film was chosen for the loading of the ciprofloxacin drug on basis of highest swelling capacity. Moreover, the successful loading of the drug was confirmed by FTIR spectroscopy. The surface morphology of hydrogel film showed the presence of rough surface and globular structures. The thermal analysis showed that the presence of the drug increased the thermal stability of the hydrogel film. The in vitro ciprofloxacin drug release studies showed that the hydrogel films effectively released the drug in a controlled manner when immersed in a phosphate buffer solution with a pH of 7.4. The drug release data was fitted in the First-order, Higuchi and Korsmeyer-Peppas models to study the kinetic modeling of drug released. The results showed that the Korsmeyer-Peppas model was the best-fitted model and the estimated value of diffusion exponent (n) was found to be 0.38. This value shows that drug release from the hydrogel film followed a Fickian diffusion. The antibacterial assay indicated good antibacterial action against *E.coli* and *S. aureus* bacteria and MTT assay indicated the cytocompatibility of film against HaCaT Cell lines. Thus, the overall results suggested that CMTKG/PVA/GG hydrogel film has significant potential for the delivery of ciprofloxacin drug in biomedical applications.

In the next study, zeolite-embedded CMTKG/PSMA composite hydrogel was synthesized for the removal of cationic crystal violet dye. The influence of zeolite on various factors such as maximum swelling index, porosity, morphology, and viscoelastic properties of CMTKG/PSMA hydrogel were investigated. The loading of zeolite particles into the hydrogel matrix was confirmed by XRD, FTIR and FE- SEM characterization. Moreover, BET analysis concluded that the estimated specific surface area was 20.176 m^2g^{-1} while the estimated pore diameter and pore volume were 23.907nm and 0.138 cm^3 g^{-1}, respectively. The CMTKG/PSMA hydrogel showed 81 % maximum CV dye removal while the presence of zeolite increased this value up to

93 %. The maximum adsorption capacity (Q_{max}) of zeolite-embedded hydrogel was obtained as 123.60 mg g^{-1}. The adsorption data was fitted in the Langmuir model with R^2 = 0.9942. In addition, both pseudo-first-order and intraparticle diffusion kinetic models were used to follow the kinetic rate of the CV adsorption. Furthermore, the regeneration studies of dye were performed for hydrogel which showed 82% dye desorption efficiency. Thus, zeolite-loaded CMTKG/PSMA hydrogels can be used as a promising adsorbent for the removal of cationic dyes.

6.2. Future Prospects

As natural and nontoxic polysaccharides, TKG and CMTKG-based composite hydrogels have a lot of potential to deliver drugs. Their special qualities, like being able to bind a lot of water, sticking to mucous membranes, and being able to be chemically changed, make them good material for several drug delivery methods. Future research should focus on cross-linking TKG or CMTKG with other polymers or bioactive chemicals to develop multifunctional hydrogels capable of precise and safe drug delivery. Hydrogels based on TKG or CMTKG that are responsive to external factors like pH, temperature, or ionic strength could enable the targeted release of drugs, improving therapeutic efficacy and reducing side effects. Also, TKG and CMTKG-based composite hydrogels need further investigation for their possible uses in tissue engineering and regenerative medicine. Owing to their biocompatibility and resemblance to the extracellular matrix, these hydrogels can be utilized to fabricate scaffolds that promote cell growth, division, and differentiation. The effect of zeolites in TKG or CMTKG-based hydrogels can be further investigated for different applications such as agronomical, drug delivery, scaffold & tissue engineering, and wastewater treatment. To fully leverage the potential of TKG and CMTKG-based composite hydrogels, collaboration among researchers, business partners, and regulatory agencies is essential.

6.3. Social Impact

My research on novel composite hydrogels based on TKG and CMTKG biopolymers has the potential to make a significant societal impact in several areas. These polymeric materials have the potential to be used in various fields such as biomedical, tissue

engineering, agricultural, heavy metal, and dye removal applications. In this research work, TKG and CMTKG-based nanocomposite hydrogels were synthesized. These materials show the ability for targeted release of antibiotic drugs. The synthesized nanocomposite hydrogels can also be used for tissue engineering applications. To address wastewater treatment challenges, a zeolite-loaded CMTKG-based hydrogel was synthesized. This hydrogel demonstrated promising potential for removing cationic dyes. Although, these zeolite-loaded hydrogels can be used in toxic metal removal, agricultural, biomedical, tissue engineering, and textile industry. They can be used as micronutrients and fertilizer carriers due to their excellent swelling capacity. Thus, the developed composite hydrogel shows excellent potential as a drug delivery carrier and adsorbent for dye removal applications.

LIST OF PUBLICATIONS FROM THESIS

- **Indu Rani,** S.G. Warkar and Anil Kumar, "Nano ZnO embedded Poly (ethylene glycol) diacrylate cross-linked carboxymethyl tamarind kernel gum and poly (sodium acrylate) composite hydrogels for oral delivery of ciprofloxacin drug and their antibacterial properties," ***Mater. Today Commun.,*** vol. 35, no. June 2022, p. 105635, 2023, doi: 10.1016/j.mtcomm.2023.105635. **(I.F. = 3.8) (SCIE)**

- **Indu Rani**, S.G.Warkar and Anil Kumar, "Removal of cationic crystal dye using zeolite embedded carboxymethyl tamarind kernel gum (CMTKG) based hydrogel adsorbents," ***ChemistrySelect,*** vol. 8, no. 29, 2023, doi: 10.1002/slct. 202301434. **(I.F. = 2.3) (SCIE)**

- **Indu Rani,** S.G.Warkar and Anil Kumar, "A Silver nanoparticle embedded tamarind kernel gum/ poly (sodium acrylate) nanocomposite for sustainable release of doxycycline," ***ChemistrySelect,*** vol. 9, no. 14, p. 2024, 2024, doi: 10.1002/slct.202400168. **(I.F. = 2.3) (SCIE)**

- **Indu Rani,** S.G.Warkar and Anil Kumar, " Synthesis and characterization of novel carboxymethyl tamarind kernel gum- poly(vinyl alcohol)/ guar gum- based hydrogel film loaded with ciprofloxacin for biomedical applications," ***International Journal of Biological Macromolecules***, p.136766, 2024, doi: http://doi.org/10.1016/j.ijbiomac.2024.136766. **(I.F. =7.7) (SCIE)**

Other Publications

- **Indu Rani,** Ekta Yadav, Komal Pandey, Khusbhu, S.G.Warkar, Anil Kumar. Synthesis and application of zinc-loaded carboxymethyl tamarind kernel gum and xanthan gum-based superabsorbent hydrogels to investigate the effect on sesame plant growth, ***Polym. Bull.,*** no. 0123456789, 2024, doi: 10.1007/s 00289-024-05150-y. **(I.F. = 3.2) (SCIE)**

Conference presentation

1. Presented paper in international e-Conference on " Nanomaterials and

Nanoengineering APA NANOFORUM-2022" organized by NPL, Delhi from 24-26th February 2022.**(Oral presentation)**

2. Presented paper in international e-Conference on "Recent Advancements in Chemical Sciences: Health, Environment, and Society (ICRACS-2022)" organized by the Department of Chemistry, Deshbandhu College, University of Delhi during 8 and 9th April 2022. **(Oral presentation)**

3. Presented paper in "International Conference on Advances in Chemical Sciences and Nanocomposites-ACSN 2022" jointly organized by Zakir Husain Delhi College & ISAS on 1st and 2nd April 2022. **(Oral Presentation)**

4. Attended conference on "2nd Indian Analytical Congress " organized jointly by Indian Society of Analytical Scientists, Graphic Era University, and CSIR-Indian Institute of Petroleum during 26-28 May 2022 at Graphic Era University Dehradun, UK.

Materials Today Communications 35 (2023) 105635

Contents lists available at ScienceDirect

Materials Today Communications

journal homepage: www.elsevier.com/locate/mtcomm

Nano ZnO embedded poly (ethylene glycol) diacrylate cross-linked carboxymethyl tamarind kernel gum (CMTKG)/poly (sodium acrylate) composite hydrogels for oral delivery of ciprofloxacin drug and their antibacterial properties

Indu Rani, Sudhir G. Warkar *, Anil Kumar *

Department of Applied Chemistry, Delhi Technological University, Delhi 42, India

ARTICLE INFO

Keywords:
CMTKG
ZnO NPs
ZnO loaded hydrogels
Ciprofloxacin
Drug delivery
Antimicrobials studies

ABSTRACT

In this research work, a novel hydrogel network based on carboxymethyl tamarind kernel gum/poly (sodium acrylate) was synthesized by using poly (ethylene glycol) diacrylate (PEGDA) as a cross-linker. Zinc Oxide nanoparticles (ZnO NPs) were prepared via the hydrothermal synthetic method and developed ZnO NPs embedded within CMTKG/Poly (sodium acrylate) hydrogel for the controlled release studies of ciprofloxacin drug. Various techniques such as FTIR, XRD, FESEM, and TEM were used to characterize the synthesized ZnO NPs, pure hydrogel, and hydrogel nanocomposites. Various parameters such as drug loading (DL %), drug entrapment (DE %), gel content, and porosity were estimated for all the synthesized hydrogel nanocomposites. The results of swelling and rheological studies of hydrogel nanocomposites concluded that the embedded ZnO NPs increased hydrogel's swelling and thermal stability. The water absorption data were analyzed using the Power and Schott model. The result concluded that the Schott function model fitted the dynamic swelling data. The antibacterial action of CMTKG-based hydrogel nanocomposites was studied using *E. coli* (gram-negative) bacteria with the help of the disc diffusion method. The result showed that the incorporation of ZnO NPs enhanced the antimicrobial action of ciprofloxacin-loaded CMTKG-based hydrogels. The kinetic modelling of drug release was done using Higuchi and Korsmeyer - Peppas model. The higher value of regression coefficient (R^2) close to unity indicated that the mechanistic pathway of drug release from the hydrogels was more fitted in the Korsmeyer-Peppas model followed by Fickian diffusion.

1. Introduction

Hydrogels are cross-linked polymeric systems made up of synthetic monomers and natural polymers such as polysaccharides [1]. Hydrogels have a significant amount of porosity, making them efficient materials to absorb drugs in the aqueous mediums via physical or chemical interactions and subsequent release of the drug under physiological conditions [1]. Several stimuli like pH, temperature, and ionic strength affect drug release rate from the hydrogel. The drug released depends on the water uptake capacity of the hydrogels and the mechanism of diffusion of fluid into the matrix of hydrogel [2]. Other than the drug delivery applications, hydrogels can be used in other fields such as agriculture, metal ion sensing, heavy metal ion removal, removal of toxic dyes, and the food industry [3]. Till now, a large number of natural biopolymer-based hydrogels such as carboxymethyl guar gum [4], chitosan [5], tamarind gum [6], carboxymethyl cellulose [7] were used for the controlled release of the drug to the human body but carboxymethyl tamarind kernel gum (CMTKG) based hydrogels have not been much explored. CMTKG is a natural, non-toxic, biodegradable, and biocompatible biopolymer that is a chemically modified form of tamarind gum. It contains the polysaccharide units of D-Xylose, D-Glucose, and D-Galactose [8]. This chemical modification resulted in an enhanced life shell, swelling capacity, and high drug loading capacity [9]. There are only a few numbers of CMTKG-based hydrogel reported for biomedical applications for example Mali et.al., group reported the formation of CMTKG-based hydrogel film cross-linked via citric acid [10]. Alginate and CMTKG hydrogels were synthesized for the delivery of acyclovir as reported earlier [11]. CMTKG-based nanoparticles were synthesized for

* Corresponding authors.
E-mail addresses: sudhirwarkar@dtu.ac.in (S.G. Warkar), anil_kumar@dce.ac.in (A. Kumar).

https://doi.org/10.1016/j.mtcomm.2023.105635
Received 17 June 2022; Received in revised form 10 January 2023; Accepted 13 February 2023
Available online 14 February 2023

Check for updates

ChemistrySelect

Research Article
doi.org/10.1002/slct.202400168

Chemistry Europe
European Chemical Societies Publishing

www.chemistryselect.org

A Silver Nanoparticle-Embedded Tamarind Kernel Gum/Poly (Sodium Acrylate) Nanocomposite for Sustainable Release of Doxycycline

Indu Rani,[a] Sudhir G. Warkar,*[a] and Anil Kumar*[a]

The current work describes an eco-friendly novel synthesis of silver (Ag) nanoparticles (NPs)/Tamarind kernel gum (TKG)/Poly (sodium acrylate) (PSA) nanocomposite without the use of any toxic materials. It is a one-step route synthesis of silver nanocomposite hydrogel in which TKG and PSA are cross-linked using methylene bisacrylamide (MBA) cross-linker. The developed hydrogels were characterized using XRD, FTIR, UV-visible, FE-SEM, and TEM techniques. Doxycycline (dox) was chosen as a model drug for release studies using TKG/PSA and Ag/TKG/PSA nanocomposite. The observation is that Ag NP/TKG/PSA nanocomposite showed a pH-dependent swelling which is higher at pH 7.4 than at pH 1.2. Similarly, the cumulative drug release percentage (CDR %) using silver nanocomposite is higher at pH 7.4 than at pH 1.2. Also, the presence of Ag NPs decreased the swelling ratio (SR) of TKG/PSA hydrogel, which controls the rate of release of the dox drug. In addition, the dox release kinetics were studied using the Korsmeyer-Peppas and Higuchi model. It has been found that drug release data was fitted in the Korsmeyer-Peppas model with a higher value of regression coefficient (R^2). Thus, Ag/TKG/PSA nanocomposite showed satisfactory results for sustainable release of doxycycline drug.

Introduction

Hydrogels are three-dimensional cross-linked networks that have the potential to absorb water due to the presence of various hydrophilic functional groups. The trapped material can be released quickly or slowly depending on various external factors such as light, temperature, pressure, etc. Various inorganic materials can be embedded in hydrogels such as zeolite,[1] silica,[2] metal nanoparticles,[3] etc. Nanocomposite hydrogels are attractive materials in drug delivery fields. Various noble metals such as silver,[4] gold,[5] and platinum[6] based nanoparticles have been used in the biomedical field. However, the researchers are more interested in the synthesis of biocompatible nanoparticles. The silver nanocomposite is used most widely in the biomedical field.[7] The main role of Ag NPs in the hydrogel is to increase the electrical conductivity, optical properties, mechanical toughness, high deformability, and transparency properties.[8] However, the uniform dispersion of Ag NPs without any formation of aggregation can be achieved by embedding Ag^+ ions into a hydrogel matrix which is followed by a reducing agent like sodium borohydride. These reagents are highly toxic and they can reduce the efficiency of Ag-loaded hydrogels. Therefore, green synthesis is preferred to synthesize Ag NPs by using biocompatible biopolymers.[9] There are many reported methods to synthesize Ag NPs but in-situ synthesis of Ag NPs, hydrogels are used as porous templates with controlled size and appropriate stability.[10] Biopolymer-based nanocomposites are useful in pharmaceutical applications due to their biocompatible and biodegradable behavior. Many natural polymers such as sodium alginate, pectin, chitosan, guar gum, and carboxymethyl tamarind kernel gum (CMTKG) have been used for the development of nanocomposite hydrogels still tamarind kernel gum was not explored well. There is a reported synthesis of hydrogels of tamarind gum-co-poly(acrylamidoglycolic acid) and their silver nanocomposite for release study of doxorubicin drug.[11] In another research, the co-precipitation method was used to fabricate the nano-hydroxyapatite/chitosan-tamarind seed nanocomposite for bone tissue engineering.[12] In this present study, we have explored the development of TKG and poly (sodium acrylate) hydrogel and their Ag NP-embedded hydrogel in biomedical applications for the first time as per our knowledge. Tamarind kernel gum (TKG) is a non-toxic, biodegradable, and biocompatible polymer used in medical applications due to its viscosity-modulating properties.[13] The surface of TKG contains β-(1,4)-D-glucan with chains of α- (1,4)-D-xylopyranose and glucose residue linked with β-D-galactopyranosyl-(1,2)-α-D-xylopyranose.[14] TKG can increase the mucoadhesive properties of hydrogels. Recently, research has been devoted to synthesizing the metal nano-particle containing hydrogel. A group of researchers M. Sabzi et.al group have synthesized the PVA/Citric acid/Ag nanocomposite hydrogel for the release study of ciprofloxacin drug.[15] Thus, Ag-based nanocomposite hydrogels have gained much attention in improving the antimicrobial properties of hydrogels due to their large surface area, non-toxic behavior, and high fraction of surface atoms.[16] The Ag-based nanocomposite exhibited excellent antibiotic properties.[17] Doxycycline as a member of the semi-synthetic

[a] I. Rani, Prof. S. G. Warkar, Prof. A. Kumar
Department of Applied Chemistry
Delhi Technological University, Delhi, 110042 India
E-mail: anil_kumar@dce.ac.in
sudhirwarkar@dtu.ac.in

Supporting information for this article is available on the WWW under https://doi.org/10.1002/slct.202400168

Check for updates

ChemistrySelect

Research Article
doi.org/10.1002/slct.202301434

Chemistry Europe
European Chemical Societies Publishing

www.chemistryselect.org

Removal of Cationic Crystal Violet dye using Zeolite-Embedded Carboxymethyl Tamarind Kernel Gum (CMTKG) based Hydrogel Adsorbents

Indu Rani,[a] Sudhir G. Warkar,*[a] and Anil Kumar*[a]

In this research paper, various formulations of zeolite-loaded carboxymethyl tamarind kernel gum (CMTKG) based hydrogels were synthesized and utilized as a potential adsorbent for the removal of crystal violet (CV) dye. The swelling capacity of all the synthesized hydrogels was investigated and the composition of hydrogel which exhibited maximum swelling was used for the characterization and dye removal experiment. The CV dye was chosen as a model dye for the dye removal experiment. The structure of zeolite and zeolite embedded hydrogel was elucidated by XRD, FTIR, FE-SEM, EDX and elemental papping techniques. The adsorption experiment was investigated by varying the CV concentration, amount of hydrogel adsorbent, temperature, pH of the dye solution, adsorption time, and ionic strength. The Langmuir and Freundlich isotherm models were used to fit the adsorption data and it was observed that the data fitted well with the Langmuir model. Moreover, hydrogel's maximum dye adsorption efficiency was found at 123.60 mg g^{-1}. The adsorption kinetic studies were followed by pseudo- first-order and intraparticle diffusion kinetic models. In addition, regeneration studies were performed for the best adsorbent hydrogel using ethanol solvent and the result concluded the desorption efficiency of hydrogel (82%) over four desorption cycles.

Introduction

Nowadays, polluted water due to synthetic toxic dyes has become a serious challenge to environmental scientists. The drinking water quality is diminished a lot since few years by direct and indirect discharge of industrial toxic effluents.[1] Even a small trace of dye can harm the aquatic life of flora and fauna by disturbing the photosynthesis process.[2] Therefore, these toxic dyes must be removed from the environment. Various technologies were used for this purpose including biological degradation, chemical oxidation, photocatalytic degradation, and adsorption.[3] The removal of dyes using hydrogel as adsorbents is one of the most effective approaches owing to its low operating cost.[4] Crystal violet (CV) is a toxic dye known as methyl violet 10B and exhibited mutagenic and carcinogenic nature.[4] It is used in the textile, wood, and paper industry.[5] Hence, the removal of CV dyes from waste water using efficient organic and inorganic adsorbents is very necessary. In the past few years, hydrogels based on natural biopolymers were used as an adsorbent in dye removal applications.[6] Hydrogels are three-dimensional hydrophilic networks synthesized from synthetic and natural biopolymers. Hydrogels have high water absorption efficiency due to the presence of hydrophilic groups like hydroxy(−OH) and carboxylate(−COO).[7] However, hydrogels based on natural biopolymers showed non-toxicity, biocompatibility, and biodegradability. Also, there are a limited number of polysaccharides-based hydrogels used as adsorbents owing to the poor surface area, less capacity to form H-bonding, and low hydrodynamic volume of hydrogels.[8] Moreover, the surface properties of hydrogels can be modified by loading inorganic substances such as zeolites, clay, and nanoparticles.[9] Zeolites are tetrahedral crystalline materials occurring in form of aluminosilicate. The large surface area and porosity of zeolite are responsible for their water purification property. Only a few zeolite-based polymer composites have been reported in the removal of toxic dyes and heavy metal ions.[10] Previously, some zeolite-loaded hydrogels were used as an adsorbent due to the presence of negatively charged lattice as well as ion-exchange capacity.[11] The hydrogel composite composed of gum karaya with acrylic acid and N-isopropyl acrylamide incorporated zeolite-Y were synthesized for dye adsorption of brilliant green dye (BG).[12] In another study, a hydrogel composite composed of poly (methacrylic acid) /zeolite was synthesized for basic yellow 28 dye adsorption from an aqueous solution.[13] In research, ZSM-5 incorporated PVA/CMC/SA membrane was utilized for the dye adsorption of malachite green dye.[14] Various natural biopolymers such as guar gum, carboxymethyl guar gum, alginate, chitosan, chitin, xanthan gum, carboxymethyl cellulose, chitin, gelatin-based hydrogels were used as adsorbents for the adsorption of toxic dye from the polluted water.[15] There is limited research in which Carboxymethyl tamarind gums (CMTKG) based hydrogels were exploited as an adsorbent in dye removal applications. A hydrogel was made by grafting tamarind gum with Poly (methyl methacrylate) in the presence of CuBr catalyst and used for the removal of toxic dyes.[16] Another hydrogel nanocomposite

[a] I. Rani, Prof. S. G. Warkar, Prof. A. Kumar
Department of Applied Chemistry
Delhi Technological University, Delhi 110042, India
E-mail: anil_kumar@dce.ac.in
sudhirwarkar@dtu.ac.in

Supporting information for this article is available on the WWW under https://doi.org/10.1002/slct.202301434

International Journal of Biological Macromolecules 282 (2024) 136766

Contents lists available at ScienceDirect

International Journal of Biological Macromolecules

journal homepage: www.elsevier.com/locate/ijbiomac

Synthesis and characterization of novel carboxymethyl tamarind kernel gum - Poly (vinyl alcohol)/guar gum-based hydrogel film loaded with ciprofloxacin for biomedical applications

Indu Rani, Sudhir G. Warkar *, Anil Kumar *

Department of Applied Chemistry, Delhi Technological University, Delhi 110042, India

ARTICLE INFO

Keywords:
Antibacterial
CMTKG/PVA/GG
Ciprofloxacin
Hydrogel film
MTT assay
Drug delivery
Kinetic modelling

ABSTRACT

The current study delineates the synthesis of hydrogel films comprised of carboxymethyl tamarind kernel gum (CMTKG), poly (vinyl alcohol) (PVA), and guar gum (GG) using glutaraldehyde (GTA) as cross-linker. The hydrogel films were evaluated in terms of equilibrium swelling ratio (ESR), moisture content, thickness, wetting analysis, thermal, and mechanical analysis. The tensile strength value lies in the range of 95.80 to 149.07 MPa while elongation at break value lies in the range of 1.51 to 5.20 %. The FTIR spectroscopy confirmed the presence of hydrogen bonding between CMTKG, PVA, and GG components of hydrogel film. FE-SEM micrographs indicated the rough surfaces of hydrogel film. TGA-DTA analysis confirmed that the thermal stability of hydrogel film was found to be increased by incorporating the ciprofloxacin (CFX) drug into the hydrogel matrix. CFX was embedded in the best-swelled hydrogel film and in-vitro drug release behavior was studied at alkaline pH 7.4 phosphate buffer solution. It was found that the maximum drug release was to be 73 % after 24 h at pH 7.4. Moreover, the release data was fitted in various kinetic models such as the First-order, Higuchi, and Korsmeyer-Peppas models. The best-fitted Korsmeyer-Peppas model suggested that the release of the drug follows Fickian diffusion and the value of diffusion exponent (n) was determined to be 0.38. The cytocompatibility of the hydrogel film was analyzed by MTT assay while the antibacterial behavior of the hydrogel film against *E. coli* and *S. aureus* showed clear zone of inhibition area. Thus, the overall results indicated that CMTKG/PVA/GG hydrogel film have potential to be used in the biomedical applications.

1. Introduction

Skin plays a crucial role in protecting the human body against various types of bacterial and viral infections. Skin helps to control fluid maintenance, temperature regulation, and sensing mechanisms of the body [1]. In the medical field, skin injuries are the most common problem and to resolve this, there is a high demand for the development of new wound dressing materials in the medical field [2]. One of the most promising dressing materials is the hydrogel. Hydrogels are pH-sensitive, hydrophilic, and physically or chemically cross-linked networks. The hydrophilic functional groups present in the hydrogel are responsible for the interaction of hydrogel with various biological tissues. The external environmental conditions such as pH, temperature, and ionic strength can break the physically cross-linked networks of hydrogels. Therefore, chemically cross-linked hydrogels are required to be developed using the cross-linker agents. These are attractive materials in wound healing applications due to their specific properties such as high swelling capacity, moisture uptake, and bioactivity [3] which makes them efficient dressing materials [4]. They can absorb the wound exudates, have good flexibility, prevent bacterial growth, keep the moist restorative surroundings, and inhibit anaerobic bacteria proliferation [5]. The flexibility of the 3-D network of hydrogel allows the entrapment and transportation of antibacterial drugs [6]. The diffusion of drugs from hydrogel depends on various factors such as pH, temperature, pressure, and swelling solvent [7]. The antibacterial properties of hydrogel can be enhanced by incorporating antibiotic drugs in the hydrogel matrix [8]. The ciprofloxacin (CFX) is a synthetic, broad-spectrum, and chemotherapeutic agent belonging to the fluoroquinolone family. CFX is one of the most important biocompatible and antimicrobial drugs used for wound healing applications [9]. The half-life of the CFX drug is 4 h. CFX can inhibit DNA replication by preventing the production of folate [10]. CFX can enhance the effectiveness

* Corresponding authors.
E-mail addresses: sudhirwarkar@gmail.com (S.G. Warkar), anil_kumar@dce.ac.in (A. Kumar).

https://doi.org/10.1016/j.ijbiomac.2024.136766
Received 27 January 2024; Received in revised form 14 October 2024; Accepted 19 October 2024
Available online 22 October 2024
0141-8130/

ANNEXURE- IV

DELHI TECHNOLOGICAL UNIVERSITY

(Formerly Delhi College of Engineering)
Shahbad Daulatpur, Main Bawana Road, Delhi-42

PLAGIARISM VERIFICATION

Title of the Thesis **Development of Biopolymers Based Hydrogels for Various Applications** Total Pages **192** Name of the Scholar **Indu Rani**

Supervisor (s)

(1) **Prof. S.G.Warkar**

(2) **Prof. Anil Kumar**

Department **Applied Chemistry**

This is to report that the above thesis was scanned for similarity detection. Process and outcome is given below:

Software used: **Turnitin** Similarity Index: **7** Total Word Count: **50928**

Date: **01/11/2024**

Candidate's Signature **Signature of Supervisor(s)**

Similarity Report

PAPER NAME

INDUU PHD 30-10-24.pdf

WORD COUNT	CHARACTER COUNT
50928 Words	**273681 Characters**
PAGE COUNT	FILE SIZE
192 Pages	**5.0MB**
SUBMISSION DATE	REPORT DATE
Nov 1, 2024 1:59 PM GMT+5:30	**Nov 1, 2024 2:02 PM GMT+5:30**

7% Overall Similarity

The combined total of all matches, including overlapping sources, for each database.

- 3% Internet database
- 5% Publications database
- Crossref database
- Crossref Posted Content database
- 3% Submitted Works database

Excluded from Similarity Report

- Bibliographic material
- Quoted material
- Cited material
- Small Matches (Less then 10 words)
- Manually excluded sources
- Manually excluded text blocks

Summary

BIO-DATA

Dr. Indu Rani has completed her Ph.D. from Delhi Technological University, Delhi in the Department of Applied Chemistry during 2020-2024. Before this, she completed her Master's in Chemistry from Hansraj College, Delhi University in the year 2016 and her Bachelor of Science from Sri Venkateswara college, Delhi University in the year 2014. She has qualified NET- JRF, and GATE exams. She was a recipient of a Junior Research Fellowship (JRF) and Senior Research fellowship (SRF) from the Council of Scientific and Industrial Research (CSIR), India. She was also a recipient of Innovation in Science Pursuit for Inspired Research (INSPIRE) scholarship during her graduation and post-graduation period. Her research interest includes the development of biopolymers-based hydrogels for various applications.